6-1986

Characterization of the Rheological, Optical, and Flow-Induced Structural Features of Polymer Liquid Crystals

David Neal Lewis
University of Tennessee - Knoxville

To the Graduate Council:

I am submitting herewith a dissertation written by David Neal Lewis entitled "Characterization of the Rheological, Optical, and Flow-Induced Structural Features of Polymer Liquid Crystals." I have examined the final electronic copy of this dissertation for form and content and recommend that it be accepted in partial fulfillment of the requirements for the degree of Doctor of Philosophy, with a major in Polymer Engineering.

John F. Fellers, Major Professor

We have read this dissertation and recommend its acceptance:

Kermit E. Duckett, Donald C. Bogue, Joseph E. Spruiell

Accepted for the Council:
Dixie L. Thompson

Vice Provost and Dean of the Graduate School

(Original signatures are on file with official student records.)

To the Graduate Council:

I am submitting herewith a dissertation written by David Neal Lewis entitled "Characterization of the Rheological, Optical, and Flow-Induced Structural Features of Polymer Liquid Crystals." I have examined the final copy of this dissertation for form and content and recommend that it be accepted in partial fulfillment of the requirements for the degree of Doctor of Philosophy, with a major in Polymer Engineering.

John F. Fellers

John F. Fellers, Major Professor

We have read this dissertation
and recommend its acceptance:

Kenneth E. Duncan

Donald C. Bogue

J. E. Spruiell

Accepted for the Council:

Carl Minkel

Vice Provost
and Dean of the Graduate School

CHARACTERIZATION OF THE RHEOLOGICAL, OPTICAL, AND FLOW-INDUCED STRUCTURAL FEATURES OF POLYMER LIQUID CRYSTALS

A Dissertation

Presented for the

Doctor of Philosophy

Degree

The University of Tennessee, Knoxville

David Neal Lewis

June 1986

DEDICATION

This dissertation is dedicated to my Lord and Savior, Jesus Christ, without whose help and guidance this research would not have been successfully completed.

ACKNOWLEDGEMENTS

First, the author wishes to express his profound appreciation to his parents, Hugh and Alma Lewis, for their encouragement and guidance throughout his graduate studies.

Second, the author expresses his deep appreciation to his advisor, Professor John F. Fellers, for the opportunity to work with him in this project and for his guidance, advice and encouragement throughout his doctoral program.

Third, the author expresses his appreciation to the members of his doctoral committee, Professor Donald C. Bogue, Professor Joseph E. Spruiell, and Professor Kermit E. Duckett, for their input and advice in his dissertation research.

Fourth, the author is indebted to the Material Science and Engineering Department for their financial support of his doctoral studies.

Fifth, the author would like to thank W.J. Jackson of Tennessee Eastman for supplying the polyesters used in his research. The author would also like to thank the Dow Chemical company and Hercules, Inc. for supplying the cellulosic polymers used in his research.

Sixth, the author would like to thank Ted Long and his coworkers in the Electronic Shop, Tommy Thompson and

his coworkers in the Machine Shop, and Al Carter and his coworkers in the Facilities Shop.

Finally, the author extends his many thanks to all his many associates and faculty advisors in the Polymer Engineering program, particularly Ken Zieminski, Greg Farell, George Webster, John Flood, Carl Wust, Mukareem Cakmak, Subbu Venkatraman, Professor Edward S. Clark and Professor James L. White, for their advice, constructive conversations, and input during his doctoral program.

ABSTRACT

Two related sets of experiments were conducted to explore the interaction between supramolecular structures, material properties, and flow-induced stresses in selected lyotropic and thermotropic polymers. The first set of experiments focused on the quiescent and rheological characterization of the polymers. The objective was to develop a flow-structure model based on the general phenomenological features of the liquid crystalline state. The second set of experiments concerned the characterization of the crystal structure, crystalline orientation, and tensile properties of a model thermotropic polymer, melt spun under varying conditions of extrusion rate, extrusion temperature, drawdown ratio, and die exit conditions. The objective was to determine the most effective process conditions for enhancing both orientation and tensile properties.

The principal materials examined were hydroxypropyl cellulose (HPC), ethyl cellulose (EC), poly(p-benzamide) (PBA), and poly(p-oxybenzoate-co-ethylene terephthalate) (POB/PET 60/40). HPC, EC and PBA formed lyotropic solutions. EC and POB/PET 60/40 formed thermotropic melts.

Quiescent characterization revealed the presence of birefringent 'polydomain' structures at certain polymer concentrations or melt temperatures. Rheological studies revealed the presence of 'domain flow' stresses associated

with these structures. The magnitude of this stress was associated with the 'domain loading' effect of a densely packed polydomain structure. The shear stress and first normal stress difference (N_1) both were generally represented by a shear rate dependent, three region response curve. The low shear region exhibited a plateau associated with the plastic flow behavior. The moderate shear region was quasi-linear and tended to have a slope less than one. For the shear stress the slope represented the degree of shear thinning. For N_1 the slope represented the degree of plastic flow suppression. A stress saturation plateau was found at high shear rates.

The crystalline orientation and tensile properties of POB/PET 60/40 were most improved by extrusion temperatures exceeding the melt transition of the POB rich phase at 255^{o}C. The crystalline orientation was limited to a maximum value of 0.75 for all process conditions. Under certain conditions, tensile strength and modulus were improved by employing an isothermal die exit chamber.

TABLE OF CONTENTS

CHAPTER PAGE

IV. (Continued)

CHAPTER PAGE

IV. (Continued)

LIST OF TABLES

TABLE PAGE

LIST OF FIGURES

FIGURE PAGE

FIGURE PAGE

FIGURE PAGE

FIGURE PAGE

CHAPTER I

INTRODUCTION

Liquid crystalline polymers represent a class of technologically important plastics with several unique characteristics. These polymers possess a degree of structural order as solutions and/or melts. These same conditions, with some notable exceptions [195], completely disrupt all structural order in conventional semicrystalline polymers. Generally, semicrystalline polymers show structural order only upon solidification. The presence of structural order in polymer liquid crystals during processing is responsible for their potential in forming highly oriented fibers, films, and moldings, which possess both high modulus (stiffness) and high strength.

The 'structurally ordered' or 'anisotropic' state in polymer liquid crystals results from the presence of either:

1. a rigid main chain backbone comprised of phenyl or other aromatic ring structures, or

2. a semiflexible main chain that is sterically restricted to rigid rodlike and/or extended chain conformations. Anisotropic states in polymeric mesophases only exist under certain conditions of temperature and/or solute concentrations; these conditions specify the liquid

crystalline region of the phase diagram. The liquid crystal state is formed by the packing of the polymer chains into supramolecular associations known as 'domains'.

The presence of 'domains' in polymer liquid crystals affects the rheology and, thereby processing, of these polymeric materials. The flow behavior or rheology of polymer liquid crystals is quite unusual compared to typical amorphous and semicrystalline polymers; the behavior most closely resembles that of highly filled conventional polymers containing very small particles. Both filled polymers and liquid crystalline polymers exhibit 'yield' or 'domain flow' stress behavior just prior to flow initiation; unfilled polymers do not exhibit 'yield' stresses. However, the flow behavior shows some aspects that are completely different from even filled polymer systems. Polymeric mesophases are easily oriented at low shear rates and typically show lower viscosities than either filled or unfilled polymers of similar molecular weight. Liquid crystalline polymers show three distinct regions of flow behavior with increasing shear rate:

1. at low shear rates, the flow is characterized by shear thinning and 'yield' or 'domain flow' stresses,

2. at intermediate shear rates, the flow is characterized as quasi-Newtonian, and

3. at high shear rates, the flow is characterized by shear thinning behavior [18].

The solid state structure of flow oriented polymer liquid crystals consists of a relatively highly oriented outer 'skin' layer surrounding a less oriented core [216]. This 'skin-core' structure is more pronounced than in non-liquid crystalline polymers processed under the same conditions. The main reasons this oriented skin layer remains after solidification are

1. the stress-induced orientation decays away very slowly and

2. the initial level of stress-induced orientation is much higher at the boundary surfaces during flow than at the flow's centerline. The pronounced difference in the skin and core orientation levels also exists because of the fact that the skin solidifies before the core, upon encountering either a coagulant (in the case of solution processing) or a cooler temperature zone (in the case of melt processing).

The research presented in this dissertation is an examination of the factors which govern how processing changes the structure of polymer liquid crystals. The objective of this research is threefold:

1. to determine which process variables are most important in enhancing chain orientation and mechanical properties,

2. to discover which of these process variables are general characteristics of the liquid crystalline state

and not limited to the particular polymer, and

3. to develop a phenomenological framework to explain the interactions of the microstructure and the flow stresses during processing.

The liquid crystalline polymers used in this research were selected on the basis of two criteria:

1. the polymers should be representative of the spectrum of liquid crystalline types (thermotropic, lyotropic, nematic, cholesteric, and smectic), and

2. the polymers should be available in reasonable quantities from either a commercial or noncommercial source.

CHAPTER II

LITERATURE REVIEW

1. GENERAL CLASSIFICATION OF LIQUID CRYSTALS

Materials which form liquid crystals or mesophases may be classified in several ways. Two general classification schemes exist for all liquid crystals. The first, developed by Friedel [91] in 1922, is based on the structural arrangement adopted by the quiescent liquid crystal. The second is based on the thermodynamic pathway, or transition, from the disordered isotropic state to the ordered liquid crystalline or anisotropic state. Liquid crystals may also be classified on the basis of molecular weight. Mesophases formed from low molecular weight substances are called 'small molecule liquid crystals'. Mesophases formed by high molecular weight polymers are called 'polymer liquid crystals' or 'macromolecular liquid crystals'.

Structurally, three classes of liquid crystals have been designated (a) nematic, (b) cholesteric, and (c) smectic [91]. The nematic class or state can be thought of as a collection of rigid rods which have an average alignment in the axial direction but little alignment or order in the transverse direction. The cholesteric state is usually considered as a twisted or helical nematic state (hence, it is sometimes considered as a subclass of

the nematic state). This state is formed by liquid crystals which contain non-racemic, optically active or chiral groups [51]. In the cholesteric state, the molecules are arranged in uniform layers of one dimensional order normal to the twist axis. The distance for a 360 degree turn of this structure is called the 'pitch', p [240]. The smectic state is a layered structure with two dimensional order [240]. Several forms of the smectic mesophase are known: S_A, S_B, S_C, S_D, S_E, S_F, S_G, S_H, and S_I [42]. The smectic A (S_A) phase is characterized by the molecules being arranged parallel to one another and in layers normal to the molecular long axis [57]. In the smectic C (S_C) structure, the long axes of the molecules are tilted in the layer planes [57]. The S_A, S_C, and S_F mesophases are known as unstructured smectics, since the molecules are positioned in a random parallel arrangement in each layer [42]. Smectic D (S_D), unlike the other smectics, does not possess a layer structure; the molecules are packed in a cubic type arrangement [42]. The remaining smectics: S_B, S_E, S_G, S_H, and S_I are known as structured smectics, since each layer forms a two dimensional unit cell or lattice [42]. In these smectics, the molecules are arranged in unit cells with hexagonal (S_B), tilted hexagonal (S_I), monoclinic (S_G and S_H), or orthorhombic (S_E) character [42, 57]. Structures of the nematic, cholesteric, and smectic classes are shown in Figure 1.

Nematic

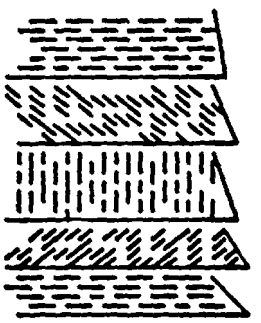

Cholesteric

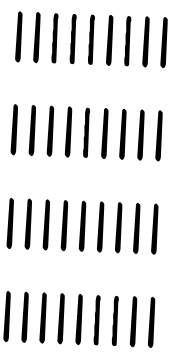

Smectic A

Figure 1. Representative Structures for Nematic, Cholesteric, and Smectic A Classes.

Liquid crystals are also classified according to the phase transition from isotropy to anisotropy. Isotropic materials which become anisotropic through purely thermal processes (heating and cooling) are called thermotropic liquid crystals [240]. Similarly, isotropic solutions which become anisotropic under the influence of solvents or through changes in solute concentration are called lyotropic liquid crystals [240].

2. SMALL MOLECULE LIQUID CRYSTALS

Liquid crystals were first discovered by Reinitzer [200] in 1888, followed by Lehman [145-147] in 1889 through 1890. Since their time, numerous small molecule chemical species have been observed to exhibit liquid crystalline behavior. Small molecule liquid crystals and polymeric liquid crystals share several characteristics which appear to be intrinsic to the liquid crystalline state. This is particularly true in examining the effects of electric or magnetic fields. Both small molecule and polymer liquid crystals exhibit elastic moduli called Frank constants when exposed to magnetic fields [71]. Both small molecule and macromolecular liquid crystals show some similarities when subjected to imposed electric fields, since both exhibit conductive type flow patterns [136]. Small molecule and polymer mesophases also show similarities in the optical appearance or 'textures' they

both exhibit in nematic, cholesteric, or smectic states [18]. Thus low molecular weight liquid crystals have served as standards or models by which the liquid crystal state of polymers can be evaluated.

These low molecular weight compounds can be divided into three major groups or classes. The first and largest class is comprised of rigid, planar, aromatic compounds with structures of the form [240]

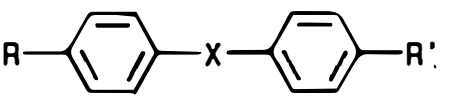

(1)

where R and R' are alkyl or aromatic groups and the central group X includes the structures of diagram (2).

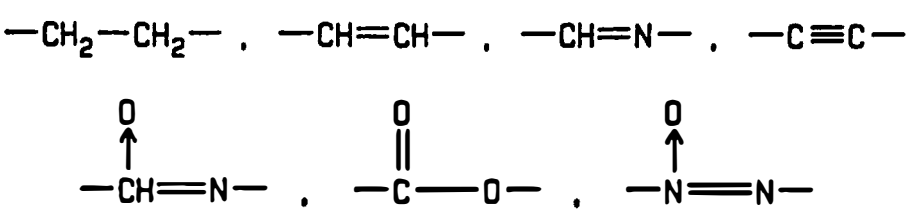

(2)

Widely studied examples of this group are shown in diagrams (3) through (6).

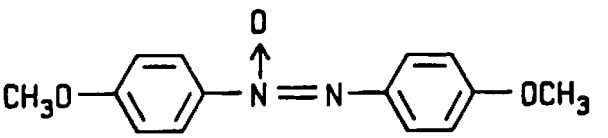

(3)

p-azoxyanisole (PAA),

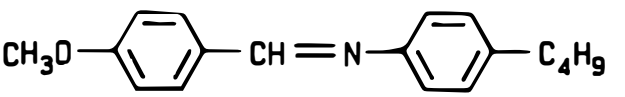

(4)

N-(p-methoxybenzylidene)-p-butylaniline (MBBA),

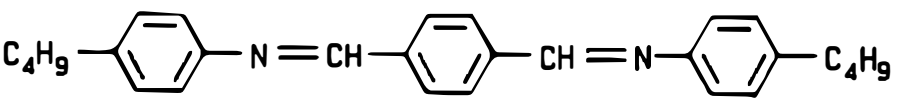

(5)

terephthal-bis(p-butylaniline) (TBBA), and

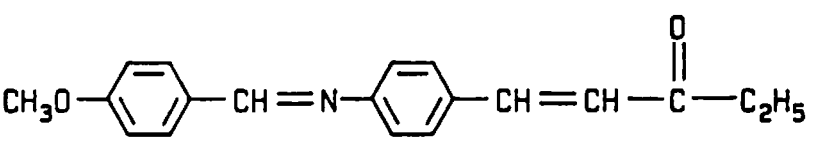

(6)

ethyl-anisal-p-amino-cinnamate (EAPAC).

These compounds undergo thermotropic mesomorphosis. Compounds like p-azoxyanisole (PAA) and N-(p-methoxy-benzylidene)-p-butylaniline (MBBA) form the nematic state in the melt [59]. Other compounds like terephthal-bis(-p-butylaniline) (TBBA) and ethyl-anisal-p-amino-cinnamate

(EAPAC) exhibit both thermotropic smectic phases and nematic phases [59,61].

Derivatives of cholesterol are the second major class of small molecule liquid crystals. These compounds include the cholesteric moiety shown below:

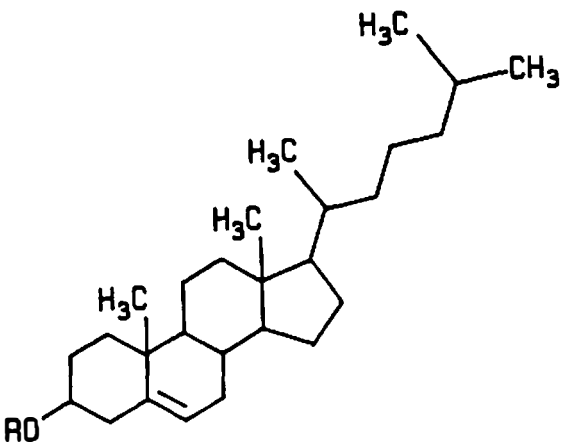

(7)

where R represents a carboxylic acid group. Cholesteric derivatives contain chiral or optically active molecules which induce the twist or pitch in the mesomorphic state. Examples of cholesterol derivatives include cholesterol benzoate, cholesterol propanoate, and cholesterol formate which are esters of cholesterol and organic acids such as benzoic acid, propanoic acid, or formic acid [240].

Amphiphilic compounds are the third major class of small molecule liquid crystals [240]. In contrast to the first two classes, these compounds undergo lyotropic mesomorphosis. Materials which form soaps like sodium laurate or N-n-dodecyl pyridium chloride are common examples of amphiphilic liquid crystals [240]. Amphiphilic compounds

generally form spherical micelles in dilute or isotropic solutions, but form the smectic A (S_A) state when the concentration neccessary to form an anisotropic solution is attained. Chemically, amphiphillic compounds show extreme polarization (i.e. ionic character) and have a flexible, nonrigid structure.

3. MACROMOLECULAR LIQUID CRYSTALS

A. Classification

Unlike the discoveries of small molecule liquid crystals, or even the discovery of polymers themselves, the discovery of macromolecular or polymer liquid crystals is relatively recent. Since their discovery in 1950, some 15 classes of polymers have been reported to form liquid crystals in solutions or melts. These 15 classes of polymers can be divided into three structural groups:

1. polymers which contain mesogenic groups in the main chain,

2. polymers which have rigid chains due to intra-helix hydrogen bonding, and

3. polymers which possess pendant or side chain mesogenic groups [55]. Polymers placed in the first category include aromatic polyamides, aromatic polyhydrazides, aromatic polyazomethines, aromatic polyurethanes, aromatic copolyesters, aromatic polyesteramides, aromatic polythioesters, aromatic polyethers,

polyisocynates, cellulosic polymers, heteropolysaccharides like xanthan gum, and wholly aromatic polyheterocylics like poly(bisbenzthiazole) (PBT) [28]. Synthetic polypeptides are the only polymers included in the second group. Polymers categorized in group three include polyacrylates and polysiloxanes.

Synthetic polypeptides were the first polymers found to exhibit liquid crystalline behavior. These polymers were initially investigated at Courtaulds in the late 1940's for their potential in forming synthetic silk fibers [23]. The liquid crystalline nature of synthetic polypeptides was first reported in 1950 by Courtaulds' researchers Elliott and Ambrose [80]. Other Courtaulds' researchers, notably Robinson [202-205], made extensive investigations of one synthetic polypeptide, poly(γ-benzyl-L-glutamate) (PBLG). PBLG was observed to form birefringent, lyotropic solutions at concentrations ranging from 17 wt% to 34 wt%, depending on polymer molecular weight and solvent character. Robinson [202] also observed two phenomena which are usually associated with lyotropic liquid crystal formation:

1. the unexpected viscosity decrease with increasing concentration at the onset of anisotropic phase formation, and

2. the formation of optically observed 'textures'.

In the case of PBLG, the 'textures' consisted of parallel

band structures associated with the twist length or 'pitch' of the helical superstructure.

Chemical structures of several synthetic polypeptides are represented by diagrams (8) through (12) [240,241]

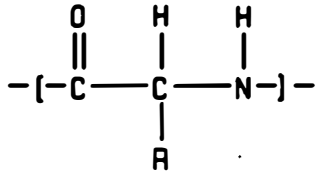

(8)

where R may be

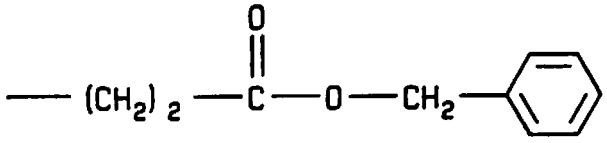

(9)

for poly(γ-benzyl-L-glutamate) (PBLG),

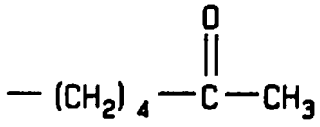

(10)

for poly(ε-carbobenzyloxy-L-lysine) (PBCL),

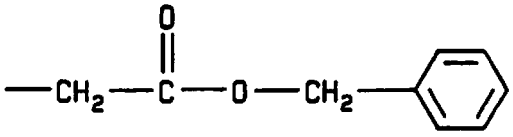

(11)

for poly(β-benzyl-L-aspartate) (PBAP), and

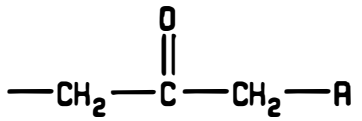

(12)

for poly(γ-alkyl-L-glutamate). R' can be methyl, ethyl, propyl, butyl, amyl, hexyl, or cyclohexyl.

Synthetic polypeptides, particularly PBLG, are mainly studied at the present time as model systems for understanding the nature of the liquid crystalline state in lyotropic polymer systems. The quiescent structure of PBLG solutions has been studied extensively by DuPre and coworkers [71,187,188,222]. The deformation effects of external electric and magnetic fields, which yield Frank [87] elastic constants, have been investigated by several researchers, notably in the United States by DuPre et al. [71-76,82,187,222] and in Japan by Iizuka and coworkers [114,136]. The effects of external fields on polymer liquid crystals was reviewed by both DuPre [71] and Krigbaum [136] in 1982.

Aromatic polyamides were the second group of polymers observed to form liquid crystals. Many of these polymers were first developed by Dupont researchers, particularly Kwolek [142,143] and Morgan [19,20,168], in the mid 1960's and early 1970's. Aromatic polyamides have structures represented by diagrams (13) and (14)

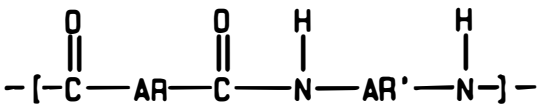

(13)

where AR and AR' may be

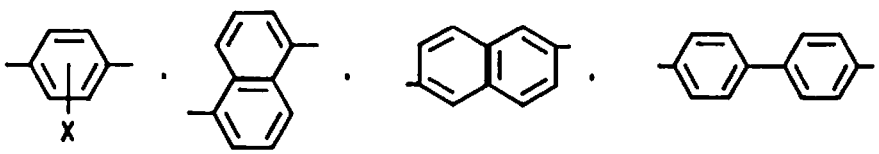

(14)

and X = H, Cl, Br, F or SO_3H. Two of these aromatic polyamides, poly(p-benzamide) (PBA) (structure 15) and poly(p-phenylene terephthalamide) (PPTA) (structure 16), have received the most attention [142].

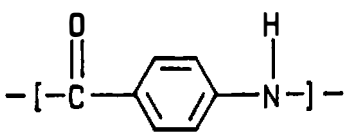

(PBA) (15)

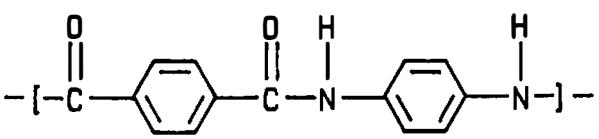

(PPTA) (16)

The latter polymer, PPTA, has been commercialized by Dupont under the tradename Kevlar®. Both PBA and PPTA form nematic liquid crystalline solutions in sulfuric acid (SA) in concentrations around 10 wt% depending on polymer

molecular weight [142]. The concentration needed to induce the onset of the anisotropic or liquid crystalline state was found to be inversely proportional to polymer molecular weight as noted by Papkov et al. [142], Kwolek et al. [137], and Morgan et al. [20]. The phase diagrams of PPTA, PBA, and other lyotropic polyamides were also observed to depend on solution temperature as well as polymer concentration [141].

Aromatic polyamides forming thermotropic, nematic liquid crystalline states have been reported by Adduci et al. [3] and Griffin et al. [93]. Adduci et al. [3] reported thermotropic behavior in aromatic polyamides with the structures shown in diagrams (17) and (18).

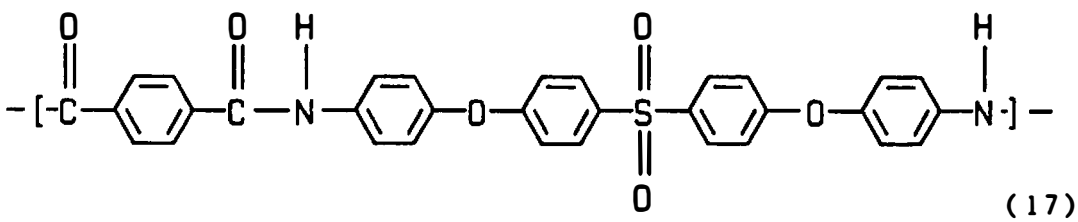

(17)

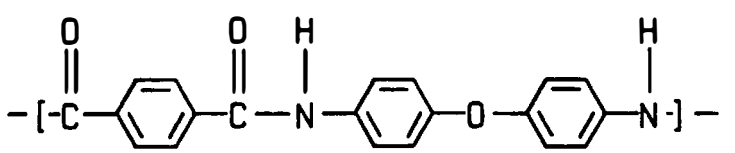

(18)

Whereas Griffin et al. reported thermotropic behavior in aromatic polyamides represented by diagram (19)

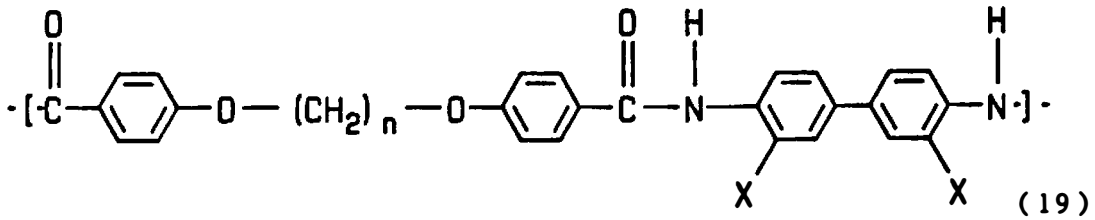

(19)

where n = 10 to 12 and X may be Cl, CH_3, or OCH_3.

Aromatic copolyesters were the third group of polymers observed to exhibit liquid crystalline behavior. Commercial interest in this group of polymers results from the ability of these polymers to form melt processable thermotropic mesophases. Melt processing or fabrication techniques are generally less expensive than the solution processing methods used for lyotropic polymers like PPTA.

The development of thermotropic aromatic copolyesters was pioneered by researchers at Tennessee Eastman, notably Jackson [119,120,138,139] and McFarlane [156,157]. Jackson et al. [120] described the synthesis and properties of poly(p-oxybenzoate-co-ethylene terephthalate) (POB/PET) copolyesters containing from 60 to 90 mol% p-oxybenzoate units (POB). These aromatic copolyesters were prepared by high temperature melt polymerization of p-acetoxybenzoic acid and poly(ethylene terepthalate). The POB/PET copolyesters contain the molecular structures shown in diagrams (20) and (21).

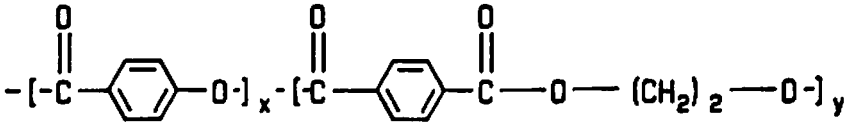

(20)

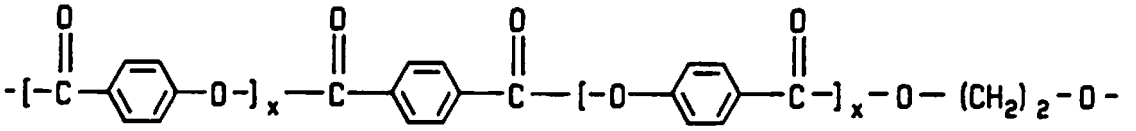

(21)

The variables x and y generally range from two to six units. The POB/PET copolyesters containing at least 60 mol% POB units were observed to form nematic melts above 240°C. McFarlane and coworkers described other aromatic copolyesters which formed thermotropic liquid crystals. These copolyesters were of the general form

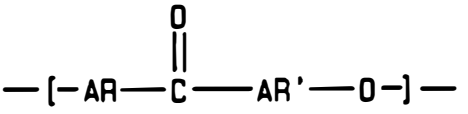

(22)

where AR may be the structures

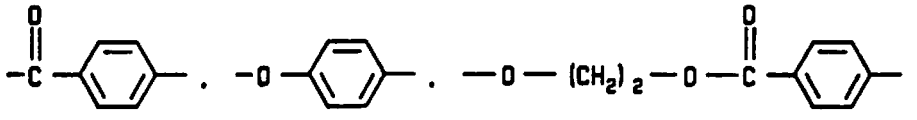

(23)

and AR' may consist of the structures in diagram (24).

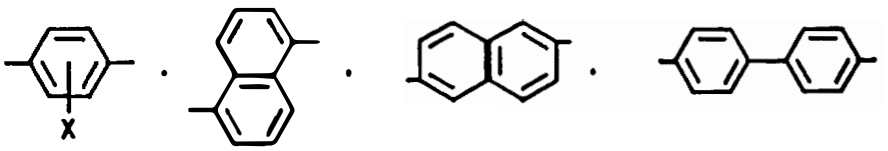

(24)

X can represent Cl, Br or OCH_3. Pletcher [191] and Kleinschuster [133,134] of Dupont, described similar classes of aromatic copolyesters containing the units

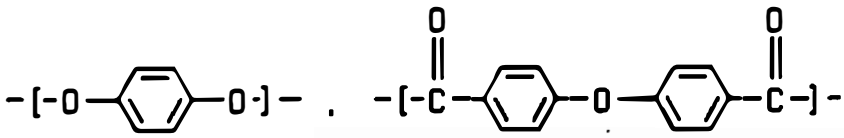

(25)

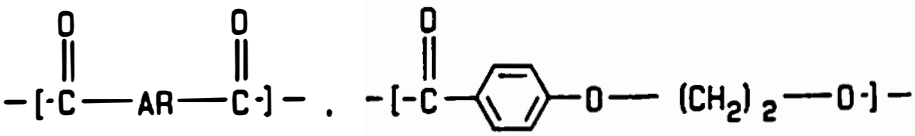

(26)

where AR may be the structures of diagram (24).

Cottis et al. [56], of the Carborumdum Co., in a 1976 patent, described melt spinnable aromatic copolyesters containing the moieties shown in diagram (27)

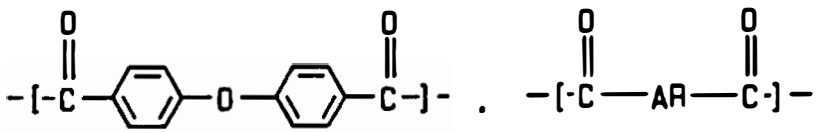

(27)

where AR may be the structures of diagram (24).

One of these aromatic copolyester compositions in the Cottis et al. patent, synthesized from terephthalic acid,

p-hydroxybenzoic acid, and p,p'biphenol, was sold to Dartco, a subsidary of Dart and Kraft, Inc. and commercialized under the tradename Xydar® [53]. The first reported commercial application of Xydar® was a new line of heat stable oven containers, by Dart and Kraft's Tupperware subsidary, marketed under the tradename Ultra 21® [58].

More recently, Celanese corporate researchers, principally Calundann [47], Warner [236], and Wissbrun [242], have reported studies of thermotropic aromatic copolyesters containing moieties of the type

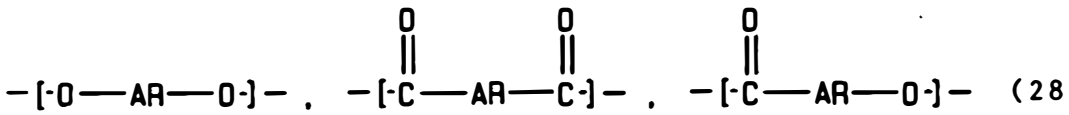

(28)

where AR may be the structures of diagram (24) or the structures of diagram (29) below

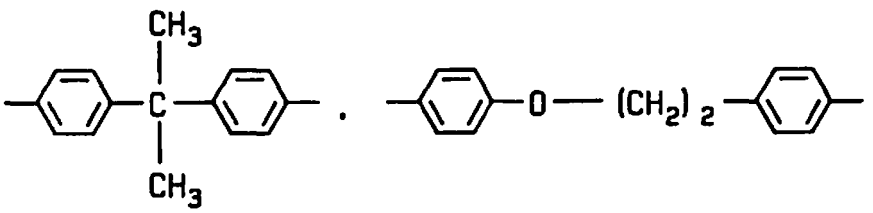

(29)

and where X is a halogen group.

Recently, Krigbaum and Watanabe [137] reported aromatic copolyesters which form smectic A mesophases. These copolyesters have a general structure of the type

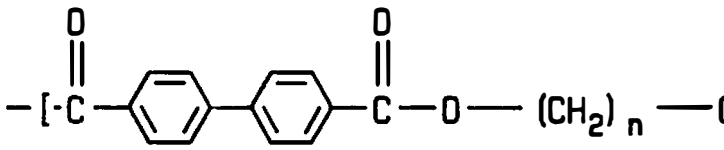

(30)

where n = four, six, eight, or ten.

Cellulosic derivatives are the fourth class of polymers observed to form liquid crystalline or mesomorphic states. Examples of this class include hydroxypropyl cellulose (HPC), cellulose acetate (CA), cellulose acetate butyrate (CAB), ethyl cellulose (EC), cellulose nitrate (CN), cellulose triacetate (CTA), and cellulose itself. All of the above materials form lyotropic liquid crystalline states in certain solvents. HPC and EC form thermotropic as well as lyotropic liquid crystals [216,226]. The general repeating unit of the cellulose derivatives is shown in Figure 2. Lyotropic behavior in cellulose and cellulose derivatives was reviewed in 1983 by Gilbert and Patton [93].

The most extensively studied member of this class has been HPC [29,30,180,208,238]. Samuels [208] first reported studies on solution cast films of HPC in 1969. These studies indicated the polymer structure existed in the solid state as a collection of rigid rods or

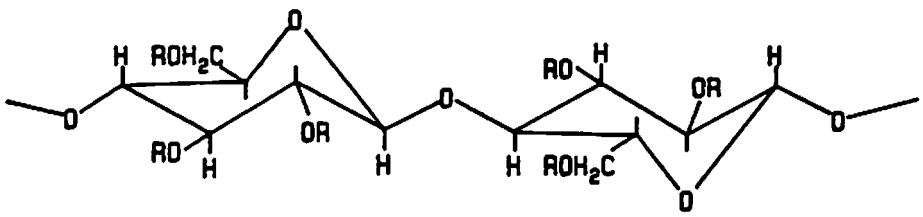

Figure 2. Representative Structure of the Repeat Unit for Cellulose and Cellulose Derivatives. The variable R can represent groups like H, $-CH_3$, $-C(O)CH_3$, $-C_2H_5$, and $-CH_2-CH(OH)-CH_3$ among others.

crystalline microfibrils. The liquid crystalline nature of HPC, however, was not known until the published work of Werbowyj and Gray [238] in 1976. They reported HPC formed a lyotropic cholesteric mesophase in water. Other studies of HPC in water solutions, notably Onogi et al. [180], found that HPC formed the cholesteric state in concentrations above 53 wt% polymer. They also observed the formation of negatively birefringent spherulitic 'domains', ca. 20 to 80 microns in size, for solution concentrations greater than 70 wt%. Bheda et al. [29,30] reported studies of HPC in different solvents, namely acetic acid (AA), water (W), dichloroacetic acid (DCA), dimethylacetamide (DMA), and ethanol (EA). Bheda and coworkers observed the critical concentration for the onset of anisotropy, C*, in HPC solutions decreased with increasing solvent acidity. They also observed the formation of fingerprint type 'textures' in some HPC solutions.

Studies of other cellulosic derivatives were reported by Bheda [29]. Conclusions were (a) that EC formed negatively birefringent spherulitic 'domains', (b) that CTA formed positively birefringent 'domains', and (c) that CA and CAB did not form any well defined structures in solution.

Aharoni [6] reported studies of cellulose acetate (CA) in 30 different solvents and observed that C*

generally decreased with acid strength in moderate to strong acid solvents. These studies also noted that C* decreased with increasing (solvent) molar volume with respect to weakly acidic, neutral, or basic solvents.

Several recent studies of cellulose itself have noted that it can form lyotropic solutions. Mixed solvents such as N-methylmorpholine oxide and water [52,88,111,171], ammonia and ammonium thiocynate [111], and trifluroacetic acid and methylene chloride [187] have been reported to form lyotropic, cholesteric solutions with cellulose at concentrations exceeding 10 wt%.

Thermotropic liquid crystalline behavior was reported in 1981 for HPC and in 1982 for EC. HPC was observed to form birefringent melts in the temperature range of 160°C to 200°C [216,226]. EC was observed to form thermotropic melts in the temperature range of 180°C to 200°C [226].

The fifth class of polymers observed to form liquid crystals are the polyisocynates. These polymers have a general structure represented by diagram (31) [8]

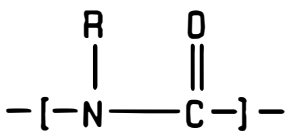

(31)

where R is an alkyl group of four to twelve carbon units

long or arylalkyl structures represented by diagram (32).

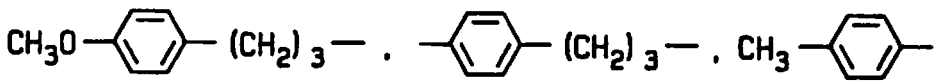

(32)

Millich [156], in 1975, first reported the liquid crystalline nature of the polyisocynates. The rigid rod-like character of the polyisocynates, however, has been known since the work of Burchard [46] in 1963, among others [45,123,214,231,232].

Studies of the polyisocynates by Aharoni and coworkers [4,5,8,9] have indicated that several of these polymers form lyotropic as well as thermotropic mesophases. Lyotropic and thermotropic behavior were observed in poly(n-butyl isocynate), poly(n-hexyl isocyanate), poly(n-octyl isocynate), and poly(n-nonyl isocynate). Solutions and melts formed were nematic.

Aromatic polyhydrazides and poly(amide-hydrazides) comprise the sixth class of polymers found to form liquid crystals. Although these polymers were first discovered in 1964 [89,90], liquid crystalline members of this class were not reported until 1976 [105]. Hartzler [105] and Morgan [169], both of Dupont, reported about 30 homopolymer and copolymer compositions which formed lyotropic solutions in 101% sulfuric acid or flurosulfonic and

sulfuric acid mixtures. Fibers with tenacities of 1.3 GPa to 1.5 GPa were dry-jet wet spun from anisotropic solutions containing ca. 20 wt% polymer. One of these polyhydrazides is poly(oxalic-chlorophthalic hydrazide), whose structure is shown below.

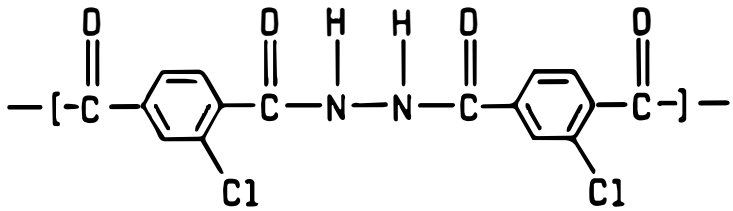

(33)

The seventh class of polymers observed to form liquid crystals were the wholly aromatic polyheterocyclics. These polymers have been studied in some detail by Berry and coworkers [28,54,79,233]. These polymers form lyotropic solutions in strong protic acids like methane sulfonic acid (MSA) and sulfuric acid (SA). Structures of two of these polymers are shown below [28].

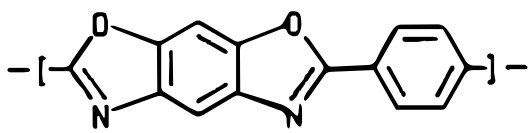

(34)

Poly(benzbisoxazole) (PBO)

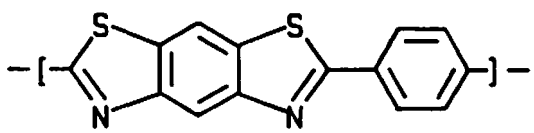

(35)

Poly(benzbisthiazole) (PBT)

The eighth and ninth classes of polymers observed to form liquid crystals are the side chain polymers of polyacrylates and polysiloxanes. These polymers have a flexible main chain with rigid, mesogenic pendant groups or side chains. Most of the polyacrylates and polysiloxanes which are liquid crystalline form thermotropic nematic or smectic states [83], although some polyacrylates have been reported to form lyotropic gels in certain solvents [215]. The literature on side chain polymers has been recently reviewed by Finkelmann [83]. Polyacrylates have a general repeating structure of the form [83]

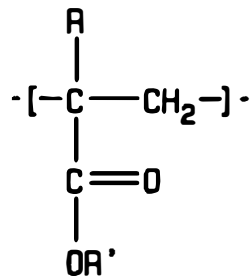

(36)

where R = H or CH_3 and R' may include the structures

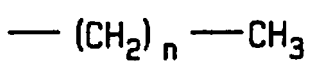

(37)

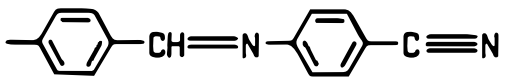

(38)

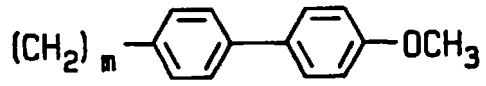

(39)

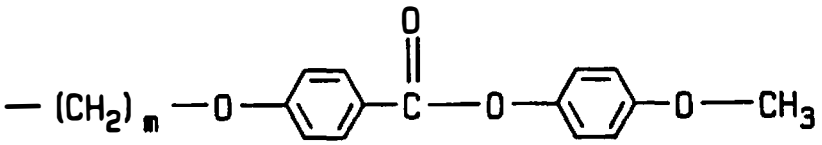

(40)

where m = two to eight units.

Polysiloxanes have a general structure of the form [83]

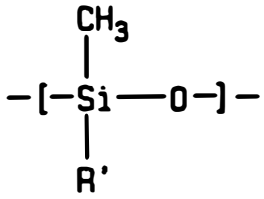

(41)

where R' includes structures (37) through (40).

Polyazomethines were the tenth class of polymers found to exhibit liquid crystalline behavior. These polymers form thermotropic nematic and smectic mesophases. Guillion and Skoulios [99], in 1978, synthesized the first thermotropic polyazomethine. This polymer exhibited a smectic B (S_B) mesophase and possessed the structure shown by diagram (42).

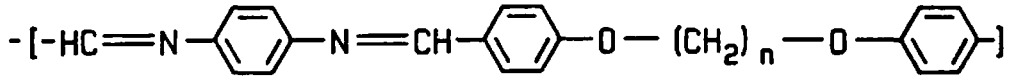

(42)

Samulski and Wiercinski [211] described other thermotropic azomethines with structures represented by diagram (43)

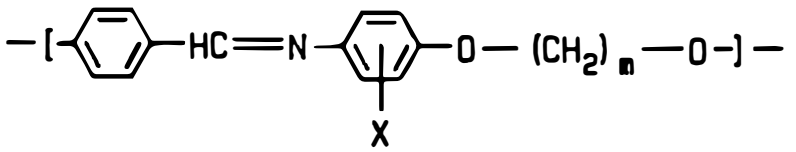

(43)

where X = H, Cl, or OCH_3 and m = two to twelve units.

Polyurethanes were the eleventh class found to exhibit liquid crystalline phases. Iimura and coworkers [117] observed that polyurethanes consisting of 3,3'-dimethyl-4,4'-biphenyldiyl disocynate and α,ω-alkanediols with five to twelve methylene units formed thermotropic phases in the range of 175°C to 230°C. The structure of these polyurethanes are of the form

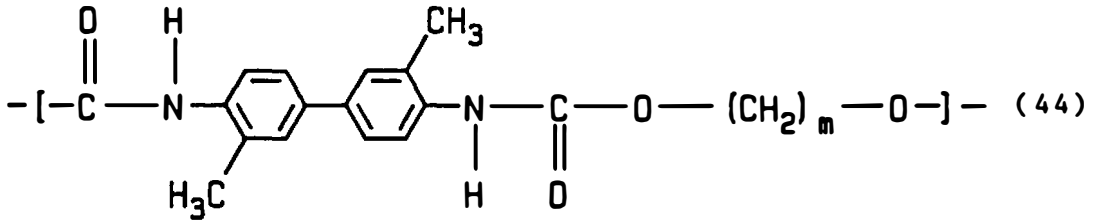

(44)

where m = five to twelve.

Aromatic poly(ester-amides) were the eleventh class of polymers found to form liquid crystals. Jackson and Kuhfuss [121,122] reported the synthesis and properties of several thermotropic poly(ester-amides). Representative structures are shown in diagrams (45) through (47).

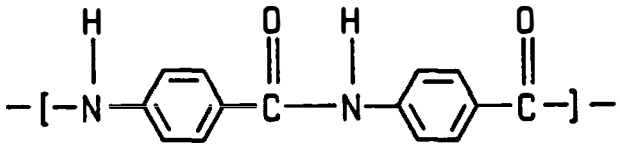

(45)

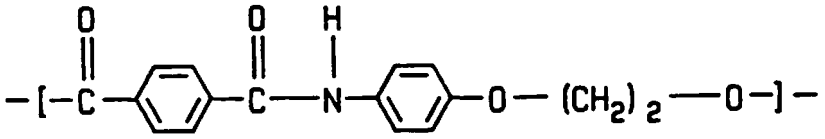

(46)

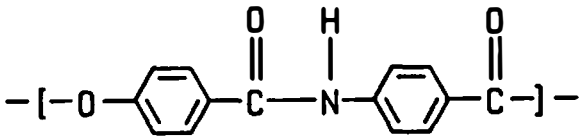

(47)

Heteropolysaccharides, like xanthan gum, are the twelfth class of polymers observed to be liquid crystalline. Xanthan gum is a biosynthesized, heteropolysaccharide containing D-glucose, D-mannose, and D-glucuronate in the mole ratio 2.8/2.0/2.0 [160]. Xanthan gum has been observed to form lyotropic solutions in water at concentrations as low as 1.0% [151]. The liquid crystalline nature of xanthan gum was first observed by Salamone et al. [207] in 1982.

The thirteenth class of polymers observed to form liquid crystals are the poly(thioesters). Laus et al. [144] synthesized poly(β-thioesters) with the structure represented by diagram (48)

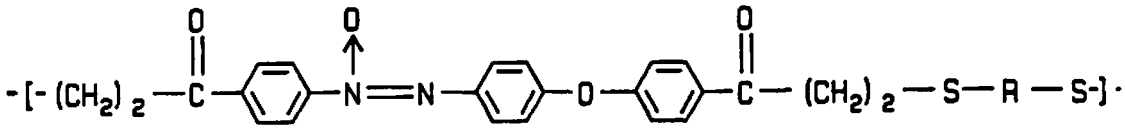

(48)

where R may be the structures of diagram (49).

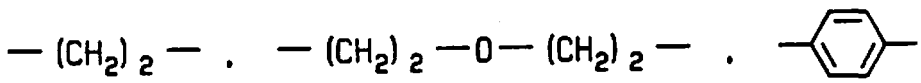

(49)

These polymers were found to exhibit thermotropic nematic states above 150°C.

The most recent class of polymers found to exhibit liquid crystalline behavior are the aromatic polyethers. Percec and coworkers [190] observed that polyethers synthesized from α,ω-di(bromo)alkanes and 4,4'-dihydroxy-α-methylstilbene containing from three to eight methylene groups formed smectic and nematic melts betweem 80°C and 200°C. A general chemical structure of these polyesters is shown by diagram (50)

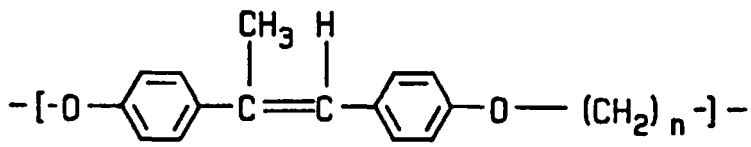

(50)

where n ranges from three to eight.

B. Quiescent Features

The anisotropic or directional nature of the liquid crystalline state in polymeric mesophases gives rise to the unusual properties of these materials as compared to typical amorphous and crystalline polymers. The most striking properties of polymer liquid crystals concern their optical behavior. Melts or solutions of polymeric mesophases, unlike typical isotropic polymers, transmit light between crossed polars and show birefringent colors. The quiescent condition in polymer liquid crystals is usually characterized by the formation of aggregated spherulitic 'domains' or polycrystalline 'textures' [18]. These 'textures' are quite sensitive to boundary conditions [71] and are characterized by the formation of defects or 'disclination' lines [87,162]. The interaction of a boundary surface with a polymer mesophase may cause static distortions in the liquid crystalline director, $\underline{n}$, which is a vector representing the average alignment of the molecular long direction or chain axis direction [59]. These static deformations are governed by the 'curvature elasticity theory' as proposed by Frank [87] in 1958

$$G_{el} = 0.5\, k_{11}(\text{div}\ \underline{n} + k_1/k_{11})^2 + 0.5\, k_{22}(\underline{n}\cdot\text{curl}\ \underline{n} - k_2/k_{22})^2 + 0.5\, k_{33}(\underline{n}\cdot\text{grad}\ \underline{n})^2 - k_{12}(\text{div}\ \underline{n})(\underline{n}\cdot\text{curl}\ \underline{n}) \qquad (1.0)$$

where G_{el} is the elastic (Gibbs) free energy density, k_i, k_{ii} are the elastic constants or moduli (of order 10^{-7} dyne), and $\underline{n}$ is the director. The 'curvature elasticity theory' is based on several assumptions [221]:

1. there is long range orientational order in liquid crystals,

2. the liquid crystal has uniaxial symmetry,

3. the distortions in the director which give rise to elastic energy result from only splay (k_{11}), twist (k_{22}), or bend (k_{33}) deformations, and

4. the curvature restoring stresses (or torques) are proportional to the curvature strains (Hooke's law). The forms of the three types of deformations are shown in Figure 3. Equation (1.0) takes on certain forms depending on the nature of the liquid crystalline state: nematic, cholesteric, or smectic A [221]

1. nematic case: $k_1/k_{11} = k_2/k_{22} = k_{12} = 0$

$$G_{el} = 0.5\, k_{11}(\text{div } \underline{n})^2 + 0.5\, k_{22}(\underline{n}\cdot\text{curl } \underline{n})^2 + 0.5\, k_{33}(\underline{n}\cdot\text{grad } \underline{n})^2 \qquad (1.1)$$

2. cholesteric case: $k_1/k_{11} = k_{12} = 0$, $k_2/k_{22} > 0$

$$G_{el} = 0.5\, k_{11}(\text{div } \underline{n})^2 + 0.5\, k_{22}(\underline{n}\cdot\text{curl } \underline{n} - k_2/k_{22}) + 0.5\, k_{33}(\underline{n}\cdot\text{grad } \underline{n})^2 \qquad (1.2)$$

3. smectic A case: curl $\underline{n} = 0$

$$G_{el} = 0.5\, k_{11}(\text{div } \underline{n})^2 \qquad (1.3)$$

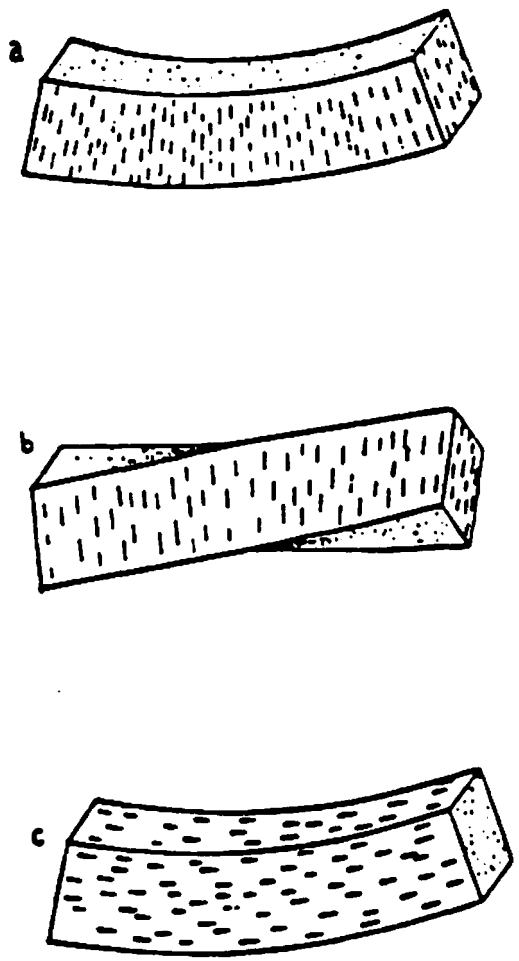

Figure 3. Spatial Representations of the Static Deformations in a Liquid Crystal. (a) Splays, (b) Twists, and (c) Bends.

Source: Stephen, M.J. and Straley, J.P., Rev. Mod. Phys. 46, 617 (1974)

Other forms of the smectic state, S_B through S_I, have symmetries higher than the uniaxial case and are not described by Frank's theory. The 'curvature elasticity theory' has several implications regarding the formation of 'textures'. The small magnitude of the Frank elastic constants, which are about 22 orders of magnitude smaller than Young's moduli [71], indicate that liquid crystals are very sensitive to external forces. The presence of a boundary surface, such as a glass slide, may cause localized orientation in the director near the surface, thereby distorting that part of the director with respect to the bulk of the liquid crystal [162]. The presence of chain ends can also cause local distortions in the director; this was pointed out by Meyer [162]. These local distortions also affect the molecular orientation at some distance from the disturbing influence, since the molecules act cooperatively in a liquid crystal. The preferred arrangement of the molecules near a disturbance results in the formation of 'disclinations' or discontinuities in the director [162]. These 'disclinations' are analogous to dislocations or defects in crystals [59].

Optical studies of nematic polyester melts have shown that particular types of line 'disclinations' occur [164]. Mackley et al. [153] observed that 'disclinations' of integer order ($\pm$ 1) occurred in the POB/PET 60/40 copolyester. Kleman et al. [127] observed 'disclinations' of

half integer order ($\pm$ 0.5) in a polyester with the structure represented by diagram (51).

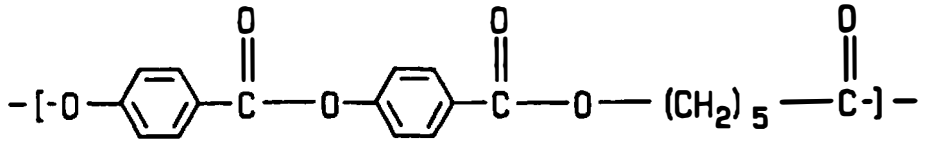

(51)

Kleman et al. noted these kinds of 'disclinations' are mainly due to twist type deformations, at the expense of splay and bend type deformations. The splay constant, k_{11}, was observed to be approximately three times larger than the bend constant, k_{33}, whereas both were larger than the twist constant, k_{22}. This implies the distortions giving rise to 'disclinations' tend to occur by the path of least resistance, which is the twist deformation mode. Kleman et al. also noted that some bend deformations occur along with twist deformations. Meyer [162] reinforced Kleman et al.'s observations by pointing out that splay deformations are largely inhibited by the length of the molecular chains in polymer liquid crystals.

More recently, Noel and coworkers [175] have observed 'disclinations' of integer order in the nematic melt of a methyl hydroquinone/pyrocatechol/terephthalic acid copolyester. This copolyester has a structure of the type illustrated by diagram (52).

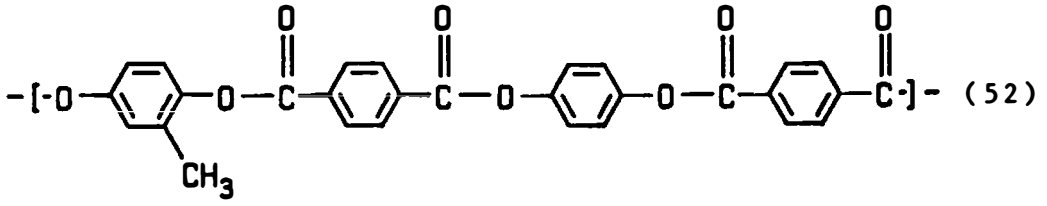

(52)

Noel et al. suggested that 'disclinations' of integer order seemed to be preferred in polymeric mesophases. This tendency was supported by the earlier observations on lyotropic polymer systems by Millaud [164], who attributed the 'disclinations' to a radial splay type distortion. The apparent strong dependence of the splay constant on molecular length, however, would tend to favor twist-bend distortions as the formation pathway for 'disclinations' [162].

Meyer [162] has observed a different mechanism for the formation of 'disclinations' in cholesteric polymers. Solutions of PBLG confined between thinly spaced glass surfaces produced the normally expected twist 'disclination' lines. However, PBLG solutions confined in cells with an air interface instead of glass formed compensated splay and bend 'domains' separated by 'disclination' lines. These splay distortions were stablized by the change in sign at the air interface, which made the total splay contribution to the system neglible.

Krigbaum and Watanabe [136] have observed 'textures' characteristic of smectic A type liquid crystals in

polyesters of p,p'bibenzoic acid and tetramethylene glycol or hexamethylene glycol comonomers. Batonnet, fan-shaped, and focal conic 'textures' were observed. Meyer [162] has pointed out that smectic A 'textures' can only result from radial splay distortions, since both twist and bend distortions are forbidden by Frank's theory in smectic mesophases.

C. Theoretical Rheological Models

The unusual rheological and rheo-optical behavior of polymer liquid crystals has been the subject of several extensive reviews: Baird [21] in 1978, Wissbrun [243] in 1981 and, more recently, Asada and Onogi [18] in 1983. The latter two reviews discussed general features of the rheology of polymer liquid crystals in terms of a qualitative, phenomenological flow-structure model, originally proposed by Asada and Onogi [18] in 1979. This model is illustrated in Figure 4. The Asada-Onogi model describes three distinct regions of flow behavior in polymer liquid crystals: at low shear rates, region I, where the flow is characterized by pronounced shear thinning and coexistant 'yield' stresses; at intermediate shear rates, region II, where the flow is characterized as quasi-Newtonian or shear rate independent; and at high shear rates, region III, where the flow is characterized as shear thinning. As noted by Wissbrun, this model shows qualitative

(A)

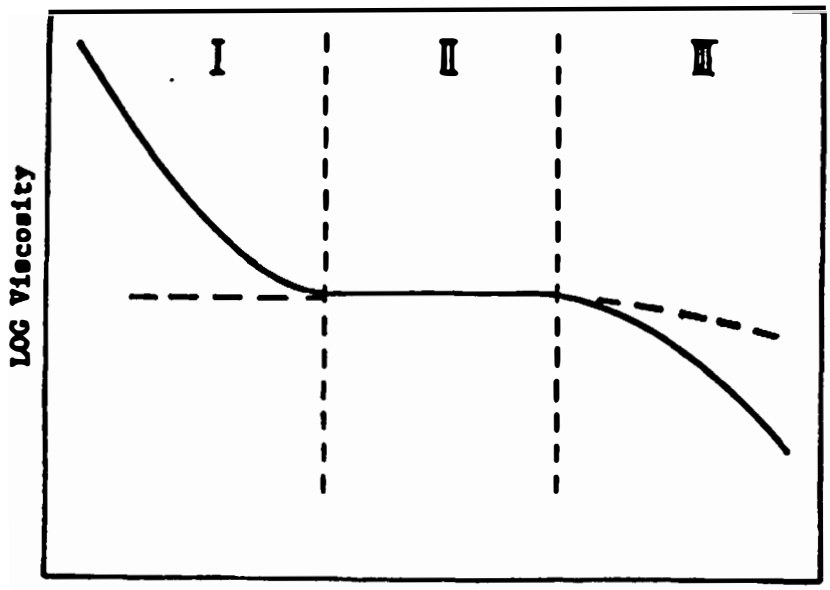

(B)

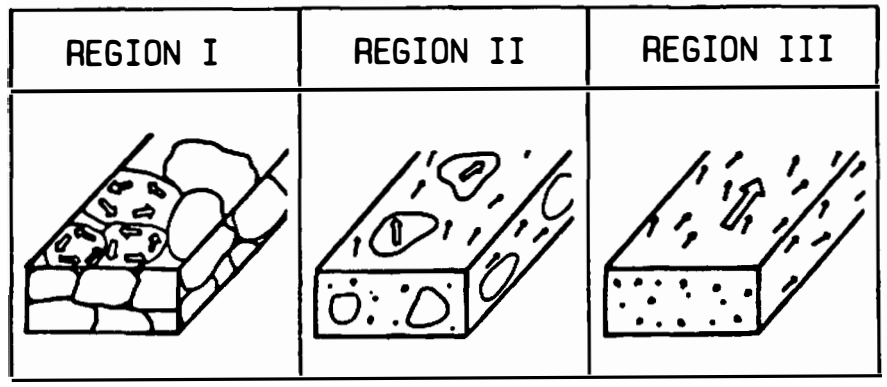

Figure 4. Onogi-Asada Model Representing the Viscosity Response (A) and Structural Changes (B)in Polymer Liquid Crystals. In Part (A), the Solid Line is the Liquid Crystalline Phase and the Dotted Line is the Isotropic Phase. In Part (B), the Shear Direction is from Left to Right.

Source: Asada, T., Muramatsu, H., Watanabe, R and Onogi, S., Macromol. 13, 867 (1980); Asada, T. and Onogi, S., Polym. Eng. Rev. 3, 323 (1983)

similarities to the flow-induced 'texture' model proposed by Pochan [192], to describe flow behavior in low molecular weight, thermotropic cholesterol derivatives. The bulk of this section is viewed in the context of the Asada-Onogi model. At present, no quantitative phenomenological or molecular based theory has been formulated to treat all three regions of flow behavior as expressed by the Asada-Onogi model.

Kotaka [135], in 1959, proposed the first constitutive expression to model the behavior of semidilute solutions of rod-like macromolecules. This theory was an extension of Kirkwood's [127] general theory of irreversible processes in macromolecular solution as well as Prager's [193] hydrodynamic theory of dumbell shaped molecules in solution. Kotaka derived the components of the total stress tensor with the expression

$$\sigma_{ij} - \sigma^{o}_{ij} = -C \sum_{l} \langle (e_i F_l)(e_j R_{ol}) \rangle_{Av} \qquad (1.4)$$

where σ_{ij} and σ^{o}_{ij} are the components of the stress tensor in solution and medium (solvent), respectively; c is the number of macromolecules per unit volume; R_{ol} is the position of each molecular segment, l, relative to the molecular center of mass; e_i and e_j are the unit vectors in the direction of the velocity field, and F_l is the hydrodynamic force. The expression was solved by averaging it with respect to the angular distribution

function $f(\theta,\Psi)$, which represents the orientation of the molecular axis with respect to the flow direction. The summation over l is taken over all the elements in a macromolecule: $-n \leq l \leq +n$. The result is expressed in terms of a power series of the ratio of shear rate, g, to rotary diffusion coefficient, D. The final form of equation (1.4) can be represented by

$$\sigma_{ij} - \sigma^{o}_{ij} = ckT \sum_{l} C_{l} (g/D)^{l} \qquad (1.5)$$

where σ_{ij}, σ^{o}_{ij}, g, D, and l, are as defined earlier; C_l is a coefficient dependent on $-n \leq l \leq +n$; k is the Boltzman constant, and T is the absolute temperature of the solution. This expression predicts in the presence of intermolecular interactions a small positive primary normal stress difference, N_1, as well as a large pulling force in the flow direction. Kotaka's constitutive expression appears to be applicable only to region II or region III flow, since no expression is included for the 'yield' stress.

Doi [62], in 1981, proposed a molecular based theory for the hydrodynamics of concentrated solutions of rod-like macromolecules, extending the earlier framework proposed by Doi and Edwards [63]. This theory introduced an orientation order tensor, S_{ij}, and related the stress tensor, σ_{ij}, to it through a change in the free energy

density. The final expression is a constitutive expression of the form

$$\sigma_{ij} = [(ck_BT)/(2D_{ro})][-(\partial S_{ij}/\partial t) + G_{ij}] \qquad (1.6)$$

where σ_{ij} is the deviatoric part of the stress tensor, c is the number of macromolecules per unit volume, k_B is the Boltzman constant, T is the absolute temperature, D_{ro} is the rotary diffusion coefficient, $(\partial S_{ij}/\partial t)$ is the rate of change in the orientational order tensor with time, and G_{ij} is a tensor relating components of the velocity gradient tensor and the orientational order tensor. Doi's theory predicted the following:

1. the order parameter, S, increases discontinuously at concentrations greater than 0.889 ϕ^*, where ϕ^* is the volume fraction of nematic phase formed;

2. the rheo-optical extinction angle, χ, does not approach 45^o at zero shear rate in the nematic phase;

3. the ratio of shear viscosity to isotropic phase viscosity at $\eta = \eta^*$ versus the ratio of the volume fraction of isotropic and nematic phases forms a universal plot independent of molecular weight (η/η^* versus C/C^*);

4. a viscosity peak or maximum occurs in this universal plot at the critical volume fraction ratio, where $C = C^*$;

5. the shear viscosity in the isotropic phase, η, depends on the third power of the concentration, c^3, and sixth power of molecular weight, M^6; and

6. the primary normal stress difference, N_1, is a proportional function of shear rate, $\dot{\gamma}$, and not $\dot{\gamma}^2$, in the nematic phase. Wissbrun [243] noted that Doi's theory appeared to show reasonable agreement with available experimental data, however, the agreement was limited to region II or quasi-Newtonian flow behavior. The limitations were due to four assumptions [62,196,243]:

1. the orientational order vector (i.e. the director) does not vary with position,

2. the polymer is monodisperse (that is the M_w/M_n ratio is equal to one),

3. the flow is limited to relatively low shear rates, and

4. the flow occurs in the absence of magnetic and other external fields.

Marrucci [154] has extended Doi's theory to include the effects of external magnetic fields. This extension allowed the extraction of the Leslie [148] viscosity coefficients, α_1 through α_6. These coefficients, as formulated for polymer liquid crystals, are different in magnitude from those predicted in the Ericksen, Leslie, and Parodi (ELP) [185] theory for low molecular weight

nematic liquid crystals. Marrucci's final form of equation (1.6) is the expression [145]

$$\underline{\underline{\sigma}} = [(ck_BT)/(2D_{ro})][\ \alpha_4\ \underline{\underline{A}} + \alpha_5\ \underline{n}\ \underline{n}\cdot\underline{\underline{A}} + \alpha_1(\underline{\underline{A}}:\underline{n}\ \underline{n})\underline{n}\ \underline{n} + \alpha_2\ \underline{n}\ \underline{n}\cdot\underline{\underline{B}} + \alpha_3\ \underline{\underline{B}}\cdot\underline{n}\ \underline{n}\ ] \tag{1.7}$$

where $\underline{\underline{\sigma}}$ is the viscous part of the stress tensor; c, k_b, T, and D_{ro} are as defined in Doi's theory. In the common term $[(ck_BT)/(2D_{ro})]$, the Leslie coefficients, α_1 through α_6, are defined by equation (1.8).

$$\alpha_1 = -2S^2\ , \quad \alpha_2 = -S[1 + 3S/(2 + S)],$$
$$\alpha_3 = -S[1 - 3S/(2 + S)], \quad \alpha_4 = (2/3)[1 - S]$$
$$\alpha_5 = 2S, \quad \alpha_6 = 0 \tag{1.8}$$

The tensors $\underline{\underline{A}}$ and $\underline{\underline{B}}$ are the symmetric and asymmetric parts of the velocity gradient tensor $\underline{\underline{L}}$ and are defined by

$$\underline{\underline{A}} = 0.5(\underline{\underline{L}} + \underline{\underline{L}}^T) \quad \text{and} \quad \underline{\underline{B}} = 0.5(\underline{\underline{L}} - \underline{\underline{L}}^T) \tag{1.9}$$

where $\underline{\underline{L}}^T$ is the transpose of $\underline{\underline{L}}$.

Prilutski and Metzner [196,197] have expanded the Marrucci-Doi theory to cover high shear rates in steady shear flow and elongational flow. Predictions of this expanded theory included:

1. the primary and secondary normal stress differences are linearly dependent on shear rate at low shear

rates, but level off to a maximum value at high shear rates;

2. the ratio of elongational viscosity to shear viscosity (Trouton's ratio) is five at low shear rates, and

3. the fluid at high stretch rates is extension thinning. The expressions for steady shear viscosity, primary normal stress difference, elongational stress, and Trouton's ratio are given by equations (2.0) through (2.3):

$$\eta_s = [(ck_bT)/(6D_{ro})][(1-S)^2(1+2S)(1+1.5S)] /[(1+S/2)^2] \quad (2.0)$$

$$N_1 = [(ck_bT)/(6D_{ro})][(1-S)^{1.5}(1+2S)^{.5}(1+1.5S)] /[(1+S/2)^2] \quad (2.1)$$

$$\sigma_{xx} - \sigma_{yy} = 3ck_bT[S(1-C/3-CS/3-2CS^2/3)] \quad (2.2)$$

$$\eta_{ex}/\eta_s = 3[(1+S/2)^2]/[(1-S)(1+1.5S)] \quad (2.3)$$

where η_s is the shear viscosity, N_1 is the primary normal stress difference, $\sigma_{xx} - \sigma_{yy}$ is the elongational stress, η_{ex}/η_s is the Trouton viscosity ratio, C is the dimensionless concentration corresponding to U in Doi's theory [62], c is the concentration of molecules per unit volume, k_b, D_{ro}, and S are as defined earlier, and T is the absolute temperature.

Chaffey and Porter [49, 50] have attempted to theoretically explain the flow of solutions containing semidilute concentrations of rod-like macromolecules at high shear rates. Extensions to existing flow theories of Brenner [41] for dilute concencentrations and Doi-Edwards [63] for semidilute concentrations were used to identify and extract the most important dimensionless parameters of the solutions under conditions of shear flow. The parameters so identified were the relative viscosity, η_r; the shear rate, G; the primary normal stress difference, S; the axial ratio, p; and the volume fraction of macromolecules, v. A sixth parameter, U, was introduced to describe the flow orientation of the macromolecules, caused by a torque balance of hydrodynamic forces and molecular interaction forces. Predictions from the Porter-Chaffey extension were compared with experimental values obtained from the data of lyotropic polypeptide solutions studied by Kiss and Porter [130]. For dilute concentrations, theoretical and experimental values tended to agree in both region II, the quasi-Newtonian flow region, and region III, the shear thinning region. For semidilute concentrations, theory and experiment tended to correlate in region II but not region III. In region II at semidilute concentrations, the shear viscosity, η, was predicted to be proportional to the molecular volume and axial ratio product, v^3p^6, and the primary normal stress

difference, N_1, was predicted to be proportional to v^5p^{13}. The experimentally obtained shear viscosity matched the theoretically predicted value. However, the primary normal stress difference was observed experimentally to be proportional to v/p, not v^5p^{13}. In region III, the shear viscosity could not be fitted by integer exponents for v and p, but was experimentally observed to be $v^{1/3}p^{2/3}$. The trend of the primary normal stress difference with shear rate was predicted to be linear in region II and level off to some maximum in region III at low values of v. With inclusion of the parameter U at high values of v, the theory predicted N_1 to exhibit negative values at certain flow orientations. These predicted values, how-ever, severely underestimated the experimentally observed N_1 values.

A brief mention can be made of the more conventional flow theories applied in an attempt to describe the flow behavior of liquid crystalline polymers. An inherent limitation of these models is their prediction of an elongational viscosity to shear viscosity ratio (Trouton's ratio) of three. The experimental work of Prilutski [196] suggests that Trouton's ratio is much greater than three. In addition, these models suffer from the limitation of nonapplicability to region I, an inherent limitation of the Marrucci-Doi [154] theory.

Baird [22] has applied the five parameter, semi-empirical Bird-Carreau [32] model and a simplified version of the Hand [103] anisotropic fluid theory to experimental data from isotropic and nematic solutions of PPTA/SA. The forms of the Bird-Carreau [32] model used to predict steady shear viscosities and primary normal stress coefficients were

$$\eta = \sum_k [\eta_k /(1 + (\lambda^{(1)}_k \dot{\gamma})^2] \quad (2.4)$$

$$\Psi_1 = N_1/\dot{\gamma}^2 = 2\sum_k [\eta_k \lambda^{(2)}_k /(1 + (\lambda^{(1)}_k \dot{\gamma})^2] \quad (2.5)$$

where $\lambda^{(n)}_k = \lambda_n [\ 2 /(k+1)]^{\alpha}n$ for n = 1,2 and η is the shear viscosity; Ψ_1 is the primary normal stress coefficient: η_k, λ_k, and α_n are material parameters determined from the data, and $\dot{\gamma}$ is the shear rate. The Bird-Carreau model tended to fit the data well at high shear rate for nematic PPTA solutions. However, it did not fit the data well at low shear rates. The Hand [108] model was simplified to pseudo-anisotropic forms for the shear viscosity and primary normal stress coefficient

$$\eta = (m + n\dot{\gamma}^2)/(p + q\dot{\gamma}^2) \quad (2.6)$$

$$\Psi_1 = 1 /(p + q\dot{\gamma}^2) \quad (2.7)$$

where η, Ψ_1, and $\dot{\gamma}$ are as defined earlier and m, n, p, and q are material parameters derived from the data.

Berry and coworkers [79,233] have applied a simplified version of the integral BKZ [27] model to isotropic and nematic solutions of poly(1,4 phenylene-2,6 benzobisthiazole) (PBT) in methane sulfonic acid (MSA). Equations (2.8) and (2.9) show the forms of the model used

$$\eta = \sum \eta_i \, (1 - q_{K,i}) \tag{2.8}$$

$$\eta^2 \, N_1 = \sum \eta_i \, \tau_i \, (1 - q_{K,i} \, p_{K,i}) \tag{2.9}$$

where η is the shear viscosity, N_1 is the primary normal stress difference, $q_{K,i}$ and $p_{K,i}$ are strain rate related functions, η_i and τ_i are material parameters derived from the data. The model predicted well for the isotropic solutions and was partially applicable to region II and region III of the nematic solutions. Solutions exhibiting region I behavior could not be fitted, due to the presence of 'domains' or related 'textures'. Berry and coworkers suggested a parameter incorporating a critical strain rate function might allow the model to fit region I behavior.

Viscosity behavior of several polymer liquid crystals has been fitted with the empirical Herschel-Bulkley [109] model

$$\sigma_{12} = \sigma_y + K(\dot{\gamma})^n \tag{3.0}$$

where σ_{12} is the shear stress, σ_y is the 'yield' stress, K and n are power law type material constants, and $\dot{\gamma}$ is the

shear rate. This model is not a complete constitutive model, since it can only fit shear stress behavior.

Warren [237] was the first to use this model to successfully fit viscosity data of liquid crystalline nitrocellulose (NC) solutions in dimethylacetamide (DMA). Experimentally determined values of the 'yield' stress were in the 1.0 kPa to 19 kPa range. Values of the material constant, K, ranged from 2.5 kPa-s to 13.5 kPa-s and the exponent, n, averaged about 0.3.

Lewis and coworkers [224] reported the Herschel-Bulkley model fitted, with a precision of 0.98 or better, melt viscosity data from thermotropic polymers of POB/PET 60/40, HPC and EC. In the case of POB/PET 60/40, the values of 'yield' stress decreased exponentially from 20.6 kPa at 190^{o}C to 75 Pa at 340^{o}C; values of K ranged from 27.7 kPa-s to 29 Pa-s over the temperature range and n averaged about 0.6. For HPC, the 'yield' stress ranged from 6.4 kPa (160^{o}C) to 0.9 kPa (190^{o}C), K decreased from 1.9 kPa-s (160^{o}C) to 0.9 kPa-s (190^{o}C) and n averaged about 0.6. For EC, the 'yield' stress ranged from 5.9 kPa (180^{o}C) to 3.1 kPa (200^{o}C), K decreased from 48 kPa-s to 25 kPa-s over the same temperature range, and n decreased from 0.52 to 0.28.

In conclusion, the Marrucci-Doi [154] theory as expanded by Metzner and Prilutski [196,197] appears to adequately model region II and region III behavior of

polymer liquid crystals. However, in order for this theory to also predict region I behavior, a 'yield' stress tensor, or more aptly named 'domain flow' stress tensor, is needed in the constitutive expression. This 'domain flow' stress tensor represents the 'yield-like' response of the 'domains' before flow occurs. The means for including this tensor as part of the total stress expression is by analogy to the total stress expression in low molecular weight liquid crystal systems, given by [96]

$$\sigma_{ij} = -p\delta_{ij} + \sigma^{o}{}_{ij} + \sigma^{1}{}_{ij} \tag{3.1}$$

where σ_{ij} is the total stress, $p\delta_{ij}$ is the isotropic pressure term, $\sigma^{o}{}_{ij}$ is the stress term dependent on the elastic free energy, G_{el}, and $\sigma^{1}{}_{ij}$ is the viscous or deviatoric stress term. In low molecular weight nematics, $\sigma^{o}{}_{ij}$ and $\sigma^{1}{}_{ij}$ are given by equations (3.2) through (3.4)

$$\sigma^{o}{}_{ij} = -\rho\,(\partial G_{el}/\partial n_{k,i})n_{k,j} \tag{3.2}$$

$$\begin{aligned} \text{where } 2\rho G_{el} = {} & k_{22}\, n_{i,j}n_{i,j} + (k_{11} - k_{22} - k_{24})\, n_{i,i}n_{j,j} \\ & (k_{33} - k_{22})\, n_i n_j n_{k,i} n_{k,j} + k_{24}\, n_{i,j}n_{j,i} \end{aligned} \tag{3.3}$$

$$\begin{aligned} \sigma^{1}{}_{ij} = {} & \alpha_1\, n_k n_p A_{kp} n_i n_j + \alpha_2\, n_i N_j + \alpha_3\, n_j N_i \\ & + \alpha_4\, A_{ij} + \alpha_5\, n_i n_k A_{kj} + \alpha_6\, n_j n_k A_{ki} \end{aligned} \tag{3.4}$$

where $n_{()}$ are the unit vectors representing the director, k_{ii} are the Frank [87] elastic constants, α_i are the Leslie [148] viscosity coefficients, $A_{()()}$ is the strain

rate tensor, and $N_{()}$ are the vectors representing the velocity of the director with respect to the fluid [148].

The term σ^{o}_{ij} represents the Ericksen [96] stress in the case of low molecular weight nematics. This stress arises from the spatial variation in the director [62]. Doi [60] neglected this term in his flow theory, which assumed a uniform director (i.e. the director did not vary with position).

In polymer liquid crystals, the stress term σ^{o}_{ij} can be assumed to relate to the 'yield' stress, σ_{y}, or 'domain flow' stress tensor, σ_{df}. Intuitively, the 'domain flow' stress tensor should be some function of (a) the number of 'domains', (b) the size of the 'domains', and (c) the Frank [87] elastic constants. The number of 'domains' appear to be both concentration and molecular weight dependent [16,29,180,189]. 'Domain' size tends to decrease with increasing polymer molecular weight [189]. The number of 'domains' tend to increase with increasing polymer concentration [16,180]. Wissbrun [243] notes the magnitude of the Frank [87] elastic constants accounts for the 'yield' stresses of small volumes (15×10^{-3} cm^{2}), but not the whole sample volume. Morphological investigations of liquid crystalline HPC and EC solutions by Nishio and coworkers [173,174] support the contention the stress needed to deform an individual 'domain' is very small. In fact, the stresses imposed by the proximity of a boundary

surface is sufficient to deform all 'domains' into a fibrillar 'texture' [173,174]. Only in the interior of the sample volume were undeformed 'domains' observed [173,174]. These observations would suggest the Frank [87] constants can represent the moduli of individual 'domains' and the Ericksen [96] stress can represent the localized stress on a 'domain' in a polymer liquid crystal. These assumptions, if valid, would suggest a 'domain flow' stress tensor represented by the form

$$\sigma^{o}_{ij} = Z\,[\rho\,(\partial G_{el}/\partial n_{k,i})n_{k,j}] \qquad (3.5)$$

where σ^{o}_{ij} is now the 'domain flow' stress tensor and Z is a function defined by

$$Z = f(N_D,\ D_D,\ N_{MD},\ p) \qquad (3.6)$$

where N_D is the number of 'domains' in the sample volume, D_D is the size of an individual 'domain', N_{MD} is the number of macromolecules per 'domain', and p is the axial ratio of the macromolecules. At Z = 1, the 'domain flow' stress would become equivalent to the Ericksen [96] stress.

D. Rheological And Rheo-Optical Behavior

Phase Transition Effects On Viscosity

The unusual flow behavior of polymer liquid crystals was first observed in the viscosity versus concentration

behavior of lyotropic polymer solutions. In these solutions, viscosity is not a monotonic function of concentration. Viscosity intially increases with concentration, approaches a maximum value, then decreases to some minimum value at some intermediate concentration. At higher concentrations the viscosity tends to make an upturn in value. The viscosity maximum is similar to that observed in phase inversion of two phase rubber in styrene solutions during polymerization [26]. In contrast, single phase polymer solutions exhibit a continuous, monotonic increase in viscosity with concentration. Viscosity versus concentration effects have been observed in these classes of lyotropic polymers: synthetic polypeptides [107,130,202], aromatic polyamides [13,15,142,168,184], cellulosic polymers [29,226], polyheterocyclics [28], and polyisocynates [7].

Robinson [202] observed that an isotropic PBLG solution in dioxane exhibited a much higher apparent viscosity than a more concentrated, fully liquid crystalline solution. Hermans [107] observed similar phenomena in PBLG/m-cresol solutions. Hermans represented his observations in the form of fixed shear stress, viscosity versus concentration plots. These plots exhibited viscosity maxima at low shear stresses for high molecular weight PBLG samples. Above a critical shear stress, viscosity increased monotonically with concentration and exhibited no viscosity

maxima. Kiss and Porter [184] reported observations, similar to those of Hermans, for solutions of PBLG in m-cresol and PCBL in m-cresol. Shear rates above 1000 s^{-1} were observed to suppress or completely eliminate the viscosity versus concentration maxima in the solutions.

Papkov et al. [184] observed viscosity versus concentration phenomena in solutions of PBA in dimethylacetamide (DMA) and lithium chloride. The behavior was very similar to that reported for the polypeptide solutions [107,130]. Papkov and coworkers attributed the viscosity maximum to the formation of the liquid crystalline phase in the solution upon reaching the critical concentration, C*. They observed that a plot of the viscosity ratio, η_o/η, versus the concentration ratio, C/C*, exhibited at viscosity maximum corresponding to C = C*, independent of molecular weight. This was an experimental verification of Doi's [62] theory.

Bheda [29] correlated polarized optical microscopy observations with viscosity versus concentration behavior in several lyotropic cellulosic polymer solutions and concluded the viscosity maximum corresponded to the critical concentration, C_A, marking the onset of the biphasic region. This biphasic region consisted of a discontinuous anisotropic or liquid crystalline phase in a continuous isotropic phase. In this context C_A is eqivalent to C*.

Aharoni [7] also correlated polarized optical microscopy observations with viscosity versus concentration behavior in solutions of polyisocynates. In a 50/50 poly(n-hexylisocynate-co-n-propylisocynate) in toluene solution, a shoulder of the viscosity concentration peak coincided with C* or C_A and not the viscosity maximum. The viscosity maximum corresponded to the onset of a phase inversion of isotropic and anisotropic phases. This second biphasic region consisted of a discontinuous isotropic phase in a continuous anisotropic phase.

Plots of other rheological properties with respect to concentration also exhibit maxima and minima associated with phase transitions. Aoki and coworkers [13,15] and Baird [22] all reported that plots of the primary normal stress coefficient, Ψ_1, versus concentration, in PPTA/SA solutions, exhibited maxima and minima. Bheda [29] reported similar behavior in the related primary normal stress difference, N_1, versus concentration behavior of HPC/AA solutions. Suto [226] reported the presence of maxima and minima in 'yield' stress versus concentration plots of EC/chloroform solutions.

In several thermotropic copolyesters, analogous behavior exists with viscosity versus mesogen content plots at constant temperature and shear rate. Jackson and Kuhfuss [120] observed viscosity maxima in POB/PET copolyesters corresponding to 30 mol% POB groups and viscosity

minima corresponding to 60 mol% POB groups. Prasadarao and coworkers [194] report similar plots for terpolyesters prepared from p-actoxybenzoic acid (PAB), hydroquinone diacetate (HQ), tetramethylterephthalic acid (TMT), and poly(ethylene terephthalate) (PET). These plots exhibited viscosity maxima corresponding to 40 mol% (PAB/HQ/TMT) groups and viscosity minima correponding to 58 mol% (PAB/HQ/TMT) groups.

Region I Flow Behavior

Region I of the Onogi-Asada [18] flow-structure model is characterized by flow behavior embodying pronounced shear thinning and concomitant 'yield' or 'domain flow' stresses. This behavior primarily occurs at relatively low shear rates. Physically region I flow behavior can be interpreted as viscoplastic flow of a microstructure consisting of 'domains' or 'textures'. Each 'domain' or 'texture' consists of polymer chains organized into aggregates or associations possessing local order. Region I behavior has been observed in both lyotropic and thermotropic polymers.

Papkov and coworkers [184], in 1974, were the first to report flow behavior in lyotropic polymers possessing region I characteristics. Viscosity data for anisotropic solutions of 5 wt% to 7 wt% PBA in dimethylacetamide-4% LiCl were obtained from a concentric cylinder rheometer.

At shear rates less than 1 s^{-1}, 'yield' stresses on the order of 0.5 Pa were observed.

Aoki and coworkers [13,15] obtained steady shear and dynamic viscoelastic data for anisotropic 10 wt% and 12 wt% PPTA/SA solutions at 25°C in a cone and plate rheometer. Steady shear viscosity data corresponding to region I were observed over a shear rate range of 0.01 s^{-1} to 10 s^{-1}. The viscosities on average showed a 0.5 decade drop in magnitude per decade increase in shear rate. Observed 'yield' stresses were on the order of 70 Pa. Primary normal stress coefficients, Ψ_1, were on the order of 6 kPa-s^2, but decreased rapidly over the 0.01 s^{-1} to 10 s^{-1} shear rate range. Correspondingly, the primary normal stress differences, N_1, increased toward a maximum plateau on the order of 8 kPa for 10 wt% and 3 kPa for 12 wt% solutions. At frequencies correponding to the steady shear rates, the dynamic viscosities, η', were about 0.2 decade in magnitude lower than the steady shear viscosities. Plots of the storage modulus, G', versus frequency exhibited a tendency to form a frequency independent plateau at low frequencies; at higher frequencies, G' increased linearly with frequency. The ratio of loss shear modulus to storage modulus, G"/G' or tan δ, indicated the solutions exhibited an elastic solid-like response characteristic of a gel-like structure.

Kiss, Orrel and Porter [128] reported both rheological and rheo-optical studies of a gel-like 33.2 wt% PBAB/m-cresol solution. Rheological measurements were made in a cone and plate rheometer; rheo-optical measurements were made in a transparent parallel plate device. Shear viscosities exhibited pronounced shear thinning with coexistant 'yielding' behavior. Positive primary normal stress differences, N_1, in the range of 0.5 Pa to 3.0 Pa were observed. These tended to show a quasi-linear increase with shear rate. Both shear viscosities and primary normal stress differences exhibited significant hysteresis with respect to ascending and descending shear rates. The dynamic storage modulus, G', and dynamic viscosity, η', showed significant sensitivity to strain amplitude. This indicates the presence of a gel type structure. Rheo-optical observations indicated the existence of supramolecular aggregates or 'domains'. These 'domains' were approximately 100 microns in size and showed resistance to shear elongation at shear stresses below 200 Pa.

Asada and coworkers [16,17] have reported rheological and rheo-optical measurements for two lyotropic polymers possessing region I behavior: (a) a racemic, nematic 40 wt% PBG/m-cresol solution and (b) a cholesteric, 61 wt% HPC/W solution. Simultaneous measurements of steady shear viscosity and rheo-optical intensity data were made in a

specially equipped, transparent quartz, cone and plate rheometer. In the case of the PBG/m-cresol solution, component intensities of flow birefringence, $I_{//}$ and I_X, and optical rotation, I_E, were measured over a 0.01 s^{-1} to 100 s^{-1} shear rate range. Small wavy changes in amplitude for $I_{//}$ and I_X and a decrease in magnitude for I_E, due to dynamic light scattering, occurred above a low shear rate, $\dot{\gamma}$ = 0.07 s^{-1}. These effects were attributed to the shear-induced deformation and coalescence of an intial 'multi-domain' structure. The 61 wt% HPC/W solution exhibited region I viscosity behavior as well, but in a shear rate range of 0.02 s^{-1} to 0.6 s^{-1}. In this shear rate range the spectrum did not recover completely to its original values at cessation of shear. This behavior was interpreted as a partial shear-induced disorientation of the cholesteric structure due to a 'yielding' type flow.

Onogi, White and Fellers [180] reported rheo-optical studies of anisotropic 55 wt% HPC/W solutions and 10 wt% PPTA/SA solutions. These solutions were sheared between parallel glass slides separated by spacers; shear rates in the range of 0.1 s^{-1} to 10 s^{-1} were obtained. Both anisotropic solutions contained birefringent microstructures or 'domains'. Each 'domain' consisted of tangentially arranged rod-like macromolecules. The HPC/W solution exhibited a birefringence overshoot below a shear rate of 2.4 s^{-1}. Steady state birefringence at a lower shear

rate, 0.1 s^{-1}, required more than three minutes of shearing. Similar behavior occurred in the PPTA solution. Below a shear rate of 0.2 s^{-1} attainment of steady state birefringence took seven minutes. Many distinct small 'domains' could be observed in the flow field at shear rates of 0.1 s^{-1} or below. Below a critical shear rate both solutions showed flow behavior which can be interpreted as region I.

Suto [227] reported viscosity and 'yield' stress data for anisotropic 35 wt% to 45 wt% EC/chloroform solutions, via a concentric cylinder viscometer. Pseudoplastic or shear thinning behavior and concomitant 'yield' stresses were observed at shear rates below 0.5 s^{-1}. Hysteresis in the viscosity curves was observed for increasing and decreasing shear rates. 'Yield' stresses ranged from 1.5 Pa to 9.5 Pa in magnitude over the concentration range at 25^{o}C. At 35 wt% the 'yield' stress exhibited an increase in value with temperature from 1.5 Pa to 4.5 Pa. A similar anomalous increase was observed with the viscosity. This behavior apparently indicated a temperature related phase transition effect.

Warren [237] reported shear and 'yield' stress measurements on 47.5 wt% to 60 wt% nitrocellulose (NC) /N,N'dimethylacetamide (DMA) solutions. Measurements were made with a specially designed slit die in a capillary rheometer. 'Yield' stresses ranged from 1 kPa to 19 kPa

over the concentration range. The relationship between extrusion pressure, the time to reach steady state, and the presence of pressure overshoots indicated thixotropic behavior in the NC/DMA solutions.

Horio and coworkers [110] reported dynamic viscoelastic and steady state viscosity measurements on a 60 wt% HPC/W solution via a cone and plate rheometer. Viscosity behavior corresponding to region I was apparent at shear rates below 1.0 s^{-1}. At frequencies corresponding to the 0.1 s^{-1} to 1.0 s^{-1} (region I) shear range, the dynamic storage modulus, G', and the dynamic loss modulus, G", tended to form frequency independent plateaus. This behavior was in constrast to isotropic HPC solutions for which G' and G" declined sharply. The dynamic viscosity, η', exhibited frequency dependence below 1.0 rad s^{-1} and was on average 0.2 decade lower in magnitude than the corresponding shear viscosity. The steady state viscosity exhibited strong shear thinning behavior on the order of 0.5 decade decrease in value per decade increase in shear rate.

Berry and coworkers [79] reported creep viscosity and shear stress measurements on nematic PBT/MSA solutions via a cone and plate rheometer. Solutions containing 60 g kg^{-1} to 80 g kg^{-1} of PBT exhibited strong shear thinning viscosity behavior below 0.005 s^{-1}. Behavior of the stress growth function, $\sigma J_{\sigma}(t)$, at small strain rates did

not indicate the presence of 'yield' stresses. The behavior was attributed to the flow induced depopulation of 'domains', or locally ordered 'textures'. These 'domains' contained rod-like macromolecules which were oriented perpendicularly to the flow direction just prior to the initiation of flow.

Prud'homme and coworkers [151] measured the transient shear stress behavior of anisotropic xanthan gum (XG)/water (W) solutions in a cone and plate rheometer. Flow birefringence observations were made in a transparent parallel plate device. Transient overshoots, undershoots, and hysteresis effects were all cited as evidence of microstructure in the solutions. Observations of flow birefringence indicated that persistant birefringent regions were formed from the presence of 'domains'; these regions persisted after the cessation of shear. Earlier viscosity measurements of XG/W solutions by Whitcomb and Macosko [239] and Sanderson [212] indicated that solutions with 1.0 wt% XG or greater exhibited strong shear thinning behavior reminiscent of region I flow at shear rates below 1000 s^{-1}.

Jackson and Kuhfuss [120] reported the earliest rheological studies indicating region I flow behavior in thermotropic copolyesters. Shear melt viscosities were measured on different compositions of POB/PET copolyesters in a capillary rheometer. Viscosity data of a liquid

crystalline POB/PET 60/40 copolyester at 275°C indicated that region I, or possibly region III, shear thinning behavior occurred at shear rates below 10^4 s^{-1}.

Wissbrun [242] reported more extensive rheological measurements of POB/PET 60/40. Steady state viscosity data were obtained from a cone and plate rheometer at low shear rates and a capillary rheometer at high shear rates. Dynamic viscoelastic measurements were made on a rheometer using cone and plate or parallel plate geometry in an oscillatory mode. Flow behavior characteristic of region I was observed in the 0.1 s^{-1} to 1000 s^{-1} shear rate range at temperatures ranging from 170°C to 280°C. Steady shear viscosities exhibited on average a 0.5 decade decrease in magnitude per decade increase in shear rate. At 170°C the complex viscosity, η^*, was one to two decades higher in magnitude than the corresponding shear viscosity. At 210°C the magnitude difference was about one decade. At higher temperatures no apparent differences were observed in η and η^*. The primary normal stress difference, N_1, could not be determined at temperatures below 210°C, due to large 'yield' stresses in the material. No apparent die swell was observed at these same temperatures. At temperatures in the 240°C to 280°C range, N_1 increased linearly with shear rate and ranged from 100 Pa to 500 Pa in magnitude over a decade in shear rate. At temperatures below 240°C the dynamic storage modulus, G', tended to

form a frequency independent plateau at low frequencies. At 280°C the dynamic storage modulus exhibited a linear relationship with frequency at low frequencies.

Jerman and Baird [124] measured the shear viscosity and die swell behavior of both POB/PET 60/40 and POB/PET 80/20 in a capillary rheometer. Both copolyester compositions exhibited a drop of 0.5 decade in value in the viscosity per decade increase in shear rate over the range studied. Significant extrudate contraction was observed at temperatures below 260°C in POB/PET 60/40 and 285°C in POB/PET 80/20. Examination of the entrance pressure loss data for both copolyesters indicated the melts showed significant elastic behavior, but the elastic energy was mostly used in orienting the molecules in the flow direction. This manifested itself as minimal elastic recovery and neglible die swell behavior.

Recently, Gottis and Baird [94] reported extensive measurements of the steady shear viscosities and primary normal stress differences for thermotropic melts of POB/PET 60/40 and POB/PET 80/20. These measurements were obtained from both cone and plate and parallel plate rheometers. The 60/40 copolyester was examined in the 250°C to 285°C temperature range; the 80/20 material was examined in the 310°C to 340°C temperature range. The viscosity data for both copolyesters exhibited pronounced shear thinning behavior at shear rates below 100 s^{-1}. The

average drop in viscosity for both copolyesters was about 0.5 decade per shear rate decade. The viscosities declined slightly with respect to increasing temperature and tended to 'group together' or overlap. Stress growth experiments indicated that some change occurred in the initial structure. Stress relaxation experiments did not, however, indicate the presence of 'yield' stresses. For the POB/PET 60/40 material, the primary normal stress differences increased linearly with shear rate. This was in accord with Doi's [62] prediction that N_1 is proportional to the first power of the shear rate. The 80/20 copolyester, however, was observed to have apparent negative N_1 values at shear rates below 10 s^{-1}. The values varied in the -1 kPa to -100 Pa range and tended toward positive values with respect to increasing shear rate and gap distance. Above 10 s^{-1} the values of N_1 were positive and increased linearly with shear rate.

Bickel and coworkers [31] reported steady shear rheological measurements of an apparent POB/PET 50/50 copolyester. Shear stress data and primary normal stress difference data were obtained from a cone and plate rheometer. Viscosity behavior characteristic of region I was observed with shear rate at 243°C. The shear stresses increased in a quasi-linear fashion with shear rate. The slope of the plot, however, was less than one. This indicated shear thinning or psuedoplastic behavior. The

measured primary normal stress differences were about 1/3 the shear stresses in magnitude. The primary normal stress differences exhibited a linear increase with shear rate.

Prasadarao, Pearce and Han [194] reported steady state viscosities and primary normal stress differences, N_1, on copolyesters synthesized from p-acetoxybenzoic acid (PAB), hydroquinone diacetate (HQ), tetramethylterephthalic acid (TMT), and poly(ethylene terephthalate) (PET). Measurements were made on a cone and plate rheometer at 260°C. Compositions containing 46 mol% of the mesogen (PAB/HQ/TMT) or more were liquid crystalline. Plots of shear viscosity versus shear rate exhibited pronounced shear thinning at shear rates below 100 s^{-1}. The average decrease in viscosity averaged about 0.7 decade in value per decade increase in shear rate. Plots of shear viscosity versus shear stress indicated the presence of 'yield' stresses; these ranged from 7 Pa to 5 kPa in magnitude depending on mesogen content. Negative N_1 values were observed in the compositions containing from 46 mol% to 67 mol% mesogen; these ranged from -100 Pa to -800 Pa and did not show any apparent trend with shear rate. Positive N_1 values were observed for the composition containing 75 mol% mesogen; the N_1 data exhibited a gradual increase with shear rate.

Simoff and Porter [218] reported steady state viscosities and die swell measurements on a nematic copolyester synthesized from 50 mol% 1,2 bis(4-hydroxyphenyl) ethane (BPE), 40 mol% isophthalic acid (IP), and 10 mol% 2,6 naphthalene dicarboxylic acid (ND). Measurements were made in a capillary rheometer in the 285°C to 340°C temperature range. The copolyester exhibited pronounced shear thinning, averaging 0.4 decade in value decrease per shear rate decade increase, in the 1 s^{-1} to 1000 s^{-1} shear rate range. Significant extrudate contraction was observed in the copolyester below 330°C.

Suto, White and Fellers [227] have reported steady state viscosity and dynamic viscoelastic measurements on thermotropic HPC and EC melts. Measurements were made on a cone and plate rheometer in the case of steady state measurements and on an eccentric rotating disk rheometer in the case of dynamic measurements. Steady shear viscosity data exhibited a 0.5 decade decrease in value per decade increase in shear rate for HPC melts in the 160°C to 190°C temperature range; this phenomena in HPC was also reported earlier by Shimamura et al. [216]. Similar behavior was observed in EC melts in the 180°C to 200°C temperature range. Measurements of the primary normal stress differences were complicated by the presence of 'yield' stresses. After baseline corrections for 'yielding' behavior, HPC melts exhibited N_1 values in the

1 kPa to 10 kPa range. The dynamic complex viscosity, η^*, was slightly larger than corresponding shear viscosities in HPC and EC. At temperatures below 200°C, both HPC and EC melts exhibited G' behavior that was independent of frequency at low frequencies.

In summary, several features appear to stand out as general characteristics of region I flow behavior. These can be enumerated as follows:

1. the viscosity exhibits pronounced shear thinning on the order of 0.5 decade in magnitude per decade increase in shear rate,

2. 'yield' or 'domain flow' stresses are present, although the magnitude may vary from small to large depending on temperature or concentration,

3. the dynamic complex viscosity is generally larger than the corresponding shear viscosity,

4. the dynamic storage modulus, G', tends toward a frequency independent plateau at low frequencies,

5. the primary normal stress differences and die swell may be significantly masked or depressed by the effects of 'polydomain' flow, and

6. the primary normal stress differences may be much less than the corresponding shear stresses.

Region II Flow Behavior

Region II of the Onogi-Asada [18] phenomenological model is characterized by shear independent or quasi-

Newtonian viscosity behavior. This behavior occurs at relatively intermediate shear rates. Physically region II flow behavior is interpreted as mostly 'monodomain' flow with minimal localized orientation or 'domains' still extant. Region II flow behavior has been mostly observed in lyotropic polymers.

In lyotropic polymers, region II flow behavior was first observed in synthetic polypeptide solutions at relatively low to moderate shear rates. Hermans [107] found quasi-Newtonian viscosity behavior in anisotropic PBLG/m-cresol solutions during capillary viscosity measurements.

Iizuka [115] reported the first extensive rheological measurements on nematic and cholesteric solutions of PBLG, poly(γ-ethyl-L-glutamate) (PELG), and a racemic poly(γ-ethyl glutamate) (PEG) in dioxane or methyl bromide. Solutions containing at least 13 wt% PBLG, PELG or PEG were fully liquid crystalline. Steady shear viscosities and dynamic viscoelastic properties were measured in a cone and plate rheometer over a steady shear range of 0.2 s^{-1} to 200 s^{-1} and over a frequency range of 0.2 hz to 2 hz, respectively. Quasi-Newtonian viscosity behavior was observed in the 0.2 s^{-1} to 80 s^{-1} shear range for 13 wt% PELG/dioxane and 13 wt% PBLG/dioxane solutions; shear thinning occurred above this range. The onset of shear thinning behavior showed an apparent shift to lower shear

rates with increases in concentration or change in solvent. The dynamic storage modulus, G', was observed to increase linearly in the frequency range corresponding to region II steady shear rates. Above this range G' tended to a high frequency plateau. The dynamic loss modulus, G", showed apparent frequency independence in the region II shear rate range. At higher frequencies G" decreased with frequency.

Kiss and Porter [129,130] have reported extensive rheological measurements of anisotropic, racemic PBG, PBLG, and PCBL solutions with m-cresol. Solutions containing more than 14 wt% PBG were completely nematic, whereas, solutions containing at least 14 wt% PBLG or 27 wt% PCBL were completely cholesteric. Rheological measurements were made on a cone and plate rheometer using two different cone angles and three different cone and plate diameters. Steady shear measurements were made in the 0.01 s^{-1} to 100 s^{-1} range. Dynamic oscillatory measurements were conducted in the 0.1 rad s^{-1} to 400 rad s^{-1} frequency range. PBG/m-cresol solutions exhibited apparent quasi-Newtonian behavior below 0.1 s^{-1}; the primary normal stress differences (N_1) were too small to measured below 0.1 s^{-1}. PBLG/m-cresol solutions exhibited quasi-Newtonian behavior below shear rates of 80 s^{-1}; N_1 increased to a maximum value in the vicinity of this shear rate before decreasing in magnitude. PCBL/m-cresol

solutions at concentrations between 27 wt% and 33 wt% exhibited quasi-Newtonian behavior below 20 s^{-1}. Above 33 wt% PCBL the viscosity versus shear rate plot exhibited two quasi-Newtonian plateaus, with the first below 0.2 s^{-1} and the second between 0.4 s^{-1} and 10 s^{-1}. Plots of N_1 versus shear rate for PCBL solutions exhibited quasi-linear increases with shear rate; these occurred at shear rates corresponding to the first plateau region. The dynamic viscosity showed frequency independence below 0.5 rad s^{-1} for PBG solutions. For PBLG solutions this plateau behavior occurred at frequencies below 100 rad s^{-1}. PCBL solutions exhibited complex dynamic viscosity behavior; three distinct frequency independent plateaus could be observed. The dynamic storage modulus, G', increased linearly with frequency for PBG solutions. Values of G' were not reported for PBLG solutions. In PCBL solutions, the G' versus frequency behavior was complex and exhibited slope changes at frequencies corresponding to the dynamic viscosity plateaus.

Asada and coworkers [16] reported rheo-optical measurements for racemic, nematic 20 wt% and 30 wt% PBG/m-cresol solutions. Measurements of the component flow birefringence intensities, $I_{//}$ and I_X, and optical rotation intensity, I_E, were made in a specially equipped, transparent cone and plate rheometer. Both PBG solutions exhibited quasi-Newtonian viscosity behavior in the 0.01

s^{-1} to 100 s^{-1} shear rate range studied. $I_{//}$ and I_X became periodic in form at a critical shear shear rate; I_E decreased in magnitude at this shear rate. The onset of periodicity occurred at 0.08 s^{-1} for the 20 wt% solution and at 1.0 s^{-1} for the 30 wt% solution. The critical shear rate increased about one decade for a fourfold increase in sample thickness. $I_{//}$ and I_X increased in amplitude with increasing shear rate. At constant shear rate, $I_{//}$ and I_X decreased in amplitude with increasing sample thickness. I_E decreased to an asymptotically low value with shear rate. This asymptote increased with increasing sample thickness. The behavior in $I_{//}$, I_X, and I_E were interpreted as the shear-induced formation of a continuous 'monodomain texture', with its molecules aligned mainly in the flow direction.

Kiss and Porter [131] reported rheo-optical observations of PBLG/m-cresol solutions between rotating transparent disks. The presence of bands or striations parallel to the shear direction were observed at shear rates corresponding to the end of the quasi-Newtonian flow region.

Aoki, White and Fellers [14] reported rheological measurements on anisotropic PBLG/m-cresol solutions and PPTA/SA acid solutions. Measurements were made in a cone and plate rheometer in the 0.01 s^{-1} to 1000 s^{-1} shear rate range. Solutions containing at least 14 wt% PBLG were

completely cholesteric; those containing 10 wt% or more PPTA were completely nematic. PBLG solutions showed quasi-Newtonian viscosity behavior at shear rates below 200 s^{-1}. The PPTA solutions exhibited quasi-Newtonian behavior below 1 s^{-1} at 60°C. At 25°C PPTA solutions exhibited region I type flow behavior. The primary normal stress coefficients (Ψ_1) for both PBLG and PPTA exhibited a rapid quasi-linear decrease with shear rate. Dynamic viscosity and storage modulus, G', were reported only for the PPTA solutions. The dynamic viscosity exhibited frequency independence below 1 rad s^{-1} for the 10 wt% PPTA solutions at 60°C. This frequency range was comparable to the quasi-Newtonian shear rate range for steady shear measurements. In contrast, the 12 wt% solution exhibited frequency independence at 0.1 rad s^{-1}, a decade lower than the corresponding steady shear rate. The dynamic storage modulus, G', increased linearly with shear frequency.

Baird [22] also reported rheological measurements on anisotropic PPTA/SA solutions, ranging from 10 wt% to 15 wt% in concentration. Steady shear measurements and dynamic measurements were conducted in a cone and plate rheometer at 60°C. Steady shear viscosities and primary normal stress coefficients were measured over a 0.1 s^{-1} to 100 s^{-1} shear rate range. Dynamic viscosities were measured over a 0.1 rad s^{-1} to 100 rad s^{-1} frequency range. The viscosity versus shear rate behavior for the 10 wt%

PPTA solution indicated quasi-Newtonian behavior below 0.1 s^{-1}; this was in contrast to that reported by Aoki, White and Fellers [14]. The 12 wt% and 15 wt% PPTA solutions showed apparent quasi-Newtonian behavior below 1.0 s^{-1}; the 12 wt% data agreed with that reported by Aoki, White and Fellers [14]. Plots of dynamic viscosity versus frequency indicated a frequency independent plateau below 0.1 rad s^{-1} for all three concentrations. The results for the 12 wt% solution were in agreement with Aoki and coworkers [14], however the results for the 10 wt% solution did not agree. Plots of the primary normal stress coefficient exhibited a rapid decrease with shear rate for all three concentrations.

Berry and coworkers [79] reported steady shear viscosity measurements on nematic PBT/MSA solutions. Measurements were made in a cone and plate type rheometer. PBT solutions exhibited quasi-Newtonian viscosity behavior in the 0.1 s^{-1} to 1.0 s^{-1} shear rate range.

Asada and coworkers reported rheo-optical spectral measurements of a cholesteric, 61 wt% HPC/W solution. Measurements of the spectral shift were made with a transparent quartz cone and plate rheometer, equipped with a spectrophotometer. The HPC/W solution exhibited a quasi-Newtonian viscosity plateau in the 0.6 s^{-1} to 6.0 s^{-1} shear rate range. In the 0.6 s^{-1} to 1.1 s^{-1} shear rate range, the absorbance spectrum became very broad and the

spectrum center shifted to shorter wavelengths. At shear rates greater than 1.2 s^{-1} the spectrum center disappeared. The spectrum shape recovered rapidly after shear cessation. Sharpness of the spectrum increased with time; optical observations indicated the formation of a Grandjean type 'texture'. Above a shear rate of 1.2 s^{-1}, the response of the spectrum was interpreted as a shear-induced conversion of the cholesteric helical structure into a nematic 'monodomain' structure. Microscopic observations of the boundary layers on the surfaces of the cone and plate indicated the cholesteric structure remained in these layers even at high shear. After cessation of shear, the cholesteric structure reformed by growing from the boundary layer into the interior of the sample. The twist axis of the cholesteric helical structure was observed to be normal to the cone and plate surfaces.

Onogi, White and Fellers [180] also reported rheo-optical measurements on HPC/W solutions. Flow birefringence was measured on a cholesteric 55 wt% HPC solution sheared between glass slides. At shear rates less than 1.2 s^{-1} birefringence overshoots were observed. At shear rates higher than 1.2 s^{-1} no birefringence overshoot could be observed. The irridescent color in the solution could still be observed at shear rates below 4.7 s^{-1}. The decay of the birefringence after shear was slow, taking on the order of 30 minutes to drop to an asymptotic value. The

behavior of the flow birefringence was interpreted as resulting from the formation of a shear-induced, oriented nematic structure from an initial cholesteric structure. The relaxation of the nematic structure back to a cholesteric type structure was concluded to occur rather slowly.

Prilutski [196] reported steady shear, oscillatory shear and elongational flow measurements for a liquid crystalline 40 wt% (HPC/AA) solution. Steady shear viscosities and first normal stress differences (N_1) were obtained with a cone and plate rheometer over a 0.01 s^{-1} to 100 s^{-1} shear rate range. Oscillatory or dynamic measurements of the complex viscosity and the shear storage modulus, G', were obtained by cone and plate rheometry in the 0.1 rad s^{-1} to 100 rad s^{-1} frequency range. Elongational flow measurements were conducted with a fiber spinning type apparatus under (a) gravity flow or (b) mechanical stretching flow. Extension or elongation rates ranged from 0.01 s^{-1} to 10 s^{-1}. The steady shear and complex viscosities were observed to coincide and be moderately shear thinning. The shear stress versus shear rate plots were quasi-linear and had slopes around 0.8. The observed first normal stress differences were about twice as large as the corresponding shear stresses. The N_1 data exhibited appreciable scatter, unlike the shear stress data, but tended to be linear with shear rate. The slope of the linear plot was one, which coincides with

Doi's [62] prediction. The elongational or axial stress was observed to also be a linear function of shear rate. The Trouton ratio, or the ratio of elongational viscosity to shear viscosity, was observed to have a value of nine. Doi's [62] theory predicted a value of five for all polymer liquid crystals.

Horio and coworkers [110] recently reported dynamic and steady shear measurements on a 60 wt% HPC/W solution. Their results from cone and plate measurements suggested the viscosity exhibited very little quasi-Newtonian or shear rate independent behavior. The plateau was little more than an inflection point on the viscosity versus shear rate curve at about 4 s^{-1}. The dynamic viscosity exhibited an inflection point at 4 rad s^{-1}. In this shear frequency region, the dynamic storage modulus (G') and loss modulus (G") both exhibited a linear increase with frequency. The shear viscosity behavior reported by Horio and coworkers disagreed with that reported earlier by Asada et al. [17]. The discrepancy may be related to the lower molecular weight sample of HPC used in Asada et al.'s study.

Rheological studies of thermotropic polymers reporting the presence of quasi-Newtonian viscosity behavior have been limited in number. Capillary rheometry data reported by Jackson and Kuhfuss [120] for a POB/PET 60/40 material indicated a quasi-Newtonian viscosity plateau

existed above a shear rate of 10,000 s^{-1} at 275°C. The capillary rheometry data of Wissbrun [242] for the same material at 300°C suggested quasi-Newtonian behavior below 10 s^{-1}. These observations would suggest the range of region II depends strongly on temperature.

Rheological data reported by Bickel and coworkers [31] suggested apparent quasi-Newtonian behavior at 259°C in an apparent POB/PET 50/50 copolyester. Although Bickel et al. attributed the temperature region above 250°C to be isotropic, the transmitted intensity (between crossed polars) versus temperature plot indicated the isotropic transition did not occur until about 280°C. At 259°C the transmitted intensity was substantially higher than even at the solid-liquid crystal transition point at 230°C. The shear stress versus shear rate plot at 259°C indicated quasi-Newtonian flow behavior; the primary normal stress difference increased linearly with shear rate. This behavior is qualitatively in accord with the predictions of Doi [62] for region II flow behavior. The apparent shear-induced optical 'texture' change at 40.4 s^{-1} (change from clear to milky) could be interpreted as the formation of flow instabilities or 'disclination' line formations in a previously uniform nematic state.

To summarize, several general features can be extracted from the literature on region II flow behavior. These can be enumerated as follows:

1. the viscosity is shear rate independent at moderate shear rates,

2. the primary normal stress difference linearly increases with shear rate below the transition to region III,

3. the dynamic storage modulus exhibits a linear increase with frequency, and

4. rheo-optical observations indicate the formation of a shear-induced, aligned nematic state with a uniform director.

Region III Flow Behavior

Region III of the Onogi-Asada [18] flow structure framework is characterized by shear thinning flow, without 'yield' stresses at high shear rates. Structurally, this response has been interpreted as arising from a fully aligned 'monodomain' with its director aligned in the flow direction. However, the limited number of rheological studies of region III flow behavior suggest this uniform alignment is not stable above a critical shear rate; this was noted by Wissbrun [242]. Above this critical shear rate 'disclinations' or striations appear to occur in the 'monodomain texture' [131].

Rheological studies reporting the presence of region III flow behavior in lyotropic systems are limited to four classes of polymers: synthetic polypeptides, aromatic polyamides, cellulosic derivatives and polyheterocyclics.

Hermans [107] first reported shear thinning or region III behavior in synthetic polypeptide solutions. PBLG/m-cresol solutions were observed to exhibit shear thinning behavior at high shear rates in a concentric cylinder.

Iizuka [115] reported a limited amount of high shear rate data of anisotropic solutions of PELG in dioxane, PELG in methyl bromide, PEG in methyl bromide, PBLG in dioxane and PBLG in m-cresol. Solutions containing 13 wt% PELG, PEG, or PBLG exhibited region III shear thinning behavior at shear rates above 100 s^{-1}. In contrast, solutions containing 16 wt% PELG, PEG, or PBLG showed region III behavior above 20 s^{-1}. The dynamic storage modulus, G', of the 13 wt% solutions exhibited a frequency independent plateau at comparable frequencies to the onset of steady shear thinning (100 s^{-1}). The loss modulus, G", however, decreased with frequency in the same shear frequency region. Dynamic properties were not reported on the 16 wt% solutions.

Kiss and Porter [129,130] reported extensive high shear rate rheological studies of nematic PBG/m-cresol, cholesteric PBLG/m-cresol and cholesteric PCBL/m-cresol solutions. Steady state measurements in a cone and plate rheometer were made up to shear rates of 100 s^{-1}; transient measurements were used to derive rheological measurements in the 100 s^{-1} to 16,000 s^{-1} shear rate range. The shear rate range above 100 s^{-1} was troubled by

apparent secondary flow effects. Dynamic oscillatory measurements were obtained over a 0.1 rad s^{-1} to 400 rad s^{-1} frequency range. The onset of region III flow behavior appeared to be somewhat dependent on concentration and molecular weight. Solutions of high molecular weight PBLG and PBG samples exhibited the onset of region III at 0.1 s^{-1}. Solutions of lower molecular weight PBLG samples exhibited region III behavior above 80 s^{-1}. PCBL solutions exhibited somewhat complex viscosity behavior, with solutions below 33 wt% exhibiting region III behavior above 20 s^{-1} and those above 33 wt% exhibiting region III behavior above 0.2 s^{-1}. In the dynamic viscosity versus frequency plots, the onset of region III flow behavior occurred at 0.4 rad s^{-1} in PBG solutions, 100 rad s^{-1} in PBLG solutions and 0.2 rad s^{-1} in PCBL solutions. The primary normal stress, N_1, exhibited anomalous negative values in region III. The N_1 versus shear rate curves invariably increased to an initial positive maximum, then decreased to a large negative minimum and finally increased unbounded to large positive values. These anomalous changes in N_1 appeared to be independent of cone angle or cone and plate diameter. The dynamic shear modulus, G, did not appear to approach a high frequency plateau for any of the solutions, but increased in a quasi-linear fashion with frequency.

Kiss and Porter [131] also reported rheo-optical observations coresponding to region III flow behavior in solutions of PBG or PBLG in m-cresol. These observations were made from the solutions sheared between two rotating parallel disks. Effective shear rates used were 0.5 s^{-1} to 200 s^{-1}. Striations or bands parallel to the shear direction were observed in the shear rate region corresponding to the initial positive N_1 region. Striations or shear bands perpendicular to the flow direction were observed at shear rates corresponding to the negative N_1 region. At higher shear rates a featureless field was observed; this corresponded to the second positive N_1 region.

Baird [22] reported apparent region III viscosity behavior in anisotropic PPTA/SA solutions at 60°C from cone and plate rheometry measurements. The onset of region III occurred at 0.1 s^{-1} in 10 wt% PPTA solutions and 1.0 s^{-1} in 12 wt% and 15 wt% PPTA solutions. Dynamic viscosity measurements indicated region III behavior at frequencies above 0.1 rad s^{-1} for all three solutions. Positive primary normal stress coefficients which decreased dramatically with shear rate were also observed.

Bheda [29] reported cone and plate rheometry data for two cellulose derivatives, HPC and EC. Anisotropic HPC/AA solutions exhibited shear thinning or region III behavior at shear rates above 0.2 s^{-1}. For the HPC/AA solutions,

the primary normal stress differences (N_1) exhibited a curved increase to a maximum value. Anisotropic EC/AA solutions exhibited the onset of shear thinning at shear rates above 0.1 s^{-1}. No N_1 values were reported for EC/AA solutions.

Horio and coworkers [110] observed apparent region III viscosity behavior in 60 wt% HPC/W solutions in data from cone and plate rheometry. The onset of region III was observed at ca. 8 s^{-1} for the steady shear viscosity. The dynamic viscosity exhibited an equivalent onset at a frequency of 8 rad s^{-1}. The dynamic storage and loss moduli, G' and G", respectively, showed a linear increase with frequency; no high frequency plateaus were observed.

Berry and coworkers [79] reported steady shear viscosity measurements in nematic PBT/MSA solutions. The onset of shear thinning or region III behavior was observed at shear rates above 1 s^{-1}. Normal stress data were not reported.

In studies of thermotropic polymers, Wissbrun [242] was the only researcher clearly reporting the presence of region III flow behavior. Capillary rheometry data of a 60/40 POB/PET copolyester at 300°C showed shear thinning or region III behavior above a shear rate of 20 s^{-1}. Rheological data of a different copolyester, comprised of hydroxybenzoic acid, dihydroxynaphthalene, and terephthalic acid in a 60/20/20 mole ratio, exhibited rheopectic

or shear thickening behavior above 40 s^{-1}. This anomalous viscosity behavior was also considered as a region III phemonenon.

In summary, the limited number of rheological studies encompassing region III present an incomplete picture of the flow behavior. Despite the incompleteness, a few comments can be made about the general features of region III flow behavior.

1. The viscosity-shear rate behavior in lyotropic polymers appears to be shear thinning, whereas, the behavior in thermotropic polymers may be pseudoplastic or rheopectic.

2. The onset of this shear thinning or region III viscosity behavior occurs at a lower shear rate with respect to both increasing concentration and molecular weight [16,22,196]. Polydispersity in molecular weight affects the broadness of the critical shear rate range [196].

3. The primary normal stress differences, in most cases, should approach a maximum plateau at high shear rates [196]. However, the primary normal stress differences may exhibit anomalous negative behavior, due to 'disclinations' or flow orientation instabilities [243].

4. The dynamic storage modulus, G', exhibits an apparent linear increase with shear rate, then levels off

at high shear [110,196]. The trend in the loss modulus, G", is not clear.

E. Processing and Fabrication

Six classes of polymer liquid crystals have been investigated with respect to processability or fabrication into useful products such as fibers or films. These classes include synthetic polypeptides, aromatic polyamides, aromatic polyhydrazides, cellulosic derivatives, polyheterocyclics, and aromatic copolyesters.

Synthetic polypeptides were initially investigated at Courtaulds, Ltd., in the late 1940's to early 1960's, for their potential in forming synthetic silk fibers. Ballard and coworkers [24,25] reported advantages in processing (i.e. higher spinning speeds) liquid crystalline solutions of poly(γ-methyl-L-glutamate) (PMLG) and poly(γ-ethyl-L-glutamate) (PELG) solutions over lower concentrations or isotropic solutions of these polymers. Fibers were wet-spun from anisotropic 15 wt% PMLG or PELG dopes, containing 85 wt% of a 12/5 methylene chloride/ethyl acetate solvent mixture, into a coagulation bath containing an acetone/water mixture or ethanol/water mixture. The resultant fibers were post-drawn in steam or hot water to convert the initial alpha helical crystal structure to an extended beta crystal structure. Spinning speeds of 260 m/min were attained. In contrast, the isotropic solutions

could only be spun at speeds of 17 m/min [23]. Despite the advantage in processability, however, fibers spun from anisotropic PMLG or PELG solutions did not possess higher strengths than those spun from isotropic solutions. Fibers with tensile strengths in the range of 0.26 GPa to 0.38 GPa were obtained from either type of solution. Synthetic polypeptide fibers were ultimately not commercialized because of two economic considerations:

1. the expenses involved in producing high molecular weight polypeptides and

2. the costs associated with solvent recovery and effluent waste treatment from the wet spinning process.

Kwolek [142] and Morgan et al. [19] of DuPont described the wet and dry spinning processes for forming high tenacity and high modulus fibers form liquid crystalline solutions of para-linked aromatic polyamides, like poly(p-benzamide)(PBA) and poly(p-phenylene terephthalamide) (PPTA). The later polymer, PPTA, was commercialized under the Dupont tradename Kevlar®. Kwolek [142] described aproximately 70 different combinations of aromatic polyamides and solvents for producing high strength fibers. Liquid crystalline solutions or spinning dopes contained from 5 wt% to 15 wt% polymer, the concentration depending on molecular weight and solvent character. Solvents typically included either secondary amide/lithium chloride solutions, such as N,N dimethyl-acetamide (DMA)

with 4 wt% to 8 wt% LiCl, or strong acids such as sulfuric acid. Many of the described polymer and solvent combinations were wet-spun into aqueous coagulation baths maintained at 25°C to 45°C and the resultant fibers soaked or washed in water to leach out any remaining solvent before being dried. As-spun fibers possessed tenacities in the 0.6 GPa to 1.4 GPa range and tensile moduli in the 23 GPa to 36 GPa range. Fibers were annealed or heat treated at 500°C to 600°C for a brief time period (10 to 30 seconds) to improve tensile properties. This process involved no drawing, only tension. After heat treatment the fibers exhibited greatly enhanced tensile properties with tenacities in the 1.3 GPa to 2.8 GPa range and tensile moduli in the 77 GPa to 102 GPa range.

Blades [35,36] applied the dry-jet wet spinning technique to the processing of liquid crystalline aromatic polyamide solutions. The dry-jet wet spinning technique involved extrusion of the polymer solution or spinning dope through a small air gap into a coagulation bath. The presence of the air gap allowed the extruded solution to be drawn before it solidified in the coagulation bath. Blades observed that as-spun fiber tensile properties were much improved over conventional wet spun fibers. As-spun fibers possessed tenacities in the 2.3 GPa to 4.1 GPa range and tensile moduli in the 45 GPa to 102 GPa range.

Miyoshi and coworkers [158] developed the first reported wet fabrication process for producing blown films from lyotropic PPTA and PBA solutions. The films were prepared by extrusion of a concentrated solution or spinning dope containing sulfuric acid through an annular die, then through a small air gap into an aqueous coagulation bath containing a weak base. Each extruded film was inflated with nitrogen to a blow-up ratio of three, just prior to entering the coagulation bath. The coagulated films were taken up on a wind-up roller at speeds ranging from 12 m/min to 25 m/min. Mechanical strengths of the films varied from a low of 0.21 kPa MD (machine direction) and 0.19 kPa TD (transverse direction) to a high of 0.3 kPa MD and 0.27 kPa TD.

Aoki and coworkers [15] described dry-jet wet fabrication methods for producing ribbons and tubular films from anisotropic (12 wt%) PPTA/SA dopes. Ribbons were formed by extruding the dope through a slit die into a small air gap and then into a water coagulation bath. This was followed by an alkaline rinse to neutralize any remaining acid; the ribbons were air dried after rinsing. Tubular films were produced by a similar process, except the die used was an annular die. In the case of the ribbons, fast extrusion rates, large air gaps, and low take-up rate all contributed to distorted cross-sections. The best or least distorted ribbons were produced at the

opposite of these conditions. As-extruded tubular films averaged tensile strengths in the 25 MPa MD and 1 MPa TD range. Annealing the films at 400°C for 10 minutes increased the tensile strengths to 50 MPa MD and 8 MPa TD. The tensile moduli averaged 600 MPa.

Flood and coworkers [38,84,86] made substanial improvements in the fabrication of biaxially oriented films from PPTA/SA solutions over earlier researchers. In their process, a 17 wt% PPTA/SA spinning dope is placed in a heated resevoir maintained at 70°C, then extruded through a heated annular die (also at 70°C) onto an oil coated conical mandrel. The extruded PPTA/SA solution underwent biaxial extensional flow as it passed over the mandrel and through the air gap into the coagulation bath. The coagulation bath contained water, or an ethanol/water or methanol/water mixture. The solution was extruded at a volumetric rate of 85 mL/min. The effective extension ratio was approximately three by three. Tensile strengths of the as-extruded films ranged from a low of 66 MPa MD and 90 MPa TD to 220 MPa MD and 320 MPa TD depending on coagulation conditions. The upper range of the tensile strengths were increased to 380 MPa MD and 370 MPa TD after the films were annealed at 300°C.

More recently, Flood [82] has investigated the effect of mandrel shape on the biaxial character of PPTA films. PPTA films produced with conical mandrels, with 16.5° to

30° inclinations, possessed almost equal biaxial tensile character. Tensile strengths in the 0.12 GPa to 0.14 GPa were obtained in both MD and TD; tensile moduli were obtained in the 5.1 GPa to 6.3 GPa range. Films fabricated with an ogival, or nearly parabolic, mandrel also possessed equal biaxial character. Tensile strengths in the range of 0.18 GPA to 0.19 GPa were obtained, while tensile moduli in the 4.8 GPa to 6.0 GPa range were obtained. Films produced with a hyperbolic mandrel, however, exhibited greater tensile properties in the transverse direction. The MD tensile strengths and moduli were on the order of 0.14 GPa and 4.9 GPa, respectively. The TD tensile strengths and moduli were on the order of 0.23 GPa and 7.9 GPa, respectively.

Morgan [169] reported the dry-jet wet spinning of anisotropic aromatic poly(hydrazide) solutions. Anisotropic, 20 wt% poly(oxalic-chloroterephthalic hydrazide) (POTH) solutions in either sulfuric acid (SA) or fluorosulfonic acid/sulfuric acid (FSA/SA) mixtures were spun into a water coagulation bath maintained at 1°C. The resultant fibers were then washed with water and air dried. The POTH/SA or POTH/FSA/SA solutions produced fibers with tenacities averaging 1.4 GPa and tensile moduli averaging 44 GPa.

Panar and Wilcox [182] described wet spinning and dry-jet wet spinning methods for producing moderately high

strength fibers from anisotropic solutions of several cellulose derivatives containing organic acids or chlorinated organic solvents. One example mentioned in the patent was an anisotropic solution of cellulose triacetate in trifluoroacetic acid, which was dry-jet wet spun into fibers with as-spun tenacities of 0.9 GPa. Heat treatment of the fibers at 240^{o}C, followed by a cellulose regeneration step, yielded fibers with tenacities on the order of 1.4 GPa.

Bheda [29] reported dry-jet wet spinning of anisotropic solutions of cellulose acetate butyrate (CAB) in dimethylacetamide (DMA) and cellulose triacetate (CTA) in trifluoroacetic acid (TFA). Solutions of 50 wt% CAB/DMA were extruded through a single hole spinneret of 0.8 mm in diameter, through a 2 cm air gap, and into a coagulation bath containing 50/50 DMA/water. Drawdown ratios varied from 3.4 to 8.5. Corresponding tensile strengths and tensile moduli ranged from a low of 0.07 GPa to a high of 0.09 GPa and a low of 0.8 GPa to a high of 2.36 GPa, respectively. Solutions containing 30 wt% CTA/TFA were dry-jet wet spun into a methanol coagulation bath. Drawdown ratios varied from 3.9 to 15.6. Correspondingly, the tensile strengths ranged from 0.15 GPa to 0.5 GPa and tensile moduli ranged from 2.7 GPa to 7.5 GPa.

Omatete and coworkers [178] reported dry-jet fabrication of uniaxial and biaxial films from anisotropic, 28

wt% to 30 wt% solutions of CTA in a mixed solvent which contained a dichloroacetic acid to formic acid (DCA/FA) ratio of 67 to 33. Films were produced by extruding the CTA/DCA/FA solutions through an annular die, then through a narrow air gap and into a chilled ($0^{o}C$) isopropanol coagulation bath. Uniaxial films were produced by direct extrusion of the CTA tube into the bath, whereas, the biaxial films were produced by inflating the tube with coagulant pumped from the bath. Films were slit, then washed and air dried on frames. Uniaxial films possessed tensile strengths on the order of 80 MPa and tensile moduli on the order of 0.9 GPA. Biaxial films possessed tensile strengths ranging from 150 MPa to 180 MPa MD and 140 MPa to 220 MPa TD; tensile moduli ranged from 1.3 GPa to 1.8 GPa MD to 2.0 GPa to 2.5 GPa TD.

Allen and coworkers [10,11] described the dry-jet wet spinning of liquid crystalline solutions of the aromatic poly(heterocyclic), PBT. Solutions containing 10 wt% PBT in methane sulfonic acid (MSA) or polyphosporic acid (PPA) were extruded through a multifilament spinnerette, then through a narrow air gap, and finally into a cold coagulation bath containing either MSA/water or water alone. After coagulation the fibers were wound through a wash bath and collected on a take-up roll. Extrusion rates and take-up velocities were not reported. As-spun fibers from PBT/MSA solutions possessed tensile strengths in the 0.4

GPa to 1.5 GPa range and tensile moduli in the 45 GPa to 154 GPa range. As-spun fibers from PBT/PPA solutions possessed tensile strengths in the 0.5 GPa to 2.3 GPa range and tensile moduli in the 50 GPa to 76 GPa range. After a short term heat treatment in the 200°C to 400°C temperature range, the PBT fibers possessed tensile strengths in range of 1.5 GPa to 3.2 GPa and tensile moduli in the range of 128 GPa to 320 GPa range.

Melt fabrication of thermotropic polymers was first reported in 1974. Kuhfuss and Jackson [139] reported conventional melt spinning of a POB/PET 60/40 copolyester at 275°C. Fibers produced were rather brittle, but possessed tensile strengths on the order of 0.4 GPa and moduli on the order of 25 GPa. More recent melt spinning studies of POB/PET 60/40 have been reported by Acierno and coworkers [1] in 1982 and Sugiyama and coworkers [224] in 1985.

Acierno and coworkers [1] prepared melt spun fibers by extruding a POB/PET 60/40 melt (at melt temperatures in the range 225°C to 285°C) through a 2 mm diameter orifice at a constant velocity, 0.1 m/min. Take-up velocities in the 10 m/min to 300 m/min range were used. Fibers spun at 225°C exhibited significantly higher tensile moduli than those spun at higher temperatures. At 225°C the tensile modulus increased from 10 GPa at 10 m/min to an asymptotic value of 30 GPa at 300 m/min. At a constant take-up

velocity of 300 m/min, the asymptotic value of the tensile modulus decreased with increasing temperature from 30 GPa at 225°C to 3 GPa at 285°C. Tensile strengths were reported for fibers melt spun at 245°C. The plot of tensile strength versus take-up velocity at this temperature exhibited a discontinuity at ca. 55 m/min. Tensile strengths increased from 40 MPa at 10 m/min to 220 MPa at 50 m/min. At 60 m/min the tensile strength had decreased to 100 MPa. From 60 m/min to 300 m/min the tensile strength increased to an asymptotic value of 300 MPa.

Sugiyama and coworkers [224] also reported a melt spinning study of POB/PET 60/40. Tensile properties were not reported in this study. However, the effects of extrusion temperatures and take-up ratio on fiber orientation were reported. Fibers were melt spun by extrusion of the POB/PET 60/40 melt at temperatures in the 230°C to 300°C range through a 0.74 mm diameter orifice at a constant extrusion velocities in the range of 0.085 m/min to 0.85 m/min and take-up rates in the range of 500 m/min to 1124 m/min. Fibers extruded at 0.085 m/min with no take-up showed an increase in the Hermans or c-axis orientation factor (perfect orientation $f_H = 1$) from $f_H = 0.2$ at 230°C to $f_H = 0.65$ at 280°C. At the extrusion rate of 0.85 m/min with no take-up, the orientation factor ranged from 0.45 at 230 °C to 0.65 at 280°C. An asymptote at $f_H = 0.65$ was apparent above 270°C. At this temperature the

orientation factor appeared to be unaffected by either increasing the extrusion rate or take-up rate. The asymptotic behavior of the orientation factor was interpreted as the result of 'plug' flow in the die.

Melt spinning studies of other thermotropic polyesters have been also been reported. Kleinschuster [133] described the melt spinning of a poly(chloro-1,4 phenylene-4,4'-dioxybenzoate) at 339°C. As-spun fibers showed tensile strengths averaging 0.4 GPa and tensile moduli averaging 19 GPa. A six step heat treatment process involving temperatures in the 25°C to 315°C temperature range dramatically improved the tensile properties of the fibers. Tensile strengths were quadrupled to 1.7 GPa; tensile moduli were almost doubled to 37 GPa.

Cottis and coworkers [56] described the melt spinning of copolyesters containing 50 mol% p-hydroxybenzoic acid (PHB), 25 mol% p,p'-bisphenol (BP), 17 mol% to 19 mol% terephthalic acid (TA) and 6 mol% to 8 mol% isophthalic acid (IA). The PHB/BP/TA/IP copolymers were melt spun at a temperature of 320°C, through a 1 mm diameter orifice at an extrusion rate of 200 m/min. Tensile strengths in the 1.0 GPa to 1.2 GPa range and tensile moduli in the 34 GPa to 41 GPa range were obtained.

Demartino [60] reported melt spinning studies of thermotropic copolyesters comprised mainly of 60 mol% PHB, 20 mol% TA and 15 mol% to 20 mol% of 2,6 dihydroxy-

naphthalene (2,6 DHN). Some compositions included small amounts (1 mol% to 2.5 mol%) of bisphenol A (BPA), (2.5 mol% to 5 mol%) 2,7 dihydroxynaphthalene (2,7 DHN), or (2.5 mol% to 5 mol%) poly(ethylene terephthalate). These polymers were extruded from melts at 300°C to 360°C through a 0.18 mm diameter orifice into ambient air and taken up at 52 m/min. The 60/20/20 PHB/TA/2,6 DHN base polymer exhibited tensile strengths and moduli averaging 0.8 GPa and 62 GPa, respectively. Compositions containing BPA exhibited tensile strengths and moduli on the order of 0.7 GPa and 53 GPa, respectively. Compositions containing 2,7 DHN exhibited tensile strengths and moduli averaging 0.8 GPa and 62 GPa, respectively. Compositions containing PET showed tensile strengths on the order of 0.93 GPa and tensile moduli on the order of 61 GPa.

Acierno et al. [2] reported melt spinning of polyesters containing equal molar ratios of azelaic acid (AZ) and 4,4'-diacetoxybiphenyl (ABP) or 4'-hydroxyphenyl-4-hydroxycinnamate (HPHC). The AZ/ABP polyester was extruded from a melt at 255°C through a 0.5 mm diameter orifice at 0.1 m/min. Take-up was not possible due to the brittleness of the fibers. The tensile strength and modulus of the fibers were quite low, averaging 0.04 GPa and 1.5 GPa, respectively. The AZ/HPHC polyester was spun at 210°C at an extrusion rate of 6.5 m/min. The take-up

velocity was 240 m/min. Tensile properties were of the same order as the AZ/ABP copolyester.

Zachariades and Logan [245] investigated the orientation and mechanical properties of POB/PET 80/20 films prepared by rotational molding and POB/PET 80/20 fibers prepared by melt drawing. The rotational molding apparatus consisted of a plate-plate rheometer which was heated or cooled with a respective heated or chilled input nitrogen gas flow. The molded films were prepared by forming a POB/PET 80/20 melt in the 295°C to 340°C temperature range, then compressing the melt to a thickness in the 120 to 160 micrometer range and finally shearing the melt as it was cooled to 200°C with chilled nitrogen. The sample was retrieved by stopping the rotation and cooling the film to room temperature. The shear rate used in the process was 240 s^{-1}. The melt drawn fibers were prepared from the copolyester melt in the 295°C to 330°C temperature range with a mixing extruder equipped with a varible speed take-up system. The extrusion rate was not indicated. The take-up rate was varied between 5 and 10 m/min. The mechanical properties for both of the films and the fibers varied significantly with respect to the molding or extrusion temperature. The orientation as determined by electron diffraction did not show much variation with repect to temperature. However, some loss in order was noted in the

films and fibers prepared from melts above 328°C. The films prepared at 305°C had a tensile strength of 104 MPa and a Young's modulus of 4 GPa. The films prepared at 330°C exhibited a tensile strength of 218 MPa and a Young's modulus of 19 GPa. The fibers showed a similar increase in tensile properties with respect to extrusion temperature. Fibers melt drawn at 300°C possessed a tensile strength of 115 MPa and a Young's modulus of 5 GPa. The fibers processed from the 330°C melt had a tensile strength of 225 MPa and a Young's modulus of 40 GPa. The lower mechanical properties of the fibers and films processed below 328°C were associated with the physical alignment of unmelted and undeformed POB rich 'domains'. Above 328°C the 'domains' were broken down under shear or elongational flow to form a uniform fibrillar structure. This structure was associated with the doubling of the tensile strength and the four to eight fold increase in the Young's modulus.

Ide and Ophir [113] described the melt extrusion of a copolyester containing 60 mol% p-acetoxybenzoic acid (PAB), 20 mol% 2,6 naphthalene diacetate (ND) and 20 mol% TA. The PAB/ND/TA copolyester was extruded, from a melt at 340°C, through a 0.76 mm diameter orifice at shear rates ranging from 20 s^{-1} to 2000 s^{-1}. Drawdown ratios from 1.1 to 50 were used. Tensile strengths increased from 0.1 GPa to 0.7 GPa with drawdown ratios up to 11,

then decreased to about 0.5 GPa above a drawdown ratio of 50. Tensile strengths were unaffected by increasing extrusion or shear rates. Tensile moduli decreased with shear rate from 5 GPa to 3.5 GPa at low draw ratios, but increased from 5 GPa to 50 GPa at high draw ratios.

Ide [112] recently described the melt extrusion and drawdown of copolyesters containing 60 mol% to 70 mol% 6-oxy-2-naphthoic acid (ONA), 15 mol% to 20 mol% TA and 15 mol% to 20 mol% hydroquinone diacetate (HQ). The ONA/TA/HQ copolyesters were extruded from melts at 300°C to 315°C through a 0.76 mm diameter orifice at extrusion rates ranging from 0.3 m/min to 6.2 m/min. Drawdown ratios ranged from 0.8 to 2.1. Tensile strengths and moduli appeared to be unaffected by extrusion rate, but increased dramatically with drawdown ratio. Tensile strengths in the 0.2 GPa to 0.9 GPa range and tensile moduli in the 23 GPa and 73 GPa range were obtained, depending on drawdown ratio.

Injection molding of thermotropic polyesters has been reported in several studies since 1976. Jackson and Kuhfuss [119,120] and McFarlane et al. [156] all reported the injection molding of several POB/PET compositions, with 60 mol% to 80 mol% POB and a copolyester containing 40 mol% PET, 30 mol% POB and 30 mol% hydroquinone terephthalate (HQT). The POB/PET and PET/POB/HQT copolyesters were injected into unheated molds using 1 oz and 6

oz injection molding machines to form 0.06 inch thick, 2.5 inch long tensile bars or 0.125 inch thick, 5 inch long flexure bars. Injection melt temperatures ranged from 260°C to 340°C, depending on the polyester composition. The POB/PET copolyesters exhibited tensile and flexural strengths in the 180 MPa to 300 MPa range and flexural moduli in the 12 GPa to 18 GPa range. For the PET/POB/HQT copolyester, the tensile and flexural strengths were on the order of 100 MPa and the flexural modulus was on the order of 10 GPa.

Calundann [47] described the injection molding of a copolyester synthesized from 60 mol% PAB, 20 mol% 2,6 naphthalene dicarboxylic acid (NDA) and 20 mol% hydroquinone diacetate (HQ). This 60/20/20 PAB/NDA/HQ copolyester was injection molded at 325°C into 93°C molds using an 8 oz injection molding machine. The PAB/NDA/HQ copolyester exhibited tensile strengths averaging 118 MPa, tensile moduli averaging 6.8 GPa, flexural strengths averaging 140 MPa and flexural moduli averaging 8.2 GPa.

Ophir and Ide [181] described the injection molding of a copolyester composed of 60 mol% PAB, 20 mol% NDA and 20 mol% TA. This copolyester was molded into 8.5 inch long tensile bars and 5 inch long flexure bars using a 2.5 oz injection molding machine. The injection melt temperatures ranged from 320°C to 340°C and the mold temperatures from 40°C to 100°C. The PAB/NDA/TA copolyester had

tensile strengths in the 150 MPa to 210 MPa range, flexural strengths in the 170 MPa to 180 MPa range, tensile moduli in the 15 GPa to 20 GPa range and flexural moduli in the 13 GPa to 15 GPa range.

Two melt fabrication studies have been reported for cellulosic derivatives. Shimamura and coworkers [216] reported the melt spinning of thermotropic HPC. Filaments of HPC were extruded from the melt at 180°C through a 0.74 mm diameter orifice. Extrusion rates were not reported. However, take-up rates up to 24 m/min were used to collect the filaments. The crystalline orientation in the fiber reached an asymptotic value of f_H = 0.65 above the lowest take-up rates. The HPC filaments exhibited tensile strengths on the order of 80 MPa and tensile moduli on the order of 2.5 GPa.

Farell [81] described the melt fabrication of blown HPC and EC films produced using a counter-rotating annular die. HPC was processed at 170°C through a 15 L/D, 3/4 inch screw extruder to form a thermotropic melt. The melt was forced by the extrusion pressure through an annular gap of 0.145 cm to form a tube. The still softened HPC tube was inflated by nitrogen gas to a blow-up ratio of 2.8 and taken up by hand at an extension rate of 8.25 cm/min. EC was processed under similar conditions, except the extrusion temperature was 180°C. The die rotation speed in the processing of both polymers was varied from 0

to 17.2 rev/min. The linear extrusion rate and the die rotation speed were combined into one process variable, R, which represented the ratio of tangential wall shear rate to axial wall shear rate in the die. R varied from a value of 0 to a value of 410. Orientation in HPC films could be varied from biased in the MD or extrusion direction at R = 0 to biased in the TD or circumferential direction at R = 410. For HPC films processed at R = 0, the tensile strengths averaged 25 MPa MD and 3.8 MPa TD and the tensile moduli averaged 1.4 GPa MD and 0.2 GPa TD. For HPC films processed at R = 410, tensile strengths were on the order of 14 MPa MD and 19 MPa TD and tensile moduli were on the order of 0.7 GPa MD and 1 GPa TD. Films processed from EC exhibited similar tensile behavior. EC films processed at R = 0 averaged tensile strengths of 32 MPa MD and 11 MPa TD and averaged tensile moduli of 1.8 GPa MD and 1 GPa TD. At R = 410, EC films exhibited tensile strengths on the order of 9.9 MPa MD and 16 MPa TD and tensile moduli on the order of 1.1 GPa MD and 1.3 GPa TD.

F. Crystal Structure and Morphology

Crystal Structure

The primary factors governing the solid state crystal structure and morphology of mesophase forming polymers are

1. the ability of the solidified polymer to retain orientation and structural features of the liquid crystalline state,

2. the solvent and/or temperature conditions at which the mesophase exists, and

3. the pathway along which the polymer is solidified. In the case of lyotropic polymers, the solidification pathway is determined by the temperature, type of coagulant and the stress acting on the material. For thermotropic polymers, the cooling or quenching conditions and the stress on the sample govern the solidification pathway.

Early studies of the crystal structure of lyotropic synthetic polypeptides were conducted by Courtaulds' researchers Elliott and coworkers [12,186] and Bramford and coworkers [39,40]. The structures of films and fibers produced from PMLG/m-cresol solutions and PBLG/chloroform solutions were analyzed by wide angle x-ray diffraction (WAXD) techniques. Initial analysis of WAXD patterns from PMLG fibers and films suggested the unit cell was either orthorhombic with dimensions of $\underline{a}$ = 1.035 nm, $\underline{b}$ (fiber axis) = 0.55 nm, and $\underline{c}$ = 0.598 nm, or hexagonal with the

dimensions $\underline{a}$ = $\underline{c}$ = 1.2 nm and $\underline{b}$ = 0.55 nm. Preparation of more uniform PMLG samples and improvements in obtaining clearly defined WAXD patterns indicated the initial analyses were in error. The latter WAXD patterns suggested a hexagonal unit cell with dimensions of $\underline{a}$ = $\underline{b}$ = 1.195 nm and $\underline{c}$ = 2.7 nm. Infrared dichroism and WAXD data suggested the macromolecular PMLG chains existed in an 18/5 alpha helix configuration. WAXD patterns of PBLG fibers and films indicated two crystalline forms were present. Data from PBLG films were best fitted by the macromolecular chains having an 11/3 helical configuration and being arranged in a triclinic or monoclinic unit cell with a repeat distance of 0.576 nm. WAXD patterns of PBLG fibers suggested a different unit cell and helix configuration were present. In this case, the macromolecular chains assumed the configuration of 18/5 alpha helices packed in a distorted hexagonal unit cell with dimensions of $\underline{a}$ = $\underline{b}$ = 3.5 nm and $\underline{c}$ = 2.7 nm.

Tobolsky and coworkers [158,159,209,210] conducted extensive WAXD studies of PBLG films cast from cholesteric and nematic PBLG/chloroform solutions and PBLG/ dichloroethane solutions. The WAXD patterns of the cholesteric PBLG films were interpreted as resulting from coexistant paracrystalline and cholesteric-like ordered regions. The cholesteric-like regions were envisioned as 18/5 helices arranged in microcrystalline planes, parallel to the

surface and arranged in a helical superstructure with a normal twist axis. The paracrystalline regions consisted of 18/5 helices packed in a slightly distorted hexagonal unit cell with dimensions of $\underline{a} = \underline{b} = 3.5$ nm and $\underline{c} = 2.7$ nm. In the cholesteric PBLG films, the cholesteric-like crystal structure predominated in the surface layers of the films, while the interior regions were mainly composed of the paracrystalline structure. These films possessed uniplanar molecular orientation. Nematic PBLG films were prepared by slow evaporation of cholesteric PBLG/chloroform and PBLG/dichloroethane solutions in the presence of a strong (10 kOe) magnetic field, aligned so the field direction was parallel to the film surface. Films produced in this manner possessed uniaxial molecular orientation. The WAXD patterns of the films from PBLG/chloroform solutions were interpreted as resulting from 7/2 macromolecular helices packed in hexagonal unit cells. Films produced from PBLG/dichloroethane solutions gave WAXD patterns characteristic of 18/5 helices packed in hexagonal unit cells. Annealing films produced from PBLG/chloroform solutions at 100°C for several hours converted the crystalline structure to that of the 18/5 helical form.

McKinnon and Tobolsky [159] and Elliott et al. [220] both observed three crystalline modifications in PBLG films cast from N,N dimethylformamide (DMF) solutions.

Films cast from solutions containing up to 30 wt% DMF exhibited a complex crystalline phase, composed of distorted hexagonal unit cells with dimensions $\underline{a}$ = $\underline{b}$ = 3.5 nm and $\underline{c}$ = 2.7 nm. Films from the complex hexagonal phase were slowly evaporated at room temperature and completely dried at 100°C under vaccuum. These films exhibited WAXD patterns characteristic of a poorly ordered hexagonal crystalline phase. This phase gave equatorial reflections at 1.49 nm (110), 1.28 nm (200), 0.97 nm (210), and 0.88 nm (300); it was designated as form 'A'. A second crystal modification, form 'B', was prepared by heating a concentrated 60 wt% PBLG/DMF solution at 50°C until the film solidified. These films exhibited WAXD patterns characteristic of an oblique unit cell with dimensions $\underline{a}$ = 1.588 nm, $\underline{b}$ = 1.3 nm, $\underline{c}$ = 2.908 nm, and γ = 113.7°. The crystal structure was equivalently represented by a centered orthorhombic lattice with dimensions $\underline{a}$ = 2.908 nm, $\underline{b}$ = 1.3 nm, and $\underline{c}$ = 2.7 nm.

Ito and coworkers [118] also observed the effect of solvents and casting conditions on poly(γ-alkyl-glutamates). Films cast from poly(γ-methyl-D-glutamate) (PMDG) and poly(γ-n-hexyl-L-glutamate) (PHLG) exhibited contrasting behavior with solvent type. PMDG films cast from solvents like chloroform, dichlorethane, or trichloroethane passed through a liquid crystalline state as solidification occurred. WAXD patterns indicated the

crystallites were preserved in a cholesteric-like arrangement. The microcrystallites were composed of 18/5 macromolecular helices packed in hexagonal unit cells, with lattice dimensions $\underline{a}$ = $\underline{b}$ = 1.195 nm and $\underline{c}$ = 2.7 nm. WAXD patterns also indicated the (1120) planes of the unit cells tended to be parallel to the film surface. PMDG films cast from solutions like DMF, pyridine, or dioxane also exhibited WAXD patterns characteristic of a hexagonal lattice consisting of 18/5 macromolecular helices. The unit cell dimensions were unchanged but the orientation of the unit cells changed so the (1010) planes were parallel to the film surface. Solvent type did not have any apparent effect on PHLG films, which passed through a liquid crystalline state before solidification. WAXD patterns of PHLG films indicated the hexagonal unit cells were arranged so the (1120) planes were parallel to the film surface and uniplanar in orientation. The transition from the cholesteric state to the solid state in PMDG and PHLG films is illustrated in Figure 5.

Nearly all of the structural studies on lyotropic aromatic polyamides have concerned PPTA exclusively. A number of these studies have commented on the polymorphic crystal structure of PPTA, which can exist in two crystalline forms or modifications. The crystal structure known as modification I was first reported by Tadakoro [228],

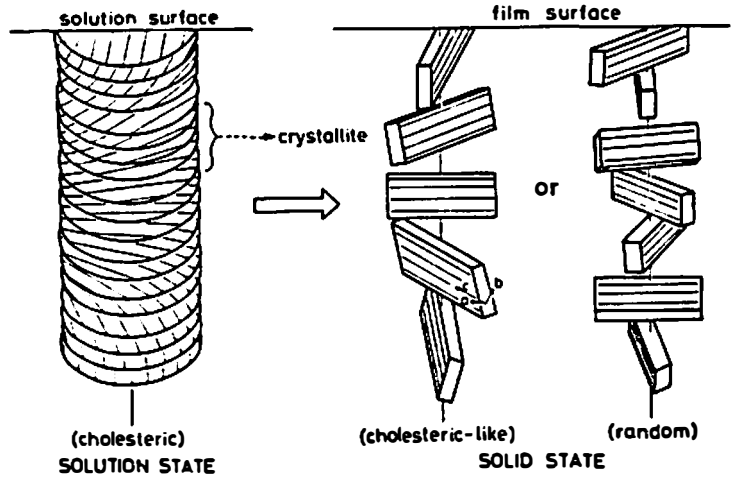

Figure 5. Schematic Representation of the Transition from Cholesteric State in Concentrated Polypeptide Solutions to the Solid State Structure of Cast Films. Parallel straight lines represent alpha-helical straight chains.

Source: Ito, K.,Kajiyama,T. and Takayanagi,M. Polym. J. (Japan) 9, 355 (1977)

and Northolt et al. [176,177]. WAXD patterns were prepared from wet spun and annealed PPTA fibers. These patterns were indexed by using a monoclinic or pseudo-orthorhombic unit cell with dimensions a = 0.787 nm, b = 0.518 nm, c (fiber axis) = 1.29 nm, and γ = ca. 90°. The modification I crystalline form gave the strongest WAXD reflections at 0.323 nm (004), 0.394 nm (200), 0.433 nm (110), and 0.645 nm (002).

Hancock, Spruiell, and White [102] first reported on the presence of a different crystalline modification in PPTA than that reported by Northolt et al. Dry-jet wet spun PPTA fibers coagulated in a 5/95 sulfuric acid/water coagulation bath exhibited two extra WAXD reflections at 0.497 nm and 0.759 nm and did not show the (110) and (002) reflections reported by Northolt et al. After annealing and hot drawing at 300°C, the fibers showed reflections at 0.398 nm (200), 0.435 nm (110), and extra reflections at 0.508 nm and 0.759 nm. Commercial Kevlar® fibers exhibited WAXD reflections at 0.448 nm (110), 0.631 nm (002) and one extra reflection at 0.759 nm. The (004) reflection in both groups of fibers studied was essentially in the same location as reported by Northolt et al.

Haraguchi and coworkers [104] also observed polymorphism in the PPTA crystal structure produced from PPTA/SA solutions. Films coagulated with water exhibited an (0k0) uniplanar molecular orientation with a crystal

structure known as modification II. The unit cell for modification II was also monoclinc or pseudo-orthorhombic, but had different dimensions than modification I. The dimensions were $\underline{a}$ = 0.8 nm, $\underline{b}$ = 0.51 nm, and $\underline{c}$ = 1.29 nm. This modification exhibited nearly the same (004) and (200) reflections as modification I, but differed from the latter structure by exhibiting an extra reflection at 0.52 nm and not exhibiting the (110) reflection. Films coagulated with water, from isotropic PPTA/SA solutions, generally exhibited modification II crystal structure and (0k0) uniplanar molecular orientation. Upon annealing, the films showed WAXD patterns characteristic of the modification I crystal structure and (h00) uniplanar molecular orientation. Films cast from anisotropic or liquid crystalline PPTA/SA solutions into water possessed the modification II crystal structure and (0k0) molecular orientation. However, these films did not transform from modification II to modification I upon annealing. Films prepared from isotropic or anisotropic PPTA/SA solutions by casting into organic solvents like methanol, acetone, or ethanol exhibited WAXD patterns characteristic of modification I crystal structure with (h00) uniplanar molecular orientation. These films also did not change crystal structures upon annealing. The formation of modification II was explained by the interference of water with the

crystallization of PPTA along the intermolecular hydrogen bond direction or b-axis direction in the unit cell.

The structural nature of fibers produced from lyotropic solutions of the poly(heterocyclic) PBT has been reported by Roche and coworkers [206]. Analysis of WAXD patterns of PBT fiber bundles indicated the structure was that of a paracrystalline two-dimensional lattice with no correlation in the monomer repeat or chain axis direction between neighboring chains. The dimensions of this two-dimensional lattice or net were $\underline{a}$ = 0.597 nm, $\underline{b}$ = 0.362 nm, and $\beta = 95.2^{\circ}$. The structure was envisioned as molecular planes packed laterally on the two dimensional net; a true three dimensional crystal structure was not apparent.

The crystal structure of a few cellulosic derivatives have been reported. Bheda [29] reported WAXD studies of dry-jet wet spun fibers from anisotropic CAB/DMA solutions and CTA/TFA solutions. The CAB fibers exhibited somewhat diffuse crystalline reflections at 0.31 nm, 0.426 nm, and 5.47 nm. The CTA fibers showed reflections at 0.374 nm, 0.406 nm, 5.43 nm, and 1.164 nm; these corresponded to the cellulose triactetate I unit cell described by Sprague et al. [219] with dimensions $\underline{a}$ = 2.26 nm, $\underline{b}$ (fiber axis) = 1.05 nm, $\underline{c}$ = 1.18 nm, and $\beta = 79^{\circ}$. CTA, as reported by Sprague et al., possessed two crystalline modifications depending on casting conditions and starting acetylation conditions. The exact type of unit cell was not

determined by Sprague and coworkers, but was concluded to be one of three types: tetragonal, orthorhombic, or monoclinc. The second modification, or cellulose triacetate II, was formed by dissolving the modification I CTA structure and reprecipitating, or by treatment of the film with formic acid [57]. CTA modification II possessed a unit cell similar to CTA type I, but with the dimensions $\underline{a}$ = 2.58 nm, $\underline{b}$ (fiber axis) = 1.05 nm, $\underline{c}$ = 1.145 nm, and β = 66.4°.

EC films, as reported by Farell [81], also possess a polymorphic crystalline structure. The various forms or modifications have not been distinguished or resolved to date.

The crystal structure of HPC was determined by Samuels [208] from the analysis of WAXD patterns of films cast from HPC/W or HPC/EA solutions. These patterns were indexed to a tetragonal unit cell with dimensions: $\underline{a}$ = $\underline{b}$ = 1.133 nm, and $\underline{c}$ = 1.5 nm. The strongest WAXD reflections were observed at 0.498 nm (003), 0.25 nm (006) and 1.133 nm (100).

Structural investigations of several thermotropic copolyesters have been recently reported by several authors. These studies have mainly concerned three types of aromatic copolyesters: poly(p-oxybenzoate-co-ethylene terephthalate) (POB/PET), poly(p-oxybenzoate-co-

naphthalene terephthalate) (POB/DHN/TA), and poly(p-oxybenzoate-co-oxynaphthalene) (POB/ON).

Wissbrun [242] was the first to report WAXD patterns from POB/PET 60/40 copolyesters. Strong reflections were observed at 0.456 nm, 0.425 nm, 0.378 nm, and 0.356 nm. These reflections corresponded closely to the spacings observed for the POB homopolymer, which exhibited strong WAXD reflections at 0.448 nm, 0.422 nm, 0.376 nm, and 0.361 nm. No reflections were observed corresponding to the PET component, which typically has reflections at 0.508 nm, 0.398 nm, and 0.347 nm.

Other studies have also noted the similarities between the WAXD patterns of POB/PET 60/40, POB/PET 80/20 and the POB homopolymer [34,92,120,125,126,224,229,244]. The similarities result from the formation of a POB rich phase in the copolyester. Nicely [172] reported, on the basis of high resolution NMR studies, the POB rich phase consisted of 80 mol% POB units, arranged in microblocks along the main chains. The WAXD patterns of the POB rich phase most resemble those of the high temperature phase III modification of the POB homopolymer [34,150]. This form occurs at temperatures above 360^{o}C and possesses an orthorhombic unit cell with the dimensions, $\underline{a}$ = 0.92 nm, $\underline{b}$ = 0.53 nm, and $\underline{c}$ = 1.24 nm [34].

Lieser and coworkers [34,150] have commented on the polymorphic crystal structure of POB. At room

temperature, two concomitant crystalline phases exist in all POB samples. The WAXD patterns of phase I crystallites can be matched with an orthorhombic unit cell, having the dimensions of *a* = 0.752 nm, *b* = 0.57 nm, and *c* = 1.249 nm [150]. Geiss et al. [92] recently proposed a similar unit cell, with the dimensions of *a* = 0.762 nm, *b* = 0.57 nm, and *c* = 1.249 nm. This unit cell corrected an earlier proposal by Economy et al. [77]. The WAXD patterns of oligmer samples of POB result from mostly phase II crystallites. The fraction of phase II was observed to decrease with increasing POB molecular weight. The unit cell of phase II is also orthorhombic and has the dimensions of *a* = 0.337 nm, *b* = 1.106 nm, and *c* = 1.289 nm [150].

Blackwell and coworkers [33,35,100,101] have described structural analyses of POB/DHN/TA and POB/ON copolyester fibers. WAXD patterns of the POB/DHN/TA copolyester were indicative of a solid state nematic structure with irregular packing of the polymer chains in the lateral dimension. Compositions ranging from 60/20/20 POB/DHN/TA to 40/40/20 POB/DHN/TA were investigated. The strongest reflections were observed along the meridional direction at 0.200 nm to 0.202 nm, 0.296 nm to 0.298 nm, and 0.313 nm to 0.348 nm, the exact positions depending on monomer ratio. All compositions exhibited strong equatorial reflections at 0.433 nm and 0.257 nm. WAXD

patterns of POB/ON copolyesters indicated an irregularly packed nematic structure with some degree of three dimensional order. Compositions ranging from POB/ON 25/75 to POB/ON 75/25 were investigated. The strongest meridional reflections were observed at 0.202 nm to 0.206 nm, 0.277 nm to 0.303 nm, and 0.67 nm to 0.81 nm, the exact positions depending on monomer ratio. The strongest equatorial reflections were at 0.26 nm and 0.45 nm.

Morphology

Two characteristic morphological features have been reported in the flow-induced solid state structure of both lyotropic and thermotropic polymer liquid crystals:

1. the presence of striations or shear bands upon cessation of shear, and

2. a distinct difference between the surface or skin layer morphology and the interior or core morphology.

The presence of striations or shear bands perpendicular to the flow direction was first reported in sheared films from anisotropic PBA/DMA solutions by Kulichikhin and coworkers [140] in 1976. The width of the striations were found to increase linearly with sample thickness. At the smallest thickness (0.25 mm) no striations could be observed. Solidified films had the appearance of slightly corregated sheet and had the tendency to split along the striation or band direction.

Banded structures were also observed in fibers produced from another aromatic polymide, PPTA. Dobb and coworkers [64,65], and later Simmens and Hearle [217], reported the presence of bands perpendicular to the fiber's long direction with a periodicity of 500 nm. These were observed by polarized microscopy at high magnification. This banding was interpreted to result from the packing of radially arranged pleated sheets of PPTA molecules in the fiber. The bands corresponded to pleats or bends every 250 nm.

Kiss and Porter [131] observed the formation of bands or striations in moderately sheared solutions of PBLG in dioxane. These striations exhibited a periodicity of 25 microns. Kiss and Porter attributed the band formation to the presence of wedge shaped planes with molecular orientation at $\pm$ 45^{o} to the shear direction.

Donald and coworkers [66-68,234] have observed the formation of shear bands perpendicular to the shear direction in several thermotropic copolyesters: POB/PET 60/40, POB/ON 70/30, poly(p-oxybenzoate-co-hydroquinone bis(p-carboxyphenoxy)ethane) (CHT/HBPE 50/50), and poly(oxynaphthalene-co-m-oxyanaline terephthalate) (ON/OAT 50/50). The periodicities of these banded structures were on the order of 0.8 micron to 1 micron. The most extensive electron diffraction and polarized microscopy studies were made on the POB/ON 70/30 and POB/PET 60/40 copolyesters.

The periodicity of the bands in POB/ON 70/30 were observed to be strongly influenced by the temperature at which the shearing took place. The band spacing decreased from 0.8 microns at 300°C to 0.2 microns at 200°C. The effect of annealing or heat treatment of the banded structure was also reported. Sheared samples of POB/PET 60/40 annealed at 300°C for 10 minutes no longer exhibited the periodic shear bands observed in unannealed samples. Examination of the banded structure in POB/PET 60/40 and POB/ON 70/30 by polarized microscopy revealed the optic axes followed a serpentine or sinusoidal variation along the shear direction. The examination of these banded 'textures' by electron diffraction suggested, however, the molecular orientation was not as sinusoidal or periodic as indicated by polarized optical microscopy. Donald and coworkers concluded the molecular optic axes did not coincide with the molecular long axes, but tracked the in-plane and out-of-plane conformations of the phenyl groups in the aromatic backbones of the macromolecules.

Zachariades and coworkers [244-246] examined the banded structure in POB/PET 60/40 and POB/PET 80/20 produced by shearing the melts between rotating parallel disks at shear rates ranging from 10 s^{-1} to 200 s^{-1}. They proposed the banded structure resulted from a macroscopic deformation of an initial spherulitic domain 'texture' during flow. The morphology suggested to result from this

'domain' reorganization was that of a homogeneously sheared monodomain skin layer surrounding a core composed of interconnected 'domains'. The director axes in these core 'domains' deviated from the shear direction up to $\pm$ 40°.

Horio and coworkers [110] studied the shear-induced formation of a perpendicular banded 'texture' in anisotropic HPC/W solutions. The formation of these bands occurred some 5 seconds after cessation of shear. This banded structure slowly transformed over several minutes to a 'polydomain' cholesteric type structure.

Nishio et al. [173,174] have studied the morphology of films cast from quiescent and sheared anisotropic HPC/W and EC/AA solutions. Films preserved from quiescent HPC and EC solutions exhibited a fibrillar skin or surface layer covering an interior of spherulitic-like 'domains'. High magnification of these 'domains' indicated each was composed of disk-like stacks crystalline lamallae. Films cast from sheared HPC and EC solutions exhibited perpendicular bands to the shear direction. The bands produced at high shear (300 s^{-1}) were more distinct than those produced at low shear (70 s^{-1}). The bands were observed by polarized optical microscopy to have a spacing or periodicity of 1.2 microns and to exhibit an optic axis tilt in each band ranging from 15° to 24° with respect to the shear direction. Examination of the solid films by

scanning electron microscopy (SEM) indicated a pleated or kinked morphology had formed with periodicities corresponding to the bands observed in polarized optical microscopy. Nishio et al. suggested the bands formed from the contractural strain imposed upon relaxation of the shear stresses after cessation of shear.

The presence of an oriented skin and less oriented core morphology in polymer liquid crystals have been reported by several authors. Shimamura, White and Fellers [216] were the first to document the distinct morphological differences between the skin and the core of polymer liquid crystals. Shimamura et al. examined the extrudates and frozen section of the capillary reservior from HPC extruded in an Instron capillary rheometer. Microtomed sections of the reservior, observed under SEM, revealed the surface had a fine fibrillar 'texture'. The core exhibited a coarser particulate type 'texture'. Extruded filaments examined by WAXD and SEM indicated the skin layer was more oriented and fibrillar than the core section.

Morgan and coworkers [170] examined the morphology of dry-jet wet spun PPTA fibers. These fibers also exhibited a skin-core type morphology. The skin layer, as examined by SEM fracture topology, was concluded to be 0.1 micron to 1 micron thick and have a fibrillar crystalline structure. The core was observed to be composed of 60 nm wide

lamallar blocks of crystalline fibrils with defect layers every 200 nm to 250 nm along the fiber axis. These defect layers were assumed to result from concentrations of the chain ends of the PPTA macromolecules. Unlike the core, the skin layer was assumed to have a random chain end distribution.

Panar and coworkers [183] also examined the skin and core morphology of dry-jet wet spun PPTA fibers. SEM photomicrographs of etched PPTA fibers suggested that the core was composed of fibrillar bundles 600 nm wide joined by tie fibrils to adjacent bundles. Each fibril appeared to be composed of ordered 35 nm thick lamellae stacked along the fibril length. The banded structure reported by Dobb et al. was observed to be superimposed on the fibrillar bundles. The fibrillar bundles were assumed to be packed in the pleated sheet structure within the core. The skin was assumed to be composed of a more continuous fibrillar structure than the core.

Joseph, Wilkes and Baird [125,126] observed morphological differences between the skin and core sections in POB/PET 60/40 copolyesters. Microtomed sections of injection molded plaques were examined by SEM and WAXD. The morphology of the skin and core differed, depending on the molding temperature. At low molding temperatures (235^{o}C), crystallites composed of a POB rich phase with dimensions of 2 microns to 10 microns were observed in

fractured samples. At high molding temperatures (260°C to 280°C) these crystallites were not observed. At 235°C the topology was a fine, grainy type structure, whereas at 280°C the topology was that of a coarse fibrillar structure. Analyses of the skin sections by electron spectroscopy indicated that the layers were composed mainly of the POB rich phase. Analyses of the core sections indicated that the PET rich phase was the major component. Comparisions of WAXD patterns of the skin and core sections indicated the skin had higher molecular orientation than the core. Joseph et al. explained the separation of the two phases in the skin and core layers as a difference in viscosities between the two phases. The POB rich phase migrated to the skin layers because it had a lower viscosity than the PET rich phase.

CHAPTER III

EXPERIMENTAL

1. MATERIALS

A. Polymers

Polymers examined in this research were hydroxypropyl cellulose (HPC), ethyl cellulose (EC), poly(p-benzamide) (PBA), 60/40 poly(p-oxybenzoate-co-ethylene terephthalate) (POB/PET), poly(p-oxybenzoate) (POB), and polystyrene (PS).

HPC was obtained in the form of a granular white powder under the tradename Klucel®, type E, from Hercules, Inc. This cellulose ether had been prepared by a reaction of alkali cellulose and propylene oxide. This polymer had a nominal weight average molecular weight ($\bar{M}_w$) of 60,000 g mol^{-1}, an average degree of substitution (DS) of 3.0, and an average molecular substitution (MS) of 4.0 [44].

EC was obtained as a granular white powder from Dow Chemical company under the tradename Ethocel®. The cellulose ether had been prepared by reacting alkali cellulose with ethylene chloride. This polymer had a number average molecular weight ($\bar{M}_n$) of 24,000 g mol^{-1}, and ethoxy content of 48%, and a degree of substitution (DS) of 2.5 [70].

PBA was obtained in the form of coarse, yellow-brown chips as synthesized by Harwood [106]. This aromatic polyamide was synthesized from p-aminobenzoic acid, using a solution polymerization process. This polymer had a weight average molecular weight ($\bar{M}_w$) of 13,000 g mol^{-1}.

POB/PET 60/40 was obtained in the form of white pellets from the Tennessee Eastman Company. This polyester was prepared by high temperature melt polymerization of 60 mol% p-acetoxybenzoic acid and 40 mol% poly(ethylene terephthalate). The procedure was described by Jackson and Kuhfuss [120]. The weight average molecular weight was not reported, however the intrinsic viscosity (I.V.) was reported to be 0.6.

POB was obtained as a tan colored powder from the Carborundum company under the tradename Ekonel T101®. This polymer was prepared by high temperature melt polymerization of p-acetoxybenzoic acid. The procedure was described by Economy et al. [77]. The number average molecular weight ($\bar{M}_n$) was reported to be 20,000 g mol^{-1}.

PS was obtained in the form of clear pellets from the Dow Chemical company under the tradename Dow Styron 678U®. This polystyrene had a weight average molecular weight ($\bar{M}_w$) of 214,000 g mol^{-1} and had a molecular weight distribution ($\bar{M}_w/\bar{M}_n$) of 2.6 [152].

B. Solvents

Distilled water (W) was used as obtained from a water still without further purification.

Formic acid (FA) was obtained in the form of a 90% solution in water from the Fisher Scientific company. It was used without further purification.

Toluene (T) was obtained in the form of a reagent grade solvent from the Fisher Scientific company. It was used without further purification.

N,N dimethylacetamide (DMA) was obtained in the form of a purified grade from Pfaltz and Bauer, Inc. It was dried over molecular sieves prior to use. A solution of 3 wt% lithium chloride, LiCl (Fisher Scientific), in DMA was prepared by dissolving 30 g of vaccuum dried LiCl powder with hot DMA. The DMA and LiCl were mixed, until dissolved, at 70°C in a 1000 ml erlenmeyer flask using a combination hot plate/magnetic stirrer. The 1 kg of solution was allowed to cool and was stored in a sealed dark bottle prior to use.

2. SAMPLE PREPARATION

A. Solutions

Concentrated polymer solutions were prepared in 200 g batches on the basis of weight percent (wt%) polymer in the solution. Amounts of polymer and solvent calculated

to give a certain weight percent concentration were weighed in 500 ml beakers on an Ohaus® two pan balance to the nearest 0.1 g. The weighed polymer was transferred to an 8 oz glass Oster® blending jar. The weighed solvent was then added to the jar. A stainless steel set of blades, or Oster® processing unit, and a 2 mm thick teflon gasket were placed on top of the blending jar and secured with teflon tape. A phenolic cap was used to seal the jar. The sealed blending jar was then inverted and placed on a mixing stand. The mixing stand consisted of a one horse-power, General Electric continuous duty electric motor equipped with a mixing adapter and mounted in a Unistrut® frame. The duration of the mixing was for four 15 minute intervals. Between each interval, the jar was removed and agitated several times, then replaced on the mixing stand. After the dissolution was observed, the contents of the blending jar were transferred to a 1000 ml beaker and placed in a vaccuum chamber. The vaccuum chamber was evacuated to remove air entrained in the solution during mixing. After deaeration, the solution was placed in a glass jar, labeled and sealed until used. Solutions prepared by this method were

1. hydroxypropyl cellulose in water (HPC/W): 10 wt%, 20 wt%, 30 wt%, 40 wt%, 50 wt%, and 60 wt%,

2. hydroxypropyl cellulose in formic acid (HPC/FA): 10 wt%, 20 wt%, 30 wt%, 40 wt%, 50 wt% and 60 wt%,

3. ethyl cellulose in formic acid (EC/FA): 10 wt%, 20 wt%, 30 wt%, 40 wt%, 50 wt%, and 60 wt%,

4. poly(p-benzamide) in N,N'dimethylacetamide with 3 wt% LiCl (PBA/DMA): 3 wt%, 6 wt%, 8 wt%, 10 wt%, and 12 wt%, and

5. polystyrene in toluene (PS/T): 10 wt%, 20 wt%, 30 wt%, 40 wt%, 50 wt%, and 60 wt%.

B. Bulk Polymers, Sheets and Films

Bulk polymers were used in the form received (pellets or powders), or in the forms of compression molded sheets and thin films. Prior to use or compression molding, the polymers were dried in 200 g batches in a vaccuum oven for 24 hours. HPC and EC were dried at 80°C, while POB/PET 60/40 and POB were dried at 130°C. These polymers were placed in nitrogen purged jars and sealed until used.

Sheets and thin films of the polymers were prepared by hot compression molding on a Wabash 24 ton hydraulic press, equipped with heated 12 inch square platens. Sheets for rheological studies were prepared by placing a mound of dried polymer pellets or powder on a 10 inch square sheet of aluminum foil or on a bare 10 inch square stainless steel photographic plate. The sheet or foil was placed on the bottom platen of the hydraulic press. An aluminum frame spacer, with frame dimensions of 10 inch square by 1 mm thick, was placed around the mound on the

foil or plate. A second plate or foil sheet was placed on top of the spacer and mound. The gap between the top and bottom platens of the press was reduced until the covering foil sheet or plate contacted the top platen. The polymer was allowed to preheat at the pressing temperature for 2 minutes, then the lower platen was slowly raised to compress the melt. At full compression, a force of 12 tons was maintained for a duration of 1 minute. The bottom platen was then lowered and the plates or foil sheets removed. In the case of EC, the foil sheets containing the polymeric sheet were allowed to air cool. In the case of POB/PET 60/40, an ice water quench bath was used to cool the plates. The POB powder was compression sintered between photographic plates and allowed to air cool after the plates were removed from the press. Thin film samples of HPC, EC, and POB/PET 60/40 were prepared by placing a small of amount of polymer on a sheet of Kapton® polyimide film, covering with a second sheet and placing them on the bottom platen of the hydraulic press. The heating and compression step were the same as described before. The resultant polymer films were allowed to air cool after removal from the press. The HPC and EC polymers were pressed into 0.2 mm thick films, while the POB/PET 60/40 polymer was pressed into 0.02 mm thick films. Pressing temperatures for fabricating sheets and films were: 160^{o}C

for HPC, 180°C for EC, 240°C for POB/PET 60/40, and 290°C for POB.

Specimens for cone and plate rheological measurements were prepared by cutting the 1 mm thick compression molded sheets into 1 inch squares using a razor edge cutting tool. The cut squares were dried under vaccuum and stored in a desicator prior to use. Thin film specimens for optical microscopy studies were prepared by cutting the larger films into 1 cm long by 0.5 cm wide sections, then drying the sections under vaccuum, and finally storing the samples in a dessicator.

C. Fibers

Fibers were melt spun from POB/PET 60/40 pellets placed in Merz-Colwell Instron capillary rheometer. Two spinning setups were used for preparing the fibers. The first setup, used for nonisothermal melt spinning, employed a conventional capillary die with an orifice diameter of 0.74 mm and a length to diameter (L/D) ratio of 50. The second setup, used for isothermal melt spinning employed a capillary die of the same dimensions, but designed to fit into the upper part of an isothermal chamber having a 2.5 cm heated zone beneath the die exit. Diagrams illustrating the two setups are shown as Figures 6 and 7. In each setup, fibers were extruded into a water bath before being wound on a take-up roll. In the first

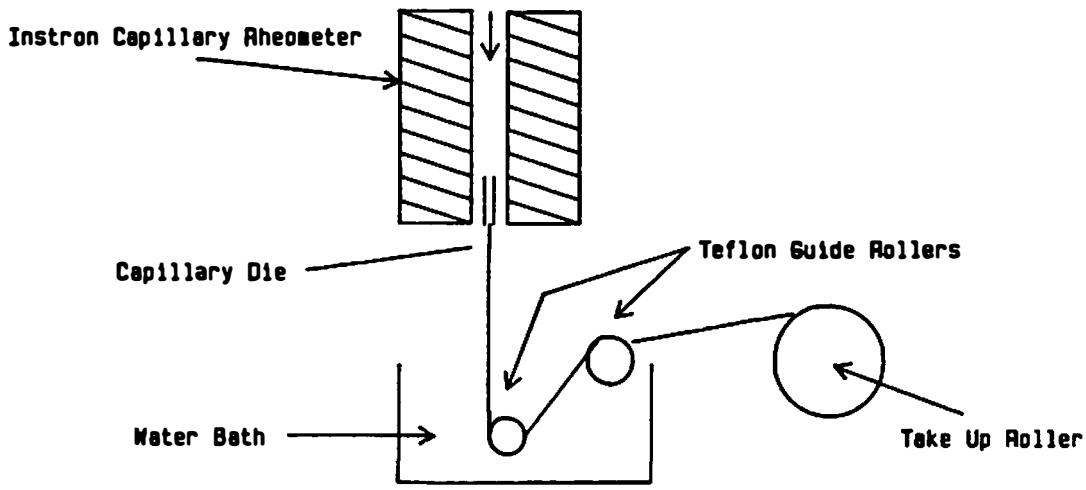

Figure 6. Diagram Illustrating the Nonisothermal Melt Spinning Setup for POB/PET 60/40 Fibers.

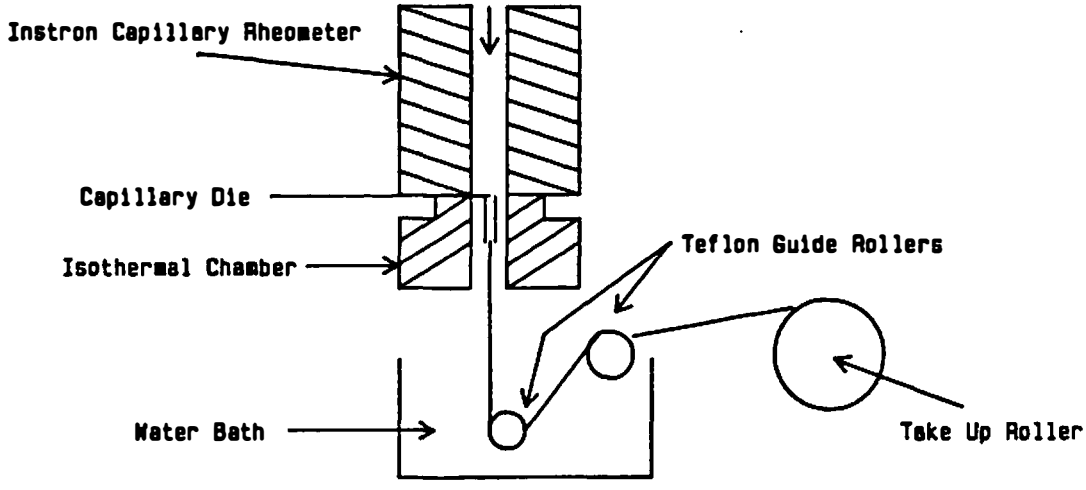

Figure 7. Diagram Illustrating the Isothermal Melt Spinning Setup of POB/PET 60/40 Fibers.

setup, the water bath was located about 2 cm beneath the die. In the second setup, the water bath was located about 2 cm beneath the isothermal chamber. Fibers were spun at three melt temperatures: 240°C, 260°C, and 270°C. The temperature of the isothermal chamber was also maintained at the selected melt spinning temperatures. Four extrusion rates in the range of 0.21 m/min to 2.1 m/min were used. Fibers were wound onto a 7.3 cm diameter take-up roll attached to a variable speed electric motor. Constant drawdown ratios of 50, 100, 200, and 500 were maintained at each extrusion rate by selecting an appropriate take-up velocity in the 10.5 m/min to 425 m/min range.

3. CHARACTERIZATION METHODS

A. Differential Scanning Calorimetry

Thermal transitions in HPC, EC, and POB/PET 60/40 were characterized by using a Perkin Elmer DSCII differential scanning calorimeter. Samples, weighing 8 mg to 10 mg, were cut from compression molded films and placed into sample pans and sealed. Pure metal reference standards of indium (T_m = 156°C), tin (T_m = 231°C), and lead (T_m = 327°C) were used to calibrate the temperature ranges used. HPC was characterized over the temperature range of 50°C to 250°C, EC over the range of 50°C to 300°C, and POB/PET 60/40 over the range of 50°C to 450°C. The heating or scanning rate in each case was 20°C per minute.

B. Polarized Optical Microscopy

The optical tranmissivity between crossed polars of the polymer solutions and melts was determined on a photodetector equipped, Leitz Ortholux polarized optical microscope. The detector was an International Light SE 010 solid state silicon type photodetector connected to an International Light IL 700 research radiometer. The radiometer provided the photodetector's power and readout capability. The radiometer's output signal was recorded on a Heath SR-205 single pen chart recorder.

Solution samples were placed on cavity slides, possessing a single cavity with dimensions 10 mm diameter by 0.5 mm deep. The samples were examined mainly by optical observation at 100 X magnification. The transmission characteristics were only qualitatively noted, since the objective was to determine which sample concentrations were isotropic and which were liquid crystalline.

Quantitative transmitted intensity measurements on molten polymer samples were determined from films heated on microscope hot stages. Polymer film specimens were placed on clean, dry microscope slides and covered with a 22 mm square glass cover slip. The cover slips were set in place with a high temperature resistant cement. HPC and EC films were examined using a microscope hot stage capable to 300^{o}C, whereas the POB/PET 60/40 films were

examined using a 450°C capable hot stage. Both stages were controlled by an Electromax temperature controller in conjunction with a ramp function voltage divider. This system provided a heating rate of 3°C per minute.

C. Cone and Plate Rheometry

Measurements of shear viscosity, shear stress, and the primary normal stress difference were made on a cone and plate equipped, Rheometrics Mechanical Spectrometer (RMS), model 7200. A block diagram of the RMS 7200 [198] is shown in Figure 8.

Solution samples were examined on the RMS 7200 employing a specially designed cone and plate test fixture set, illustrated in Figure 9. The design of this test fixture set provided an oil filled sealing enclosure around the sample when the gap was set. This seal isolated the sample from the outside air and minimized concentration changes due to solvent evaporation. The characteristics of this cone and plate test fixture set were cone angle = 0.1 rad, cone and plate diameters = 2.54 cm, and gap setting = 0.125 mm. Measurements were made at room temperature, 26°C.

Molten polymer samples were examined using the standard cone and plate test fixture set [199], illustrated in Figure 10. Characteristics of the standard test

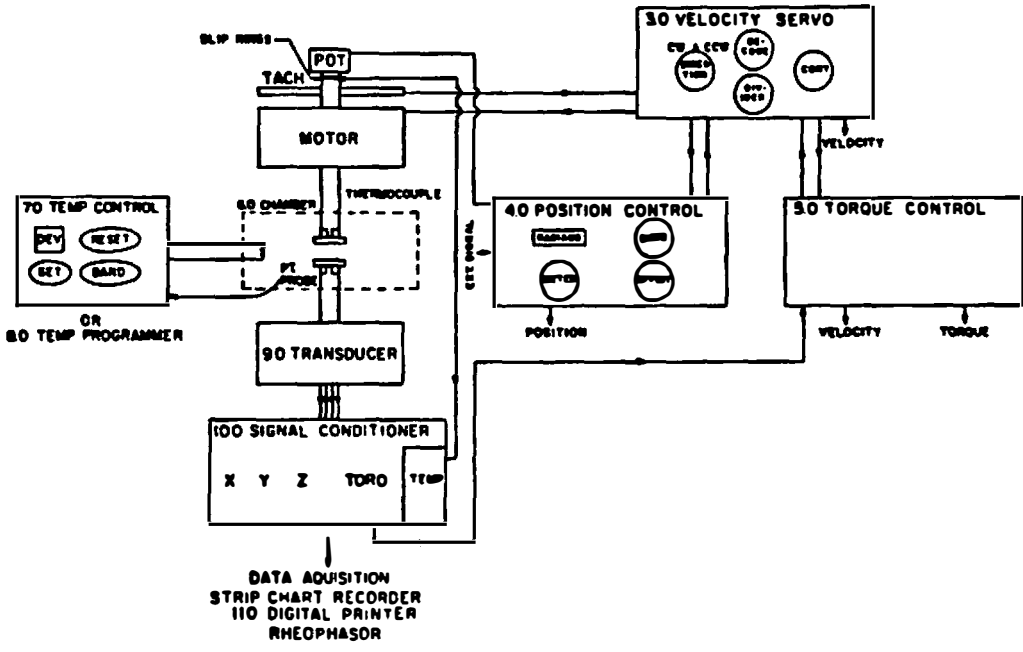

Figure 8. Block Diagram of the Rheometrics Mechanical Spectrometer Model 7200 Used for Cone and Plate Measurements.

Source: Rheometrics Mechanical Spectrometer model 7200 Electronics Manual, Rheometrics,Inc. (1974)

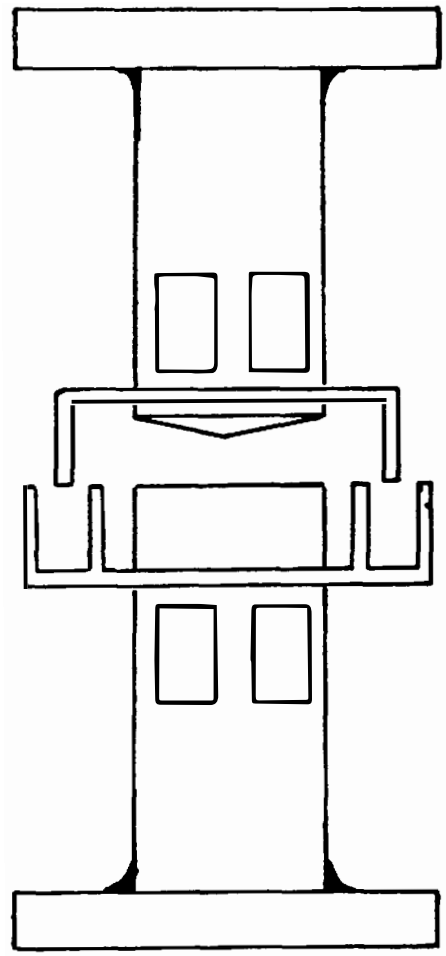

Figure 9. Diagram Illustrating a Specially Designed Cone and Plate Test Fixture Used for Study of Polymer Solutions.

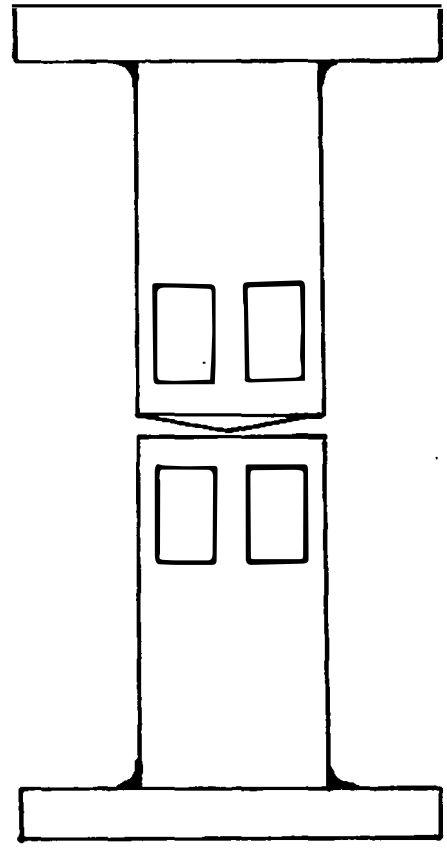

Figure 10. Diagram Illustrating the Standard 2.5 cm Cone and Plate Test Fixture for Study of Polymer Melts.

Source: Rheometrics RMS 7200 Test Fixture Description Brochure, Rheometrics, Inc. (1976)

fixture set were cone angle = 0.1 rad, cone and plate diameters = 2.54 cm, and gap setting = 0.05 mm. A nitrogen purged, heated environment chamber was placed around the standard test fixture set to maintain the melt temperature in an non-oxidative atmosphere. Rheological measurements were conducted on EC in the 180°C to 210°C temperature range, and on POB/PET 60/40 in the 190°C to 340°C temperature range. Shear rates in the range of 0.1 s^{-1} to 500 s^{-1} were used for measurements on polymer solutions, while shear rates in the 0.01 s^{-1} to 1 s^{-1} range were used for measurements on polymer melts. At each shear rate used, force traces of the torque, or rotational drag on the plate, and the normal force, or force pushing the cone and plate apart, were recorded. Based on the dimensions of the cone and plate sets used, the shear stress, σ_{12}, and the primary normal stress difference, N_1, were obtained by the equations

$$\sigma_{12}\ (Pa) = 24(kg\ g^{-1}\ m^{-1}\ cm^{-1})\ M \qquad (3.7)$$

$$N_1\ (Pa) = 40(kg\ g^{-1}\ m^{-1})\ F_z \qquad (3.8)$$

where M is the torque in units of g-cm, and F_z is the normal force in units of g. Shear viscosities were determined by dividing the shear stress by the shear rate at which it was measured.

D. Capillary Rheometry

Rheological measurements at high shear rates were made on POB/PET 60/40 melts using a Merz-Colwell Instron capillary rheometer. Capillary dies with an orifice diameter of 0.074 cm and length to diameter ratios of 10, 30, 50, and 70 were used. Shear rates in the range 1 s^{-1} to 1000 s^{-1} were used over a temperature range of 190°C to 340°C. Weissenberg corrections were made to the die wall shear rate. Bagley pressure drop corrections were made to the raw data.

Extrudate swell measurements (d/D) were made on the frozen extrudates collected at the die exit. A 30 L/D die was used at a high fixed apparent shear rate of 154 s^{-1} to produce the extrudates. Extrudates were collected at temperatures of 190°C, 210°C, 240°C, 250°C, 260°C, 280°C, 300°C, 320°C, and 340°C. Diameters of the extrudates were determined by measurement with a precision micrometer.

E. Wide Angle X-Ray Diffraction Analysis

Wide angle x-ray diffraction (WAXD) scans were made using a General Electric XRD5/F x-ray counter diffractometer in conjunction with a single crystal orienter. The diffractometer employed a copper target x-ray generator tube and a nickel foil filter to produce a beam wavelength of 0.1542 nm. A sodium iodide type scintillation counter, rotated on the orienter table by an

electric motor, was used to collect the intensity data or scintillation counts at each 2θ scattering angle. The signal output of the scintillation counter was amplified and electronically filtered using Ortec counter and pulse height discriminator modules. The output signal of the modules was directed to a single pen strip chart recorder to record the intensity verus scattering angle trace. A schematic of the single crystal orienter setup is shown in Figure 11.

Fiber orientation measurements were conducted using the same counter diffractometer and single crystal orienter, as described earlier, in conjunction with a Digital Equipment PDP 15/35 minicomputer. An Ortec interface controller and digital to analog converters in the PDP minicomputer were used to collect the intensity data at various chi (χ) angle positions of the mounted fiber specimen. A real time Fortran program, written by Professor J.E. Spruiell, instructed the minicomputer to position the sample, collect the intensity data, process the data, and generate the average $\cos^2\chi$ values used to determine the orientation factor. The (006) reflection plane was used for the POB/PET 60/40 fiber samples c-axis fiber orientation measurements.

A brass sample holder, illustrated in Figure 12, was used to mount the POB/PET 60/40 fibers for fiber orientation measurements. Fibers were wound horizontally in a

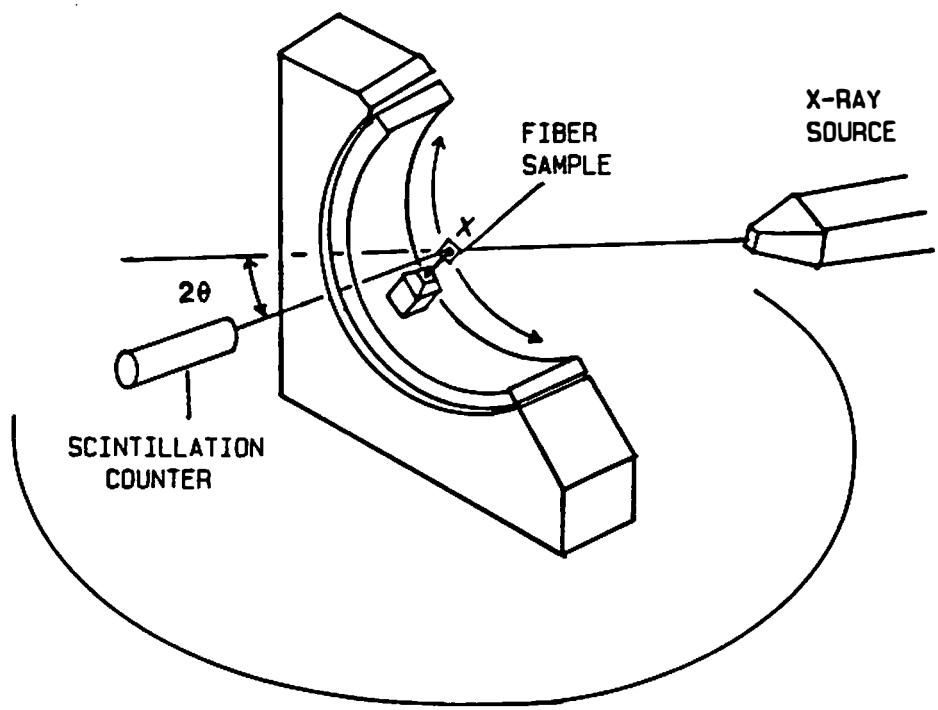

Figure 11. Schematic Diagram of the Single Crystal Orienter Used for WAXD-Based Crystalline Orientation Measurements of POB/PET 60/40 Fibers.

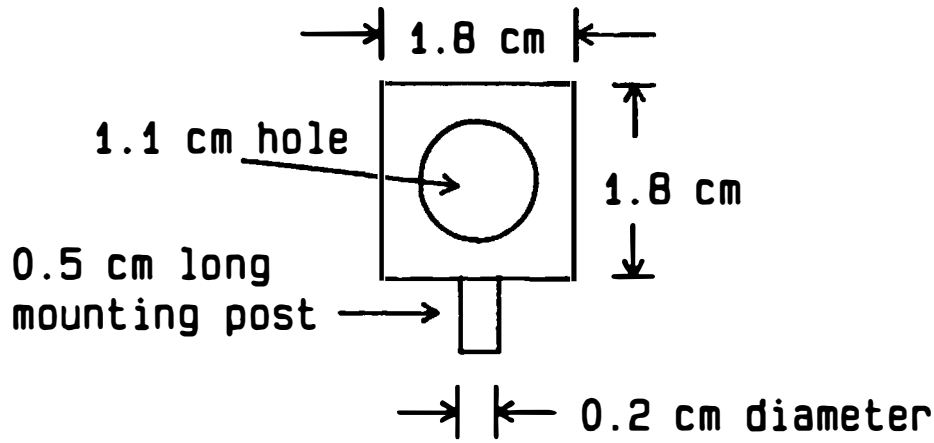

Figure 12. Diagram of Brass Holder Used to Mount POB/PET 60/40 Fibers for Crystalline Orientation Measurements.

parallel arrangement on the brass sample holder. Several layers were used to provide a 1 mm thick specimen for fiber orientation measurements. Diffractometer scans of the POB homopolymer sheet and POB/PET 60/40 films were also made using samples taped to the brass sample holders.

F. Tensile Property Measurements

Determinations of the tensile strength, initial modulus, and percent elongation were made on selected POB/PET 60/40 fiber specimens by using a Instron Tensile Tester, model 1122. A 500 g load cell and pneumatic clamps with a clamping force of 15 lbs were employed in testing the samples. An extension rate, or crosshead speed, of 2 mm/min was used in conjunction with a chart recorder speed of 200 mm/min.

Samples were prepared by mounting single filaments on a 1.25 inch wide by 3 inch long card possessing a 1 inch square center cut out. This provided a gage length of 2.54 cm. Filament diameters were determined at 100 X magnification with an optical microscope employing a stage micrometer.

CHAPTER IV

RESULTS AND DISCUSSION

1. QUIESCENT CHARACTERIZATION

A. Solutions

Results

Solutions of HPC/W, HPC/FA, EC/FA and PBA/DMA were all examined by polarized light microscopy to identify qualitatively the specific concentrations exhibiting liquid crystalline behavior. Solutions containing up to 30 wt% HPC/W, 20 wt% HPC/FA, 20 wt% EC/FA, or 6 wt% PBA/DMA showed no light transmission between crossed polars. Only an optically dark field was observed at these concentrations. Solutions containing more than 40 wt% HPC/W, 30 wt% HPC/FA, 30 wt% EC/FA or 8 wt% PBA/DMA transmitted light between crossed polarizers. Optical observations under typical 'darkfield' conditions revealed the presence of bright and dark regions in 40 wt% HPC/W, 30 wt% HPC/FA, 30 wt% EC/FA and 8 wt% PBA/DMA. Higher concentrations of HPC/W, HPC/FA, EC/FA, and PBA/DMA exhibited optically bright fields under crossed polars as well as birefringent colors.

Discussion

Concentrations below 40 wt% HPC/W, 30 wt% HPC/FA, 30 wt% EC/FA, or 8 wt% PBA/DMA exhibited the optical behavior of isotropic polymer solutions. Solutions at the intermediate concentrations of 40 wt% HPC/W, 30 wt% HPC/FA, 30 wt% EC/FA, and 8 wt% PBA/DMA showed optical behavior characteristic of biphasic solutions containing discontinuous anisotropic phase regions. The bright regions corresponded to the anisotropic phase regions, whereas the dark regions represented observable portions of the continuous isotropic phase. Solutions at even higher concentrations exhibited optical characteristics of single phase, anisotropic solutions. These solutions were fully light transmitting under normal 'darkfield' conditions. Spherulitic 'domains' were observed in several of the more concentrated HPC and EC solutions. Birefringent colors were observed in all anisotropic HPC, EC and PBA solutions and appeared to result from the presence of 'polydomain' or 'multitextured' microstructures. These structures apparently cause position dependent diffraction and retardation of the transmitted light. This would give rise to the birefringent colors in the solutions when observed between crossed polars.

B. Melts

Results

Quantitative measurements of the transmitted light intensity between crossed polars, or 'darkfield' light transmissivity (DLT) were made on film samples of HPC, EC and POB/PET 60/40 with respect to temperature. Subsequent measurements of the thermal characteristics of these same polymers were obtained with differential scanning calorimetry (DSC). Figures 13 through 15 show composite plots of the DLT versus temperature trace along with the DSC versus temperature trace for each of the three polymers.

The composite plot of HPC, shown in Figure 13, exhibits the DSC and DLT traces obtained over a temperature range of 20°C to 250°C. The main feature of the DSC trace is a solitary, broad endothermic peak centered at 192°C. The apparent end points of this endotherm are at 174°C and 219°C, respectively. The DLT trace illustrates that both solid and molten forms of HPC transmit light under normal 'darkfield' conditions. Three significant aspects of the DLT trace are

1. a gradual monotonic increase in the transmitted intensity from 110°C to 180°C,

2. an apparent intensity maximum at 185°C, and

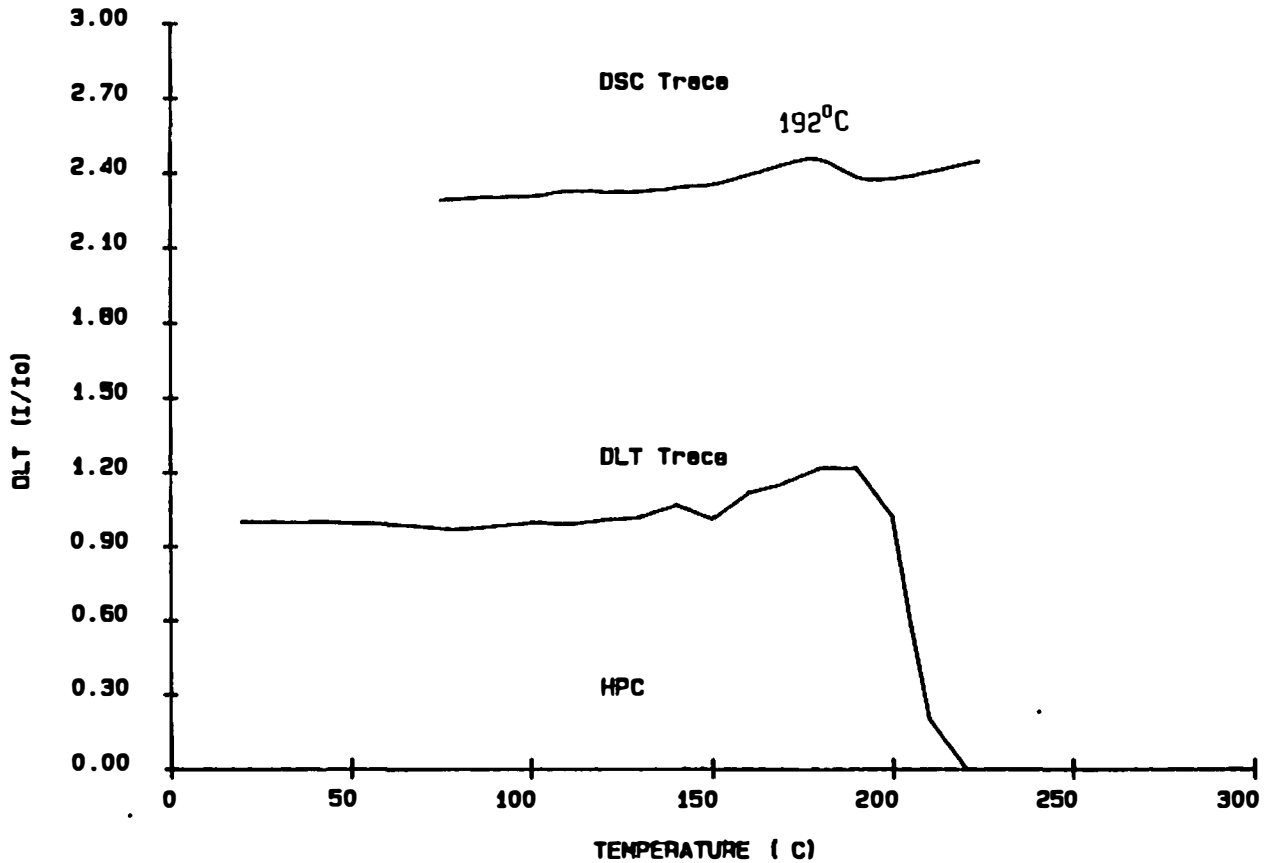

Figure 13. DSC and DLT Traces for HPC from 20°C to 250°C.

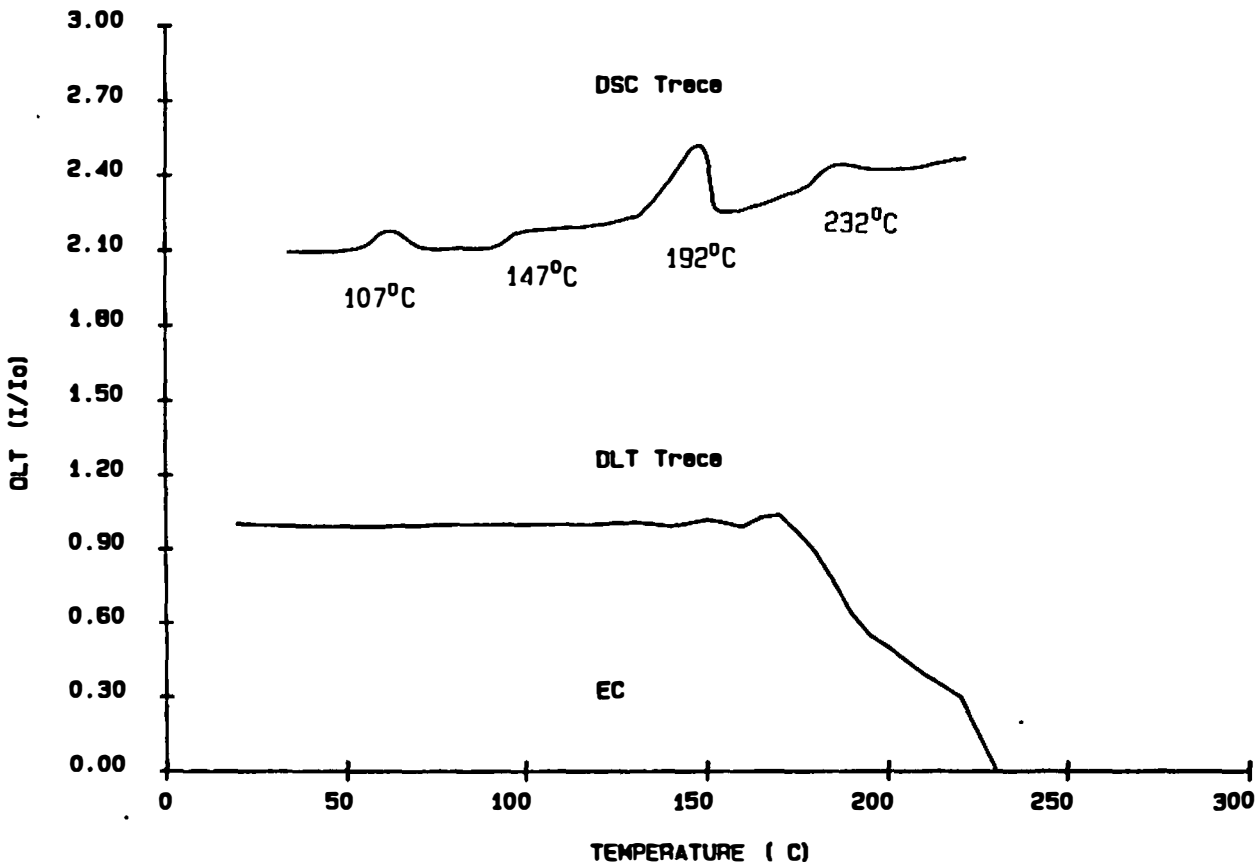

Figure 14. DSC and DLT Traces for EC from 20°C to 250°C.

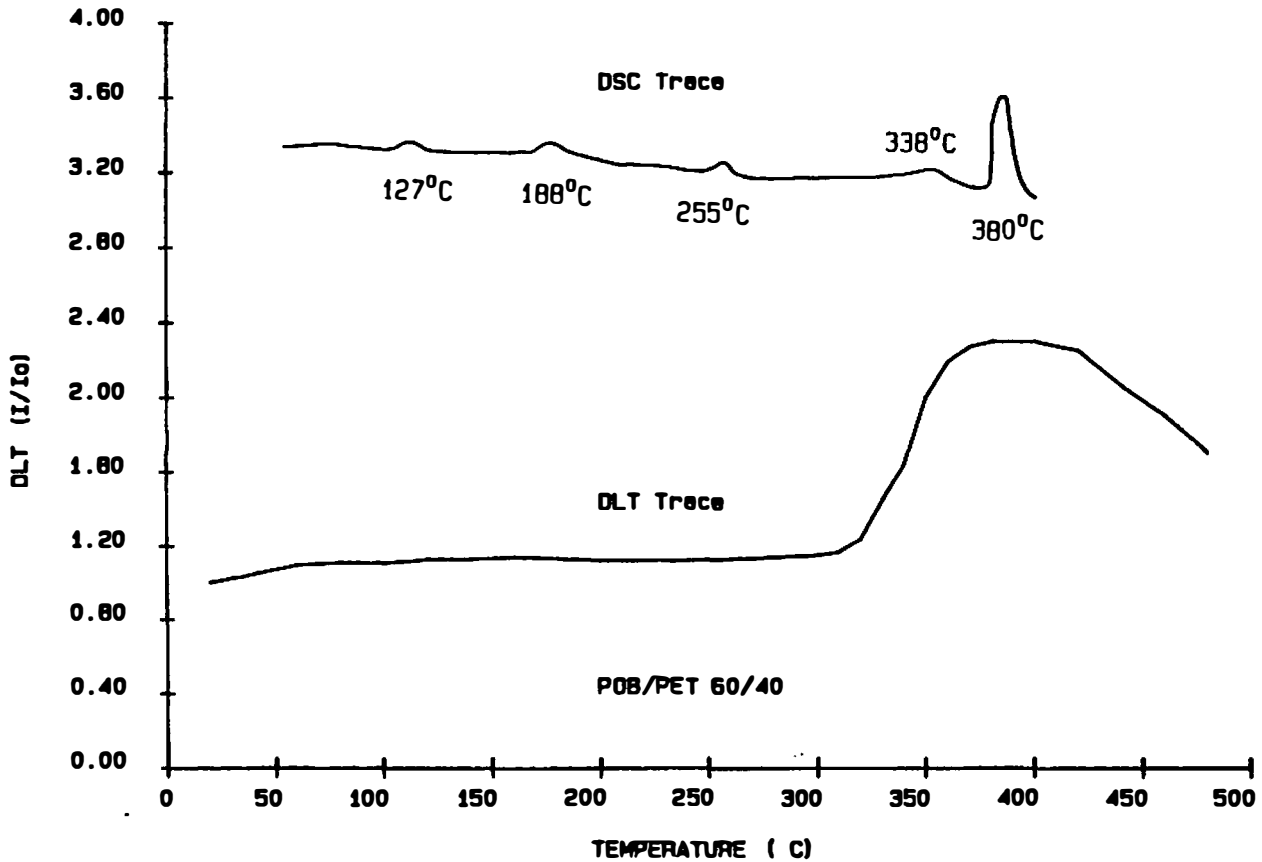

Figure 15. DSC and DLT Traces for POB/PET 60/40 from 20°C to 500°C.

3. a steep decline in the transmitted intensity from 200°C to 220°C. At 220°C the value of the transmitted intensity becomes zero.

In Figure 14, the DSC and DLT traces for EC are presented. These traces were obtained over a 20°C to 300°C temperature range. The DSC trace exhibits four transitions centered, respectively, at 107°C, 147°C, 192°C, and 232°C. The companion DLT trace shows that both solid and molten forms of EC, like HPC, transmitted light under crossed polarizers. The main features of the DLT trace are

1. a level value in the transmitted intensity from 20°C to 150°C,

2. a slight increase in the transmissivity from 150°C to 170°C,

3. a fairly steep decline in the transmissivity from 170°C to 200°C, and

4. a steeper decline in the transmitted intensity from 200°C to 230°C. At 230°C, the transmissivity becomes zero.

Figure 15 shows the composite plot of POB/PET 60/40. This plot shows the DSC and DLT traces taken over the temperature range of 20°C to 500°C. The DSC trace exhibits five endothermic transitions located at 127°C, 188°C, 255°C, 338°C, and 380°C. The DLT trace has four notable features:

1. a gradual curvilinear increase in the intensity between 20°C and 300°C,

2. a steep transmitted intensity increase from 300°C to 380°C,

3. an apparent transmissivity peak in the 380°C to 410°C region, and

4. a significant decline in the transmissivity above 410°C.

Discussion

The broad endotherm observed in the DSC trace for HPC in Figure 13 represents the caloric uptake in response to the liquid crystal to isotropic transition. Optical observations of the sample under 'darkfield' conditions indicate that a birefringent melt is formed above 160°C. Earlier microscopy studies on molten HPC films by Shimamura et al. [216] and Suto et al. [227] concluded that HPC existed as a liquid crystalline melt between 160°C and 205°C. The close correspondence of the endotherm with the transmissivity peak in the companion DLT trace is further evidence for assuming both represent the anisotropic to isotropic transition phenomenon. The DLT trace approaches a peak value at 185°C, a temperature before the endotherm's center point. The decay in the DLT trace from 195°C to 220°C corresponds to the decline of the DSC endotherm. At 220°C the end points of the DLT trace and the DSC endotherm correspond. The appearance of

the DLT peak just prior to the peak temperature of the endotherm suggests that a pretransitional ordering phenomenon takes place in the melt.

The DSC trace for EC in Figure 14 is more complicated than for HPC, since four distinct thermal transitions are observed. The first endotherm at 107°C is close to the vaporization temperature of water. This probably represents the loss of the water of crystallization. The second endotherm at 147°C occurs near the observed melting in the sample at 150°C. The presence of a fairly large endotherm at 192°C and a second small endotherm at 232°C suggests the presence of two concomitant liquid crystalline phases. The two step decline of the DLT trace from 170°C to 232°C seems to support this interpretation. The DLT trace shows a small intensity peak about 170°C, which can be associated with a pretransitional ordering phenomenon in the melt. Between 170°C and 200°C, the transmissivity declines about 40%. This may represent the transition of a first liquid crystalline phase. Between 200°C and 232°C, the transmissivity declines to zero. This may represent the transition of a second minor liquid crystalline phase. The reported polymorphic structure of solid EC films [81] may represent this solidified polymorphic liquid crystalline state.

The DSC trace for POB/PET 60/40 in Figure 15 can also be interpreted in terms of a polymorphic liquid

crystalline state. Recent investigations of POB/PET 60/40 by Sawyer [213], Joseph et al. [125,126] and Nicely [172] all suggest the copolyester contains two phases (1) a POB rich phase and (2) a PET rich phase. High resolution nuclear magnetic resonance (NMR) studies of POB/PET 60/40 melts suggest the POB rich phase is composed of 80 mol% POB units, principally in the form of randomly distributed dimer, trimer and tetramer POB sequences in the main chain [172]. These NMR studies also indicate the PET rich phase is composed of 35 mol% POB units, mainly in the form of randomly distributed single and dimer POB sequences [172].

Interpretation of the five DSC transitions was aided by several earlier DSC studies of POB/PET 60/40 reported in the literature. Menczel and Wunderlich [161] observed an endothermic inflection at 70°C and endotherms at 190°C and 250°C. Higher temperature endotherms were not reported. The endothermic inflection at 70°C was interpreted as the glass transition point of the PET rich phase. The endotherms at 190°C and 250°C were interpreted as the melting transitions of the PET and POB rich phases, respectively. Wissbrun [242] reported the locations of the transitions were affected by the copolyester's previous thermal history. Pellets and virgin polymer exhibited an endothermic inflection at 70°C and endotherms at 190°C to 200°C, and 240°C to 280°C. Quenched films showed endotherms at 130°C, 190°C and

230°C. Viney and Windle [234] reported an endothermic inflection at 70°C and endotherms at 190°C, 250°C, 340°C, and 420°C. The endothermic inflection at 70°C was interpreted as the glass transition of the PET rich phase. Based on optical observations of molten POB/PET 60/40, Viney and Windle assigned the endotherm at 190°C as a solid to smectic transition, the endotherm at 340°C as the smectic to nematic transition, and the endotherm at 420°C as the nematic to isotropic transition. The endotherm at 250°C could not be correlated with optical observations.

The most plausible interpretation of the DSC trace shown in Figure 15 (p. 150) can be made by careful evaluation of the factors gleaned from both thermal and molecular studies [119,125,126,172,213,234,242,244]. The endotherm at 127°C may represent some type of solid-solid transition in the POB rich phase. The endotherms at 188°C and 255°C correspond to the melting transitions of the PET and POB rich phases, respectively. The endotherms at 338°C and 380°C probably represent the nematic to isotropic transition points of the respective PET and POB rich phases.

The DLT trace exhibits a large, broad intensity peak corresponding to the pretransitional ordering phenomena of the two phases in POB/PET 60/40. The incompleteness of the intensity decay may represent the presence of residual high melting fragments of the POB rich phase. Jackson

[119] and Zachariades et al. [244] both reported that POB oligmers consisting of four or more repeat units degrade when heated above 400°C and do not become completely isotropic.

2. RHEOLOGICAL CHARACTERIZATION

A. Solutions

Results--Viscosity Behavior with Shear Rate

Solutions of 10 wt% to 60 wt% HPC/W, 10 wt% to 60 wt% HPC/FA, 10 wt% to 60 wt% EC/FA, and 3 wt% to 12 wt% PBA/DMA were all investigated by cone and plate rheometry. Comparative rheological measurements were conducted on 10 wt% to 60 wt% PS/T solutions, which were isotropic over the entire concentration range. The HPC/W, HPC/FA, EC/FA, and PBA/DMA solution ranged from isotropic at low concentrations to anisotropic at high concentrations. Plots of the shear viscosity versus shear rate data are shown in Figures 16 through 20.

Discussion--Viscosity Behavior with Shear Rate

An examination of the five viscosity plots reveals two contrasting features. The first contrast observed in the PS/T plot (Figure 20) and the HPC/W, HPC/FA, EC/FA and PBA/DMA plots (Figures 16 through 19) is the shapes of the viscosity curves. The PS/T plot shows a shear rate

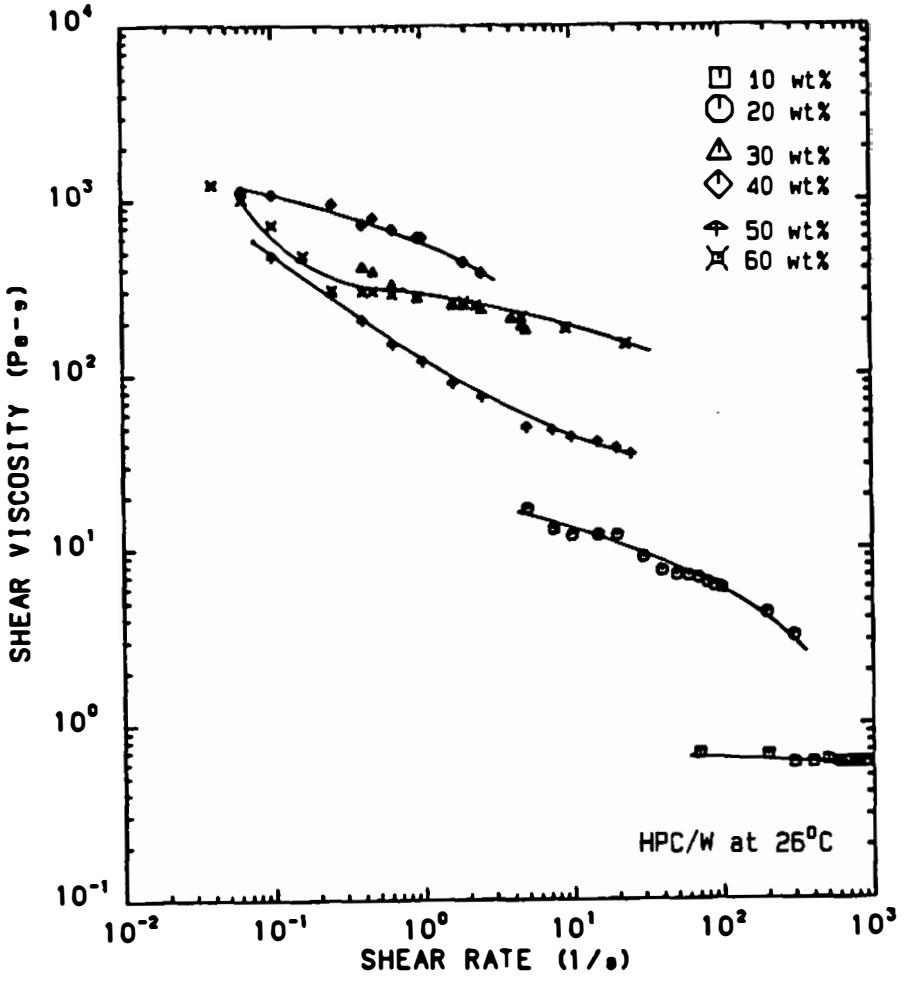

Figure 16. Viscosity Versus Shear Rate Plot of HPC/W solutions at 26°C.

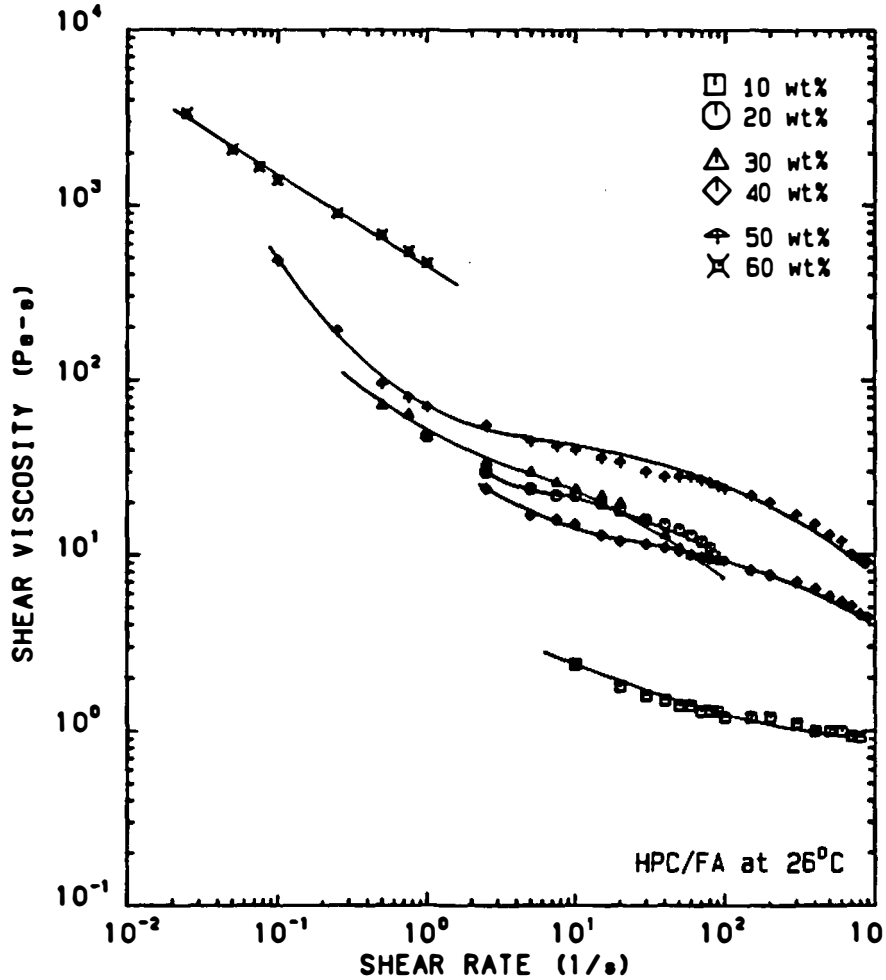

Figure 17. Viscosity Versus Shear Rate Plot of HPC/FA Solutions at 26°C.

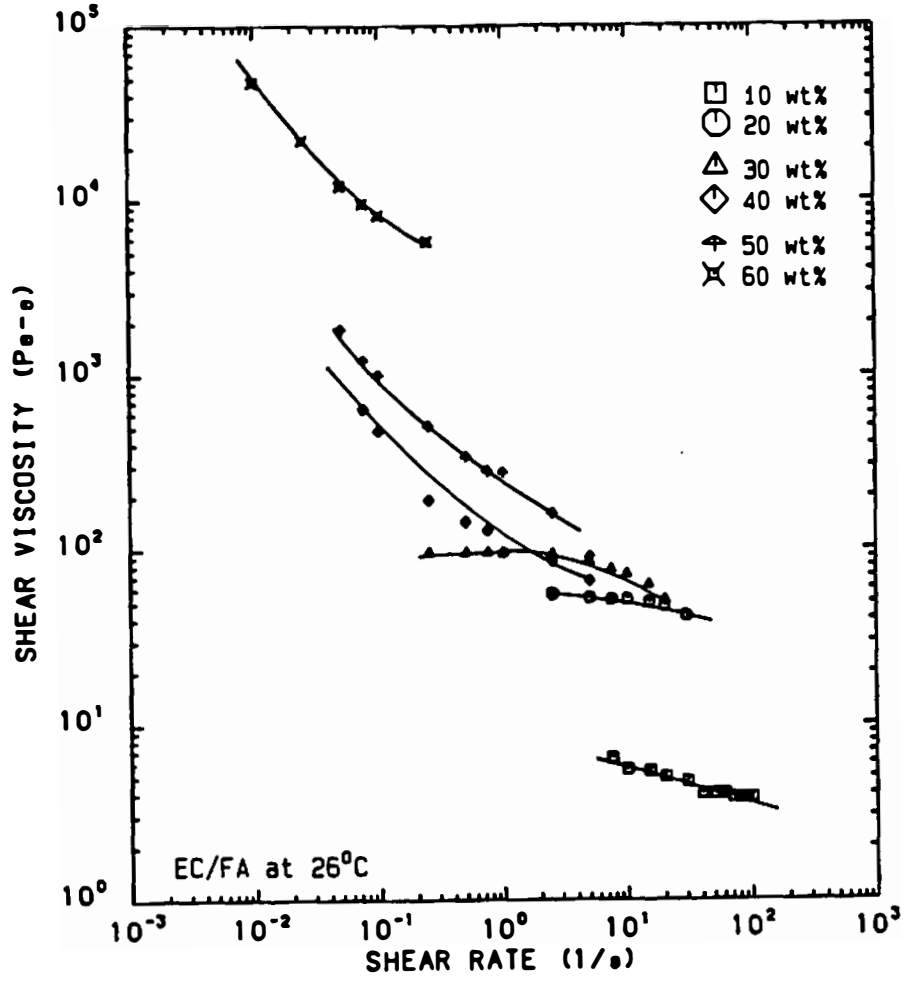

Figure 18. Viscosity Versus Shear Rate Plot of EC/FA Solutions at 26°C.

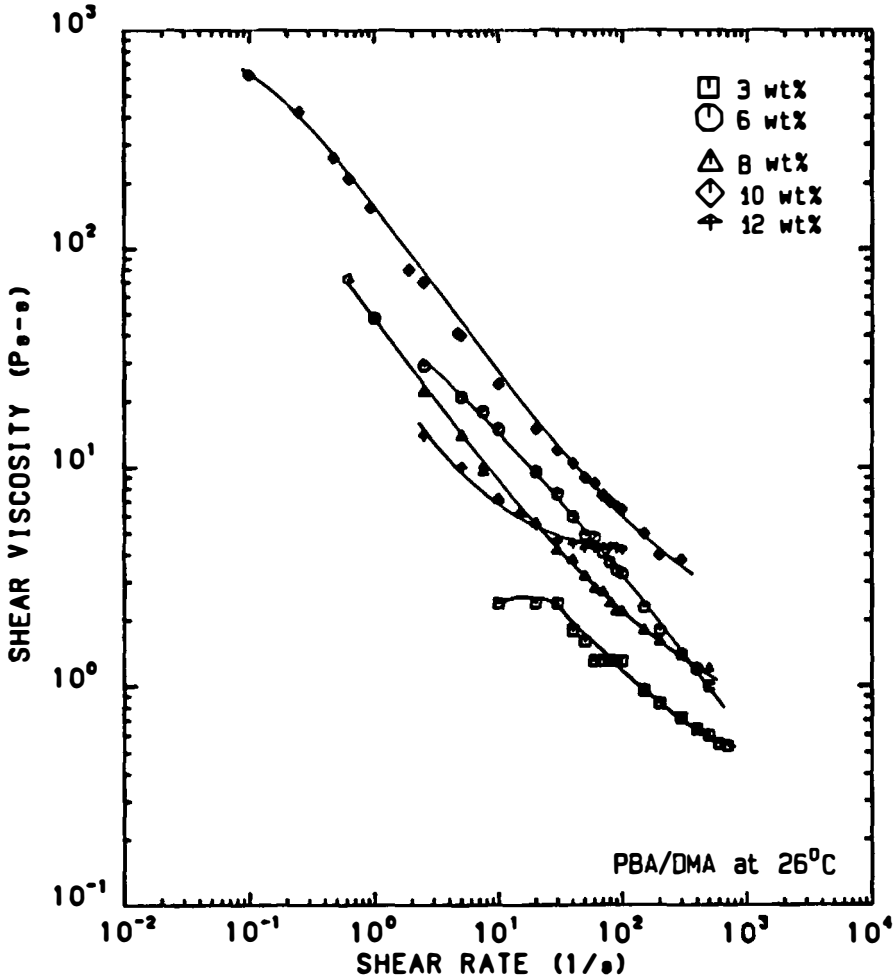

Figure 19. Viscosity Versus Shear Rate Plot of PBA/DMA Solutions at 26°C.

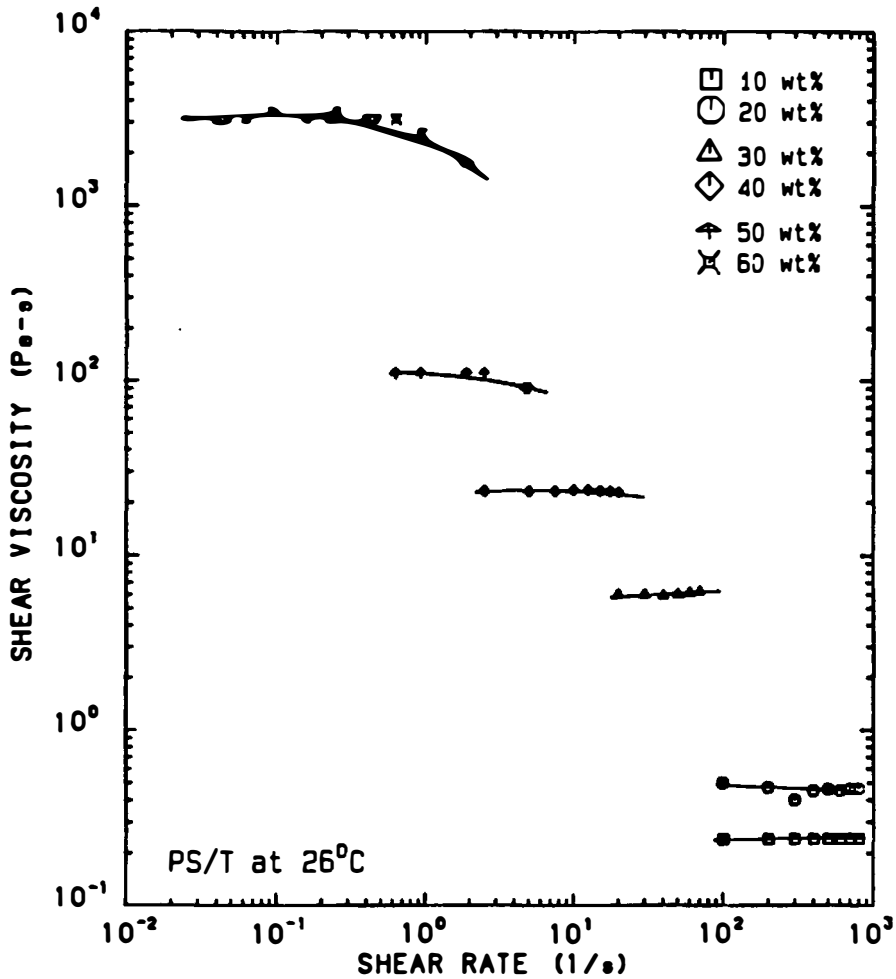

Figure 20. Viscosity Versus Shear Rate Plot of PS/T Solutions at 26°C.

independent or quasi-Newtonian viscosity response with shear rate up to concentrations of 40 wt%. At concentrations above 40 wt%, the viscosity shows quasi-Newtonian behavior at low shear rates and shear thinning behavior above 1 s^{-1}. The other four polymer solutions exhibit more pronounced shear thinning behavior in both isotropic and anisotropic solutions. The HPC and EC solutions only exhibit Newtonian or shear rate independent behavior at concentrations below 20 wt%. At concentrations above 20 wt% the solutions always exhibit some degree of shear thinning behavior. The anisotropic HPC and EC solutions exhibit pronounced pseudoplastic viscosity responses, even at low shear rates. The PBA/DMA solutions show noticeable shear thinning behavior at all concentrations investigated. With increasing PBA concentration, the solutions show pronounced psuedoplastic behavior at low shear rates.

The second contrast found between the isotropic PS/T solutions and the lyotropic polymer solutions was the relationship between viscosity and concentration. At a fixed shear rate, the PS/T plot (Figure 20) indicates a monotonic viscosity increase with respect to PS concentration. In contrast, plots of the four lyotropic polymer solutions (Figures 16-19, pp. 158-161) exhibit distinct inflection points in the viscosity-concentration relationship. These inflection points occur in the vicinity of the isotropic to anisotropic phase transition. In HPC/W

(Figure 16, p. 157) a viscosity maximum occurs at 40 wt% HPC. A viscosity minimum is observed at 50 wt% HPC. For HPC/FA (Figure 17, p. 158) the maximum occurs at 30 wt% HPC and the minimum occurs at 40 wt% HPC. In EC/FA solutions (Figure 18, p. 159) a single inflection point is observed at 30 wt% EC. Above 30 wt% polymer the viscosity begins to increase again. For the PBA/DMA solutions (Figure 19, p. 160) a viscosity maximum occurs at 10 wt% PBA. The locations of the viscosity maximum in HPC/W, HPC/W, EC/FA, and PBA/DMA solutions appear to be related to the rigidity of the respective solvated macromolecules. The HPC polymer chain forms a more extended conformer in formic acid (FA) than in water (W). This results in a lower critical concentration to form the anisotropic phase. The EC polymer chain appears to have a rigidity similar to HPC in formic acid. The PBA polymer chains are even more rigid than HPC or EC, since the former possesses a rigid aromatic backbone and the latter two polymers possess semiflexible glycosidic backbones. In PBA/DMA solutions the critical concentration is reduced to about 10 wt%.

Results--Viscosity Behavior with Shear Stress

Viscosity versus shear stress plots are presented in Figures 21 through 25 for HPC/W, HPC/FA, EC/FA and PS/T

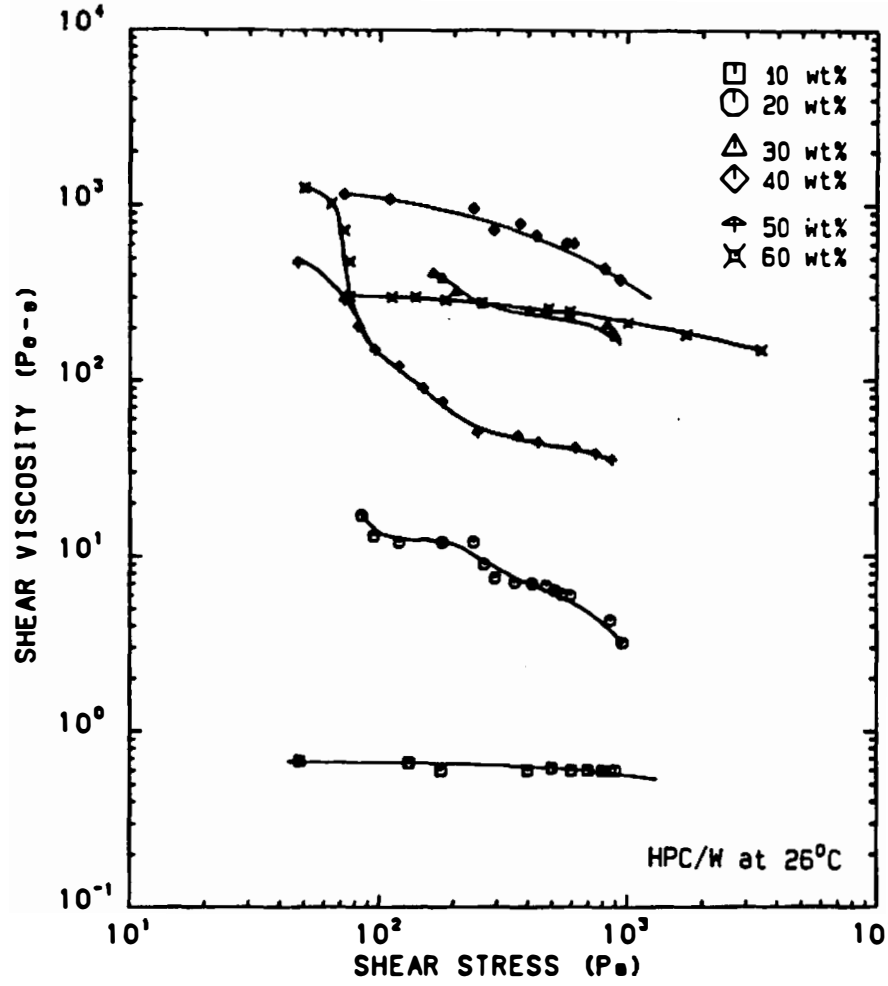

Figure 21. Viscosity Versus Shear Stress Plot of HPC/W Solutions at 26°C.

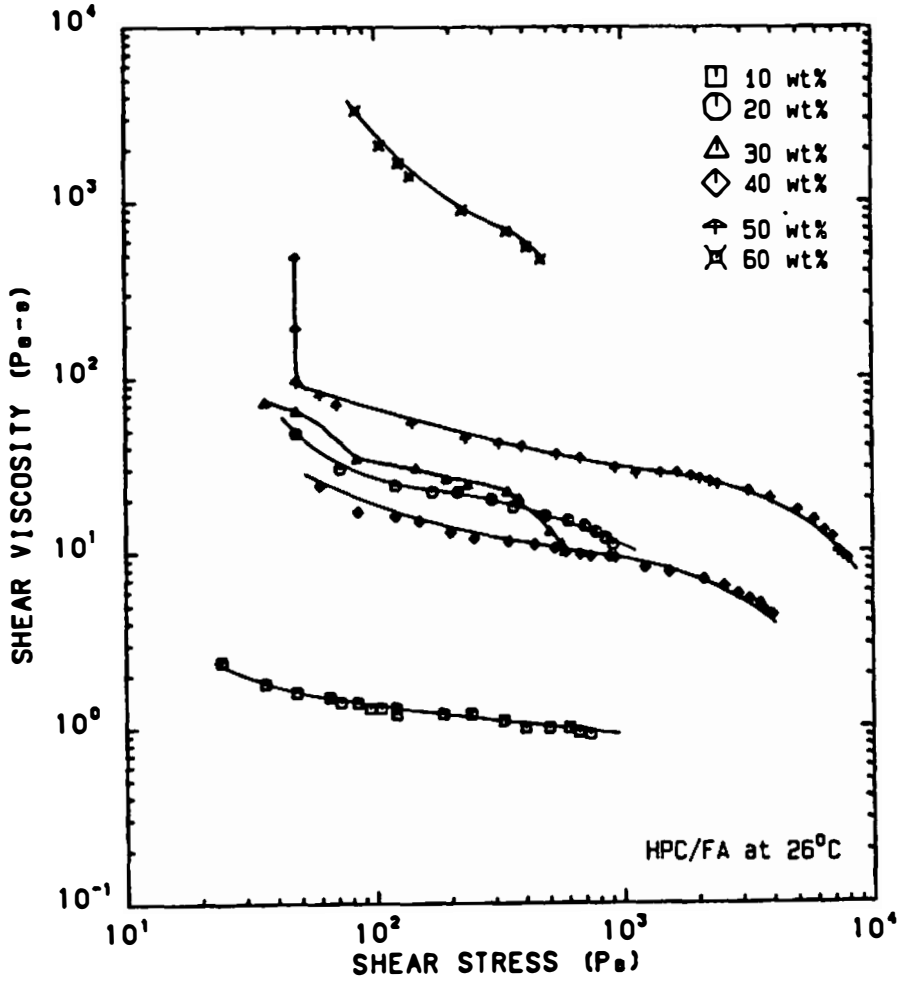

Figure 22. Viscosity Versus Shear Stress Plot of HPC/FA Solutions at 26°C.

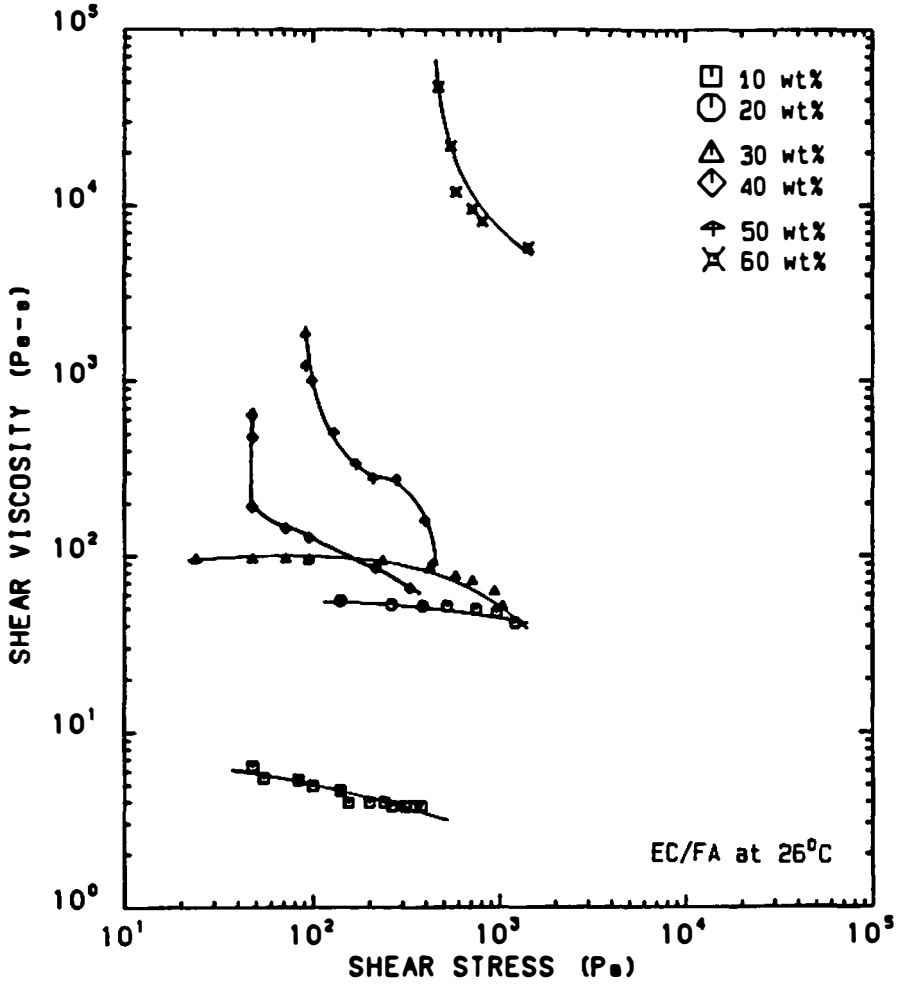

Figure 23. Viscosity Versus Shear Stress Plot of EC/FA Solutions at 26°C.

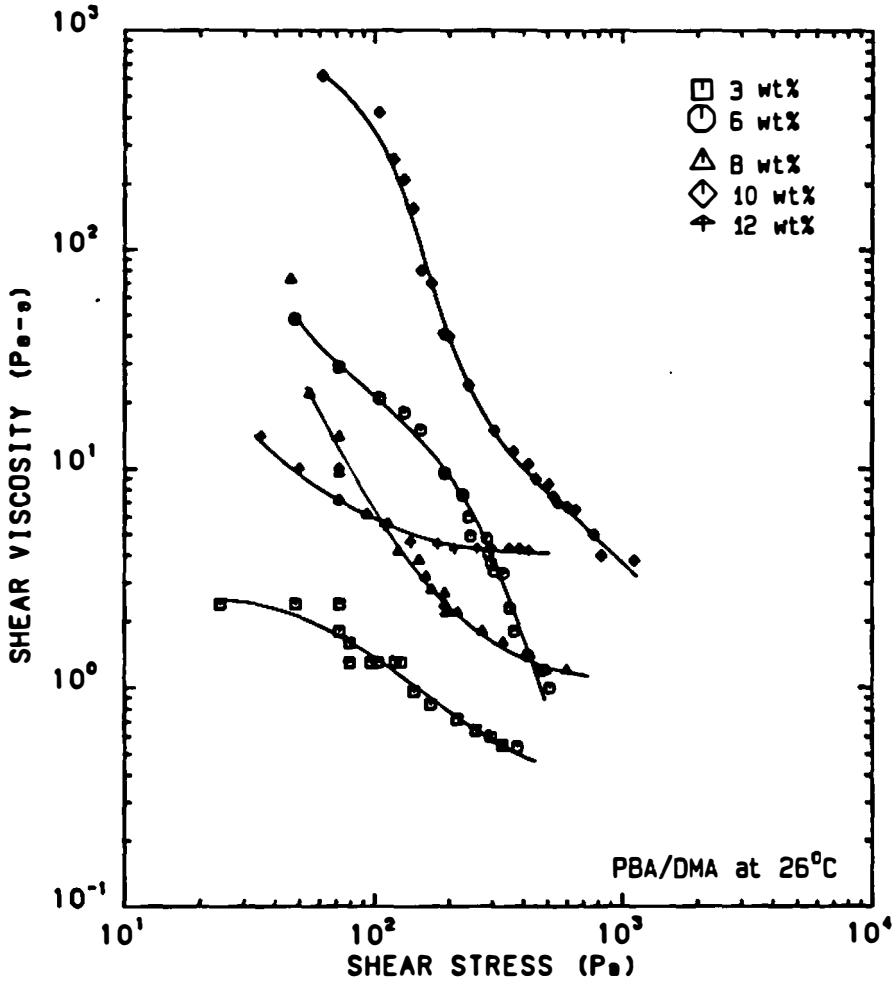

Figure 24. Viscosity Versus Shear Stress Plot of PBA/DMA Solutions at 26°C.

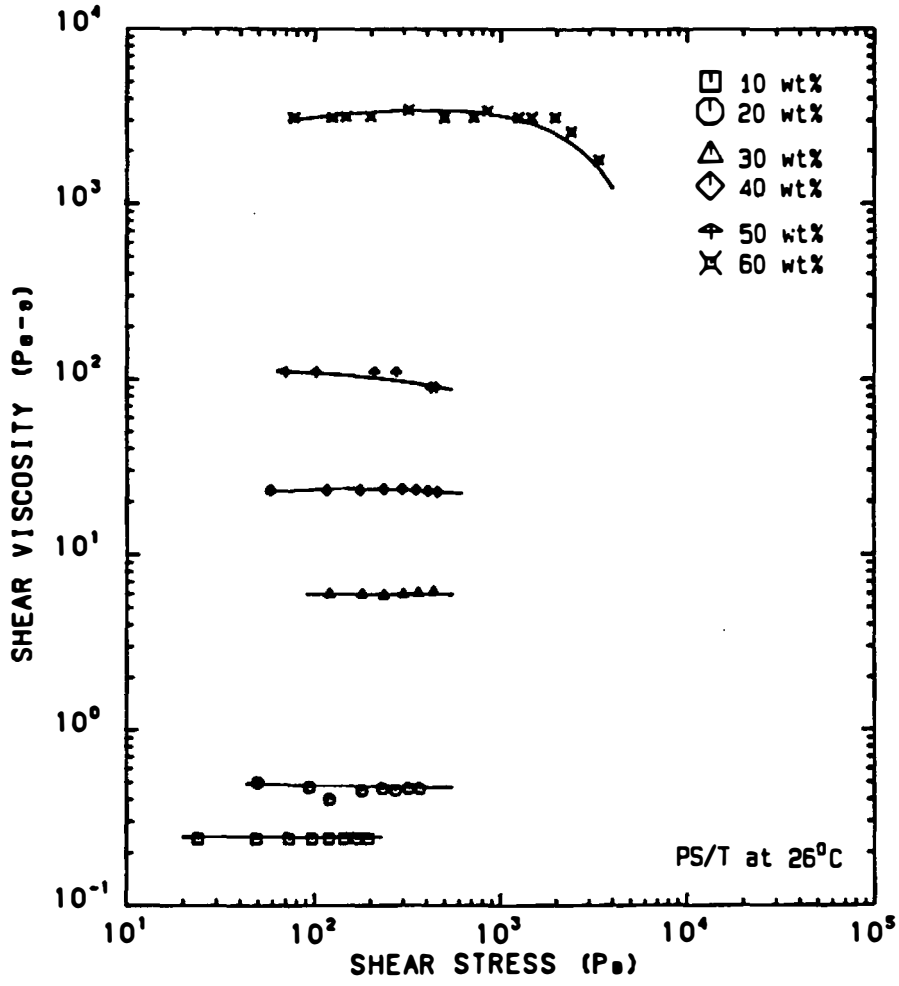

Figure 25. Viscosity Versus Shear Stress Plot of PS/T Solutions at 26°C.

solutions in the 10 wt% to 60 wt% concentration range and for PBA/DMA solutions in the 3 wt% to 12 wt% concentration range. Anisotropic solutions of HPC/W, HPC/FA, EC/FA, and PBA/DMA all exhibited viscosity versus shear stress curves with slopes approaching 90 degrees. These slopes indicated the presence of 'limiting flow stresses', which are also called 'domain flow' stresses or 'yield stresses'. The magnitudes of the 'domain flow' stresses were in most cases estimated by the use of Casson [48] plots. These plots were prepared by linear regression treatment of the low shear portion of the square roots of the shear stresses and shear rates, or $\sigma^{0.5}$ versus $\dot{\gamma}^{0.5}$. The values of the 'domain flow' stresses were obtained by squaring the intercept obtained for each plot. The use of the Casson plot in estimating values for 'limiting flow stresses' or 'yield stresses' has been described for filled polymer melts by White et al. [223,230].

Values of the 'domain flow' stresses and the linear regression correlations, or 'goodness of fit', are shown in Table 1 for anisotropic HPC/W, HPC/FA, EC/FA, and PBA/DMA solutions. Plots of the 'domain flow' stress versus concentration are shown as Figure 26. Correlation values, as determined by linear regression, are better than 0.96. These values indicate the experimental data fit the Casson form very well.

Table 1. Domain Flow Stress Values for Lyotropic HPC, EC and PBA Solutions as Obtained from Casson Plots.

Solution Type	Polymer Concentration	Domain Flow Stress	Casson Plot Correlation Value
	wt%	Pa.	
HPC/W	50	30	0.990
	60	20	0.967
HPC/FA	40	16	0.989
	50	40	0.740
	60	43	0.999
EC/FA	40	48	0.870
	50	59	0.995
	60	339	0.979
PBA/DMA	8	36	0.975
	10	40	0.961
	12	14	0.986

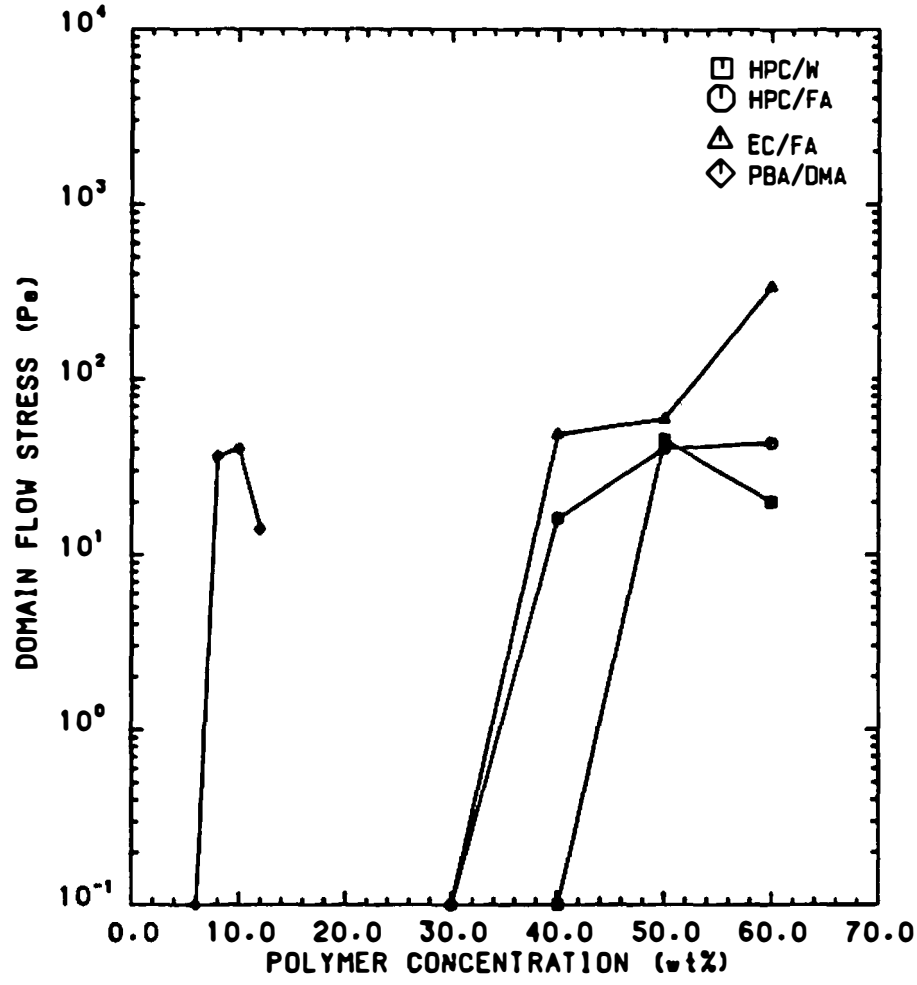

Figure 26. Domain Flow Stress Versus Concentration Plot of HPC/W, HPC/FA, EC/FA and PBA/DMA Solutions at 26 ^{o}C.

Discussion--Viscosity Behavior with Shear Stress

The viscosity versus shear stress plots for PS/T solutions in Figure 25 show predominately shear stress independent or Newtonian-like flow behavior. The viscosity data for the 50 wt% and 60 wt% solutions show some shear dependency at shear stresses exceeding 500 Pa. The behavior of these solutions can be characterized as viscoelastic flow behavior. No evidence of 'yielding' or viscoplastic flow was detected in the plots.

The viscosity versus shear stress plots, in Figures 21 through 25 (pp. 164-168), exhibit dramatic upturns with decreasing shear stress. The intial slopes of the plots show inclinations greater than 60 degrees. In some instances, the slopes approach 90 degrees or vertical inclinations. These viscosity upturns reflect the presence of 'yield' stresses and, consequently, viscoplastic flow behavior. This behavior is a feature or characteristic of materials which possess microstructure. The association of the 'yield' stresses or 'domain flow' stresses with the apparent microstructure is indicated by the plots in Figure 26. This is a graphical representation of the 'domain flow' stress versus concentration data of Table 1. These plots show the 'domain flow' stresses increase from zero to a finite value at the isotropic to anisotropic transition point. These 'finite values' or inflection points occur at 10 wt% PBA/DMA, 50

wt% HPC/W, 50 wt% HPC/FA, and 40 wt% EC/FA. Just above these intermediate concentrations, the 'domain flow' stress tends to level off or decrease in value before increasing exponentially with concentration. This region of the plot apparently occurs just prior to the onset of 'domain loading'. 'Domains' or supramolecular aggregates form when localized alignment occurs in the anisotropic phase. When a critical number of 'domains' are formed, the 'domain flow' stress begins to increase again. This 'domain loading' effect is observed in the plot for EC/FA at 60 wt%. The other solutions have not attained this point for the highest concentrations studied.

The viscoplastic flow behavior observed in anisotropic HPC, EC and PBA solutions is reminiscent of the 'yielding' behavior observed in small particle filled polymer melts [152,166,223,230]. However, the 'yielding' or viscoplastic response of anisotropic polymer solutions arises from a different mechanism than for filled systems. The 'yielding' behavior in filled systems results from the shear-induced breakdown of particle agglomerations [223]. The shearing force disrupts the particle to particle interactions. After shear cessation, new interactions are established and new particle agglomerations form which show similarities to the original microstructure. The resistance of the particle agglomerations to shear deformation is represented by the 'yield stress'. In

contrast, the 'domains' which act as the filler in anisotropic solutions deform and coalesce under shear to form a radically different microstructure. This microstructure is made up of unified 'domains' arranged parallel to the shear direction [173,246]. Unlike filled systems, the post-shear microstructure does not resemble the unsheared original microstructure. The aggregate resistance of the original 'multidomain' microstructure to shear deformation is represented by the 'domain flow' stress. This quantity is not the same as the 'yield stress', since true yield behavior does not take place during the deformation.

Results--Shear Stress Behavior

Plots of the shear stress versus shear rate are shown in Figures 27 through 30 for anisotropic HPC/W, HPC/FA, EC/FA, and PBA/DMA solutions. Comparative plots are shown for the isotropic PS/T solutions in Figure 31. Initial slopes of the shear flow portions of the shear stress versus shear rate plots are shown in Table 2.

The shear stress versus shear rate behavior of the anisotropic HPC, EC and PBA solutions was modeled by a modified version of the Herschel-Bulkley [109] expression

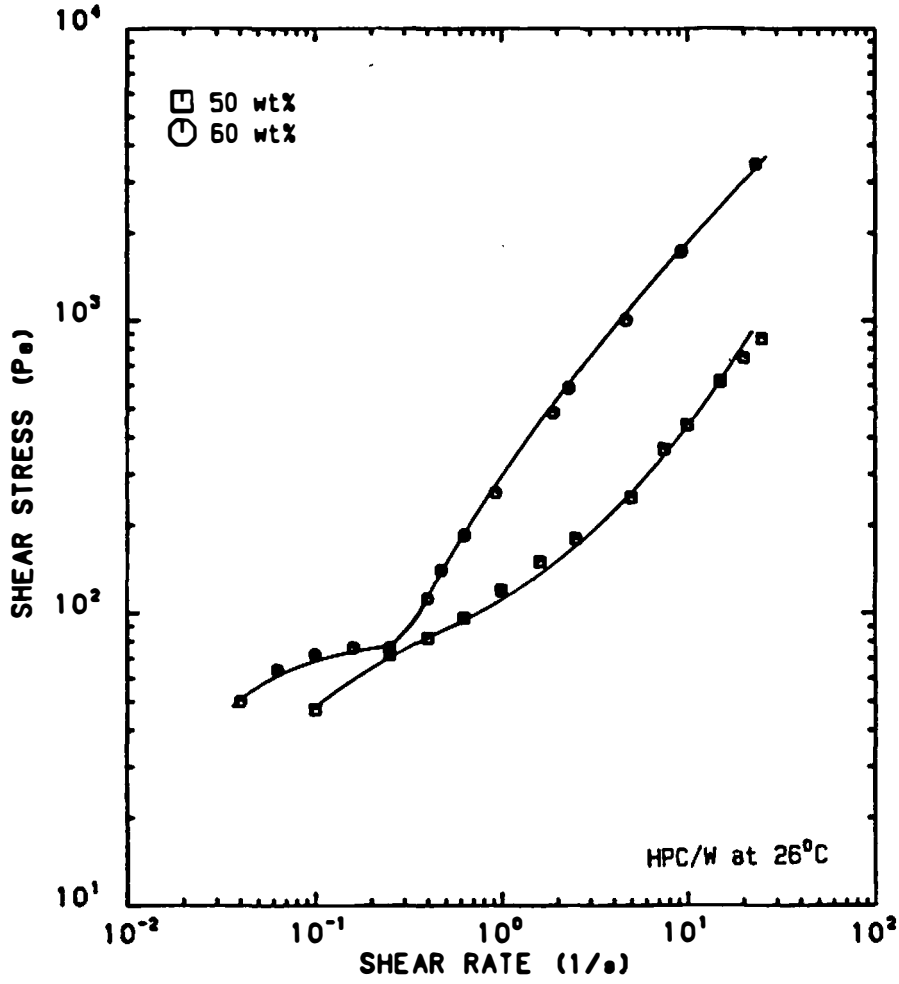

Figure 27. Shear Stress Versus Shear Rate Plot of Anisotropic HPC/W Solutions at 26°C.

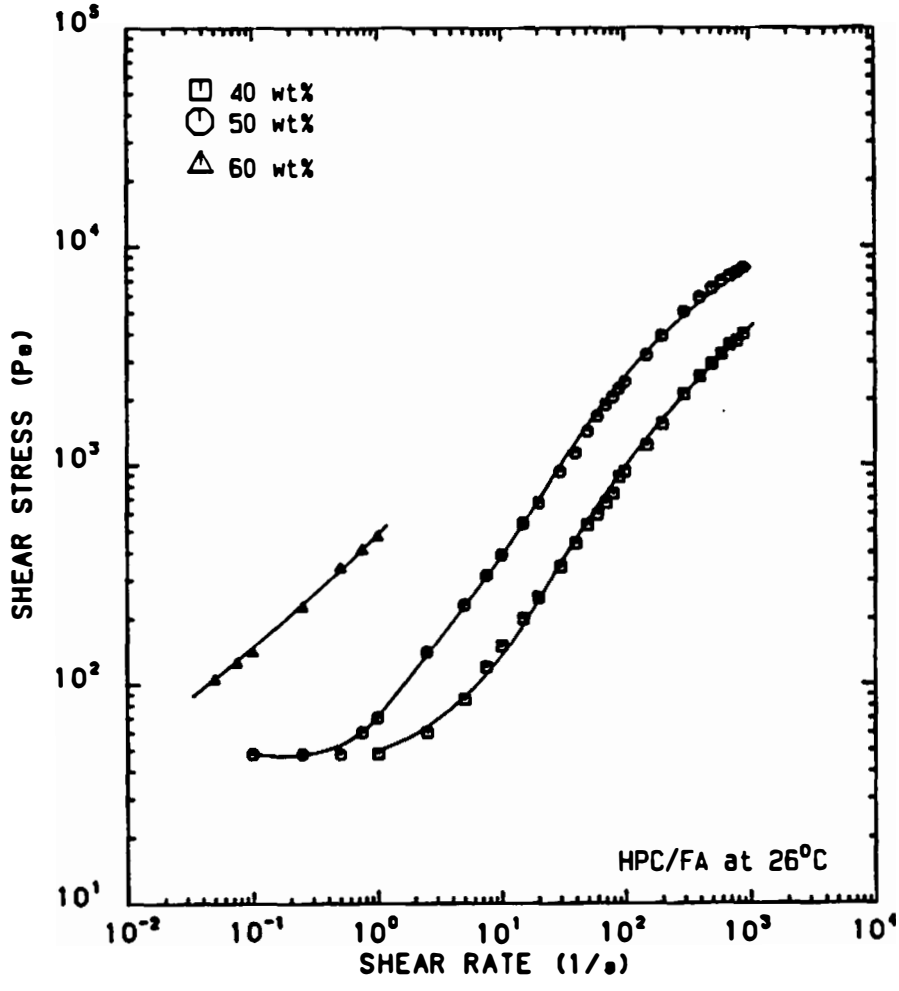

Figure 28. Shear Stress Versus Shear Rate Plot of Anisotropic HPC/FA Solutions at 26°C.

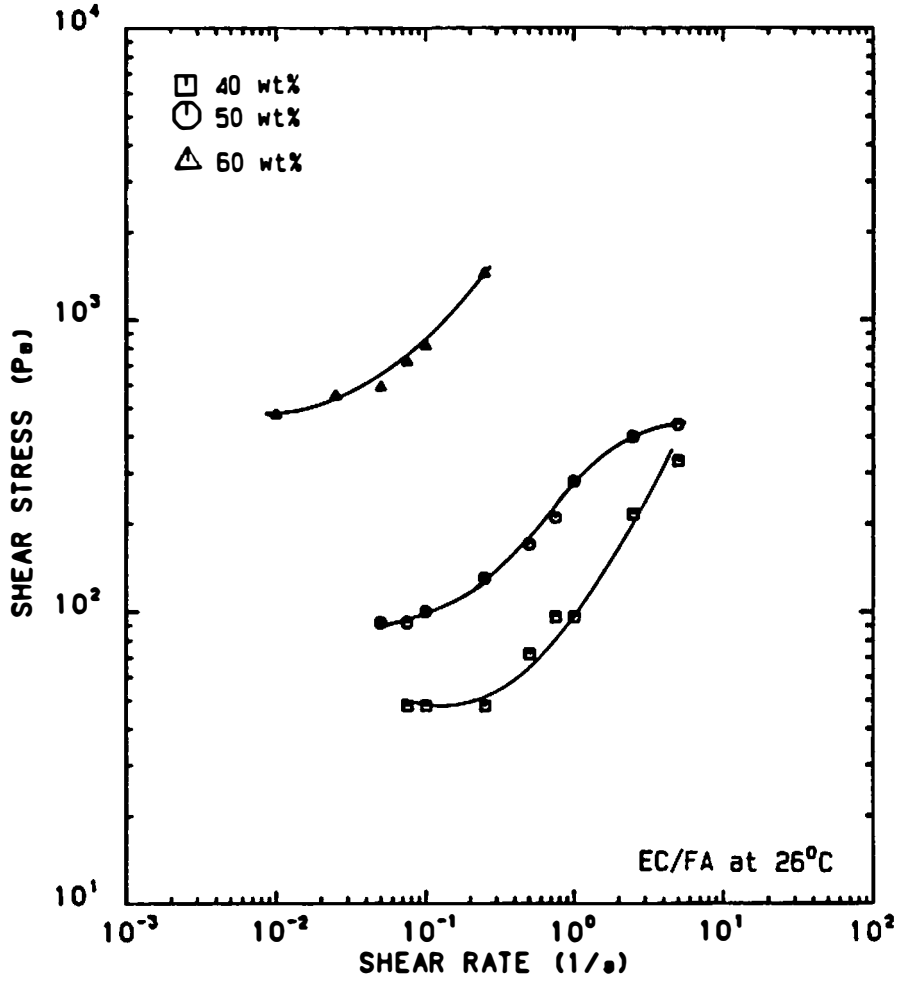

Figure 29. Shear Stress Versus Shear Rate Plot of Anisotropic EC/FA Solutions at 26°C.

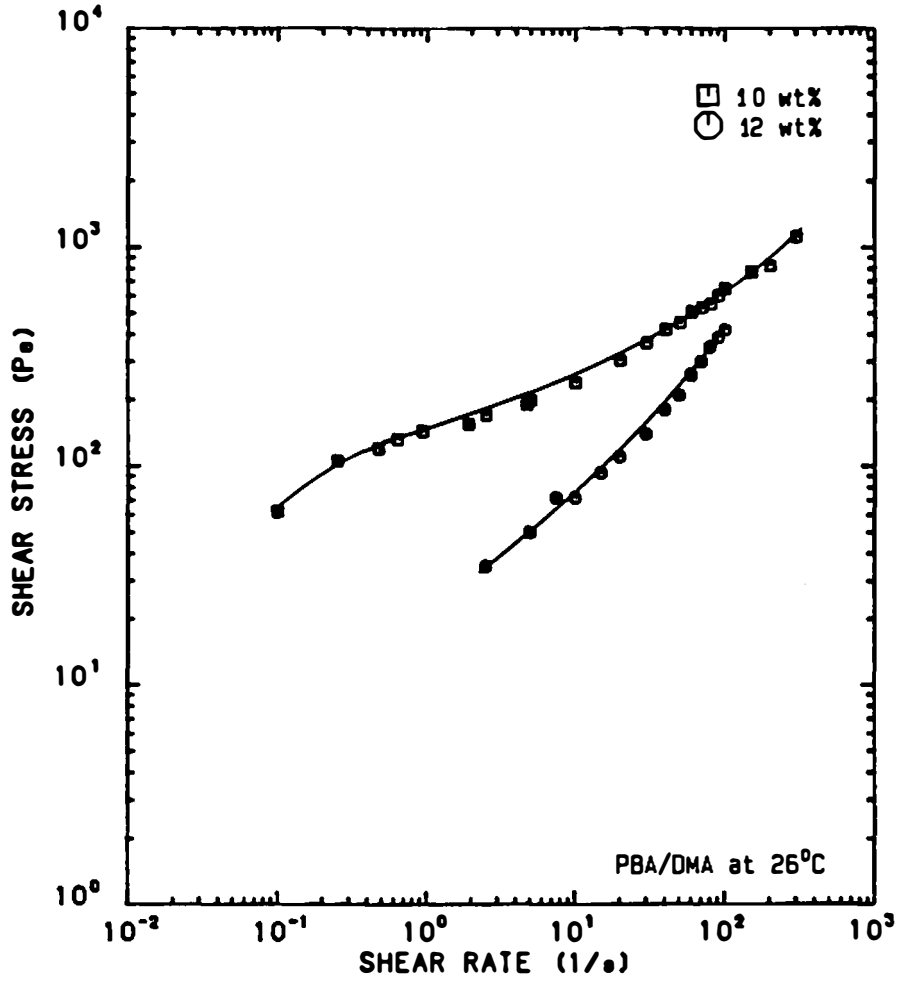

Figure 30. Shear Stress Versus Shear Rate Plot of Anisotropic PBA/DMA Solutions at 26°C.

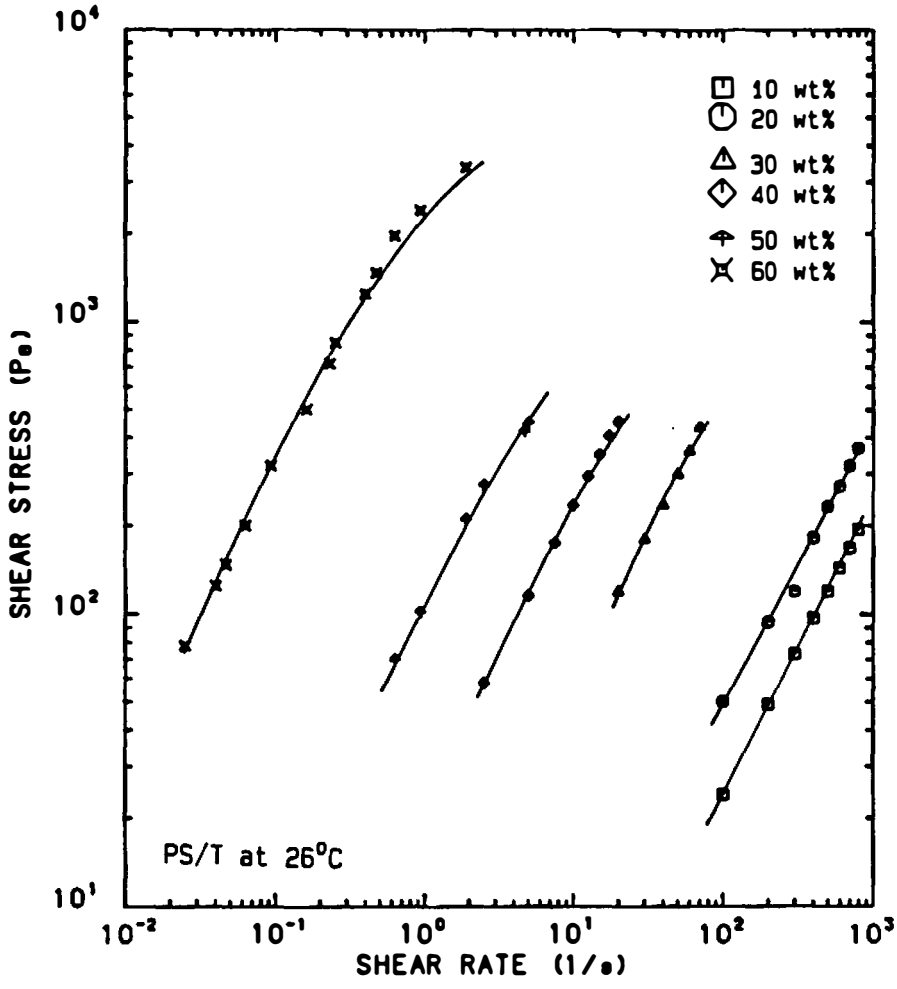

Figure 31. Shear Stress Versus Shear Rate Plot of PS/T Solutions at 26°C.

Table 2. Initial Slopes of the Quasi-linear Stress Region in the Shear Stress Versus Shear Rate Plots for HPC, EC, PBA and PS Solutions.

Solution Type	Polymer Concentration	Slope Value	Correlation Value
	wt%		
HPC/W	50	0.46	0.945
	60	0.84	0.999
HPC/FA	40	0.75	0.999
	50	0.64	0.968
	60	0.49	0.997
EC/FA	40	0.68	0.992
	50	0.41	0.986
	60	0.33	0.932
PBA/DMA	10	0.38	0.992
	12	0.82	0.994
PS/T	10	1.00	1.000
	20	0.97	0.996
	30	1.02	1.000
	40	1.00	1.000
	50	0.90	0.997
	60	1.00	1.000

(equation 3.0 on page 50)

$$\sigma_{12} = \sigma_{df} + K(\dot{\gamma})^{n} \qquad (3.9)$$

where σ_{12} is the shear stress, σ_{df} is the 'domain flow' stress, $\dot{\gamma}$ is the shear rate, K is the power law coefficient and n is the power law exponent. In this modification, the 'domain flow' stress, σ_{df}, replaces the yield stress, σ_{y}, of the original Herschel-Bulkley expression. The parameters of the modified expression, σ_{df}, K and n, are shown in Table 3. These parameters and the correlation or fit of the modified Herschel-Bulkley expression were determined by linear regression. The experimental data for the anisotropic HPC/W, HPC/FA, EC/FA, and PBA/DMA solutions were plotted in the Herschel-Bulkley form, with the Herschel-Bulkley (HB) shear stress, log $(\sigma_{12} - \sigma_{df})$, as the y-axis and the shear rate, log $(\dot{\gamma})$, as the x-axis. Plots of log HB shear stress versus log shear rate are shown in Figures 32 through 35.

Discussion--Shear Stress Behavior

The shear stress versus shear rate plots for the PS/T solutions, Figure 31 (p. 179) are significantly different than those presented for the anisotropic HPC, EC, and PBA solutions in Figures 27 through 30 (pp. 175-178). The PS/T plots indicate the shear stress increases proportionately with shear rate at low shear and levels off or

Table 3. Parameters and Correlation Values of the Modified Herschel-Bulkley Equation for Anisotropic Solutions of HPC, EC and PBA.

Solution Type	Polymer Concentration	Domain Flow Stress	Power Law Coefficient	Power Law Exponent	Correlation Value
	wt%	Pa	Pa-s		
HPC/W	50	30	88	0.68	0.996
	60	20	234	0.90	0.996
HPC/FA	40	16	23	0.78	0.998
	50	40	61	0.77	0.995
	60	43	442	0.65	1.000
EC/FA	40	48	56	1.06	0.991
	50	59	190	0.69	0.996
	60	339	3044	0.79	0.992
PBA/DMA	10	40	98	0.38	0.993
	12	14	9	0.81	0.997

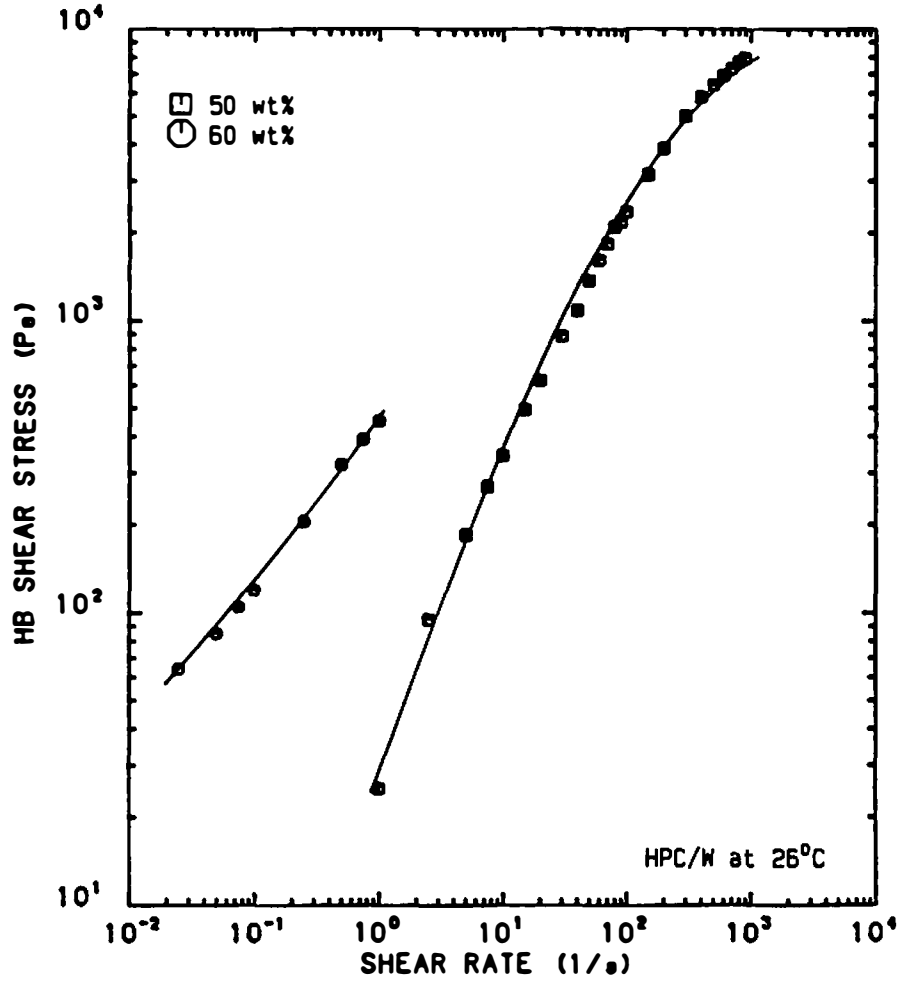

Figure 32. Herschel-Bulkley Plot of Anisotropic HPC/W Solutions.

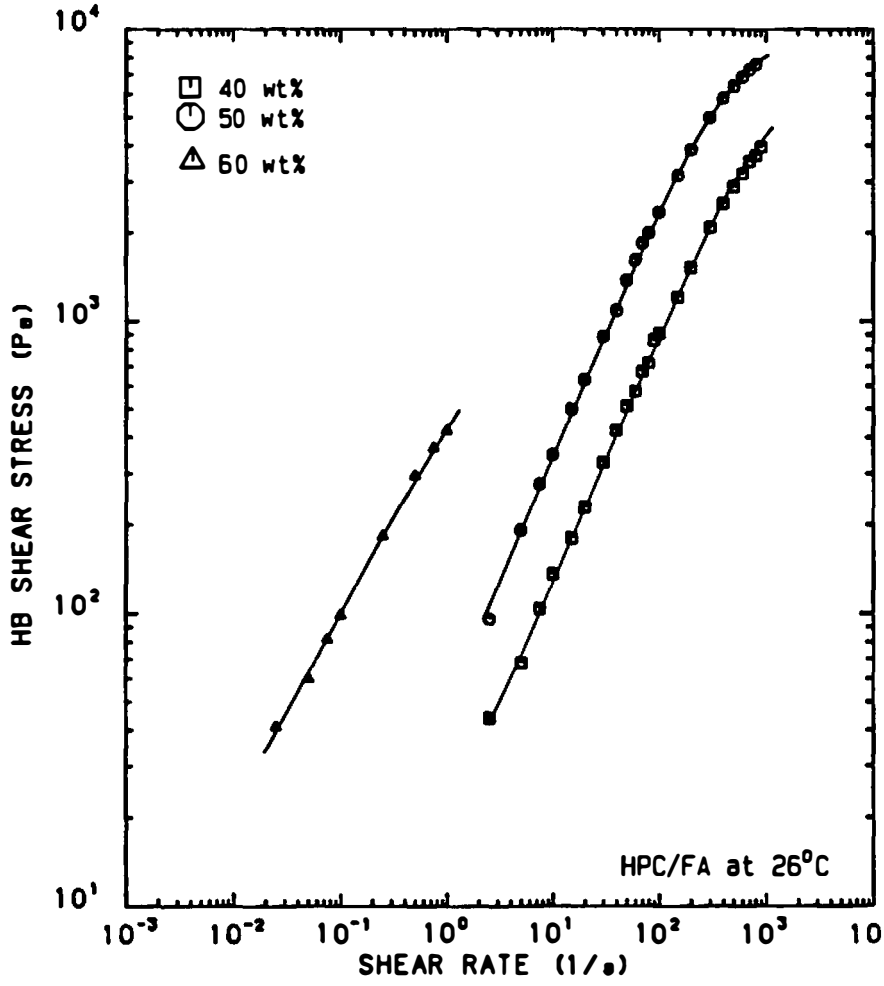

Figure 33. Herschel-Bulkley Plot of Anisotropic HPC/FA Solutions.

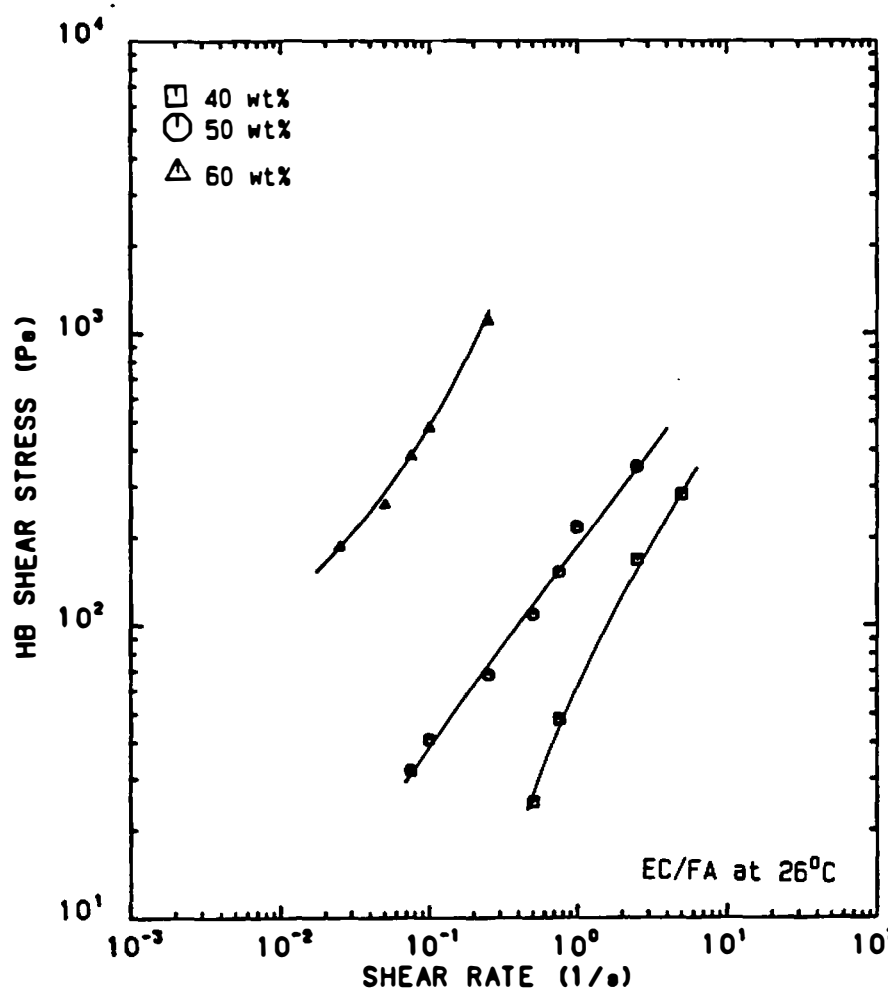

Figure 34. Herschel-Bulkley Plot of Anisotropic EC/FA Solutions.

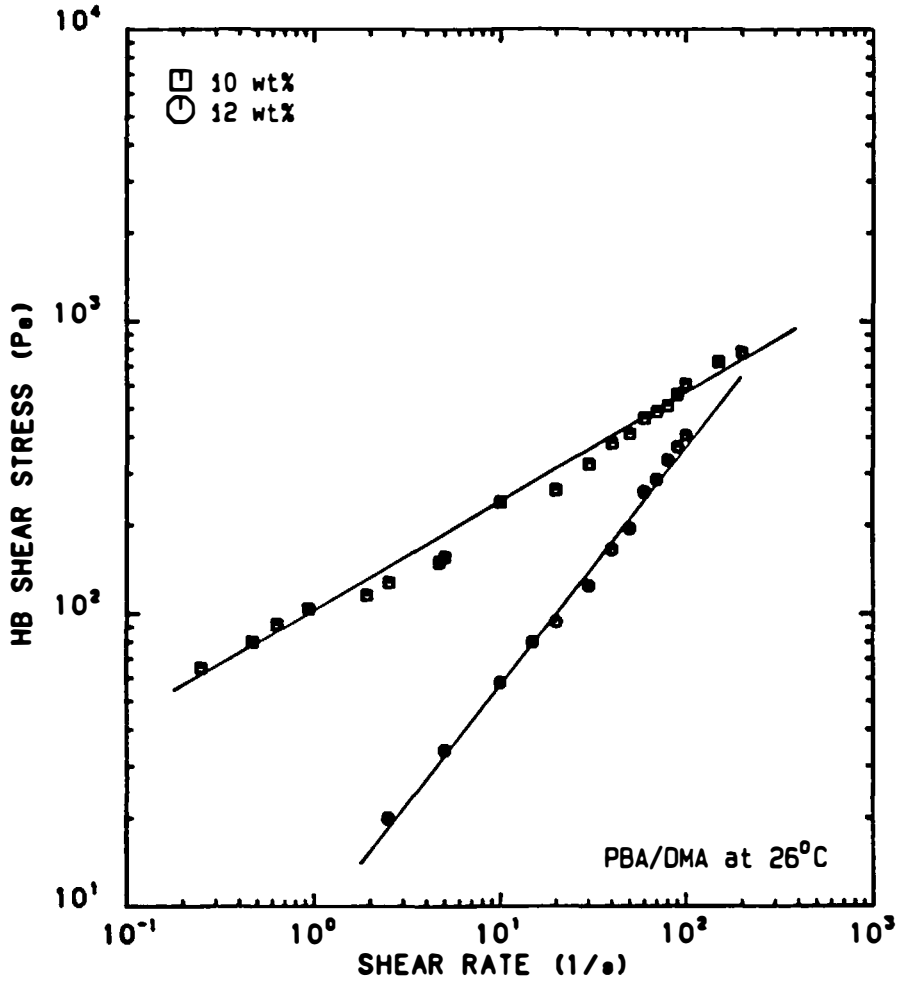

Figure 35. Herschel-Bulkley Plot of Anisotropic PBA/DMA Solutions.

saturates at high shear, particularly at concentrations exceeding 50 wt%. The proportional relationship in these plots is confirmed by Table 2 (p. 180) which indicates the slopes range from 0.9 to 1.02. The shear stress versus shear rate behavior is consistent with the flow behavior of a typical viscoelastic fluid showing shear independent viscosity at low shear rates and moderate shear thinning viscosity at high shear rates.

The shear stress versus shear rate plots for the anisotropic HPC/W, HPC/FA, EC/FA and PBA/DMA solutions, Figures 27 through 30 (pp. 175-178) tend to show three distinct regions of stress behavior. At low shear rates the stress is observed to gradually increase and level off as a constant stress plateau. At intermediate shear rates the stress is observed to increase in a quasi-linear fashion with shear rate. At high shear rates the stress tends to level off and form a stress saturation plateau. These three regions of stress represent the material response of the 'polydomain' or 'multitextured' micro-structure of the anisotropic state. The first or low low shear rate region represents the deformation of the 'domains'. The material response in this region indicates the stress builds up until the 'aggregate modulus' or 'domain flow' stress value of the 'domains' is attained. Along this constant stress plateau, the 'domains' deform and begin to unite under the shearing action. In the

second region the 'polydomain' structure is mostly unified and the polymer chains align in the flow direction. The slopes of this quasi-linear region, reported in Table 2 (p. 180), are less than one and range from 0.33 to 0.84 in value. These slopes indicate shear thinning behavior. The third or high shear rate region marks the onset of pronounced shear thinning. This stress saturation plateau appears to be related to a parallel banded 'domain' structure aligned in the flow direction [173,174].

The locations of the three stress regions appear to be shifted to lower shear rates with respect to increasing concentration for the anisotropic HPC/FA and EC/FA solutions (Figures 28-29, pp. 176-177). This shift is not observed for the HPC/W or PBA/DMA solutions (Figures 27 and 30, pp. 175 and 178). Comparisons of Figures 27 through 30 (pp. 175-178) with the 'domain flow' stress versus concentration plot in Figure 26 (p. 171) suggest the shift occurs when the 'domain flow' stress is increasing with concentration.

The shear stress versus shear rate behavior of anisotropic HPC, EC and PBA solutions is characteristic of viscoplastic type materials. These materials exhibit a 'yield-like' response at low shear rates and shear thinning behavior at moderate to high shear rates. The shear stress versus shear rate behavior of viscoplastic materials can be modeled with nonlinear Bingham type

expressions like the emperical Herschel-Bulkley [109] expression represented by equation (3.0) on page 50. For anisotropic solutions, a modified form of this expression, equation (3.9) on page 181, is used to model the 'domain deformation' behavior. Table 3 (p. 182), which represents the parameters and correlations of the data plotted in Figures 31 through 35 (pp. 179-186), indicates 'goodness of fit' parameters greater than 0.99. These high correlation values indicate the experimental data fit the Herschel-Bulkey form quite well. Figure 34 (p. 185) however, indicates that only the first two stress regions can be fitted with the Herschel-Bulkley equation. The high shear rate data, indicating the presence of the stress saturation plateau, tend to deviate from the model.

Results--First Normal Stress Differences

Figures 36 through 39 show plots of the first normal stress difference, N_1, versus the shear rate, γ, for solutions of 20 wt% to 60 wt% HPC/W, 20 wt% to 60 wt% HPC/FA, 20 wt% to 60 wt% EC/FA, and 3 wt% to 12 wt% PBA/DMA. Plots of 30 wt% to 60 wt% PS/T in Figure 40 show the N_1 behavior of an isotropic, viscoelastic polymer system. Slopes of the plots in Figures 36 through 40 are shown in Table 4. These slopes were determined by linear regression treatment of the N_1 data.

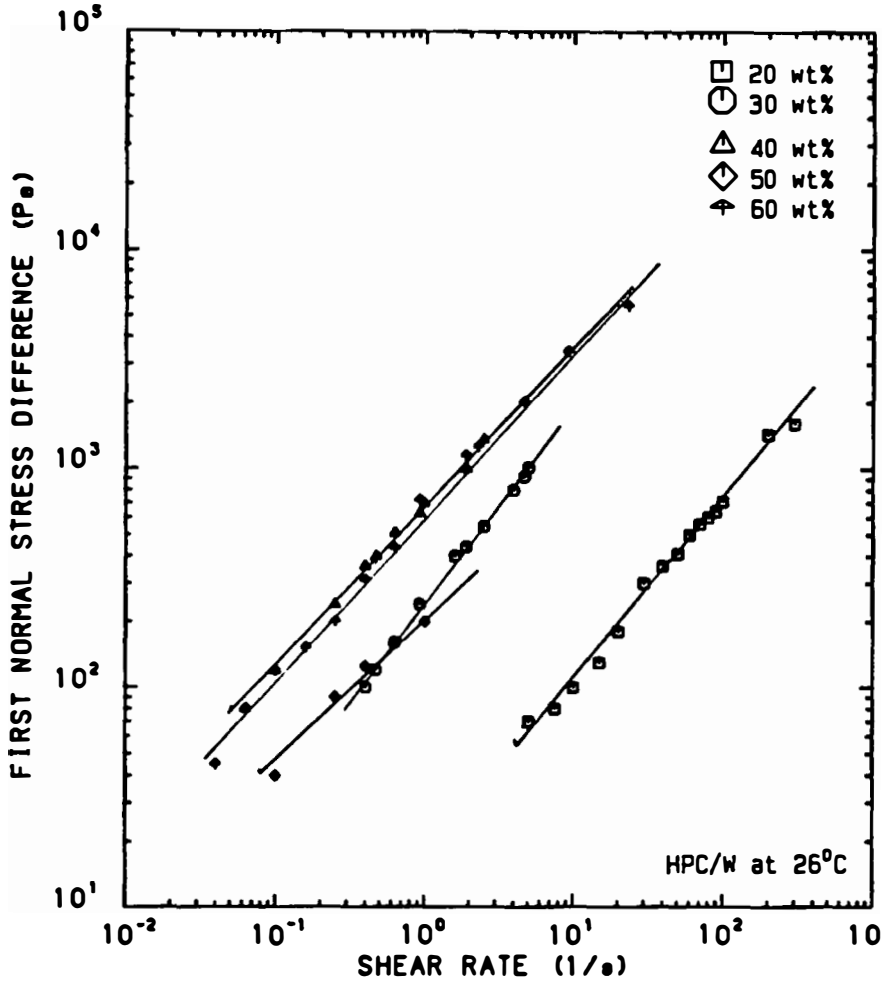

Figure 36. First Normal Stress Difference Versus Shear Rate Plot of HPC/W Solutions at 26°C.

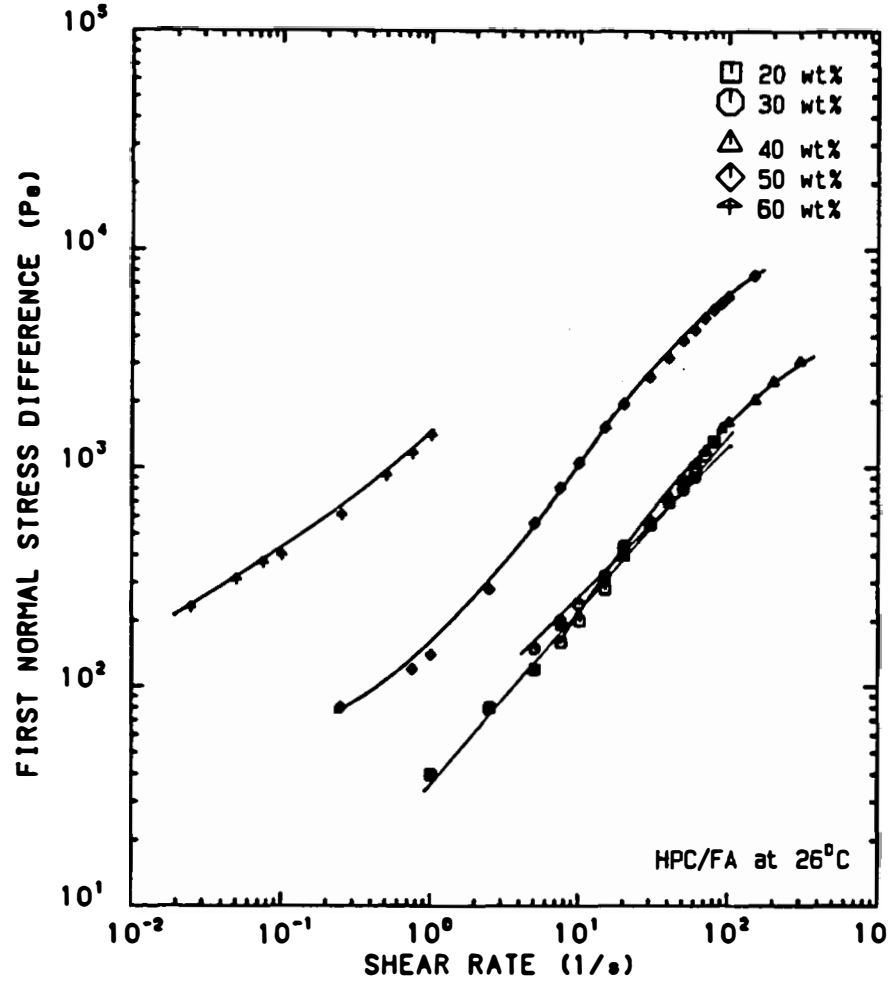

Figure 37. First Normal Stress Difference Versus Shear Rate Plot of HPC/FA Solutions at 26°C.

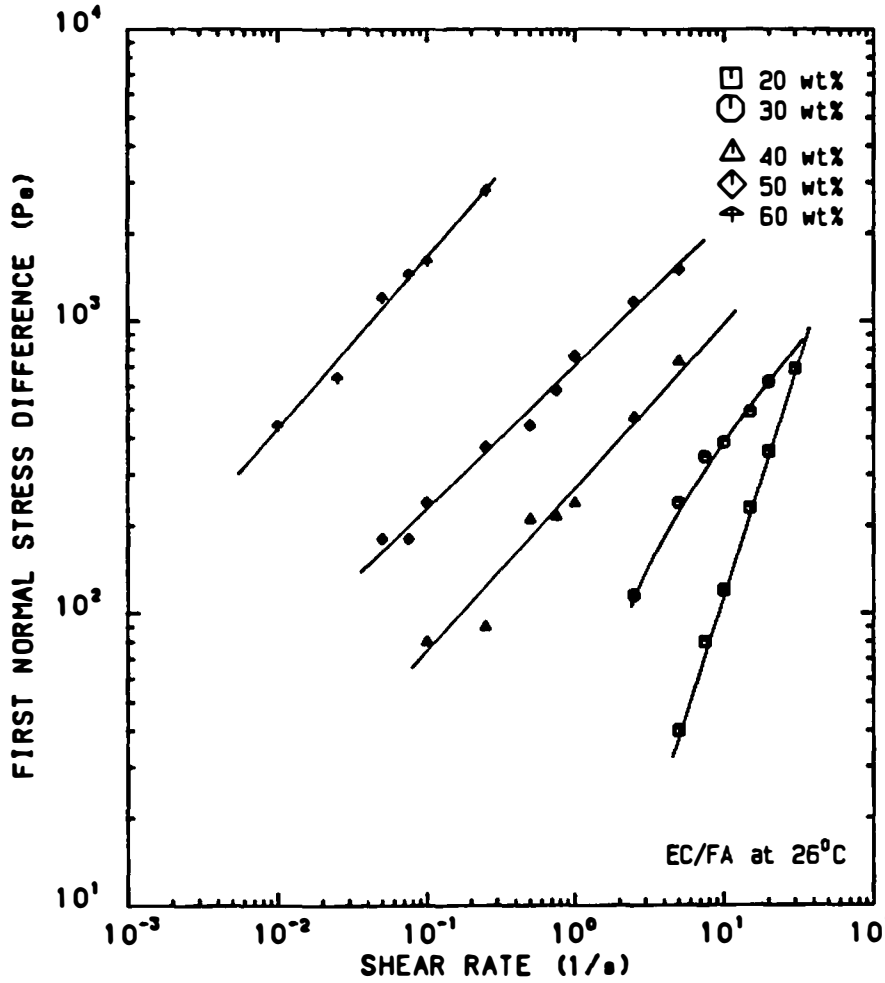

Figure 38. First Normal Stress Difference Versus Shear Rate Plot of EC/FA Solutions at 26°C.

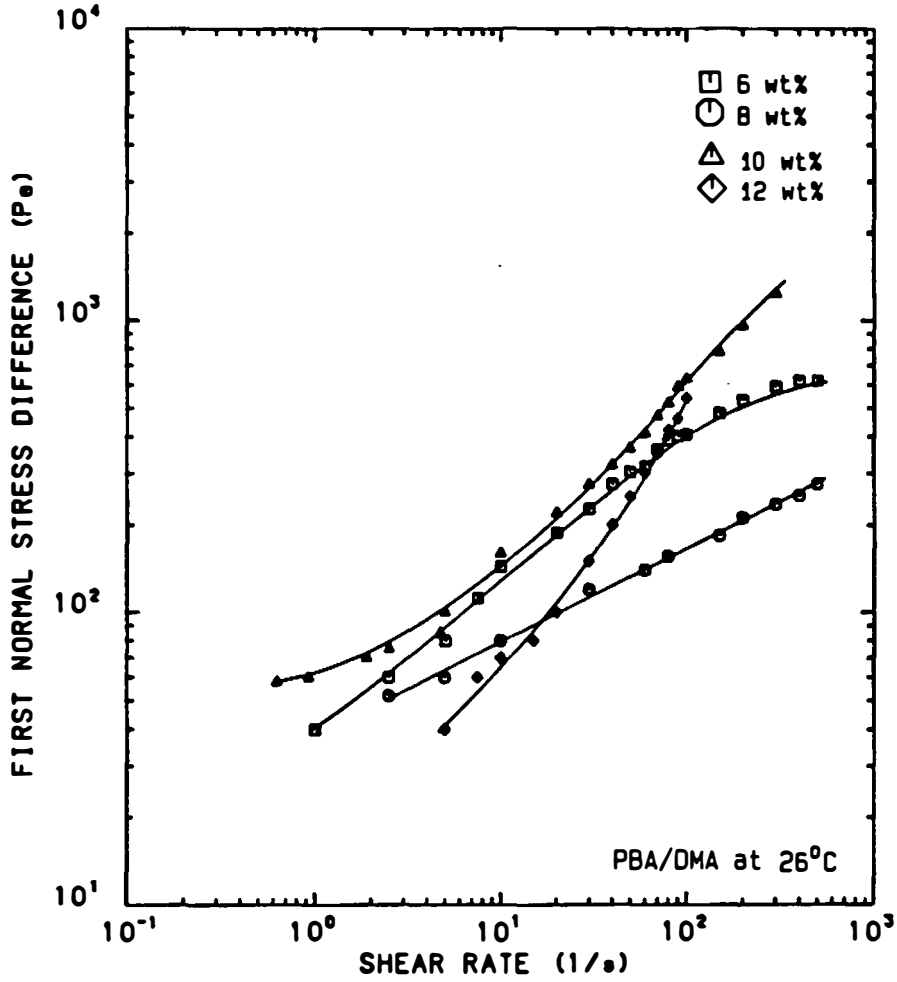

Figure 39. First Normal Stress Difference Versus Shear Rate Plot of PBA/DMA Solutions at 26°C.

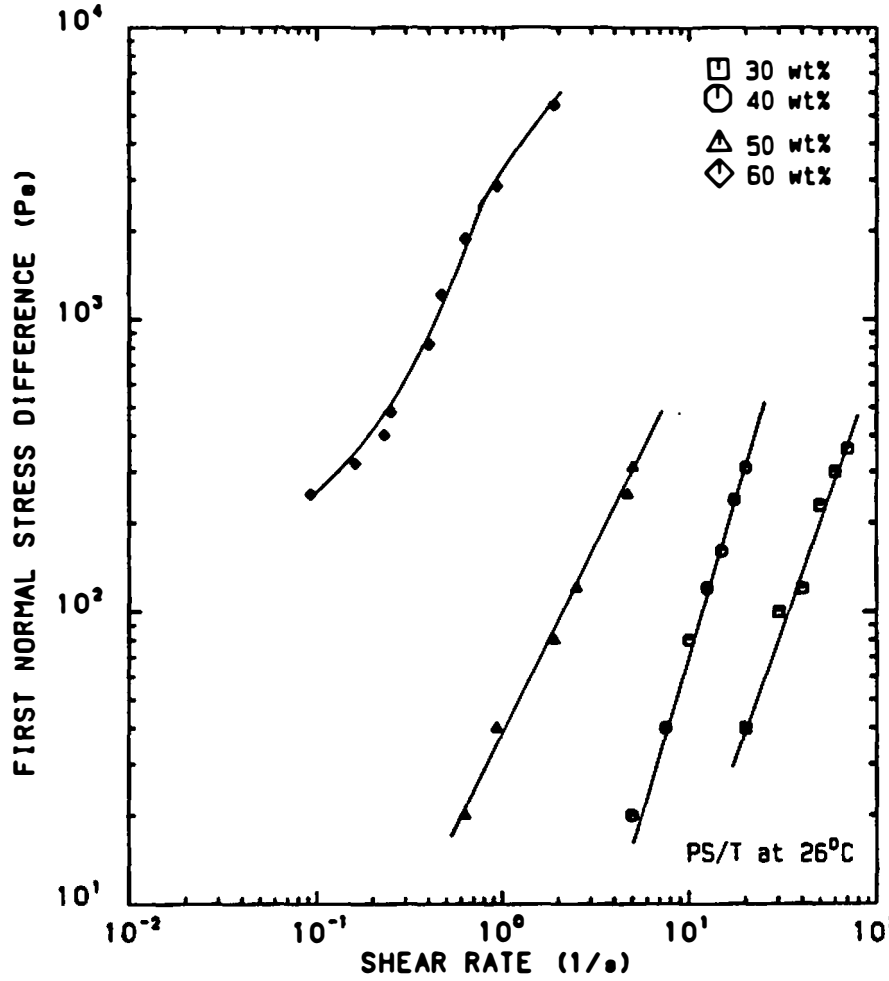

Figure 40. First Normal Stress Difference Versus Shear Rate Plot of PS/T Solutions at 26°C.

Table 4. Slopes of the First Normal Stress Difference Versus Shear Rate Plots For HPC, EC, PBA and PS Solutions.

Solution Type	Polymer Concentration	Slope Value	Correlation Value
	wt%		
HPC/W	20	0.83	0.996
	30	0.89	0.998
	40	0.75	0.998
	50	0.70	0.991
	60	0.76	0.997
HPC/FA	20	0.81	0.997
	30	0.77	0.999
	40	0.80	0.998
	50	0.82	0.999
	60	0.49	0.997
EC/FA	20	1.58	1.000
	30	0.78	0.998
	40	0.70	0.998
	50	0.50	0.995
	60	0.59	0.994
PBA/DMA	6	0.47	0.990
	8	0.33	0.991
	10	0.62	0.997
	12	0.85	0.963
PS/T	30	1.70	0.989
	40	1.99	0.999
	50	1.22	0.996
	60	1.23	0.993

Discussion--First Normal Stress Differences

Two basic differences can be discerned in the first normal stress difference, N_1, versus shear rate plots of the isotropic PS/T and the lyotropic HPC, EC and PBA solutions. The first difference concerns the shape of the plots. The N_1 plots for PS/T (Figure 40) are quasi-linear and possess slopes between 1.2 and 2.0 (Table 4). These slopes are somewhat lower than the value of two, typically observed for many viscoelastic polymers. The N_1 plots of the HPC, EC and PBA solutions (Figures 36-39) also exhibit quasi-linear character, but tend to form low shear rate plateaus at high polymer concentations. The slopes of the quasi-linear regions of these plots are less than one (Table 4), except for the 20 wt% HPC/FA solution which possesses a slope of 1.6. The slopes for remaining N_1 plots vary between 0.5 and 0.85 (Table 4). The slope predicted by Doi's theory [62] for the first normal stress versus shear rate behavior is one. Clearly, this value is not attained experimentally (Table 4). The discrepancy probably occurs because the experimentally observed N_1 values are suppressed by viscoplastic effects. These effects result from shear breakdown of the 'polydomain' microstructure. These effects are not included in Doi's theory [62], since the director is assumed not to vary with position. The presence of a 'polydomain' structure necessitates a position dependent director.

The second difference concerns the first normal stress difference versus concentration relationship. The plots for the PS/T solutions indicate N_1 tends to increase monotonically with concentration at a given shear rate. The plots for the HPC, EC and PBA solutions, however, exhibit maxima and mimima in the first normal stress difference versus concentration relationship. The behavior tends to mimic the viscosity versus concentration relationship discussed earlier on pages 162 and 163. The HPC/W plots (Figure 36, p. 190) indicate a maximum in N_1 at 40 wt% and a minimum in N_1 at 50 wt%. The HPC/FA plots (Figure 37, p. 191) show the N_1 plots at 20 wt%, 30 wt%, and 40 wt% all superimpose. Above 40 wt% N_1 increases with concentration. The EC/FA plots (Figure 38, p. 192) do not exhibit apparent maxima or minima. However, the 30 wt% and 20 wt% plots show a tendency to overlap at high shear rate. The PBA/DMA plots (Figure 39, p. 193) show an apparent N_1 maximum at 8 wt% and an apparent N_1 minimum at 10 wt%.

B. Melts

Results--Viscosity Behavior with Shear Rate

Figures 41 and 42 show the viscosity versus shear rate behavior of thermotropic melts of POB/PET 60/40 and EC. The POB/PET 60/40 melts were investigated over a 190°C to 340°C temperature range by cone and plate

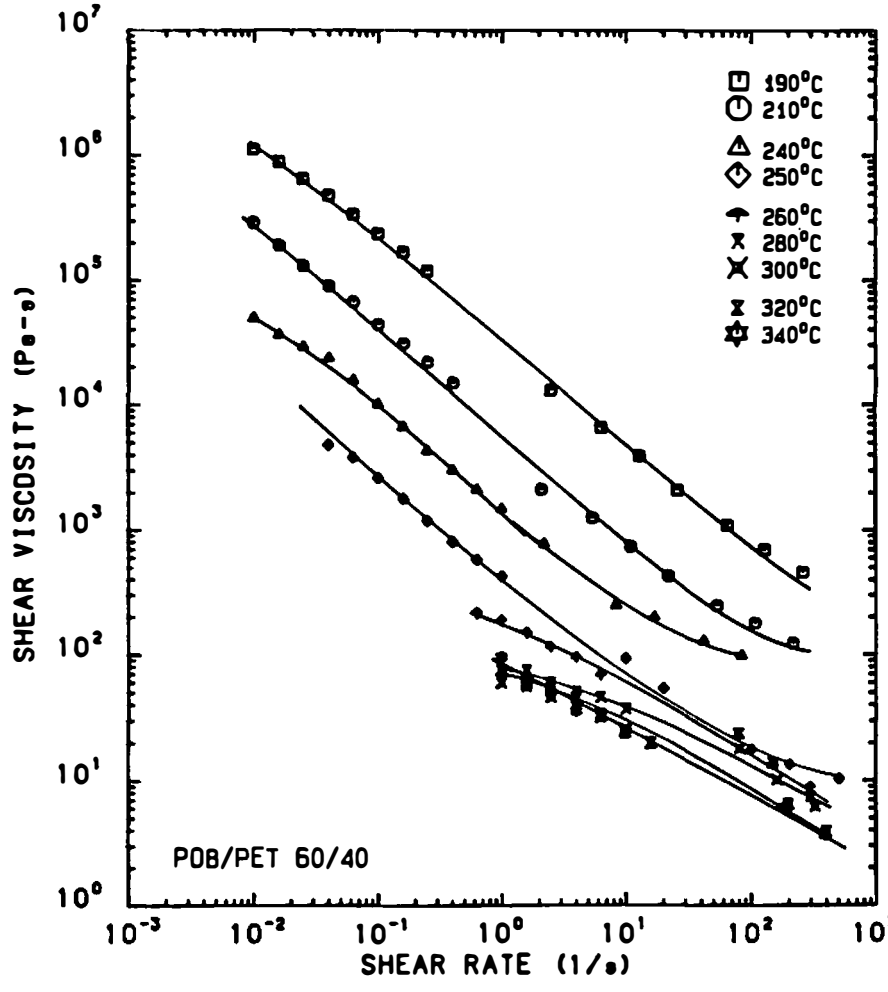

Figure 41. Viscosity Versus Shear Rate Plot of POB/PET 60/40 Melts.

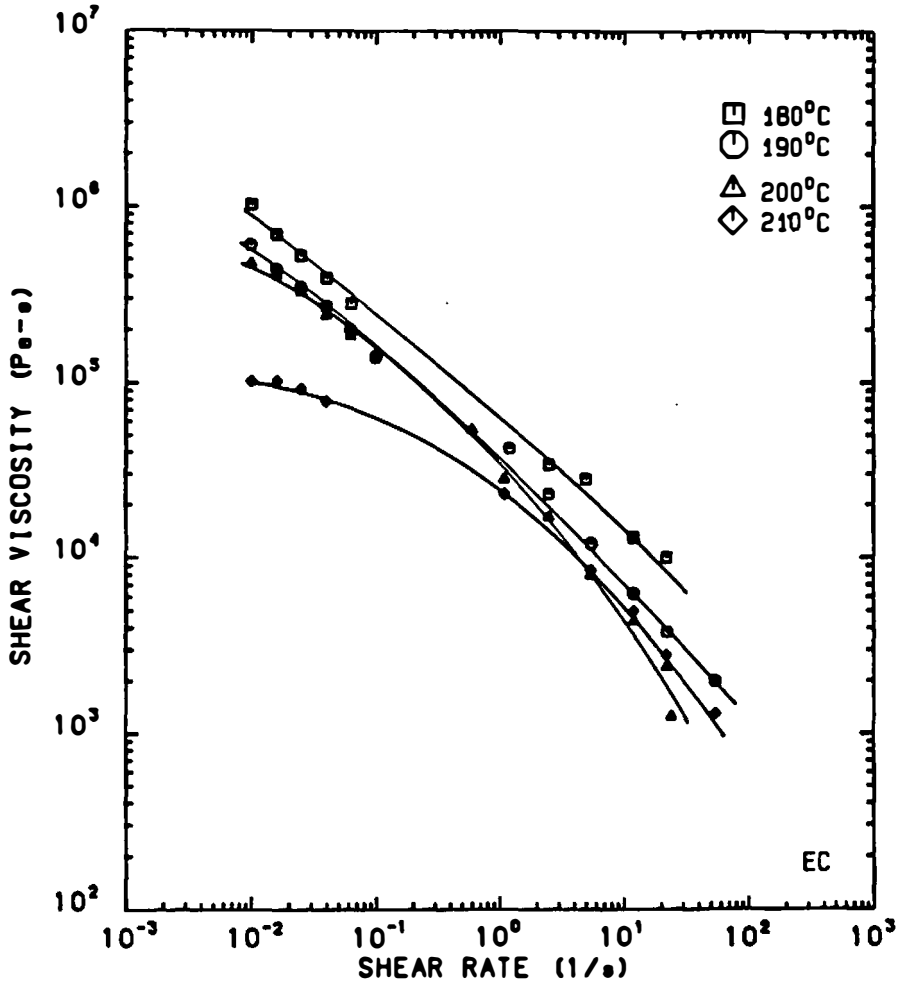

Figure 42. Viscosity Versus Shear Rate Plot of EC Melts.

rheometry and capillary rheometry. Below 260°C, the viscosity data below 1 s^{-1} are from cone and plate measurements. Above 260°C, the viscosity data below 10 s^{-1} are from cone and plate measurements. In the case of EC melts, viscosity data were obtained from cone and plate measurements below 0.1 s^{-1} for the 180°C to 210°C temperature range. The viscosity data at the same temperatures above 1 s^{-1} were replotted from capillary measurements reported by Suto, White and Fellers [227].

Comparative viscosity versus shear rate plots are shown in Figure 43 for isotropic polystyrene (PS) melts at 180°C and 200°C. These plots were constructed from viscosity data obtained by Lewis et al. [149]. The data below 0.4 s^{-1} were obtained by cone and plate measurements. Data above 4 s^{-1} represent capillary measurements.

Discussion--Viscosity Behavior with Shear Rate

The viscosity versus shear rate data for POB/PET 60/40 shown in Figure 41 are quantitatively similar to viscosity data reported by Wissbrun [242] and by Baird et al. [94,125]. The data presented by Wissbrun were obtained from capillary rheometry measurements in the 210°C to 300°C temperature range. The data presented by Baird et al. were obtained from both cone and plate rheometry and capillary rheometry in the 250°C to 285°C temperature range. The viscosity data in Figure 41 show a

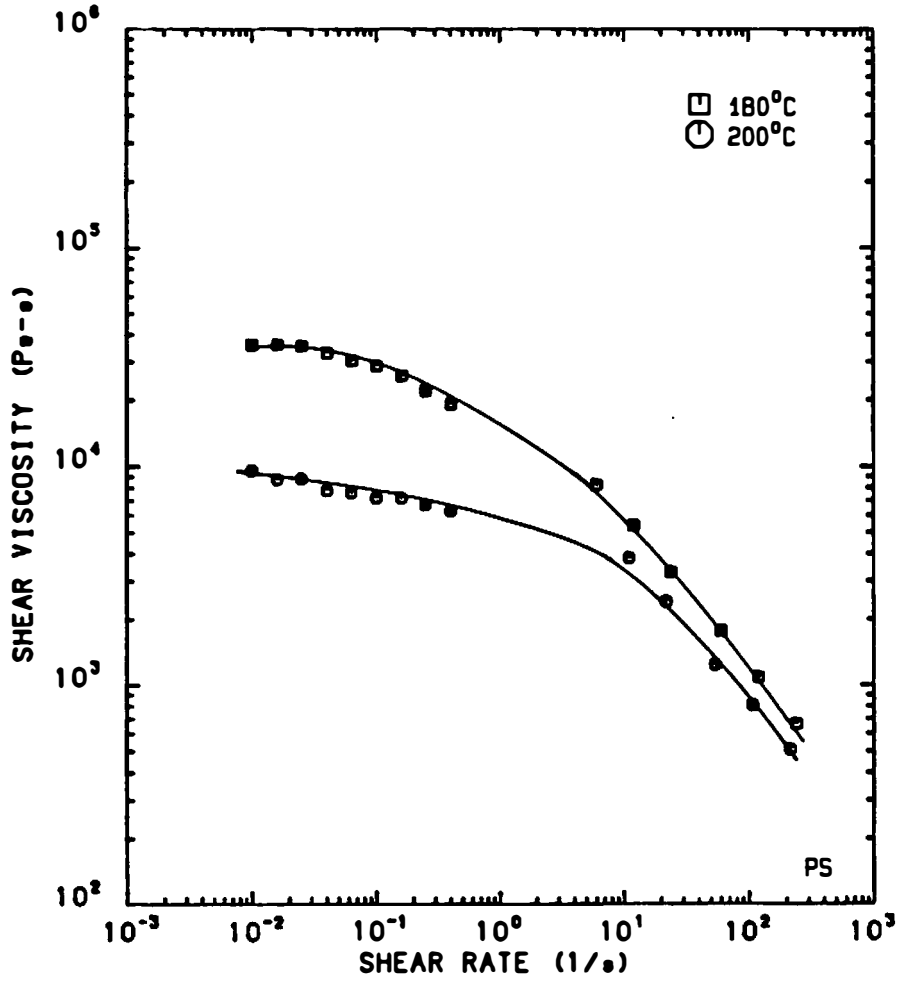

Figure 43. Viscosity Versus Shear Rate Plot of PS Melts.

steady decrease with increasing temperature in the 190°C to 260°C temperature range. Above 260°C the data begin to 'group together' and overlap. Below 250°C the viscosity curves are unbounded at low shear rates and show no tendency to form zero shear Newtonian plateaus. The curves at temperatures above 260°C show no clear trends with respect to low shear rates. From 190°C to 260°C the viscosities show an average decline of 0.8 decade per decade increase in shear rate. The viscosities above 260°C show an average decline of 0.3 decade per decade increase in shear rate. The viscosity behavior of POB/PET 60/40 appears to undergo a dramatic change in the vicinity of 260°C. This change coincides with the DSC endotherm centered at 255°C. As discussed on pages 153 through 155, this endotherm was interpreted as the melting transition of the POB rich phase. Below 260°C the viscosity behavior is influenced by the presence of unmelted POB rich 'domains'. These viscosity curves are similar in appearance to those of highly loaded, small particle filled melts [152,223]. From 190°C to 250°C the viscosity behavior of POB/PET 60/40 can be described as shear thinning viscoplastic or Region I [16] type flow behavior. Above 260°C the melt is no longer reinforced by rigid POB rich 'domains'. The viscosity behavior appears to be that of a shear thinning fluid. A 'yielding' or viscoplastic response is not evident in these curves. The

classification of these viscosity curves is a matter of conjecture. The plots may represent either Region I flow behavior or Region III flow behavior according to the Onogi and Asada [16,18,179] flow-structure model. The data of Wissbrun [242] and Baird et al. [94,124] do not clearly establish the presence of a quasi-Newtonian plateau, or Region II [18] flow behavior, at the lowest shear rates.

The viscosity data for EC melts, Figure 42, show qualitative similarities to those of POB/PET 60/40 melts. Below 200°C the viscosity curves show viscoplastic flow character and are unbounded at low shear rates. Above 200°C the viscosities tend to become shear rate independent at low shear rate. From 180°C to 200°C the viscosities show an average decline of 0.7 decade in magnitude per decade increase of shear rate. At 210°C the average drop in viscosity is about 0.4 decade. The distinct change in the viscosity behavior about 200°C can be related to a DSC endotherm at 192°C. This endotherm, as discussed on page 153, represents the anisotropic to isotropic transition of the primary liquid crystalline phase in EC. The viscosity behavior below 200°C can be characterized at shear thinning viscoplastic flow or Region I [18] flow behavior. The viscosity behavior above 200°C probably represents the viscoelastic flow behavior of the biphasic melt.

The viscosity versus shear rate plots of PS melts at 180°C and 210°C, Figure 43, show significantly contrasting flow behavior to both EC melts and POB/PET 60/40 melts. The viscosity data of PS at 180°C show quasi-Newtonian flow behavior below 0.3 s^{-1}, moderate shear thinning behavior between 0.3 s^{-1} to 10 s^{-1}, and strong shear thinning behavior above 10 s^{-1}. At 210°C the viscosity data indicate moderate shear thinning flow behavior at shear rates below 10 s^{-1} and more pronounced shear thinning behavior above 10 s^{-1}. The viscosity decrease in the moderate shear thinning region is about 0.2 decade per decade increase in shear rate. In the pronounced shear thinning regions, the viscosity decline is about 0.4 decade per shear rate decade. The viscosity behavior of PS melts can be described as a shear thinning viscoelastic flow behavior.

Results--Viscosity Behavior with Shear Stress

Figure 44 shows the viscosity versus shear stress behavior for POB/PET 60/40 over the 190°C to 340°C temperature range. The plots, obtained at 190°C to 250°C, exhibit almost vertical slopes. In contrast, the plots obtained at temperatures above 250°C show slopes with inclinations between 45 and 60 degrees.

The viscosity versus shear stress plots for EC melts are shown in Figure 45 for the temperatures in the 180°C to 210°C temperature range. The plots below 200°C exhibit

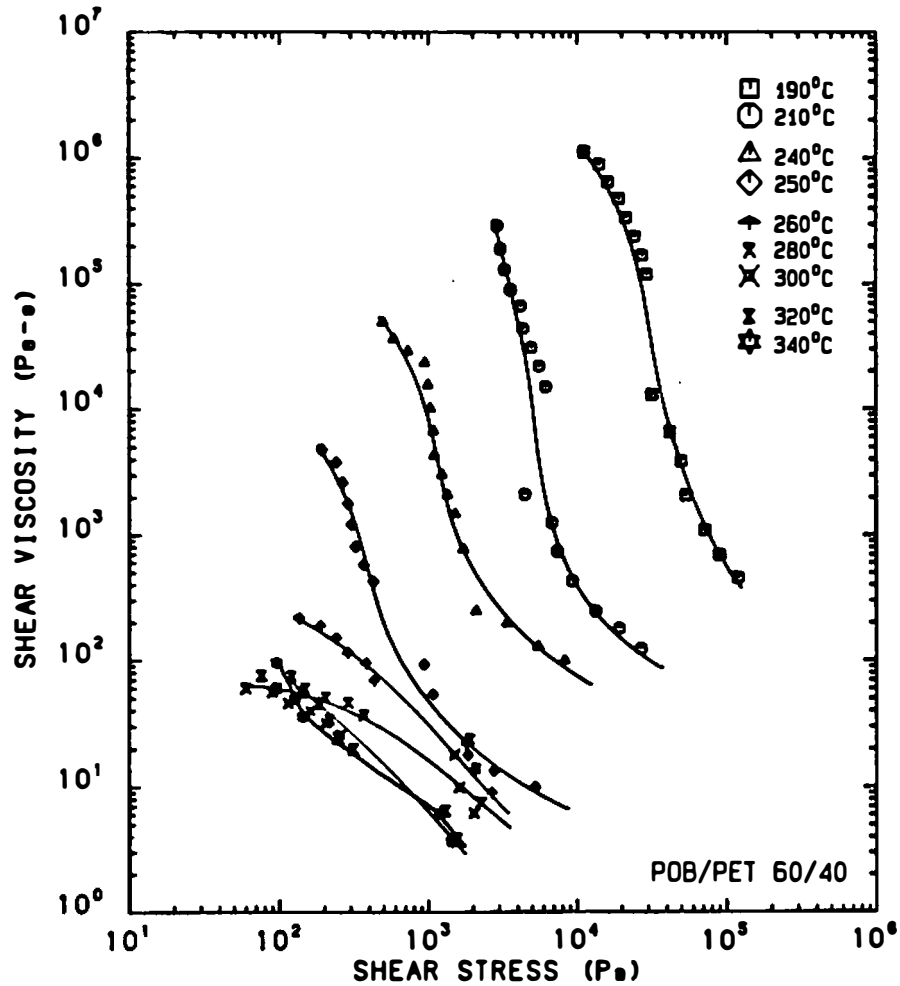

Figure 44. Viscosity Versus Shear Stress Plot of POB/PET 60/40 Melts.

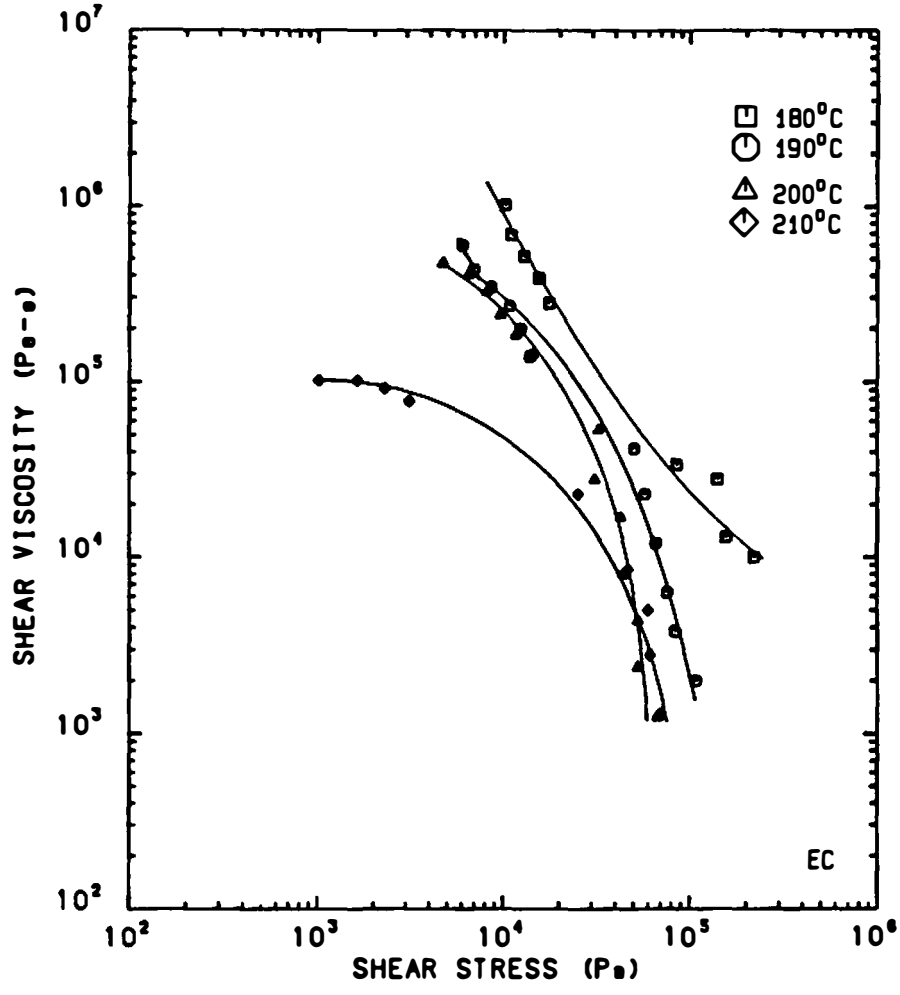

Figure 45. Viscosity Versus Shear Stress Plot of EC Melts.

slopes with inclinations between 60 and 75 degrees. The 210°C plot, however, exhibits a very shallow slope of about 30 degrees in inclination. Viscosity versus shear stress plots for PS melts at 180°C and 200°C are shown in Figure 46. These plots exhibit slopes of approaching 20 degrees in inclination at stresses below 40 kPa. Above 40 kPa, the plots exhibit slopes approaching 60 degrees.

Table 5 shows the values of the 'domain flow' stress obtained for thermotropic POB/PET 60/40 and EC melts. The values were obtained by linear regression fits of Casson [48] plots of the experimental shear stress and shear rate data. Details of the method were outlined on page 169. Figures 47 and 48 illustrate the behavior of the 'domain flow' stress with respect to temperature for POB/PET 60/40 melts and EC melts, respectively.

Discussion--Viscosity Behavior with Shear Stress

Figure 44 shows steep declines in the viscosity with respect to shear stress for POB/PET 60/40 melts below 260°C. The steep slopes of these plots indicate the presence of 'yielding' or 'domain deformation' behavior. The stresses at which the viscosity declines occur show that significant 'domain flow' stresses exist. The plots above 260°C exhibit slopes approaching 45 degrees in inclination. These shallower slopes indicate much smaller values for the 'domain flow' stresses. The shape of the plots indicate mainly shear thinning flow behavior. As

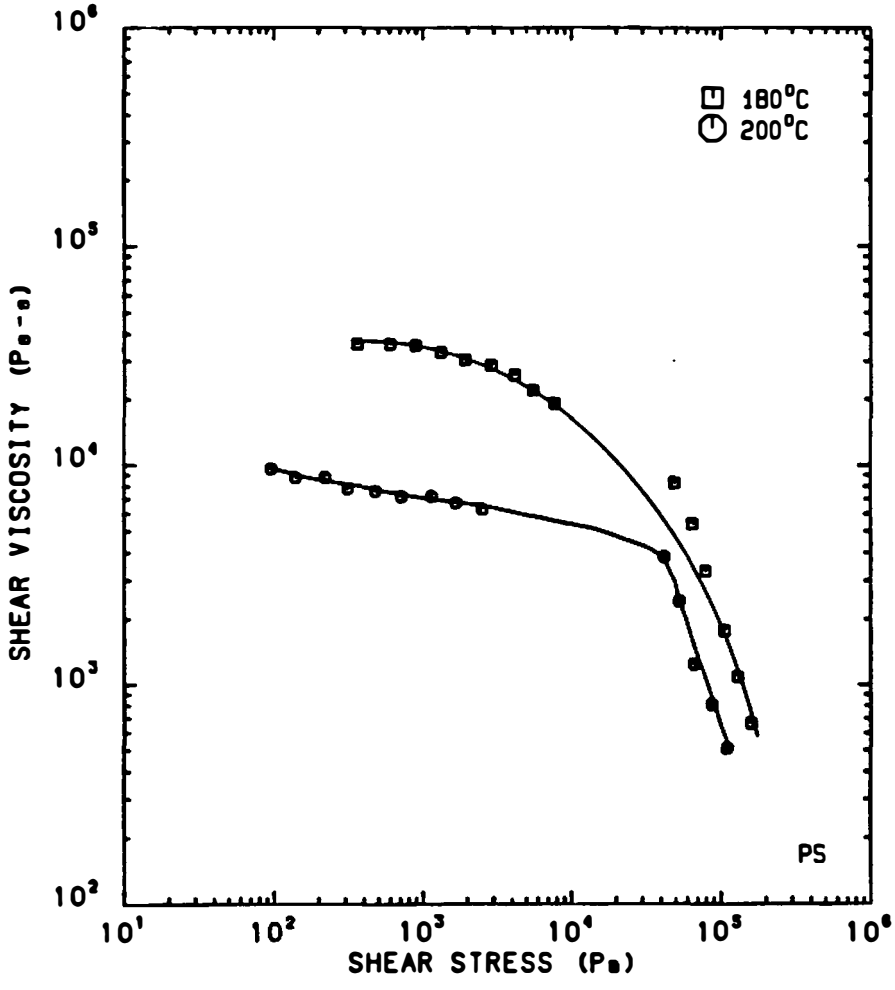

Figure 46. Viscosity Versus Shear Stress Plot of PS Melts.

Table 5. Domain Flow Stress Values for Thermotropic Melts of POB/PET 60/40 and EC as Obtained from Casson Plots.

Polymer Melt Type	Polymer Melt Temperature	Domain Flow Stress	Casson Plot Correlation Value
	^{o}C	Pa.	
POB/PET 60/40	190	20580	0.939
	210	3970	0.939
	240	840	0.987
	250	290	0.990
	260	180	0.973
	280	110	0.977
	300	60	0.989
	320	100	0.985
	340	75	0.988
EC	180	5880	0.992
	190	3870	0.999
	200	3100	0.995
	210	80	0.996

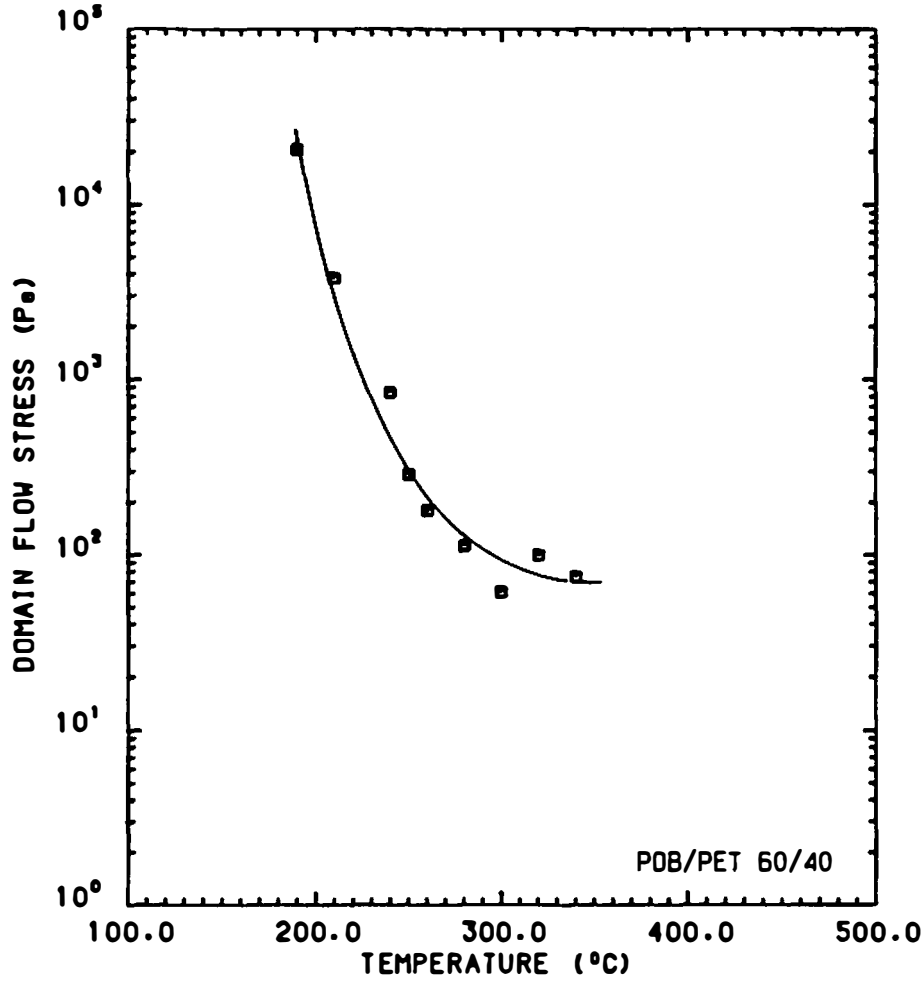

Figure 47. Domain Flow Stress Versus Temperature Plot of POB/PET 60/40 Melts.

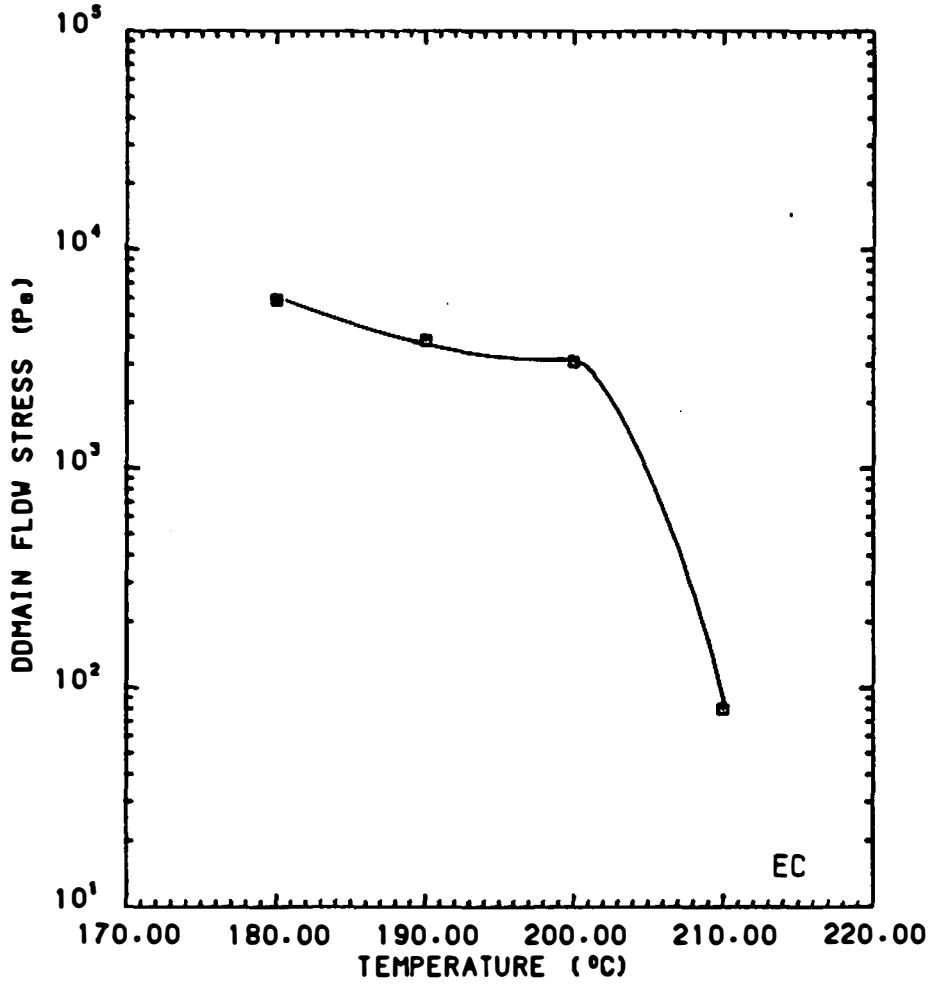

Figure 48. Domain Flow Stress Versus Temperature for EC Melts.

discussed in the previous section, the change in the viscosity behavior around 260°C relates to the melting transition of the POB rich phase at 255°C. The melt is apparently reinforced by unmelted 'domains' of the POB rich phase. This reinforcement or 'filler effect' of the POB rich 'domains' appears to be responsible for the large 'domain flow' stresses and, consequently, for the visco-plastic flow behavior. Above 260°C the POB rich phase has melted. The softened 'domains' do not provide rigid reinforcement of the melt. Consequently, the flow behavior is more shear thinning than viscoplastic. The decline in the 'domain flow' stresses with respect to temperature is clearly illustrated in Figure 47 and Table 5. The 'domain flow' stress exhibits a steep exponential decline from 190°C to 340°C. Examination of the values in Table 5 shows the 'domain flow' stress decreases from 20.6 kPa at 190°C to 0.18 kPa at 260°C. This represents 99% of the decline. From 260°C to 340°C the 'domain flow' stress approaches an assymptotic value of 75 Pa.

The viscosity versus shear stress plots of the EC melts show qualitative similarities to the plots of POB/PET 60/40. Below 200°C the plots shown in Figure 45 possess slopes between 60 and 75 degrees in inclination. This suggests the presence of significant 'domain flow' stresses as well as viscoplastic flow behavior. At 210°C the slope has decreased to 30 degrees indicating a very

small or insignificant 'domain flow' stress. The shape of the plot indicates mainly viscoelastic flow behavior, which is characterized by shear stress independence at low shear and shear thinning behavior at high shear. The 'domain flow' stress exhibits an exponential decline from 5.9 kPa at 180°C to 3.1 kPa at 200°C as shown by Figure 48 and Table 5. Above 200°C a steep decline toward zero can be observed. From 180°C to 200°C the 'domain flow' stress declines 47% in magnitude. At 210°C the 'domain flow' stress has declined by 98%.

The viscosity versus shear stress plots for PS melts in Figure 46 (p. 208) are substantially different in shape than those of POB/PET 60/40 melts below 260°C or of EC melts below 200°C. The plots of PS exhibit slopes of less than 20 degrees in inclination in the low shear region. In the high shear region, the slopes approach 60 degrees in inclination. The initial slopes do not indicate 'domain deformation' or 'yielding' behavior or the presence of 'domain flow' stresses. The shapes of the plots indicate mainly viscoelastic flow behavior. Quasi-Newtonian to slightly shear thinning flow behavior is observed at low shear, while more pronounced shear thinning behavior is observed at high shear.

The viscosity versus shear stress plots for POB/PET 60/40 and EC melts show qualitative similarities to the viscosity versus shear stress plots reported by White and

coworkers [152,223,230] for carbon black filled and calcium carbonate filled polystyrene (PS) melts. For the filled PS melts, the slopes of the plots approached 90 degree or vertical inclinations under the conditions of high volumetric loadings and/or small particle sizes of the filler material. At low volumetric loadings and/or large particles sizes, the slopes approached inclinations of about 30 degrees. For the POB/PET 60/40 and EC melts, the analogous factors appear to be the number of 'domains' and the 'domain' size. At temperatures just above the melting points, the 'domains' are probably small and rigid. The number of 'domains' is probably large. At higher temperatures, the 'domains' are less rigid and probably have a tendency to coalesce and form larger 'domains'. This would also imply the number of 'domains' decreases.

The 'domain flow' stress versus temperature plots for both POB/PET 60/40 and EC appear to be melt analogies to the 'domain flow' stress versus concentration plots for lyotropic HPC, EC and PBA solutions. Both sets of plots (Figure 26 on page 171 and Figures 47-48 on pages 210 and 211) indicate the 'domain flow' stress increases to a finite value when the anisotropic state is formed. With decreasing melt temperature or increasing polymer concentration, a plateau or minimum value is attained in the 'domain flow' stress. Below a certain melt temperature or

a certain polymer concentration, a steep exponential-like increase is observed in the 'domain flow' stress. This increase appears to coincide with the formation of a densely packed, 'multidomain' structure.

Results--Shear Stress Behavior

Plots of shear stress versus shear rate are shown in Figure 49 for POB/PET 60/40 melts in the 190°C to 340°C temperature range. Shear stress versus shear rate plots for EC melts are shown in Figure 50 for the 180°C to 210°C temperature range. Comparative plots for isotropic viscoelastic PS melts are shown in Figure 51 for temperatures of 180°C and 200°C. Table 6 indicates the slopes obtained for the initial shear flow region of the shear stress versus shear rate plots for all three polymer melts. For POB/PET 60/40 melts below 240°C, the initial shear flow portion occurs above shear rates of 2.0 s^{-1}. For melts at 240°C and 250°C, the initial shear flow region occurs at shear rates exceeding 0.3 s^{-1}. Above 260°C the initial shear flow region can be found in the 1 s^{-1} to 100 s^{-1} shear rate range. For EC at 180°C the initial shear flow region is observed in the 0.02 s^{-1} to 200 s^{-1} shear range. For the EC melts above 180°C, the initial shear flow range can be discerned in the 0.01 s^{-1} to 1 s^{-1} shear range. In the case of PS melts, the initial shear flow region is observed at shear rates below 6 s^{-1}.

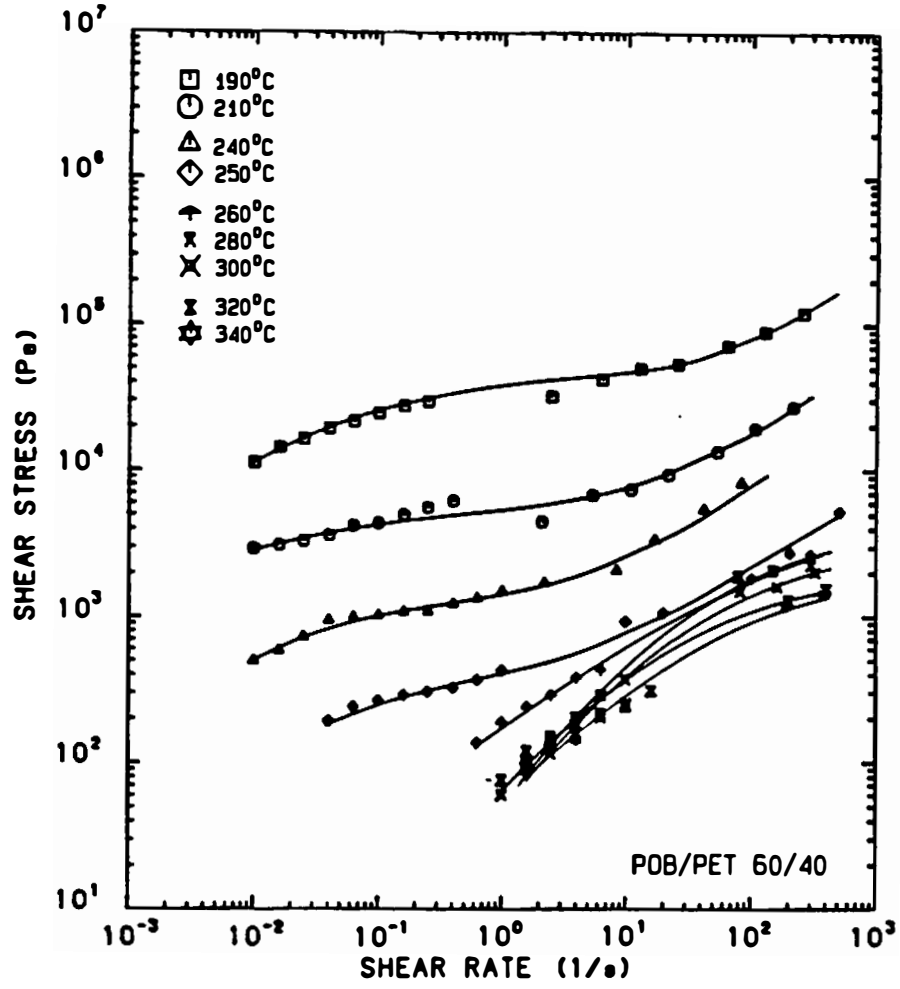

Figure 49. Shear Stress Versus Shear Rate Plot of POB/PET 60/40 Melts.

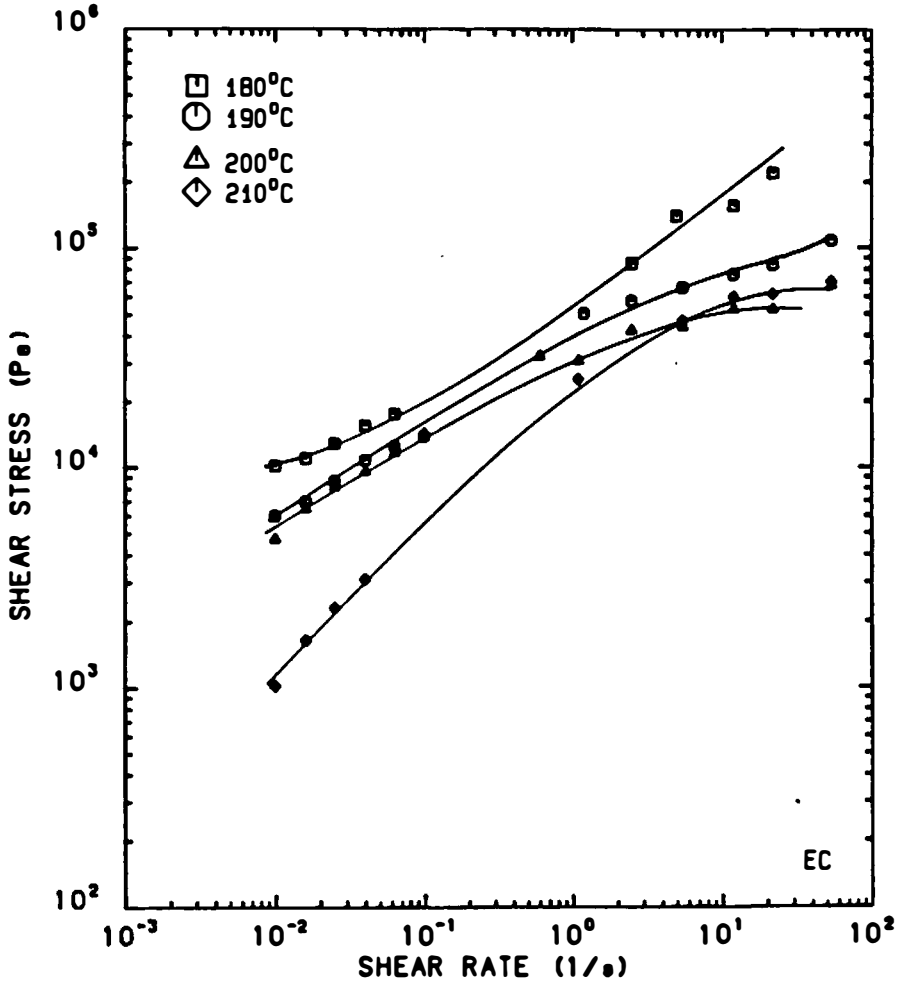

Figure 50. Shear Stress Versus Shear Rate Plot of EC Melts.

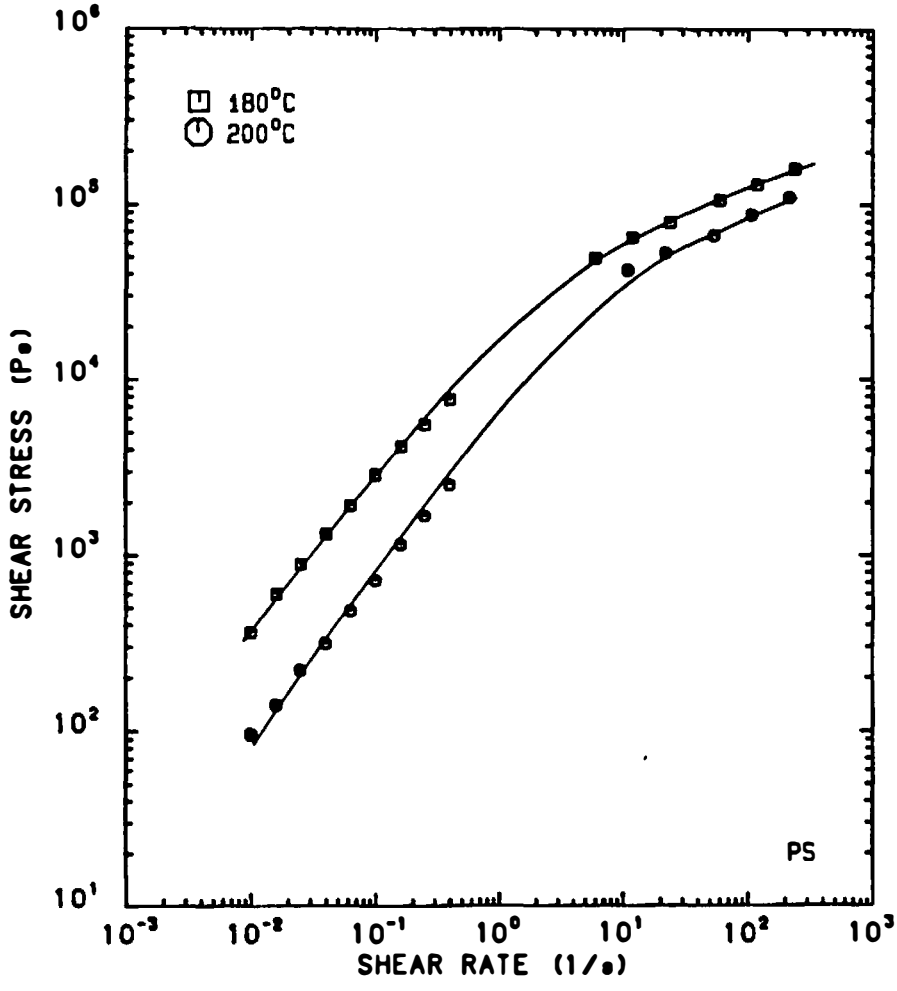

Figure 51. Shear Stress Versus Shear Rate Plot of PS Melts.

Table 6. Initial Slopes of the Quasi-linear Stress Region in the Shear Stress Versus Shear Rate Plots for POB/PET 60/40, EC and PS Melts.

Polymer Melt Type	Polymer Melt Temperature	Slope	Correlation Value
	°C		
POB/PET 60/40	190	0.28	0.990
	210	0.38	0.990
	240	0.44	0.970
	250	0.43	0.980
	260	0.52	0.998
	280	0.77	0.998
	300	0.72	0.995
	320	0.51	0.995
	340	0.51	0.998
EC	180	0.41	0.998
	190	0.44	0.996
	200	0.41	0.990
	210	0.66	0.998
PS	180	0.82	1.000
	200	0.89	0.996

The shear stress data for thermotropic POB/PET 60/40 and EC melts were fit or modeled using a modified version of the Herschel-Buckley [109] expression, equation (3.9) on page 181. Table 7 shows the correlation or fit of this equation along with the specified material parameters. Figures 52 and 53 show the experimental data for POB/PET 60/40 and EC melts as plotted in the Herschel-Bulkley form, HB shear stress, log ($\sigma_{12} - \sigma_{df}$), versus shear rate, log ($\dot{\gamma}$).

Discussion--Shear Stress Behavior

The plots from 190°C to 250°C in Figure 49 show non-linear behavior due to the viscoplastic response of the POB/PET 60/40 material. The lack of overlap between the data obtained from cone and plate measurements and capillary measurements cause some distortion in the 0.4 s^{-1} to 4 s^{-1} shear rate region. The three stress regions, discussed earlier for lyotropic HPC, EC and PBA solutions on pages 191 through 192, are not as clearly discerned in the thermotropic POB/PET 60/40 system. Figure 49 indicates that only the first two stress regions are observed. The plot at 190°C exhibits the stress buildup region below 0.3 s^{-1}. Between 0.3 s^{-1} and 2.0 s^{-1} the constant stress plateau is observed. This plateau represents the magnitude of the 'domain flow' stress. Above 2.0 s^{-1} the stress increases in a quasi-linear fashion.

Table 7. Parameters and Correlation Values of the Modified Herschel-Bulkley Equation for Anisotropic Melts of POB/PET 60/40 and EC.

Polymer Type	Polymer Melt Temperature	Domain Flow Stress	Power Law Coefficient	Power Law Exponent	Correlation Value
	^{o}C	Pa	Pa-s		
POB/PET 60/40	190	20580	12700	0.33	0.996
	210	3970	920	0.59	0.995
	240	761	760	0.50	0.996
	250	290	125	0.58	0.993
	260	180	88	0.60	0.999
	280	110	56	0.64	1.000
	300	60	40	0.67	1.000
	320	100	34	0.66	0.994
	340	75	30	0.65	1.000
EC	180	5880	48040	0.52	0.998
	190	3870	26780	0.39	0.988
	200	3100	24950	0.28	0.976

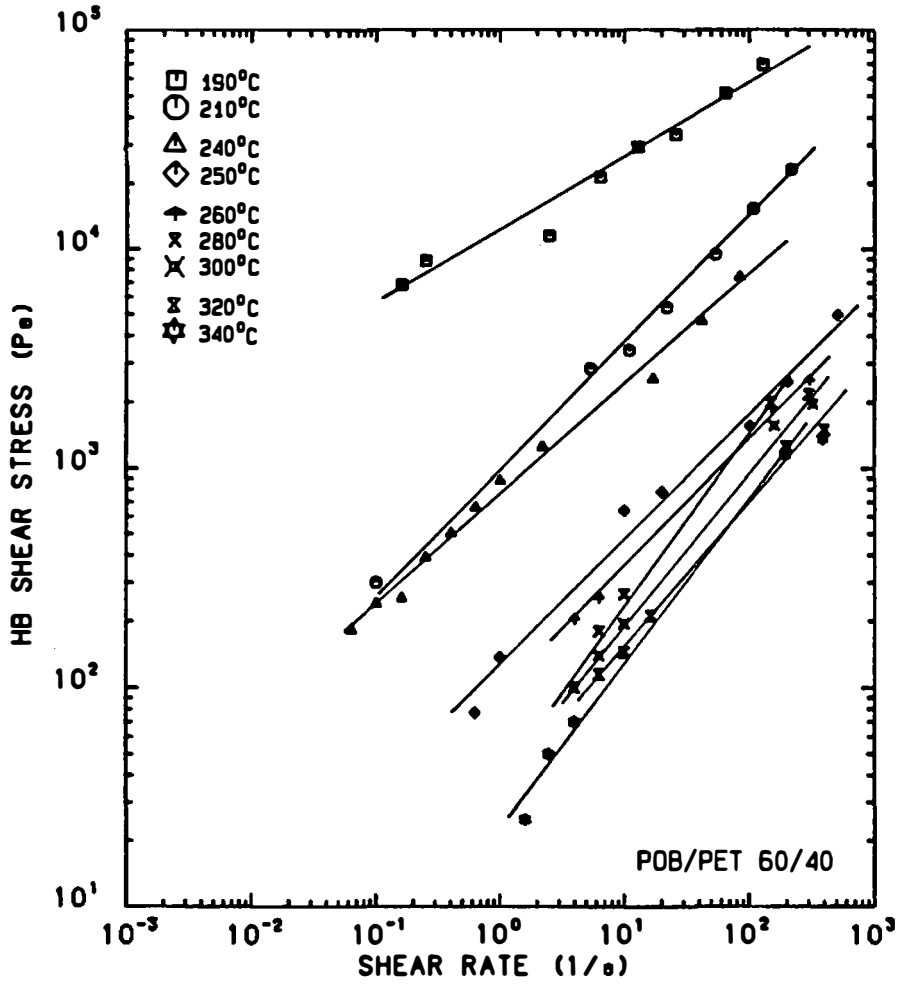

Figure 52. Herschel-Bulkley Plot of POB/PET 60/40 Melt Data.

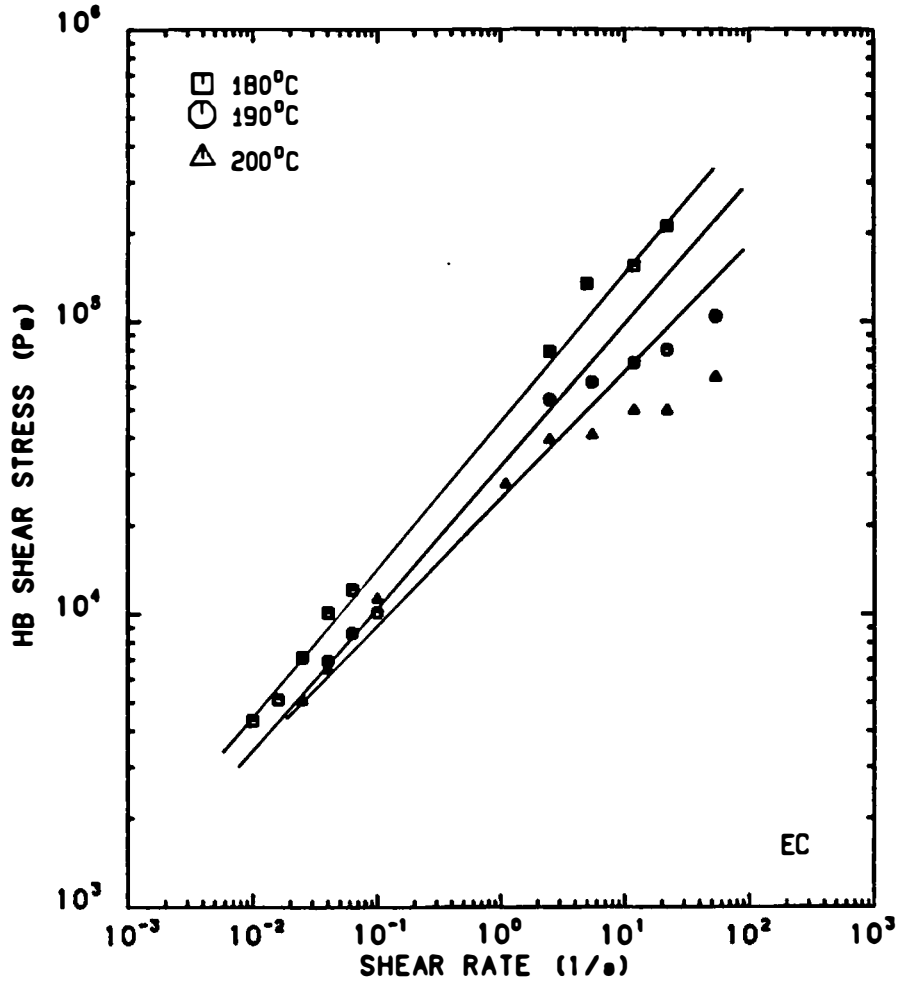

Figure 53. Herschel-Bulkley Plot of EC Melt Data.

In the plot at 210°C the stress buildup region occurs below 0.06 s^{-1}. The constant stress plateau can be discerned in the 0.06 s^{-1} to 2.0 s^{-1} shear region, although the data show some experimental scatter. Above 2.0 s^{-1} the quasi-linear shear stress region is observed. The plots at 240°C and 250°C show the stress buildup regions below 0.04 s^{-1} and 0.1 s^{-1}, respectively. The constant stress plateau, representing the 'domain deformation' response, can be observed between 0.04 s^{-1} and 0.3 s^{-1} for the 240°C plot and between 0.1 s^{-1} and 0.6 s^{-1} for the 250°C plot. The quasi-linear shear stress regions occurs at shear rates above 0.3 s^{-1} and 0.6 s^{-1}, respectively, for the two plots. The slopes of the quasi-linear shear stress or initial shear flow regions for the 190°C to 250°C are shown in Table 6 (p. 219). The slopes range from 0.28 at 190°C to 0.43 at 250°C. These slopes are substantially less than unity and indicate very pronounced shear thinning or pseudoplastic type flow behavior.

Figure 49 (p. 216) also shows the plots for POB/PET 60/40 over the 260°C to 340°C temperature range. These plots exhibit the last two stress regions. The first stress region is the quasi-linear stress or initial shear flow region. This is observed at shear rates between 1 s^{-1} and 100 s^{-1}. The slopes listed in Table 6 (p. 219) have values in the 0.51 to 0.77 range. The values indicate moderate to strong shear thinning or psuedoplastic

flow responses. Above 100 s^{-1} the plots exhibit low slope stress plateaus. These plateaus probably represent the onset of pronounced shear thinning flow behavior associated with stress saturation. The absence of the low shear rate constant stress plateau in these plots is puzzling. The values of the 'domain flow' stress as shown in Table 5 (p. 209) indicate that constant stress plateaus should be observed in the plots. This indicates the values of the 'domain flow' stress were overestimated by the Casson [48] plot method.

The shear stress versus shear rate plots for 180°C to 210°C EC melts shown in Figure 50 (p. 217) are similar to 260°C to 340°C plots of POB/PET 60/40. These plots do not show the low shear constant stress plateaus at the shear rates measured. The values of the 'domain flow' stress as observed in Table 5 (p. 209) are substantially lower than the shear stresses measured. This indicates that constant stress plateaus exist at shear rates below 0.01 s^{-1}. The plot of EC at 180°C only shows the quasi-linear stress region. The plots at 190°C, 200°C and 210°C all show the quasi-linear stress region below 1.0 s^{-1} and the stress saturation plateau above 1.0 s^{-1}. The slopes of the initial shear flow region in the 180°C, 190°C, and 200°C plots have values in the 0.4 to 0.45 range, while the slope of the 210°C plot has a value of 0.66. These values

are substantially less than unity and indicate the flow behavior is mainly shear thinning.

The shear stress versus shear rate plots for PS, shown in Figure 51 (p. 218), also show a two region stress curve. Qualitatively, these plots resemble the POB/PET 60/40 plots above 260°C and the EC plots above 180°C. The slopes obtained for the initial shear flow portion of the plots, however, are significantly higher and have values in the 0.8 to 0.9 range. These values are much closer to unity, indicating that PS is less shear thinning than either POB/PET 60/40 or EC at low shear rates. At high shear rates, the plots exhibit stress saturation plateaus similar to those of both POB/PET 60/40 and EC. This marks the onset of pronounced shear thinning or power law type flow behavior.

The shear stress versus shear rate data for thermotropic POB/PET 60/40 and EC melts were fit using a modified form of the Herschel-Bulkley [109] equation as indicated by equation (3.9) on page 181. The correlation or fit provided by this modified equation was observed to be 0.98 or better. The high correlations, as shown in Table 7 (p. 221), indicate the experimental data conform to the Herschel-Bulkley form quite well. Figures 52 and 53 also support this conclusion. The characterization of POB/PET 60/40 and EC melts as Herschel-Bulkley type fluids imply these melts will adopt a blunted rather than parabolic

velocity profile during flow. This would lead to a highly oriented skin and low oriented core solid state structure observed for these materials [224,227].

The viscoplastic flow behavior of POB/PET 60/40 melts below 260°C shows characteristics of Region I, according to the Onogi-Asada [18,179] phenomenological framework. The two part stress curve associated with this viscoplastic flow behavior appears to be consistent with a Region I type flow curve. The shear stress responses of POB/PET 60/40 melts above 260°C and EC melts below 210°C, however, are not consistent with characteristic viscoplastic or Region I [18] flow behavior. The two part stress curve of these materials may represent a variant of Region I behavior. The apparent 'domain flow' stresses are significantly smaller than the shear stresses for the EC melts. This suggests the 'multidomain' or 'polydomain' structure is very easily destroyed under shear. These two part stress curves show similarities to the predicted stress curve encompassing the quasi-Newtonian, or Region II, and shear thinning, or Region III, flow curves [196]. However, the experimentally observed slopes are less than one and indicate shear thinning rather than quasi-Newtonian viscosity behavior.

Results--First Normal Stress Differences

Plots of the first normal stress difference, N_1, as a function of shear rate are shown in Figure 54 for POB/PET

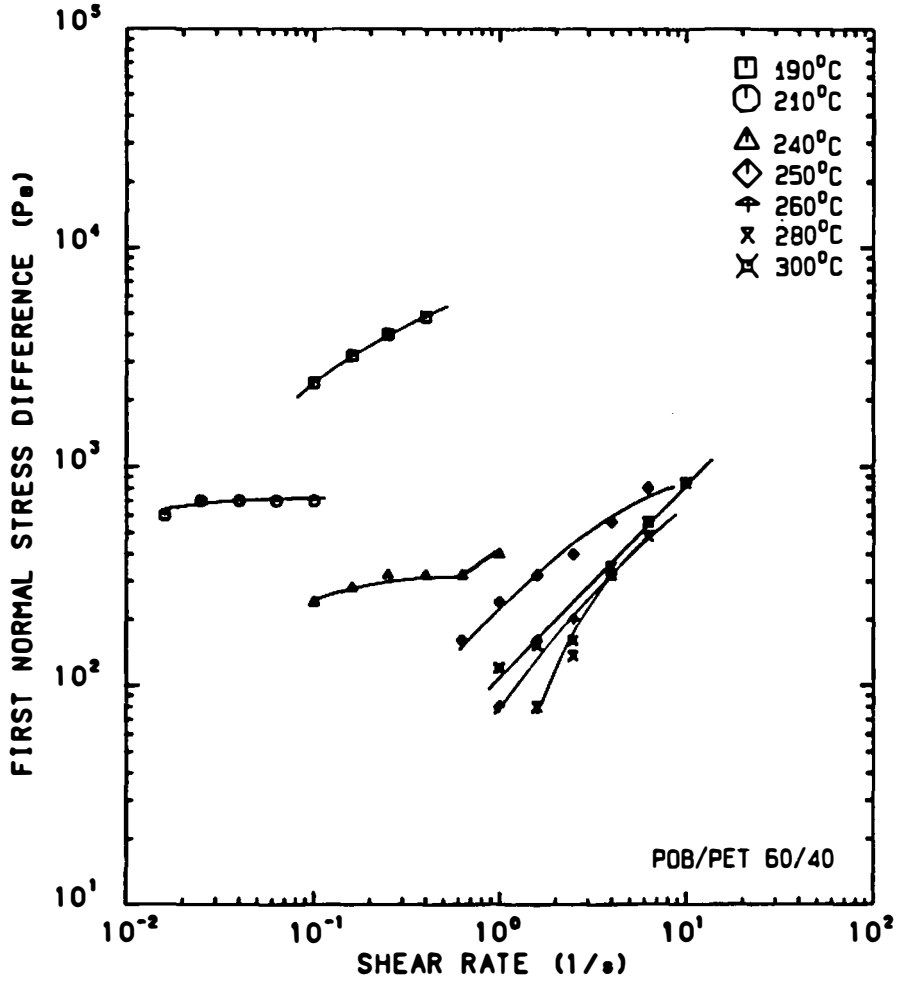

Figure 54. First Normal Stress Difference Versus Shear Rate of POB/PET 60/40 Melts.

60/40 melts. The N_1 values for POB/PET 60/40 were obtained for the 210°C to 320°C temperature range from cone and plate measurements. Related to N_1 data are the extrudate or die swell data obtained from capillary experiments. Extrudate swell data are presented as a function of extrusion temperature in Figure 55 for POB/PET 60/40 over the 190°C to 340°C temperature range. The N_1 data for EC melts obtained from cone and plate measurements in the 180°C to 210°C temperature range are shown in Figure 56. Comparative N_1 data are shown for PS melts in Figure 57. Table 8 shows the slopes of the N_1 plots in Figures 54, 56 and 57.

The first normal stress differences were determined in each case from the magnitudes of the normal or vertical thrust forces measured during cone and plate experiments. In the case of POB/PET 60/40 and EC melts, ambiguities arose as to the true magnitudes of these measured normal forces. These ambiguities are related to the sample loading process. When the sample is compressed during loading of the cone and plate instrument, resistive forces are generated which do not decay away to zero. These compressive loading forces cause a positive displacement of the normal force relaxation baseline with respect to the instrument zero baseline. At commencement of shear, the microstructure of the material is broken down so that it no longer supports the compressive load. The baseline

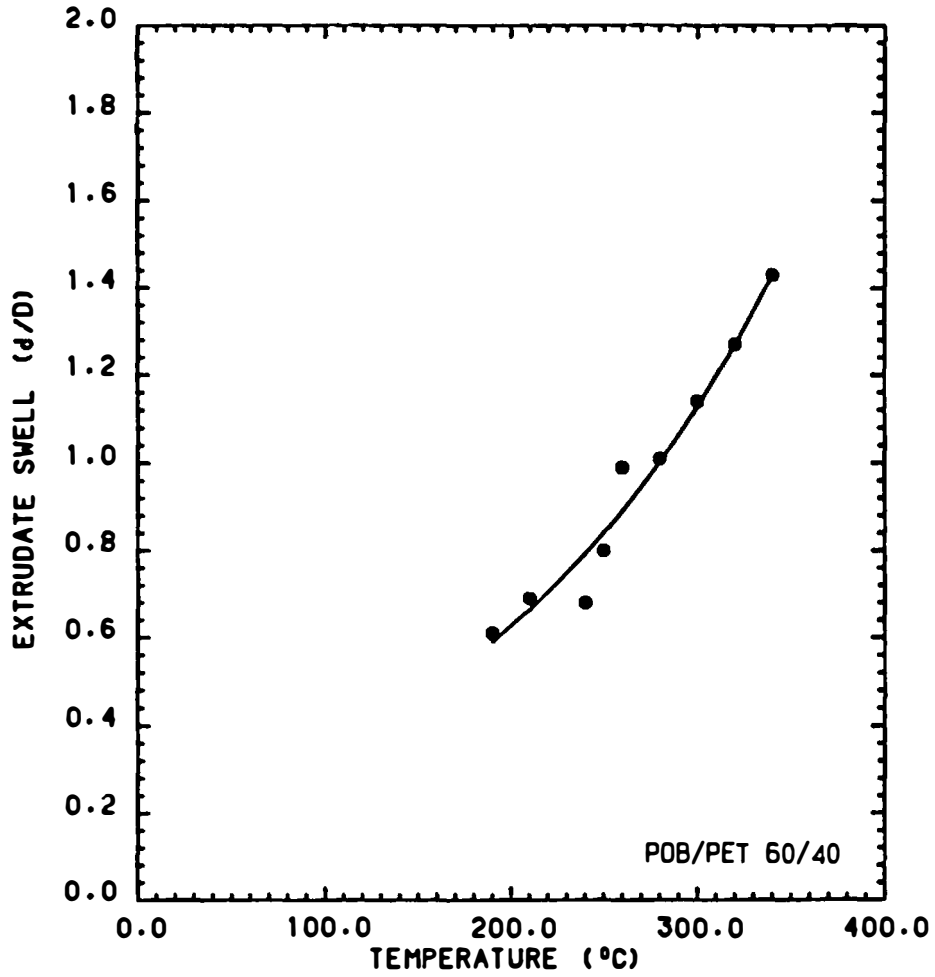

Figure 55. Plot of Extrudate Swell Versus Extrusion Temperature for POB/PET 60/40 Melts. Conditions: Apparent Shear Rate: 154 s^{-1}, L/D = 30, D = 0.074 cm

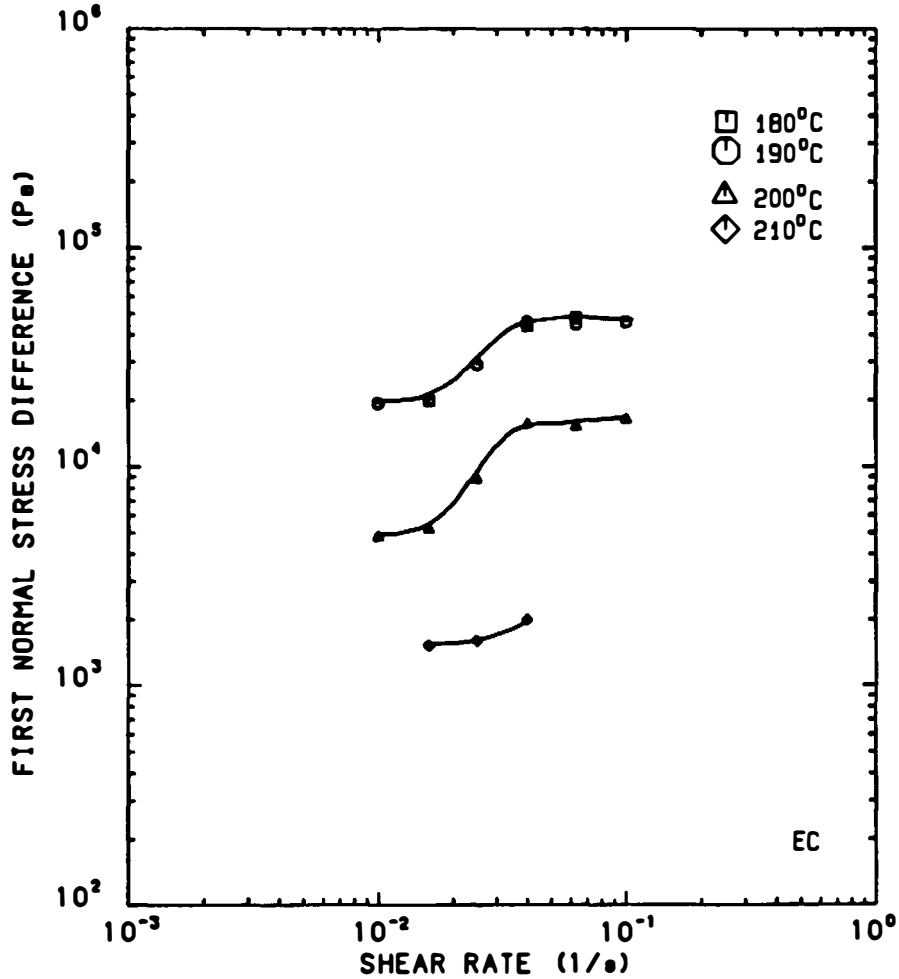

Figure 56. First Normal Stress Difference Versus Shear Rate Plot of EC Melts.

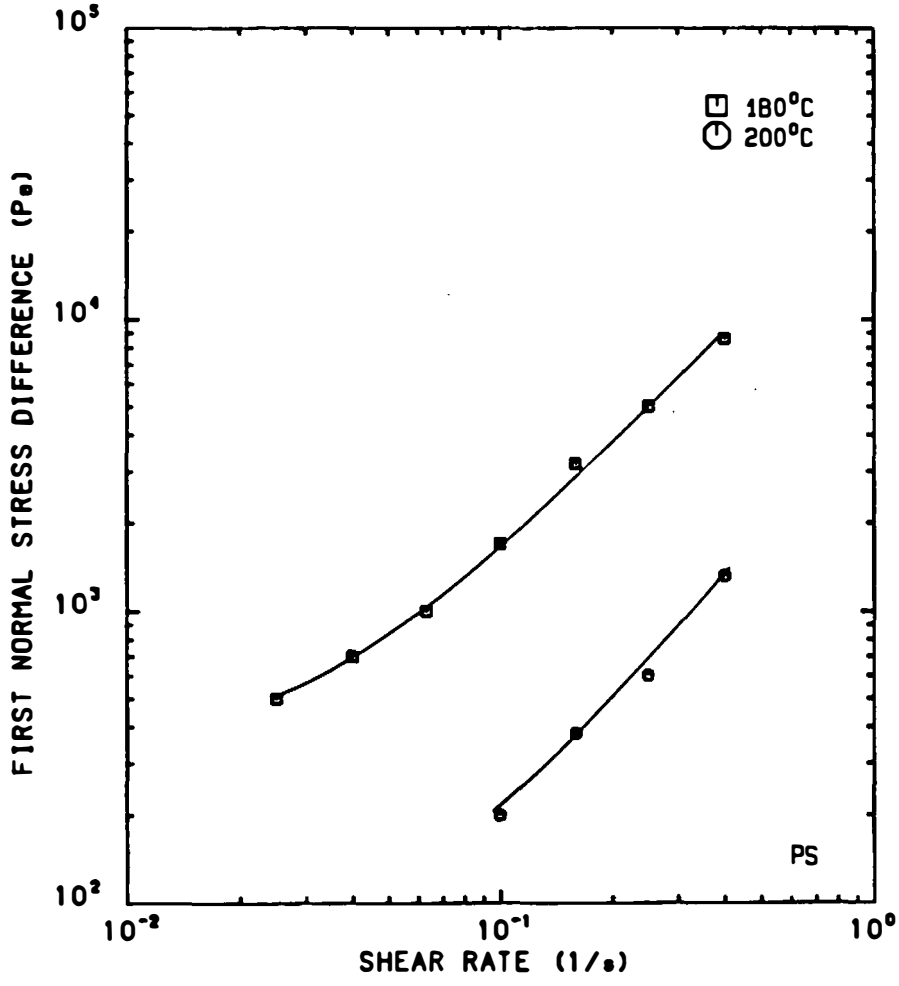

Figure 57. First Normal Stress Difference Versus Shear Rate Plot of PS Melts.

Table 8. Slopes of the First Normal Stress Difference Versus Shear Rate Plots for POB/PET 60/40, EC and PS Melts.

Polymer Melt Type	Polymer Melt Temperature	Slope	Correlation Value
	°C		
POB/PET 60/40	210	0.50	0.995
	240	0.09	0.844
	250	0.17	0.948
	260	0.67	0.997
	280	0.99	0.995
	300	1.38	0.985
	320	0.89	0.972
EC	180	0.70	0.955
	190	0.64	0.948
	200	0.88	0.960
	210	0.30	0.935
PS	180	1.12	0.998
	200	1.33	0.996

displacement is reduced during the experiment and shows variation in position with time. In the presence of these anomalies, the total thrust force is a combination of residual compressive loading forces and the normal forces generated during shear. If the compressive loading forces are not too large, the true magnitudes of the normal forces can be determined from the displacement of the normal force trace with respect to the instrument zero baseline. This baseline does not vary in position with time. For very large compressive loading effects, the normal forces cannot be separated from the resistive forces.

Similar anomalies have been reported for filled polymer melts and thermotropic HPC melts by White and coworkers [223,230]. Figure 58 illustrates the normal force anomaly for a HPC melt at 180°C as reported by Suto, White and Fellers [228]. These anomalies are not observed in isotropic viscoelastic polymer melts like polystyrene. The relaxation baseline for these polymers coincides with the instrument zero baseline prior to initiation of shear.

Discussion--First Normal Stress Differences

For POB/PET 60/40, the first normal stress differences (Figure 54, p. 228) were observed to possess positive values over the 210°C to 320°C temperature range. Data could not be obtained at 190°C due to complete

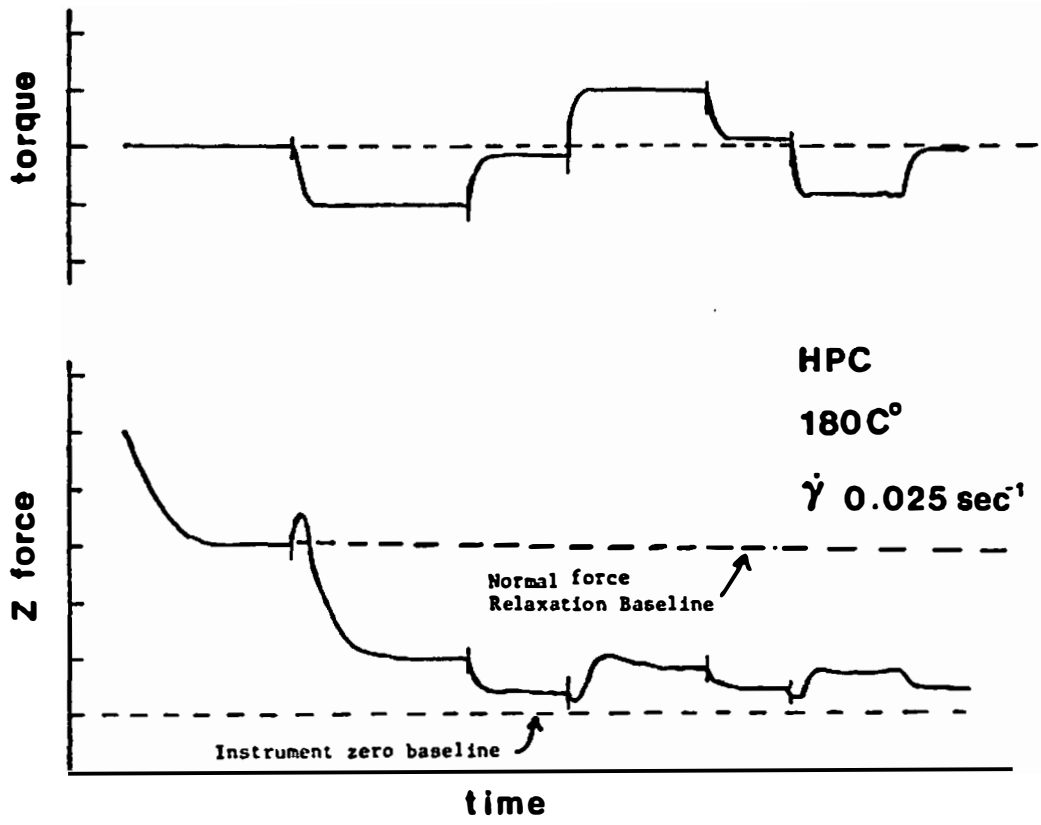

Figure 58. Torque and Normal Force Traces as a Function of Time During Measurements with HPC.

Source: Suto, S., White, J.L. and Fellers, J.F., Rheol. Acta. 21, 62 (1982)

suppression of the normal forces by the compressive loading forces. From 210°C to 250°C, the data were obtained with respect to the instrument zero baseline. However, the compressive loading forces could not be completely separated from the normal forces. The normal force traces from 260°C to 320°C did not exhibit apparent compressive loading effects. The N_1 data were obtained with respect to the relaxation baseline. The first normal stress differences from 260°C to 280°C are quantitatively similar to the results reported by Gottis and Baird [94] for the same material at 260°C to 285C.

Distinct differences in the N_1 behavior are observed at temperatures above and below 260°C. The first normal stress differences decrease with respect to temperature from 210°C to 250°C. From 260°C to 320°C the N_1 data 'group together' and tend to overlap. Below 260°C the first normal stress differences are similar in magnitude to the corresponding shear stresses. Above 260°C the N_1 values are 1.5 to 2.5 times greater in magnitude. The slopes of the N_1 plots presented in Table 8 vary significantly with respect to temperature. Below 260°C the slopes are much smaller than one and exhibit values in the 0.1 to 0.5 range. Above 260°C the slopes tend toward a value of one and show values from 0.7 to 1.4. Gottis and Baird [94] reported slopes of one for plots of N_1 versus shear rate for POB/PET at 275°C. The theories of Doi [62]

and Leslie-Ericksen [148] also predicted slopes of one for the N_1 plots versus shear rate plots of liquid crystals.

The constrasting behavior of N_1 above and below 260°C is related to the melting transition of the POB rich phase at 255°C. Below 260°C the unmelted POB rich 'domains' reinforce the melt. This reinforcement or 'filler' effect causes the presence of compressive loading forces and acts to suppress the N_1 values. This is apparent from the low N_1/σ_{12} ratios and the low values of the slopes. Similar suppression of the first normal stress differences were observed in filled polystyrene melts by White and coworkers [152,166.223,230]. Above 260°C the melt is no longer reinforced by rigid POB rich 'domains'. The first normal stress differences are not as suppressed and the compressive loading effects are absent. The N_1/σ_{12} ratios are much larger and the slopes tend toward a value of one.

Figure 55 (p. 230) shows the extrudate swell data for POB/PET 60/40 as a function of temperature. Below 260°C significant extrudate contraction is observed. Above 260°C the extrudate swell exceeds a value of one. These results are quantitatively consistent with swell data reported by Jerman and Baird [124] for POB/PET 60/40. The trend of the extrudate swell with respect to temperature parallels that of the 'domain flow' stress data with temperature (Figure 47, p. 210). The high 'domain flow'

stress region below 260°C can be correlated with extrudate contraction. Above 260°C extrudate swell becomes greater than one corresponding to the low 'domain flow' stress region. The extrudate swell behavior like the first normal stress difference behavior is related to the POB melting transition at 255°C. The same suppression effects are observed in both types of data.

The first normal stress differences for EC are shown in Figure 56 (p. 231). The N_1 data show a significant amount of experimental scatter. The data could not be completely separated from the contribution of residual compressive forces. The slopes of the plots shown in Table 8 (p. 234) are less than unity and vary in the 0.65 to 0.88 range. The magnitudes of the compressive forces were much larger than expected, since the shear stress data do not indicate significant 'yielding' or viscoplastic effects. This suggests the initial 'multidomain' structure can support a significant compressive load at rest, but not after shear.

Plots of the first normal stress differences versus shear rate, presented in Figure 57 (p. 232) for PS at 180°C and 200°C, show slopes greater than one but less than two. The normally observed slope for normal viscoelastic polymer melts is two. The plots do not indicate normal force suppression or compressive loading effects

observed in EC or POB/PET 60/40 melts. The data suggest the melt at 200°C is more elastic than the melt at 180°C.

3. IDENTIFICATION OF ORDERED PHASES PRESENT

A. Results

A WAXD film pattern of the powdered POB homopolymer, taken by H. Sugiyama [224], was used to characterize the crystalline reflections in both the homopolymer, itself, and in the POB/PET 60/40 copolymer. A plotter generated facsimile of this pattern is shown as Figure 59. The measured diffraction spacings from the WAXD film pattern were compared with wide angle (2θ) diffractometer scans of a sintered POB sheet and a representative POB/PET 60/40 fiber bundle. The diffractometer scans of the homopolymer and the copolymer are shown as Figures 60, 61, and 62.

The WAXD pattern of POB consisted of 15 diffraction rings ranging from 1.53 cm to 6.64 cm in diameter. The first (or leftmost) column in Tables 9 through 11 shows the diffraction spacings, d_{hkl}, obtained from these rings. The second column in the tables identifies the spacings of the seven strongest diffraction peaks as determined from a diffractometer scan of POB. The third and fourth columns in the tables show the calculated diffraction spacings and Miller index assignments, based on three proposed unit cells for POB [92,150]. Table 9 shows the indexation of POB based on the phase I orthorhombic unit cell proposed

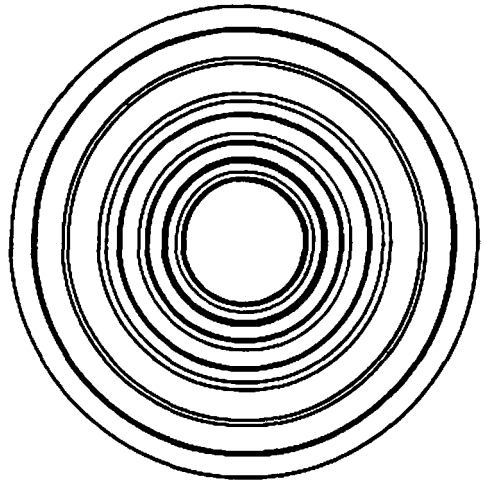

Figure 59. Plotter Generated Facsimile of POB Homopolymer WAXD Pattern.

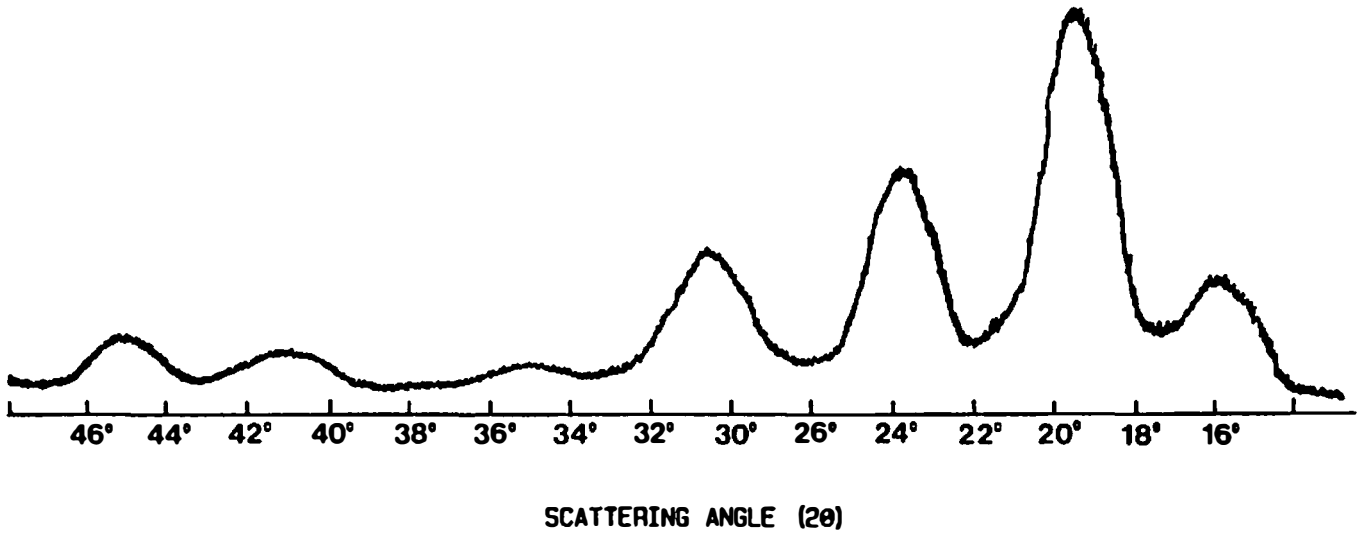

Figure 60. Wide Angle X-ray Counter Diffractometer Scan of the POB Homopolymer.

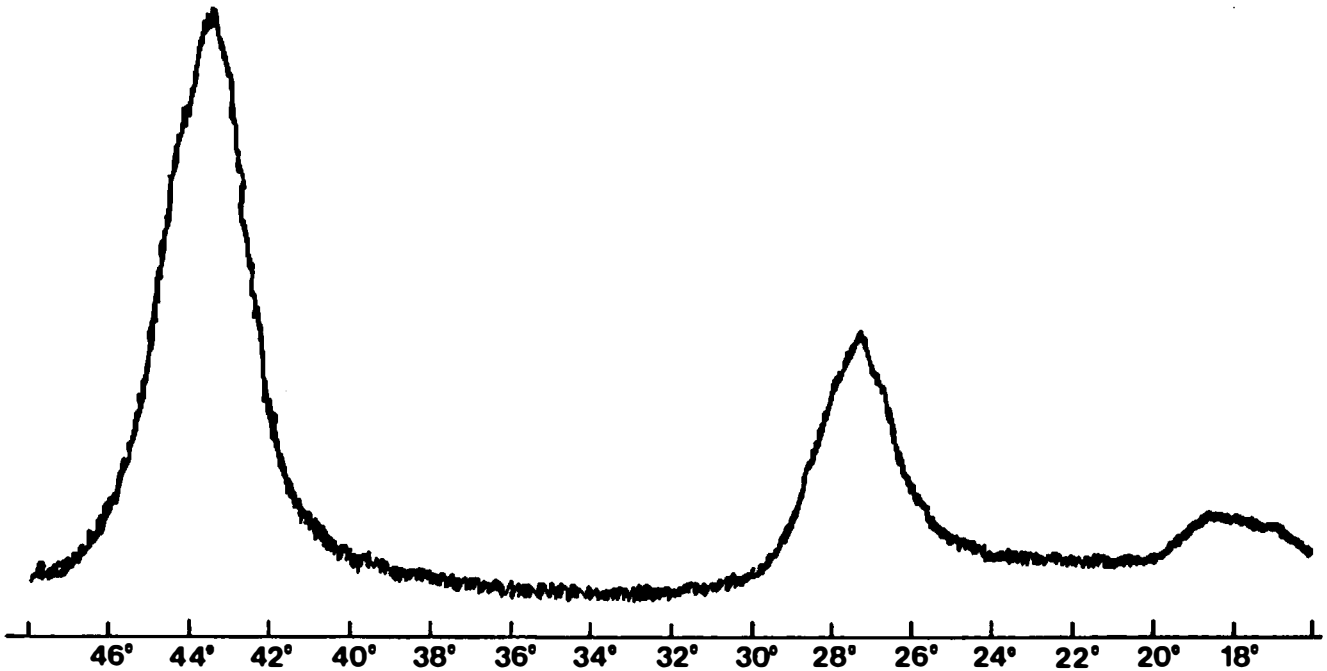

Figure 61. Meridional Wide Angle X-ray Counter Diffractometer Scan of POB/PET 60/40 Fibers.

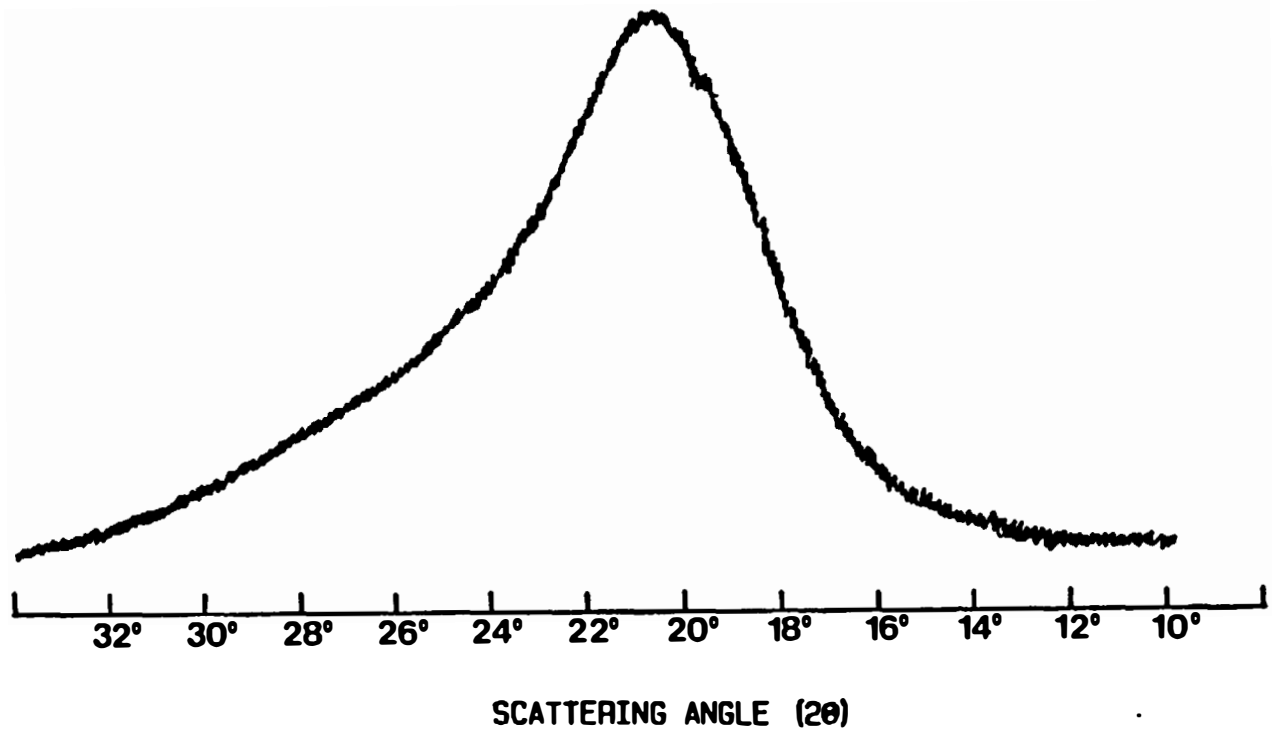

Figure 62. Equatorial Wide Angle X-ray Counter Diffractometer Scan of POB/PET 60/40 Fibers.

Table 9. Diffraction Data From 100% Poly(p-oxybenzoate) (POB) Indexed with Phase I Unit Cell of Geiss and Coworkers.

Measured[a] d_{hkl}	Measured[b] d_{hkl}	Calculated d_{hkl}	Miller Index Assignment
nm	nm	nm	h k l
0.618 (w)	---	0.628	0 0 2
0.575 (s)	0.557 (m)	0.570	0 1 0
0.521 (m)	---	0.519	0 1 1
0.462 (vs)	0.455 (vs)	0.456	1 1 0
0.437 (m)	---	0.429	1 1 1
0.381 (s)	0.374 (s)	0.381	2 0 0
0.351 (m)	---	---	---
0.310 (s)	0.312 (m)	0.314	0 0 4
0.284 (w)	---	0.285	0 2 0
0.271 (m)	0.270 (w)	0.267	1 2 0
0.234 (w)	---	0.232	3 1 0
0.230 (m)	0.232 (w)	0.228	2 2 0
0.210 (w)	0.209 (w)	0.209	0 0 6
0.198 (w)	---	0.196	0 1 6
0.190 (w)	---	0.190	4 0 0

Key: (w) = weak intensity, (m) = medium intensity, (s) = strong intensity, (vs) = very strong intensity

[a]Obtained from WAXD film pattern

[b]Obtained from Wide Angle (2θ) Counter Diffractometer Scan

Table 10. Diffraction Data From 100% Poly(p-oxybenzoate) (POB) Indexed with Phase I Unit Cell of Leiser.

Measured[a] d_{hkl}	Measured[b] d_{hkl}	Calculated d_{hkl}	Miller Index Assignment
nm	nm	nm	h k l
0.618 (w)	---	0.625	0 0 2
0.575 (s)	0.557 (m)	0.570	0 1 0
0.521 (m)	---	0.519	0 1 1
0.462 (vs)	0.455 (vs)	0.454	1 1 0
0.437 (m)	---	0.427	1 1 1
0.381 (s)	0.374 (s)	0.376	2 0 0
0.351 (m)	---	---	---
0.310 (s)	0.312 (m)	0.312	0 0 4
0.284 (w)	---	0.285	0 2 0
0.271 (m)	0.270 (w)	0.266	1 2 0
0.234 (w)	---	0.235	0 2 3
0.230 (m)	0.212 (w)	0.227	2 2 0
0.210 (w)	0.209 (w)	0.208	0 0 6
0.198 (w)	---	0.196	0 1 6
0.190 (w)	---	0.188	4 0 0

Key: (w) = weak intensity, (m) = medium intensity, (s) = strong intensity, (vs) = very strong intensity

[a]Obtained from WAXD film pattern

[b]Obtained from Wide Angle (2θ) Counter Diffractometer Scan

Table 11. Diffraction Data From 100% Poly(p-oxybenzoate) (POB) Indexed with Phase II Unit Cell of Lieser

Measured[a] d_{hkl}	Measured[b] d_{hkl}	Calculated d_{hkl}	Miller Index Assignment
nm	nm	nm	h k l
0.618 (w)	---	---	---
0.575 (s)	0.557 (m)	0.553	0 2 0
0.521 (m)	---	0.508	0 2 1
0.462 (vs)	0.455 (vs)	---	---
0.437 (m)	---	---	---
0.381 (s)	0.374 (s)	0.377	1 0 0
0.351 (m)	---	0.357	1 1 0
0.310 (s)	0.312 (m)	0.312	1 2 0
0.284 (w)	---	0.277	0 4 0
0.271 (m)	0.270 (w)	0.264	1 3 0
0.234 (w)	---	---	---
0.230 (m)	0.212 (w)	0.223	1 4 0
0.210 (w)	0.209 (w)	---	---
0.198 (w)	---	---	---
0.190 (w)	---	0.186	2 1 0

Key: (w) = weak intensity, (m) = medium intensity, (s) = strong intensity, (vs) = very strong intensity

[a]Obtained from WAXD film pattern

[b]Obtained from Wide Angle (2θ) Counter Diffractometer Scan

by Geiss and coworkers [92]. This unit cell has the dimensions $\underline{a}$ = 0.762 nm, $\underline{b}$ = 0.57 nm, and $\underline{c}$ = 1.256 nm. The indexing schemes in Tables 10 and 11 are based, respectively, on the phase I and phase II orthorhombic unit cells of Lieser [150]. The phase I unit cell has the dimensions $\underline{a}$ = 0.752 nm, $\underline{b}$ = 0.57 nm, and $\underline{c}$ = 1.249 nm, whereas the phase II unit cell has the dimensions $\underline{a}$ = 0.377 nm, $\underline{b}$ = 1.106 nm, and $\underline{c}$ = 1.289 nm. The calculated diffraction spacings and Miller index assignments in the tables were generated by inserting the appropriate unit cell parameters into a Rigaku D/Max software program called DSP [200], which ran on a Digital Equipment Corporation PDP 11/34 minicomputer.

Table 12 shows the indexed electron diffraction data of POB obtained at high temperature by Blackwell and coworkers [34]. Blackwell et al. and Lieser both reported the formation of a third crystalline phase of POB at temperatures above 360°C. The reported unit cell of phase III was orthorhombic with dimensions $\underline{a}$ = 0.92 nm, $\underline{b}$ = 0.53 nm, and $\underline{c}$ = 1.24 nm.

Table 13 shows the meridional and equatorial diffraction spacings obtained from the respective diffractometer scans of the POB/PET 60/40 copolyester fiber bundle. The meridional scan in Figure 61 shows three or four peaks depending on interpretation. The first peak, located between 16° and 19°, is relatively broad and of weak

Table 12. Electron Diffraction Data of POB at High Temperature (>360°C) Indexed with Phase III Unit Cell of Blackwell and Coworkers.

Measured[a] d_{hkl}	Calculated d_{hkl}	Miller Index Assignment
nm	nm	h k l
Equatorial		
0.462	0.460/0.459	2 0 0 / 1 1 0
0.264	0.265	0 2 0
0.230	0.230	4 0 0 / 2 2 0
First Layer Meridional		
0.331	0.334	2 1 1
Meridional		
0.617	0.620	0 0 2
0.309	0.310	0 0 4
0.206	0.207	0 0 6

[a]Electron Diffraction Data cited from Blackwell, J., Lieser, G. and Gutierrez, G., Macromol. 16, 1418 (1983)

Table 13. Diffraction Data From POB/PET 60/40 Indexed with Phase III Unit Cells.

Measured d_{hkl}	Calculated[a] d_{hkl}	Calculated[b] d_{hkl}	Miller Index Assignment
nm	nm	nm	h k l
Equatorial			
0.440 (vs)	0.460	0.440	2 0 0 / 1 1 0
Meridional			
0.485 (w)	0.487	0.487	0 1 1
0.324 (m)	0.326	0.327	0 1 3 / 2 1 1
0.207 (s)	0.207	0.207	0 0 6

Key: (w) = weak intensity, (m) = medium intensity, (s) = strong intensity, (vs) = very strong intensity

[a] Calculated scattering angle I based on Phase III unit of Blackwell and coworkers.

[b] Calculated scattering angle II based on experimentally derived phase III unit cell.

intensity. This peak can be interpreted as a single peak centered at 18.3° (0.485 nm), although some of the diffractometer scans indicate the presence of two overlapping peaks at 17.3° and 18.3°. Less ambigious diffraction peaks of medium and strong intensities occur, respectively, at 27.5° (0.324 nm) and 43.8° (0.207 nm). The equatorial diffractometer scan, Figure 62, shows a single broad diffraction peak of strong intensity at 20.2°.

Table 13 shows the indexing scheme for the POB/PET 60/40 copolyester, based on the phase III unit cell of POB as proposed by Blackwell et al. [34]. This orthorhombic unit cell was derived from electron diffraction patterns of a high temperature phase of the POB homopolymer. Blackwell et al. reported that this unit cell, with dimensions of $\underline{a}$ = 0.92 nm, $\underline{b}$ = 0.53 nm, and $\underline{c}$ = 1.24 nm, also matched the diffraction patterns of POB/PET 60/40. A better fit with the experimentally determined diffraction spacings in Table 13 was obtained by employing an orthorhombic unit cell with dimensions $\underline{a}$ = 0.88 nm, $\underline{b}$ = 0.53 nm, and $\underline{c}$ = 1.24 nm. The 'DSP' program, mentioned earlier, was used to generate the calculated diffraction spacings and Miller indices for the two unit cells.

B. Discussion

Assignment of the Miller indices for the POB homopolymer and the POB/PET 60/40 copolymer was complicated by

reported observations of polymorphism in the homopolymer. Lieser [150] reported the presence of three distinct crystalline phases in POB, depending on molecular weight and temperature. All samples of the POB homopolymer appear to contain equilibrium amounts of phase I and phase II crystallites. The fraction of phase II diminishes with increasing molecular weight. It is most prevalent in oligmer POB samples.

The WAXD diffraction data of POB, reported in Tables 9 through 11 (pp. 244-246), indicate the presence of both phase I and phase II crystallites. The diffraction spacing located at 0.351 nm is entirely due to the presence of the (110) reflection plane of the phase II unit cell. The other eight observed hkl reflection planes (020), (021), (100), (040), (130), (140) and (210), overlap with the reflection planes from the phase I unit cell. Comparison of the phase I unit cell of Lieser [150] with that of Geiss et al. [92] suggests the latter provides a slightly better fit of the experimental diffraction spacings in Tables 9 through 11 (pp. 244-246).

At temperatures above 320^{o}C oligmer samples of POB were observed to form a third crystalline form designated as phase III. This phase was reported by Lieser [150], Blackwell et al. [34] and Economy et al. [78] to be a less ordered crystalline form than phase I or phase II. The major differences between phase I and phase III unit cells

are the dimensions of the 'a' and 'b' axes. A comparison of the diffraction data in Table 12 with that of Tables 9 and 11 (pp. 244 and 246) indicates the (110) and (200) reflection planes of phase I have migrated and superimposed at a larger diffraction spacing of 0.46 nm. The (020) reflection of the phase I unit cell migrates to a smaller diffraction spacing of 0.265 nm. The (002), (004) and (006) reflections do not change. These changes are consistent with an increase in the 'a' dimension from 0.76 nm to 0.9 nm and a decrease in the 'b' dimension from 0.57 nm to 0.53 nm. The 'c' dimension remains unchanged at 1.24 nm.

A number of studies [125,126,172,213] indicate the POB/PET 60/40 copolyester consists of a POB rich phase and a PET rich phase. Examination of the equatorial (2θ) diffraction scan of the copolyester, as shown in Figure 62 (p. 243), indicates that none of the characteristic PET diffraction peaks are present. These peaks are the (010) located at 17.5°, the (110) located at 22.3°, and the (100) located at 25.7° [242]. The copolyester shows a single equatorial peak centered at 20.2°. The absence of PET equatorial peaks indicates the PET rich phase forms an amorphous solid state. The POB rich phase was reported by Nicely [172] to consist of 80 mol% POB units, predominately arranged in dimer, trimer or tetramer microblocks along the main chain. The actual sequence arrangement of

the repeat units indicated by Nicely's high resolution NMR data would be the structure shown in diagram (21) on page 19. This structural arrangement provides for two or more p-oxybenzoate sequences on each end of a terepthalic acid unit and meets the four to one POB/PET ratio inherent in an 80 mol% POB phase. This arrangement also allows the chains in the POB rich phase to crystallize with the same c-axis repeat distance of two POB units as the homopolymer. The ethylene glycol units would be incorporated as defects in the crystal structure. The location of a strong meridional diffraction peak at 43.8^{o}, or 0.207 nm, in the 2θ scan of Figure 61 (p. 242) is in good agreement with the (006) diffraction plane of both phase I and phase III unit cells. This agreement suggests the c-axis repeat distance is about 1.24 nm in the POB rich phase. Less certain are the dimensions of the a-axis and b-axis of the POB/PET 60/40 unit cell. The limited number of diffraction spacings observed for the copolyester does not allow for a reliable indexation, except by comparison with POB. Blackwell et al. [34] makes a strong case for indexing the diffractions of the copolymer with the unit cell of phase III, rather than phase I, because of two factors:

1. the less compact unit cell of phase III would be more tolerant of defects containing ethylene glycol units and

2. the sequence of the monomer units along the copolymer chain would lead to a more irregular packing arrangement than for the homopolymer in phase I. The indexing scheme, based on the phase III unit cell, is shown in Table 13 (p. 249). The Miller index for the meridional at 27.5° (0.324 nm) is probably the (013), although the (211) may also be a valid index. The equatorial peak at 20.2° (0.440 nm) is best indexed by the (200) reflection. The peak can be alternately indexed as the (110).

A better fit of the diffraction spacings for POB/PET 60/40, in Table 13 (p. 249), can be obtained by reducing the 'a' dimension of the phase III unit cell from 0.92 nm to 0.88 nm. Examination of the diffraction spacings of POB/PET 60/40 and POB/PET 80/20, reported by Wissbrun [242], Blackwell et al. [34], and Zachariades et al. [246], indicates the 'a' dimension is 0.90 $\pm$ 0.02 nm.

4. FIBER ORIENTATION MEASUREMENTS

A. Results

Orientation measurements of the c-axis or polymer chain direction were obtained for melt spun fibers of POB/PET 60/40 prepared under both nonisothermal and isothermal spinning conditions. Each melt spinning die employed had a length to diameter ratio, L/D, of 50 and a die diameter, D, of 0.74 mm. Variations in the extrusion

temperature, extrusion rate, and drawdown ratio were made in order to determine the effect of these parameters on the c-axis orientation. Determinations of the orientation measurements were facilitated by the presence of a relatively strong meridional (006) diffraction peak in the x-ray diffractometer scans of the mounted POB/PET 60/40 fiber bundles. An azimithual intensity distribution or pole figure of the (006) diffraction peak was used to obtain the $\langle\cos^2\chi\rangle$ of each sample, where χ is the angle between the c-axis and the fiber axis. The $\langle\cos^2\chi\rangle$ was used to compute the c-axis orientation by means of the Herman's [108] orientation factor, f_H, defined by the expression

$$f_H = 0.5\ [3\langle\cos^2\chi\rangle - 1] \qquad (4.0)$$

Figures 63 and 64 show the plots of the Herman's orientation factor as a function of the extrusion rate for isothermal and nonisothermal spinning conditions. The plots were made at constant drawdown ratio (V_D/V_R = 200). Figures 65 and 66 show the plots of the orientation factor with respect to drawdown ratio for isothermal and non-isothermal spinning conditions. In both sets of plots a constant extrusion rate of V_D = 0.21 m/min was used. Figure 67 shows plots of the orientation factor with respect to extrusion temperature for nonisothermal and isothermal spinning conditions. The plots were made at

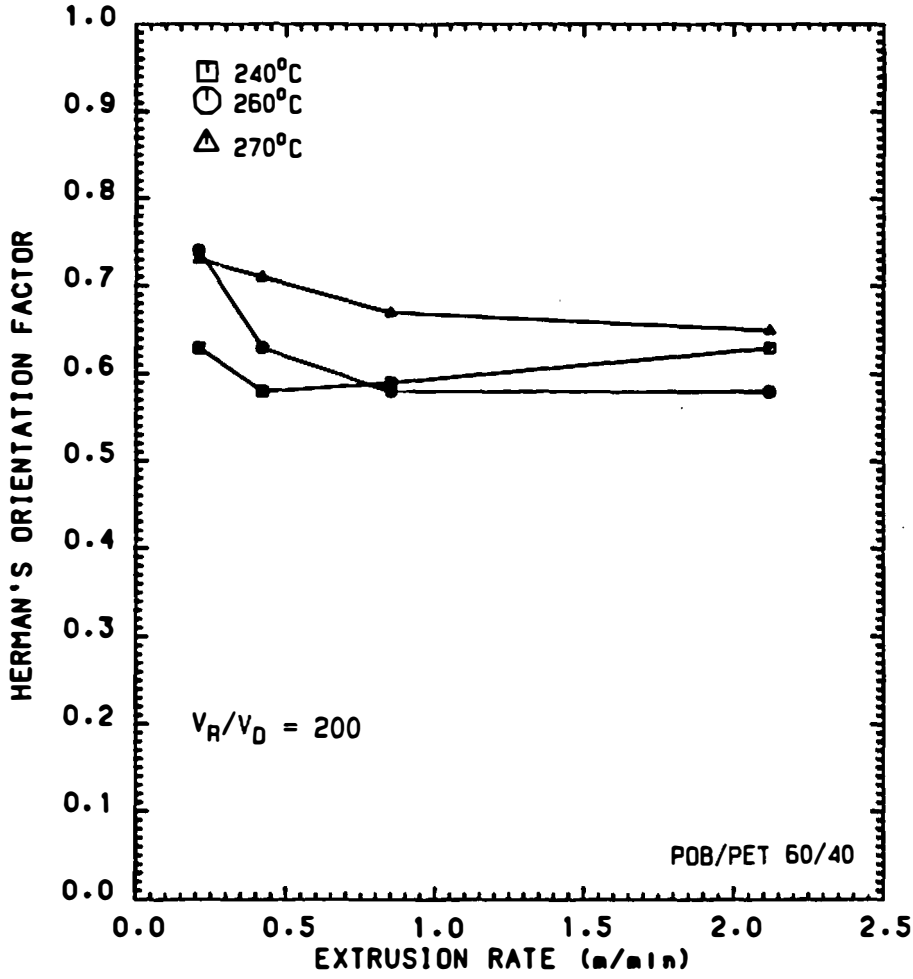

Figure 63. Plot of Herman's Orientation Factor Versus Extrusion Rate for Isothermal Melt Spun POB/PET 60/40 Fibers.

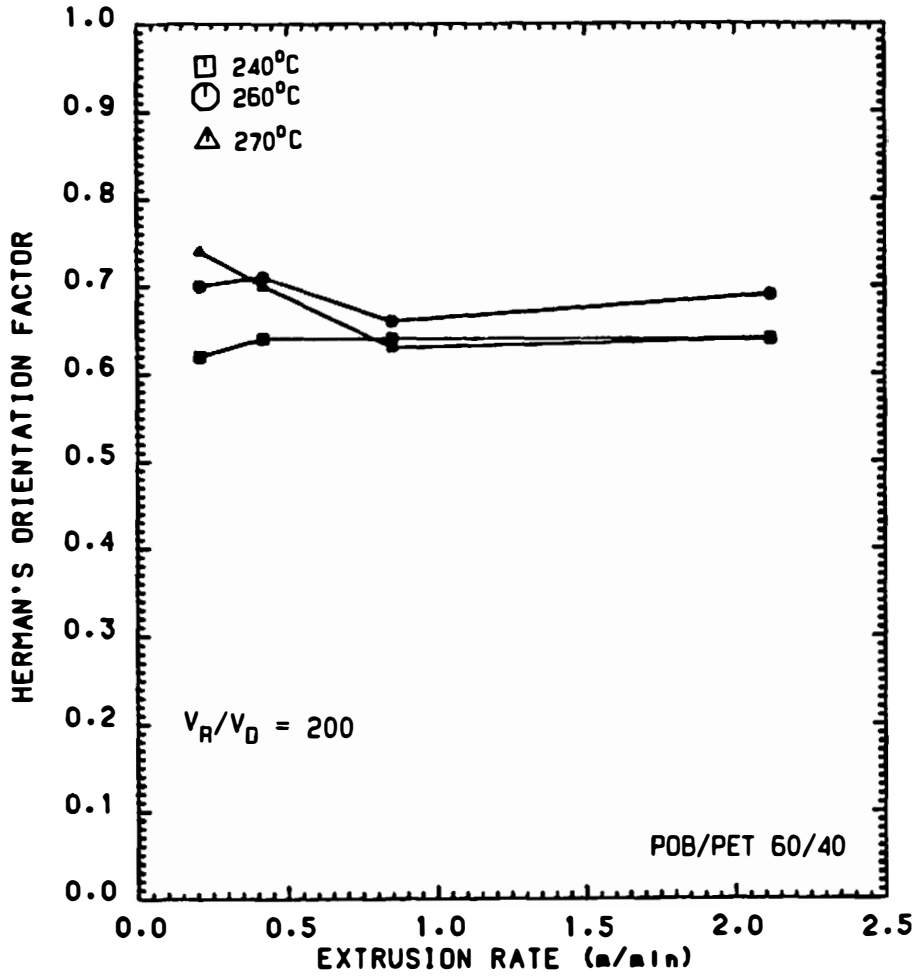

Figure 64. Plot of Herman's Orientation Factor Versus Extrusion Rate for Nonisothermal Melt Spun POB/PET 60/40 Fibers.

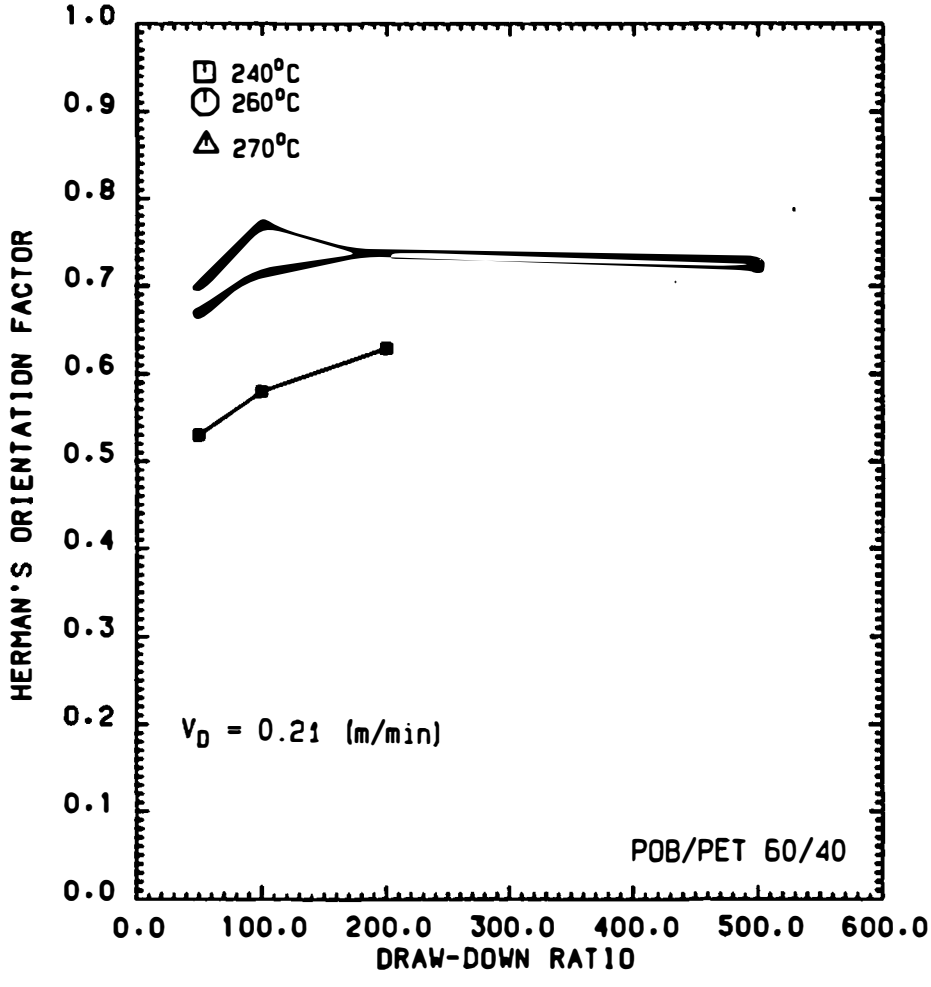

Figure 65. Plot of Herman's Orientation Factor Versus Drawdown Ratio for Isothermal Melt Spun POB/PET 60/40 Fibers.

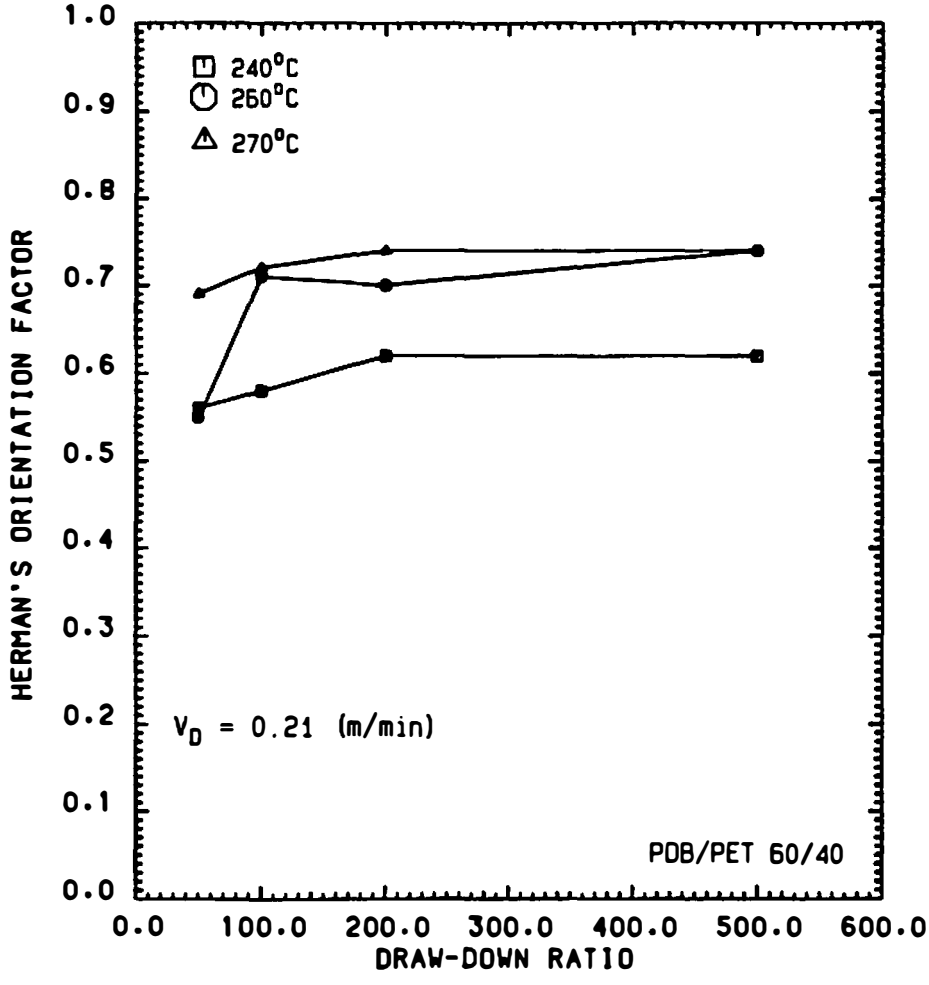

Figure 66. Plot of Herman's Orientation Factor Versus Drawdown Ratio for Nonisothermal Melt Spun POB/PET 60/40 Fibers.

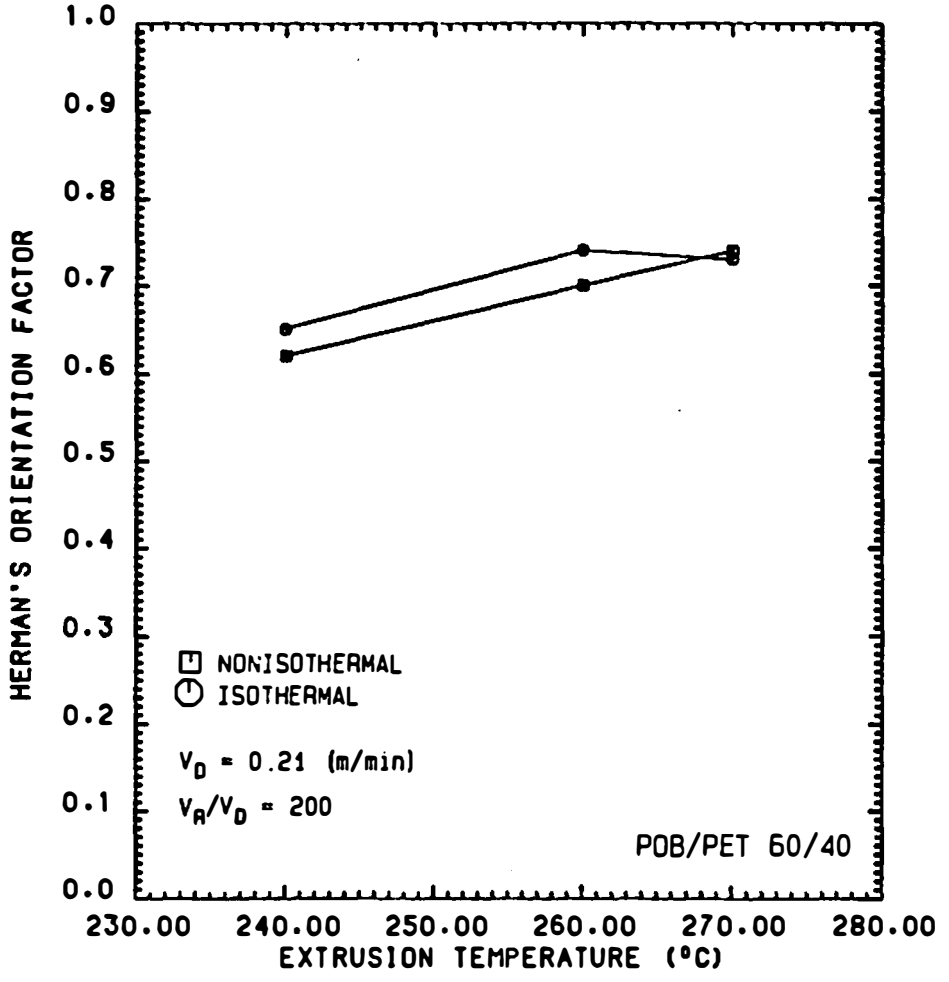

Figure 67. Plot of Herman's Orientation Factor Versus Extrusion Temperature for Isothermal and Nonisothermal Melt Spun POB/PET 60/40 Fibers.

constant drawdown ratio, V_D/V_R = 200, and constant extrusion rate, V_D = 0.21 m/min.

B. Discussion

The POB/PET 60/40 copolyester was selected as a model thermotropic system for monitoring the effectiveness of specific process variables on the enhancing c-axis orientation. The melt process variables investigated were the extrusion rate, drawdown ratio, extrusion temperature, and die exit temperature. Extrusion rates and drawdown ratios were selected to indicate the effect of a twofold, fourfold, or tenfold increase of the initial extrusion rate or initial takeup rate. Extrusion temperatures were chosen in the 240°C to 270°C range in order to monitor the change in the fiber properties in the vicinity of the POB rich phase melting transition at 255°C. Rheological properties of POB/PET 60/40 were observed to show a distinct change near 255°C. The die exit temperature was specified by either a nonisothermal or an isothermal exit region. The nonisothermal exit region specified an ambient or room temperature exit temperature and imposed a large thermal gradient on the extruded filament. This condition is an analogy to conventional wet spinning of lyotropic polymer solutions, where the solution is directly extruded into a coagulation bath. The isothermal exit condition specified the extrusion melt temperature as the die exit temperature

and imposed a minimal thermal gradient on the extruded filament. This condition was analogous to the dry-jet wet spinning process, which employs a small air gap between the die and the coagulation bath. This gap allows elongational flow to occur in the extrudate prior to coagulation. Wet spinning studies of Onogi et al. [180] and Blades [36] indicated that elongational flow in the gap was more effective than shear flow in the die for enhancing orientation in the filaments.

Figures 63 and 64 (pp. 262-263), which show the orientation factor as a function of extrusion rate, indicates orientation decreases with respect to increasing extrusion rate. This suggests the maximum orientation is developed at low shear rates. High extrusion rates appear to be detrimental to the enhancement of orientation in the copolyester. The levels of orientation for isothermal conditions were lower than those obtained under nonisothermal conditions. This indicates the 'isothermal' melt spinning analogy to dry-jet wet spinning does not apply to the POB/PET 60/40 system.

Figures 65 and 66 (pp. 258-259) show the effect of drawdown ratio on the orientation. The orientation appears to increase moderately with extrusion rate and level off at a drawdown ratio of 200. No essential differences are observed for isothermal and nonisothermal spinning conditions.

Figure 67 (p. 260) is a plot of the orientation factor with respect to extrusion temperature. This plot was made at the most favorable conditions of extrusion rate and drawdown ratio for enhancing orientation. The nonisothermal plot indicates a linear increase in the orientation factor with respect to temperature. Over the 240°C to 270°C temperature range, the orientation factor increases from 0.62 to 0.74. The isothermal plot indicates an initial increase in orientation, then a leveling off above 260°C. The final level of orientation is nearly the same as for nonisothermal spinning. The conclusion is that extrusion temperature is the most effective process variable for increasing orientation. The melting transition at 255°C appears to allow the level of orientation to increase, since the polymer chains of the POB rich phase are able to effectively enter the orientation process. Below 255°C the polymer chains are locked into rigid POB rich 'domains' and the orientation results from physical alignment of the rigid 'domains' instead of the individual polymer chains.

Several conclusions can be reached from the results presented in this section. First, the level of orientation appears to be most affected by extrusion temperature. This conclusion was also reached by Sugiyama and coworkers [225]. Second, the level of orientation appears to reach a limiting value of $f_H = 0.8$, no matter what

process conditions are employed. This supports the earlier conclusions of Takeuchi et al. [229] and Sugiyama and coworkers [225]. This suggests the level of orientation is mostly developed at low shear rates in the die and is marginally enhanced by elongational flow outside the die. In the case of isothermal spinning, the induced elongational flow does not appear to substantially enhance crystalline orientation with respect to nonisothermal conditions. This may represent an orientation limit caused by saturation of the elongational or axial flow stress [196]. Third, the level of orientation decreases with extrusion rate at a high constant drawdown ratio, suggesting that shear flow is not very effective in enhancing orientation in POB/PET 60/40. Viola et al. [235] have also reported the ineffectiveness of shear flow on enhancing molecular orientation in this copolymer. This ineffectiveness may be a result of the viscoplastic flow nature of the POB/PET 60/40 melt. In this case, the flow of the melt in the die would adopt a blunted velocity profile. This would result in the level of orientation being high in the fiber skin, but low in the fiber core. The overall level of orientation would be an average of the orientation in the skin and the core. Shimamura, White and Fellers [216] also observed this skin and core effect with melt spun filaments of thermotropic HPC.

5. TENSILE PROPERTY MEASUREMENTS

A. Results

Measurements of tensile strength, initial modulus, and strain to break were obtained on selected POB/PET 60/40 fibers prepared under both nonisothermal and isothermal melt spinning conditions. Two fixed extrusion rates of V_D = 0.21 m/min and V_D = 0.42 m/min were employed. The drawdown ratio was maintained at V_R/V_D = 200 for all the samples selected. Extrusion temperatures selected to spin the fibers were 240°C, 260°C, and 270°C. Table 14 summarizes the measured tensile properties for the selected POB/PET 60/40 fibers. Figure 68 shows a plot of stress to break versus extrusion temperature for isothermal and nonisothermal melt spun fibers prepared at V_D = 0.21 m/min. Figure 69 shows a plot of modulus versus extrusion temperature for the same fibers.

B. Discussion

Table 14 shows the tensile properties and Herman's orientation factors for the fibers melt spun at 240°C, 260°C, and 270°C. Maximum tensile strengths on the order of 490 MPa and maximum moduli on the order of 40 GPa were obtained. The tensile strengths obtained are lower than those reported for nylon or PET [10]. The tensile moduli obtained were somewhat lower that glass fibers, but higher

Table 14. Tensile Properties and Crystalline Orientation Values for Selected Nonisothermal and Isothermal Melt Spun Fibers.

Melt Temperature	Orientation Factor	Tensile Stress	Initial Modulus	Tensile Strain
^{o}C		MPa	GPa	%
Nonisothermal:	(V_D = 0.21 m/min, V_D/V_R = 200)			
240	0.62	311	27	1.4
260	0.70	331	25	1.6
270	0.74	305	26	1.6
Isothermal:	(V_D = 0.21 m/min, V_D/V_R = 200)			
240	0.65	242	30	0.9
260	0.74	451	40	1.5
270	0.73	488	41	1.6
Nonisothermal:	(V_D = 0.42 m/min, V_D/V_R = 200)			
240	0.64	278	26	1.8
260	0.71	440	29	2.1
270	0.70	450	24	2.4
Isothermal:	(V_D = 0.42 m/min, V_D/V_R = 200)			
240	0.58	206	12	2.7
260	0.63	160	12	1.9
270	0.71	422	36	1.7

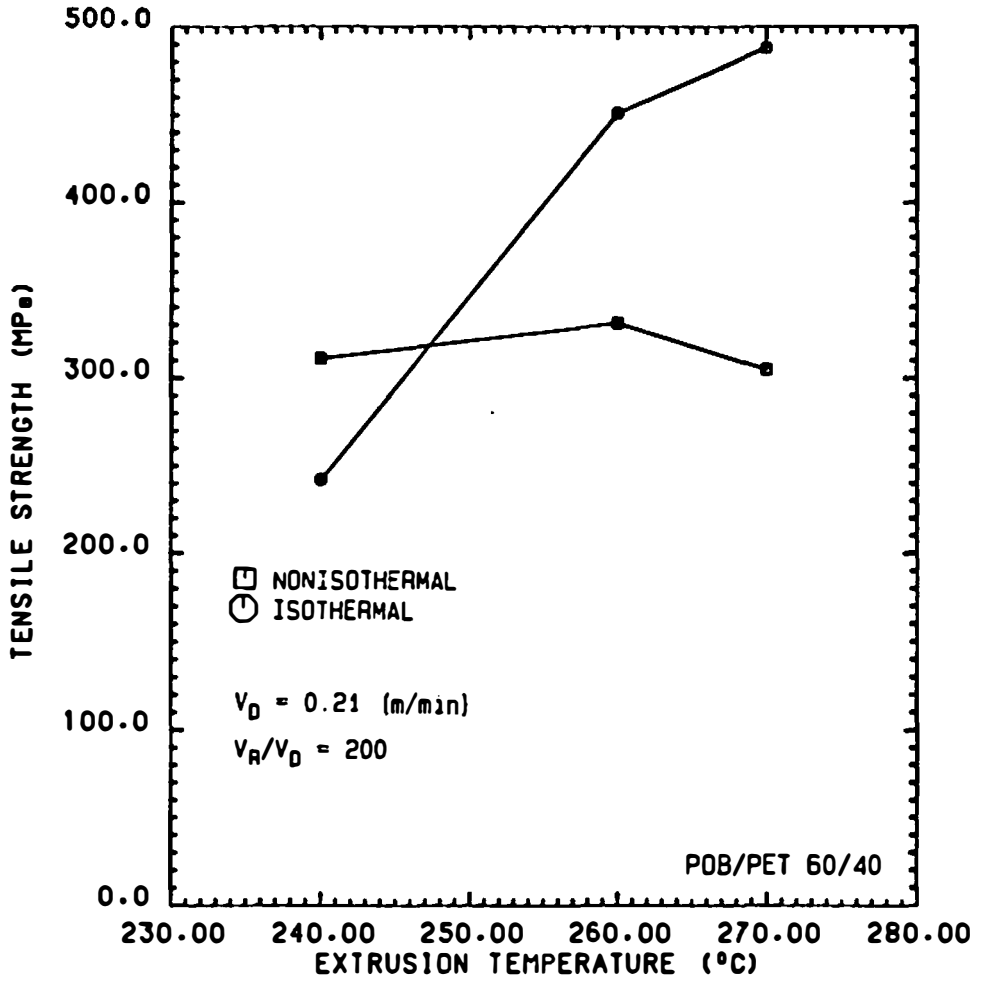

Figure 68. Plot of Tensile Strength Versus Extrusion Temperature for Nonisothermal and Isothermal Melt Spun POB/PET 60/40 Fibers.

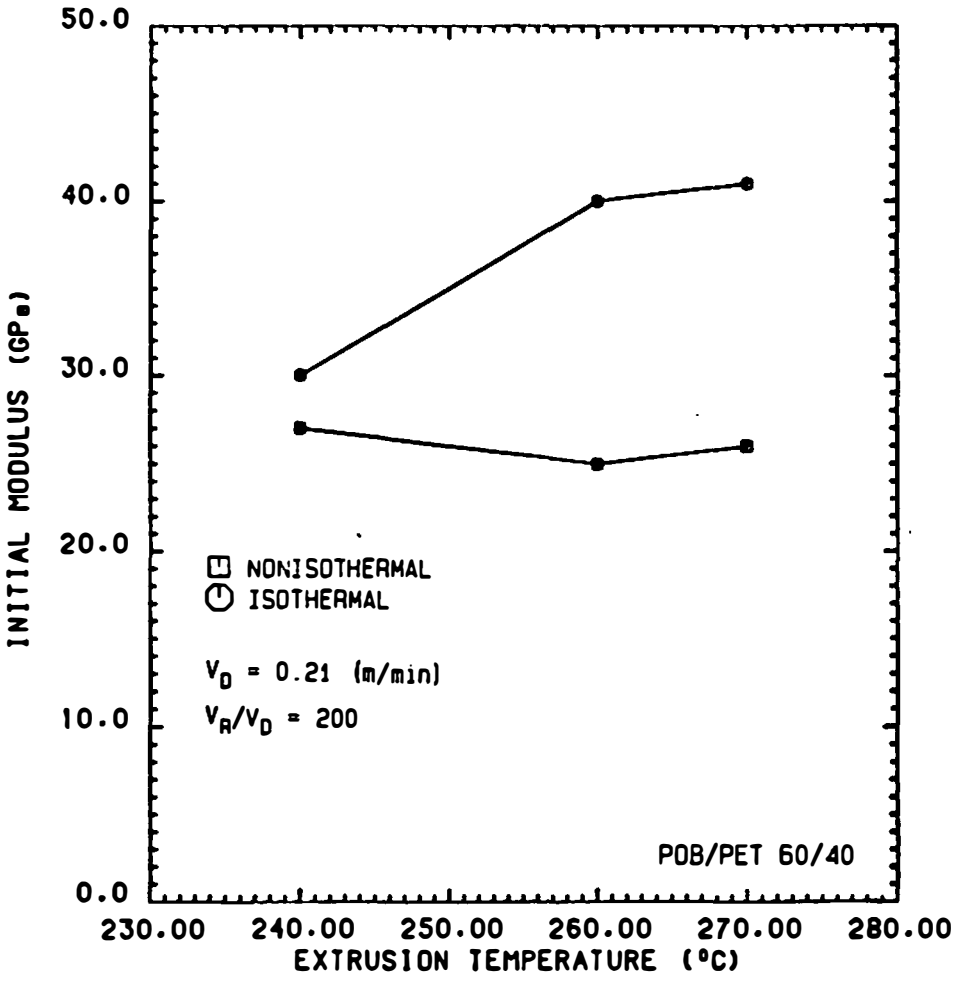

Figure 69. Plot of Initial Modulus Versus Extrusion Temperature for Nonisothermal and Isothermal Melt Spun POB/PET 60/40 Fibers.

than observed for nylon or PET [10]. The moduli and tensile strengths obtained were similar to those reported by Kuhfuss and Jackson [138] for POB/PET 60/40 fibers melt spun at 275°C. The moduli reported by Acierno et al. [1] were substantially lower than those reported by Kuhfuss and Jackson or those reported in Table 14. The fibers in the Acernio et al. study were spun at an extrusion rate of 0.1 m/min, which is less than half the lowest extrusion rate in Table 14. Acierno et al. observed the modulus to decrease with respect to extrusion temperature. The opposite trend was found with the initial modulus in Table 14 and Figure 69. The difference appears to be the result of the lower extrusion rate used in the Acierno et al. study.

A comparison of the orientation factors and tensile properties presented in Table 14 do not suggest a strict correlation between the two sets of results. Figures 68 and 69 also support this observation. Figure 69 shows the tensile strength of the nonisothermal and isothermal melt spun fibers are significantly different, although both sets of fibers have nearly identical levels of orientation. The isothermal melt spun fiber at 270°C has a Herman's orientation factor of 0.74 and a tensile strength of 305 MPa. The nonisothermal melt spun fiber at 270°C has a slightly lower Herman's orientation factor of 0.73, yet its tensile strength, 488 MPa, is 60% larger. A similar result is observed for the moduli in the two types of

fibers. These results indicate the mechanical properties of the fibers can be significantly enhanced without a corresponding increase in the crystalline orientation. This implies the crystalline orientation factor, f_H, accounts for only part of the total molecular orientation indicated to be present by the tensile property results. The level of molecular orientation in the amorphous or non-ordered phases probably accounts for the remainder.

The results in Table 14 also suggest other trends. Isothermal melt spinning appears to enhance tensile properties of the fibers extruded at 0.21 m/min, but not those extruded at 0.42 m/min. Nonisothermal melt spinning shows the opposite effect with respect to extrusion rate. The tensile strengths and moduli show a general tendency to increase with respect to extrusion temperature. The low values for the strain to break indicate the POB/PET 60/40 fibers are brittle.

CHAPTER V

CONCLUSIONS AND RECOMMENDATIONS

1. CONCLUSIONS

The research presented in this dissertation was guided by two complementary objectives. The first objective sought

1. to determine general characteristics of the liquid crystalline state based on quiescent and rheological studies of representative lyotropic and thermotropic polymers, and

2. to develop a phenomenological framework which can explain the effect of the microstructure on the flow behavior based on these general characteristics. The second objective was to determine which process variables were most effective in enhancing both molecular orientation and mechanical properties of a model thermotropic polymer.

A. General Characteristics of Mesomorphic Polymers

Three major conclusions can be drawn from the comparison of the studies of lyotropic polymers and thermotropic polymers presented in Chapter IV. The first conclusion is that certain characteristics of lyotropic polymers are analogous to those observed in thermotropic polymers. Polymer concentration in lyotropic systems and melt

temperature in thermotropic systems appear to be analogous phase transition variables. This conclusion is supported by the behavior of three material parameters with respect to these two variables. 'Darkfield' light transmissivity, which is a parameter reflecting the order in the system, is observed to increase from zero to a finite value at the isotropic to anisotropic phase transition. In thermotropic systems this transition is reached by decreasing the polymer melt temperature. In lyotropic polymers the transition is reached by increasing the polymer concentration. Two rheological parameters, shear viscosity and 'domain flow' stress, are observed to increase to a finite maximum, level off or decrease to an intermediate minimum and show a final unbounded increase with respect to either increasing concentration or decreasing melt temperature. A second conclusion drawn from the rheological studies of both systems is the 'domain flow' stress is related to the multidomain supramolecular structure. A number of quiescent morphological studies, particularly by Nishio and coworkers [173,174], have demonstrated the quiescent state of polymer liquid crystals is made up of 'domains' or locally ordered supramolecular aggregates. The behavior of the 'domain flow' stress with respect to polymer concentration or melt temperature suggests a 'domain loading' effect exists in polymer liquid crystals. The effect is similar to the volumetric loading effect of small

particles in filled polymer melts [223,230]. This suggests the 'domain flow' stress represents the aggregate resistance of the domains to shear deformation. The major third conclusion is the 'domain flow' stress is a tensoral quantity. Tensors possess force vectors in the three principle stress directions. This means the shear stress and the primary normal stress difference will both be affected by the 'domain flow' stress. The shear stress versus shear rate relationship, shown in Figure 70, possesses three stress regions when the 'domain flow' stress is significant. These three regions are the stress buildup region and the constant stress plateau at low shear, the quasi-linear stress region at intermediate shear, and the stress saturation region at high shear. The constant stress plateau represents the plastic deformation. Its magnitude is the 'domain flow' stress. The quasi-linear stress region has a slope less than one and represents the shear thinning response of the material. The stress saturation plateau at high shear represents the onset of pronounced shear thinning. When the 'domain flow' stress is small or insignificant, only the quasi-linear region and the high shear stress saturation plateau are observed.

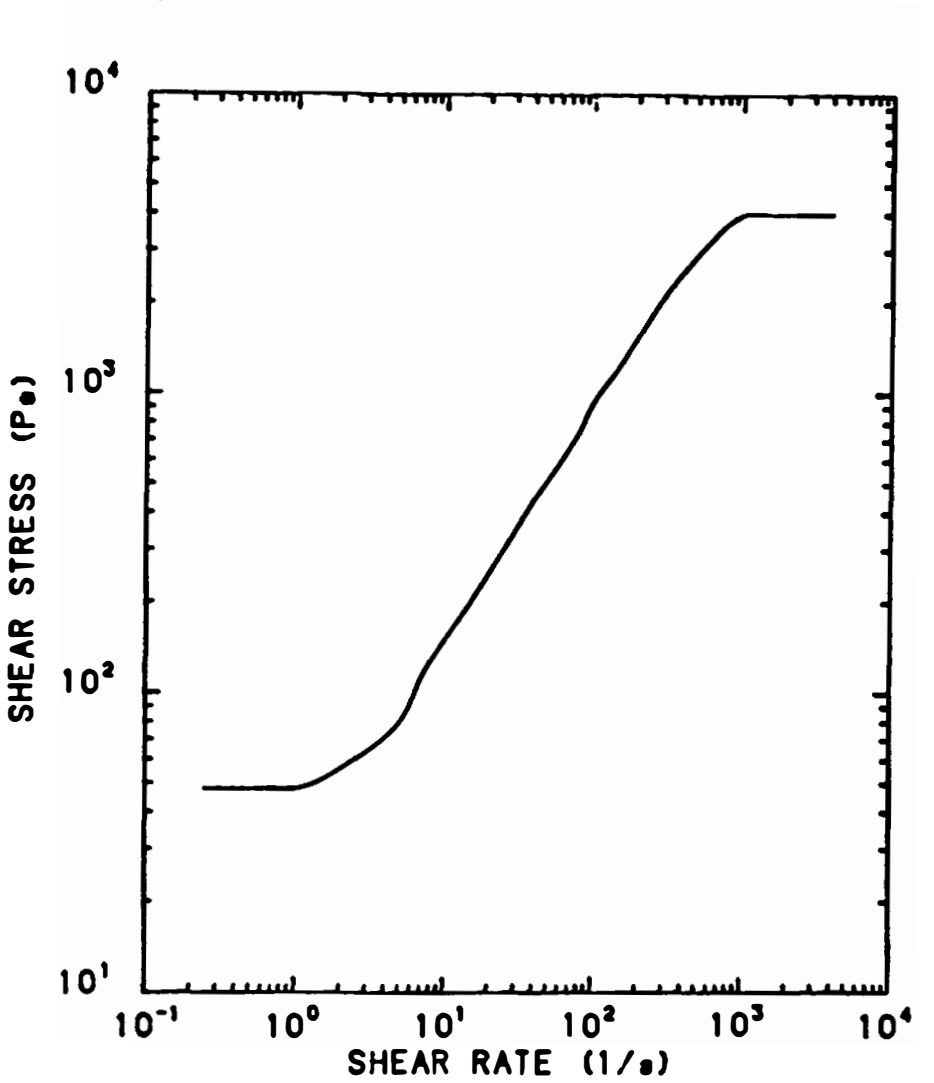

Figure 70. Diagrams Illustrating the Experimentally Observed Trends in Shear Stress Versus Shear Rate Plots of Polymer Liquid Crystals.

The primary or first normal stress difference also exhibits three regions of shear rate dependendent behavior as illustrated in Figure 71. When the 'domain flow' stress is sufficiently large, the first normal stress difference will exhibit a low shear plateau. A quasi-linear region is observed at intermediate shear rates. This quasi-linear region may have a slope of less than unity if the 'domain flow' stress is large. If the 'domain flow' stress is small, the slope of the quasi-linear region will tend toward one. At high shear rates the beginnings of a stress saturation plateau may be observed. This tendency was exhibited by some anisotropic HPC solutions.

B. Phenomenological Flow-Structure Framework

A phenomenological flow-structure model, initially proposed by Onogi and Asada [179] in 1980, has served as a convenient framework for discussing the flow behavior of both thermotropic and lyotropic polymers. This model as proposed represents a characteristic flow curve possessing three distinct shear rate regimes (See Figure 4, p. 40). At low shear rates, the flow is considered viscoplastic and exhibits both a yielding response and a shear thinning flow response. This low shear regime, called Region I, represents the deformation and flow response of a poly-domain or multitextured microstructure [16]. At moderate shear rates the flow exhibits shear rate independent or

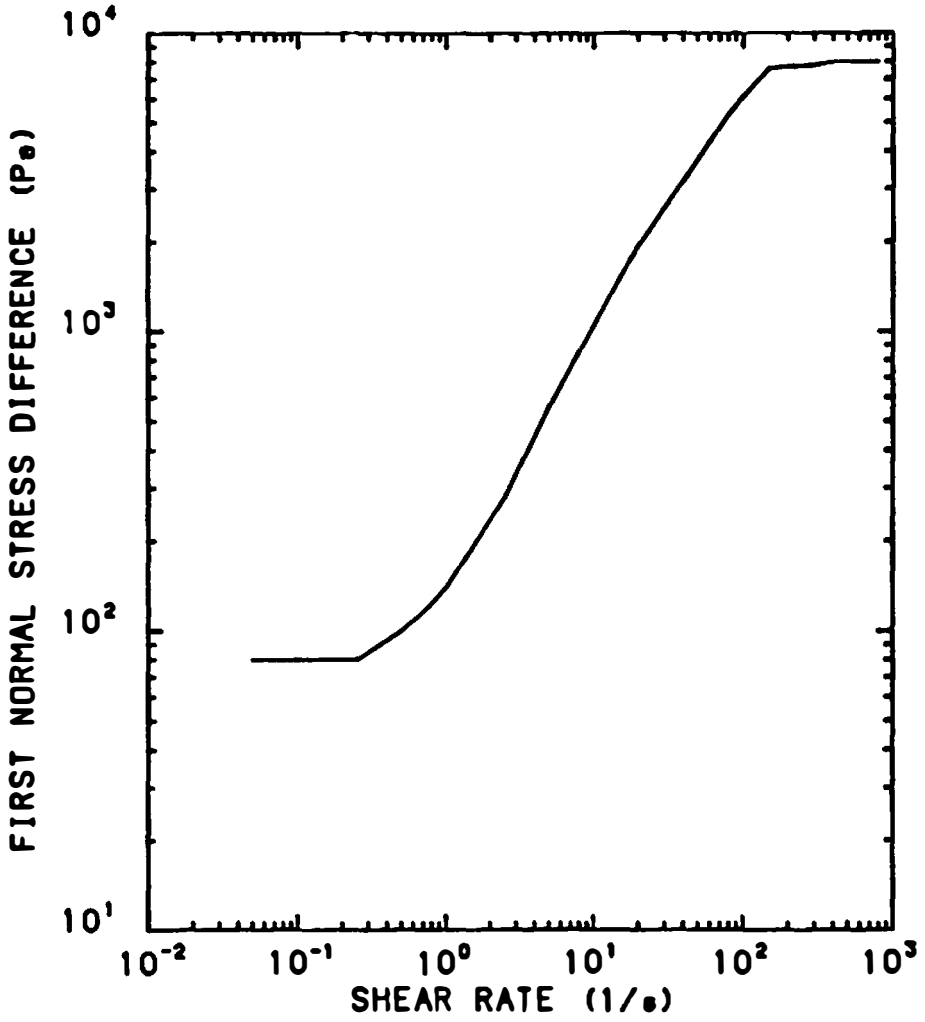

Figure 71. Diagrams Illustrating the Experimentally Observed Trends in First Normal Stress Difference Versus Shear Rate Plots of Polymer Liquid Crystals.

quasi-newtonian character. This shear regime, called Region II, represents the flow response of a mostly domain microstructure [16]. At high shear rates a second shear thinning region called Region III exists. This flow regime represents the flow of a 'monodomain' continuous phase [16].

A variety of rheological behavior is observed for lyotropic solutions of HPC, EC and PBA as well as thermotropic melts of POB/PET 60/40 and EC. These variations cannot be neatly classified by the Onogi and Asada flow-structure framework. This model is limited by its dependence on the shear viscosity behavior. A more general phenomenological framework can be based on the shear stress behavior. The shear stress versus shear rate relationship shown in Figure 72 exhibits three distinct shear regimes. The viscoplastic response of the polydomain microstructure is represented by the constant stress plateau of the regime designated as Region I. The flow in the Region II regime represents the shear-induced unification of the polydomain structure. The stress behavior in this region is quasi-linear. If the slope of the plot is unity, the model reduces to the Onogi-Asada model. The model presented in Figure 72 is more representative, since the plot can also represent a shear thinning Region II. The slope is less than unity in this case. The stress saturation plateau, represented by the Region III regime,

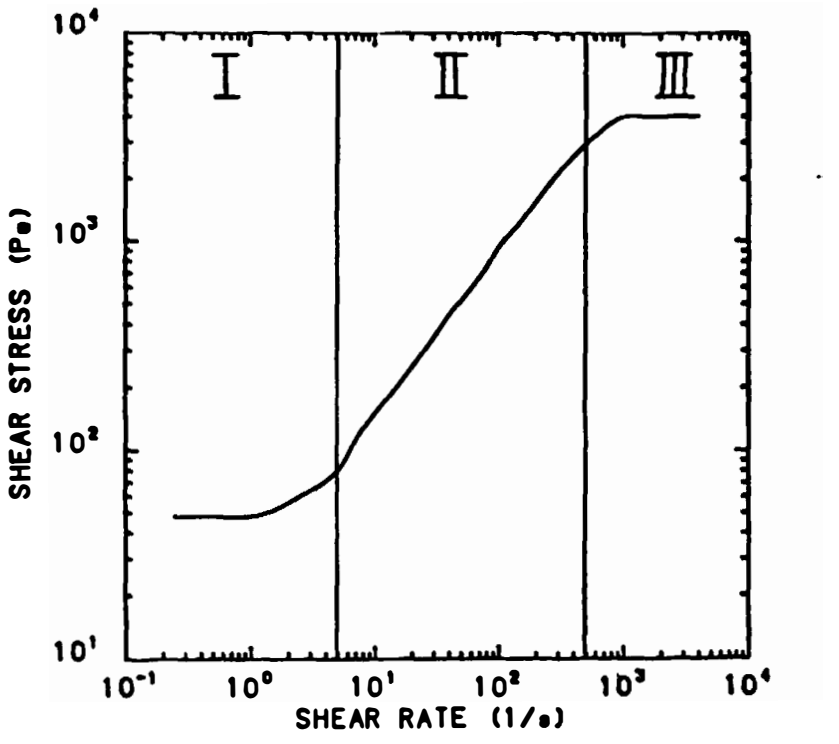

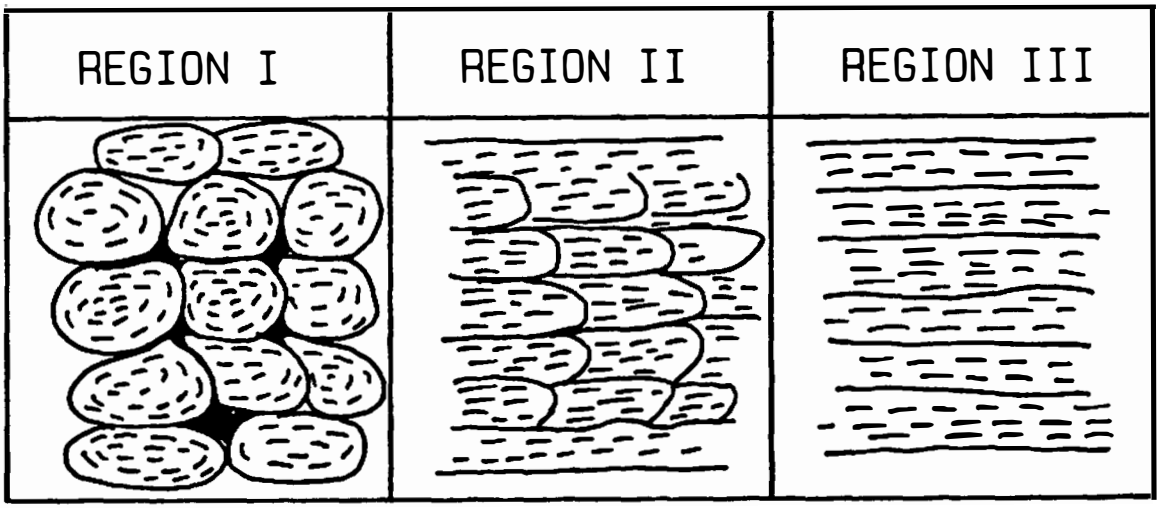

Figure 72. Diagrams Illustrating the Proposed Phenomenologically Based Flow-Structure Model for Polymer Liquid Crystals.

is the onset of pronounced shear thinning behavior. The stress response is believed to be related to the formation of a parallel band domain structure [173,174]. Nishio and coworkers [173,174] have associated the post-shear stress relaxation of this structure with the formation of transverse striations. These striations, which have been observed in a number of liquid crystalline polymers [66,67,68,110,131,234,236], represent transverse 'kinking' or 'pleating' of the parallel banded domain structure.

Region I shear stress behavior, as interpeted in light of the rheological studies presented in Chapter IV, depends on the magnitude of the 'domain flow' stress. This quantity appears to represent a 'modulus' or aggregate resistance of the domains to shear deformation. The relationship between the 'domain flow' stress and polymer concentration or melt temperature can be interpeted in terms of 'domain loading' effect. This suggests that the magnitude of the 'domain flow' stress depends on the number of domains, the size of the domains and the moduli of the individual domains. The 'domain flow' stress also appears to be a tensorial quantity since it affects both the shear stresses and the first normal stress differences.

C. Processing of Thermotropic Polymers

Three factors govern the effectiveness of processing conditions in enhancing molecular orientation and

improving mechanical properties in thermotropic polymers. These factors are the molecular arrangement, the thermal behavior and the rheological behavior.

The molecular arrangement along the polymer chains affects the molecular orientation and mechanical properties, since it governs the packing arrangement of the solid state. An irregular molecular arrangement in the polymer backbone hinders efficient packing because of unfavorable steric interactions. Consequently, this presents a barrier to a well ordered solid state. The molecular arrangement in thermotropic polymers is determined by a balance of the need for high molecular rigidity and the desirability of the lowest possible processing temperature. This compromise by necessity introduces some irregularity in the polymer backbone. The molecular irregularity is usually introduced by either the presence of 'semiflexible spacer' type repeat units between the rigid 'mesogen' units or sterically irregular aromatic moieties. In the POB/PET 60/40 polymer the ethylene terephthalate comonomer serves as the 'semiflexible spacer' between the mesogen POB units. The presence of these 'semiflexible spacers' result in defect ridden POB crystallites and appreciable amorphous regions. This heterogeneous solid state appears to be a barrier to high crystalline orientation and, consequently, high mechanical properties.

The thermal behavior of polymer liquid crystals defines the boundaries of the anisotropic or liquid crystalline region in the phase diagram. Thermal behavior affects orientation and structure by (1) defining the transition pathway to the solid state, (2) determining the crystalline growth rate, and (3) influencing the rate of deformation in the melt. In melt processing the most significant thermal parameters are the extrusion melt temperature and the die exit temperature. The extrusion temperature was found to be the most effective process variable for enhancing molecular orientation and mechanical properties for the POB/PET 60/40 system. This variable was monitored at temperatures above and below the POB rich phase melting transition at 255^{o}C. Higher orientation levels, tensile strengths and tensile moduli were observed for fibers processed above 255^{o}C. The higher properties were associated with the chain molecules of the POB rich phase effectively entering the alignment process. Below 255^{o}C the POB rich chain molecules are locked into rigid domains and the orientation is by physical alignment of the POB rich phase domains. The effect of the die exit temperature in melt spinning was investigated as an analogy to the effect of an air gap in wet spinning. The die exit temperature was specified by either of two conditions (1) room or amibient temperature or (2) the melt or extrusion temperature. The first condition imposed a large

thermal gradient on the extruded fiber, while the second condition imposed a minimal thermal gradient. The second condition represented the 'isothermal gap' analogy to the air gap in dry-jet wet spinning. Onogi et al. [180] and Blades [36] had observed for dry-jet wet spun lyotropic polymers that elongational flow in the air gap was more effective than shear flow in the die in enhancing molecular orientation and improving mechanical properties. In the case of POB/PET 60/40, the isothermal gap proved to be of little value in increasing crystalline orientation. The mechanical properties, however, were found to be substantially improved with the isothermal gap at low extrusion rate and high draw down ratio.

The rheological behavior influences the molecular orientation and the mechanical properties by determining the character of the material response during deformation. The flow behavior of polymer liquid crystals is more complex than for conventional polymers. The flow behavior at low shear is believed to be dominated by the presence of domains or locally ordered supramolecular aggregates. The 'domain flow' stress is a parameter representing the resistance of the domains to shear deformation. The viscoplastic response of the melt during flow results in a severely blunted velocity profile. This 'plug flow' response results in a the formation of a highly oriented skin layer and a poorly oriented core region. The

orientation disparity between the two regions limits the level of the average molecular orientation as determined by WAXD measurements. The flow behavior of POB/PET 60/40 below 250°C appears to represent the viscoplastic or plug flow response which leads to a skin and core solid state structure. At intermediate shear rates the flow behavior is shear rate independent. The flow at these shear rates is devoid of seperate domains and has uniform flow alignment. This condition is expected to produce high orientation. The flow behavior of concentrated PPTA/SA at 60°C appears to represent a quasi-newtonian or Region II flow response that leads to high orientation. At high shear rates the flow response of a polymer liquid crystal is shear thinning. The flow-induced orientation under these Region III conditions is expected to be lower than under Region II conditions, since the flow field is not stable. A number of studies [131,173,174] indicate that flow in Region III is beset by disclinations or striations, which cause local disruptions in the flow orientation.

2. RECOMMENDATIONS FOR FUTURE STUDIES

Despite the numerous investigations of polymer liquid crystals, a significant amount of work still needs to be done. A number of studies are needed to completely clarify the relationship between the microstructure and the flow behavior in these materials. The presence of the

three flow regions as defined by Onogi and Asada [179] has not been completely demonstrated for the presently available lyotropic and thermotropic polymers. Formation of polydomain microstructures appear to be concentration, temperature and molecular weight dependent. This allows the possibility that a polydomain structure may not exist for all extant polymer liquid crystals. Sensitive low shear experiments are needed to verify the existance of Region I for some liquid crystalline polymers and Region II for others. High shear experiments are needed to verify Region II in some thermotropic polymers. These studies should be augumented with microscopic observations prior to shear to determine the presence of a rest polydomain structure.

The 'domain loading' effect observed for polymers exhibiting Region I or viscoplastic flow behavior implies

1. the 'domain flow' stress, viscosity and primary normal stress difference all will vary with respect to sample volume, and

2. the velocity profile will be blunted rather than parabolic. The sample volume effect can be investigated by employing cone and plates of various diameters and different cone angles. The blunted velocity profile can be verified by the use of flow markers in the polymer as it flows through a slit die with viewing windows.

With regard to polymer processing, a number of studies are needed to fully explore the analogies which exist between wet spinning and melt spinning. The 'isothermal gap' analogy to the air gap in dry-jet wet spinning has been investigated for the POB/PET 60/40 material. Studies should be extended to wholly aromatic thermotropic copolyesters. A second set of melt spinning experiments should be conducted on thermotropic HPC or EC melts and comparied with analogous wet spinning experiments on lyotropic solutions of the same polymers. These comparisons would provide a means to determine the extent of the analogy beteen 'isothermal gap' melt spinning and dry-jet wet spinning.

LIST OF REFERENCES

LIST OF REFERENCES

1. Acierno, D., La Mantia, F.P., Polizzotti, G., Ciferri, A. and Valenti, B., Macromol. 15, 1455 (1982)

2. Acierno, D., La Mantia, F.P., Polizotti, G., Ciferri, A., Kribaum, W.R. and Kotek, R., J. Polym. Sci., Polym. Phys. Ed. 21, 2027 (1983)

3. Adduci, J., Chapoy, L.L., Jonsson, G., Kops, J. and Shinde, B.M., Polym. Eng. Sci. 21, 712 (1981)

4. Aharoni, S.M., Macromol. 12, 94 (1979)

5. Aharoni, S.M., J. Polym. Sci., Polym. Phys. Ed. 18, 1303 (1980)

6. Aharoni, S.M., Mol. Cryst. Liq. Cryst. 56 (Lett.), 237 (1980)

7. Aharoni, S.M., Polymer 21, 1413 (1980)

8. Aharoni, S.M. and Walsh, E.K., Macromol. 12, 271 (1979)

9. Aharoni, S.M. and Sibila, J.P., ACS Polym. Prep. 20, (1980)

10. Allen, S.R., Filippov, A.G., Farris, R.J., Thomas, E.L., Wong C.P., Berry, G.C. and Chenevey, E.C., Macromol. 14, 1135 (1981)

11. Allen, S.R., Filippov, A.G., Farris, R.J. and Thomas, E.L., in "The Strength and Stiffness of Polymers", 357, ed. by Zaccharides, A.E. and Porter, R.S., Marcel Dekker, New York, NY (1983)

12. Ambrose, E.J. and Elliott, A., Proc. Royal Soc. London A 205, 47 (1951)

13. Aoki, H., Coffin, D.R., Hancock, T.A., Harwood, D., Lenk, R.S., Fellers, J.F. and White, J.L., J. Polym. Sci., Polym. Symp. 65, 29 (1978)

14. Aoki, H., White, J.L. and Fellers, J.F., J. Appl. Polym. Sci. 23, 2293 (1979)

15. Aoki, H., Onogi, Y., White, J.L. and Fellers, J.F. Polym. Eng. Sci. 20, 221 (1980)

16. Asada, T., Maramatsu, H., Watanabe, R. and Onogi, S., Macromol. 13, 867 (1980)

17. Asada, T., Toda, K. and Onogi, S., Mol. Cryst. Liq. Cryst. 68, 231 (1981)

18. Asada, T. and Onogi, S., Polym. Eng. Rev. 3, 323 (1983)

19. Bair, T.I. and Morgan, P.W., U.S. Patent No. 3,673,143 (1972)

20. Bair, T.I., Morgan, P.W., and Killian, F.C., Macromol. 10, 1396 (1977)

21. Baird, D.G., in "Liquid Crystalline Order in Polymers", 237, ed. by Blumstein, A., Academic Press, New York, NY (1978)

22. Baird, D.G., J. Soc. Rheol. 24, 465 (1980)

23. Ballard, D.G.H., U.S. Patent No. 3,089,749 (1963)

24. Ballard, D.G.H., in "Man-Made Fibers", Vol. 2, 401, ed. by Mark, H.F., Atlas, S.M. and Cernia, E., Wiley-Interscience, New York, NY (1968)

25. Ballard, D.G.H., Griffiths, J.D. and Watson, J. U.S. Patent No. 3,121,766 (1964)

26. Bender, B.W., J. Appl. Polym. Sci. 9, 2887 (1965)

27. Bernstein, B., Kearsley, E.A. and Zappas, L.J., Trans. Soc. Rheol. 7, 391 (1963)

28. Berry, G.C., Cotts, P.M. and Chu, S., Br. Polym. J. 13, 47 (1981)

29. Bheda, J., "Characterization and Fiber Formation of Liquid Crystalline Cellulose Derivatives", M.S. Thesis, Univ. of Tennessee, Knoxville, TN (1980)

30. Bheda, J., Fellers, J.F. and White, J.L., Coll. Polym. Sci. 258, 1335 (1980)

31. Bickel, A., Shaw, M.T. and Samulski, E.T., J. Soc. Rheol. 25, 647 (1984)

32. Bird, R.B. and Carreau, P.J., Chem. Eng. Sci. 23, 427 (1968)

33. Blackwell, J., and Gutierrez, G.A., Polymer 23, 671 (1982)

34. Blackwell, J., Lieser, G., and Gutierrez, G.A., Macromol. 16, 1418 (1983)

35. Blackwell, J., Gutierrez, G.A., and Chivers, R.A. Macromol. 17, 1219 (1984)

36. Blades, H., U.S. Patent No. 3,767,756 (1973)

37. Blades, H., U.S. Patent No. 3,869,429 (1975)

38. Bodaghi, H., Kitao, T., Flood, J.E., Fellers, J.F. and White, J.L., Polym. Eng. Sci. 24, 242 (1984)

39. Bramford, C.H., Hanby, W.E. and Happey, F., Proc. Royal Soc. London A 205, 47 (1951)

40. Bramford, C.H., Brown, L., Elliott, A., Hanby, W.E., and Trotter, I.F., Nature 169, 357 (1952)

41. Brenner, H., Int. J. Multiphase Flow 1, 395 (1974)

42. Brown, G.H. and Crooker, P.P., Chem. Eng. News 61(5), 24 (1983)

43. Buhner, C., Marburg Univ. Dissert. Data (1906), cited by Bechner, G. and Kast, W., Ann. Physik. 41, 406 (1942)

44. Butler, R.W. and Klug, E.D., in "Handbook of Water Soluble Gums and Resins", Chapter 13, ed. by Davidson, R.L., McGraw-Hill, New York, NY (1980)

45. Bur, A.J., and Roberts, A.J., J. Chem. Phys. 51, 406 (1969)

46. Burchard, V.W., Makromol. Chem. 67, 182 (1963)

47. Calundann, G.W., U.S. Patent No. 4,067,852 (1958)

48. Casson, N., in "Rheology of Disperse Systems", p. 84, ed. by Mill, C.C., Pergamon Press, London U.K. (1959)

49. Chaffey, C.E. and Porter, R.S., J. Soc. Rheol. 28, 249 (1984)

50. Chaffey, C.E. and Porter, R.S., J. Soc. Rheol. 29, 281 (1985)

51. Chandrasekhar, S., "Liquid Crystals", p. 42, Cambridge Univ. Press, London, England (1977)

52. Chanzy, P. and Peguy, A., J. Polym. Sci., Polym. Phys. Ed. 18, 1137 (1980)

53. Chem. Eng. News, 62(46), 4 (Nov. 12, 1984)

54. Chu, S.G., Venkatraman, S., Berry, G.C. and Einaga, Y., Macromol. 14, 939 (1981)

55. Ciferri, A., in "Polymer Liquid Crystals", 63, ed. by Ciferri, A., Krigbaum, W.R. and Meyer, R.B., Academic Press, New York, NY (1982)

56. Cottis, S.G., Economy, J. and Wohrer, L.C., U.S. Patent No. 3,975,487 (1976)

57. Creely, J.J. and Conrad, C.M., Text. Res. J. 35, 184 (1965)

58. Daily, J.E. and Vamos, M.N., Businessweek No. 2882, 108 (Feb. 25, 1985)

59. de Gennes, P.G., "The Physics of Liquid Crystals", 3, Oxford Univ. Press, London, England (1974)

60. Demartino, R.N., J. Appl. Polym. Sci. 28, 1805 (1983)

61. Demus, D. and Richter, L., "Textures of Liquid Crystals", 16, Verlag Chemie, Weinhein, NY (1978)

62. Doi, M., J. Polym. Sci., Polym. Phys. Ed. 19, 229 (1981)

63. Doi, M. and Edwards, S.F., J. Chem. Soc., Faraday Trans. II 74, 560 (1978); 74, 918 (1978)

64. Dobb, M.G., Johnson, D.J. and Saville, B.P., J. Polym. Sci., Polym. Phys. Ed. 15, 2201 (1977)

65. Dobb, M.G., Johnson, D.J. and Saville, B.P., Philos. Trans. Roy. Soc. London A 294, 483 (1977)

66. Donald, A.M., Philos Mag. A 47, L13 (1983)

67. Donald, A.M., J. Mater. Sci. Lett. 3, 44 (1984)

68. Donald, A.M., Viney, C. and Windle, A.H., Polymer 24, 155 (1983)

69. Donald, A.M. and Windle, A.H., Coll. Polym. Sci. 261, 793 (1983)

70. Dow Chemical Co., Ethocel Information Brochure (1981)

71. DuPre', D.B., in "Polymer Liquid Crystals", 165, ed. by Ciferri, A., Krigbaum, W.R. and Meyer, R.B., Academic Press, New York, NY (1982)

72. Duke, R.W. and DuPre', D.B., Macromol. 7, 374 (1974)

73. Duke, R.W. and Dupre',D.B., J. Chem. Phys. 60, 2759 (1974); 63, 143 (1975)

74. DuPre', D.B., Duke, R.W., Hines, W.A. and Samulski, E.T., Mol. Cryst. Liq. Cryst. 40, 247 (1977)

75. DuPre', D.B. and Hammersmith, J.R., Mol. Cryst. Liq. Cryst. 28, 365 (1974)

76. DuPre', D.B. and Samulski, E.T., in "Liquid Crystals: The Fourth State of Matter", 218, ed. by Saeva, F.D., Marcel Dekker, New York, NY (1979)

77. Economy, J., Storm, R.S., Matkovich, V.I. and Cottis, S.J., J. Polym. Sci., Polym. Chem. Ed. 14, 2207 (1976)

78. Economy, J., Volksen, W. and Geiss, R.H., Mol. Cryst. Liq. Cryst. 105, 289 (1984)

79. Einaga, Y., Berry, G.C. and Chu, S.G., Polym. J. (Japan) 17, 239 (1985)

80. Elliott, A. and Ambrose, E.J., Disc. Faraday Soc. 52, 571 (1956)

81. Farell, G.W., "A Rotating Annular Die for Control of Biaxial Orientation in Melt Processed Thermotropic Cellulose Derivatives", M.S. Thesis, Univ. of Tennessee, Knoxville, TN (1984)

82. Fernandes, J.R. and DuPre', D.B., Mol. Cryst. Liq. Cryst. 72 (Lett.), 67 (1981)

83. Finkelmann, H., in "Polymer Liquid Crystals", 35, ed. by Ciferri, A., Krigbaum, W.R. and Meyer, R.B., Academic Press, New York, NY (1982)

84. Flood, J.E., "The Formation and Characterization of Biaxially and Uniaxially Oriented Poly (p-Phenylene Terephthalamide) Films from Liquid Crystalline Solutions", M.S. Thesis, Univ. of Tennessee, Knoxville, TN (1982)

85. Flood, J.E., "A Kinematic Approach to the Formation and Characterization of Biaxially Oriented Poly(p-Phenylene Terephthalamide)", PhD. Dissertation, Univ. of Tennessee, Knoxville, TN (1985)

86. Flood, J.E., White, J.L. and Fellers, J.F., J. Appl. Polym. Sci. 27, 2965 (1982)

87. Frank, F.C., Disc. Faraday Soc. 25, 19 (1958)

88. Franks, N.E. and Varga, J.K., U.S. Patent No. 4,145,532 (1979)

89. Frazer, A.H., Sweeny, W. and Wallenberger, F.T., J. Polym. Sci. Pt.A 2, 1157 (1964)

90. Frazer, A.H. and Wallenberger, F.T., J. Polym. Sci. Pt.A 2, 1137, 1147, 1171 (1964)

91. Friedel, G., Ann. Phys. (Paris) 18, 273 (1922)

92. Geiss, R., Volksen, W., Tsay, J. and Economy, J., J. Polym. Sci., Polym. Lett. Ed. 22, 433 (1984)

93. Gilbert, R.D. and Patton, P.A., Prog. Polym. Sci. 9, 115 (1983)

94. Gottis, A.D., and Baird, D.G., J. Soc. Rheol. 29, 539 (1983)

95. Griffin, A.C., Britt, T.R. and Cambell, G.A., Mol. Cryst. Liq. Cryst. 82(Lett.), 145 (1982)

96. Groupe d'Etude des Crystaux Liquides (Orsay), J. Chem. Phys. 51, 816 (1969)

97. Guha-Sridhar, C., Hines, W.A. and Samulski, E.T., J. Chem. Phys. 61, 947 (1974)

98. Guha-Sridhar, C., Hines, W.A. and Samulski, E.T., J. Phys. (Paris) 36, C1-269 (1975)

99. Guillon, D. and Skoulious, A., Mol. Cryst. Liq. Cryst. 49(Lett.), 119 (1978)

100. Gutierrez, G.A., Chivers, R.A., Blackwell, J., Stamatoff, J.B. and Yoon, H., Polymer 24, 937 (1983)

101. Gutierrez, G.A. and Blackwell, J., Macromol. 17, 2744 (1984)

102. Hancock, T.A., Spruiell J.E. and White, J.L., J. Appl. Polym. Sci. 21, 1227 (1977)

103. Hand, G.L., J. Fluid Mech. 13, 33 (1962)

104. Haraguchi, K., Kajiyama, T. and Takayanagi, M., J. Appl. Polym. Sci. 23, 903 (1979); 23, 915 (1979)

105. Hartzler, J.D., U.S. Patent No. 3,966,656 (1964)

106. Harwood, D., "Unique Mechanism of The Complex Liquid Crystalline Phase Behavior of Poly(Chloro-p-Phenylene Terephthalamide) in N,N'Dimethyl Acetamide Solvent: Revealed by Light Scattering Photometry", PhD Dissertation, Univ. of Tennessee, Knoxville, TN (1984)

107. Hermans, J.J., J. Colloid Sci. 17, 638 (1962)

108. Hermans, J.J., Hermans, P.H., Vermass, D., and Weidinger, A., Rec. Trav. Chim. 65, 427 (1946)

109. Herschel, W.H. and Bulkley, R, Proc. Amer. Soc. Test. Mater. 26(II), 621 (1926)

110. Horio, M., Kamei, E. and Uchimura, H., Nihon Reoroji Gakkaishi (J. Soc. Rheol. Japan) 13, 25 (1985)

111. Hudson, S. and Cuculo, J.A., J. Macromol. Sci., Rev. Macromol. Chem. C18, 1 (1980)

112. Ide, Y., U.S. Patent No. 4,468,364 (1984)

113. Ide,Y. and Ophir, Z., Polym. Eng. Sci. 23, 261 (1983)

114. Iizuka, E., Polym. J. (Japan) 4, 401 (1973)

115. Iizuka, E., Mol. Cryst. Liq. Cryst. 25, 287 (1974)

116. Iizuka, E., Keira, T. and Wada, A., Mol. Cryst. Liq. Cryst. 23, 13 (1973)

117. Iimura, K., Koide, N., Tanabe, H. and Takeda, M., Makromol. Chem. 182, 2569 (1981)

118. Ito, K., Kajiyama, T. and Takayanagi, M., Polym. J. (Japan) 9, 355 (1977)

119. Jackson, W.J., Br. Polym. J. 12, 154 (1980)

120. Jackson, W.J. and Kuhfuss, H.F., J. Polym. Sci., Polym. Chem. Ed. 14, 2043 (1976)

121. Jackson, W.J. and Kuhfuss, H.F., U.S. Patent No. 4,182,842 (1980)

122. Jackson, W.J. and Kuhfuss, H.F., J. Appl. Polym. Sci. 25, 1685 (1980)

123. Jennings, B.R. and Brown, B.L., Eur. Polym. J. 7, 805 (1971)

124. Jerman, R.E. and Baird, D.G., J. Soc. Rheol. 25, 275 (1981)

125. Joseph, E., Wilkes, G.L. and Baird, D.G., Polym. Eng. Sci. 25, 377 (1985)

126. Joseph, E., Wilkes, G.L. and Baird, D.G., Polymer 26, 689 (1985)

127. Kirkwood, J.G., J. Polym. Sci. 12, 1 (1959)

128. Kiss, G., Orrell, T.S. and Porter, R.S., Rheol. Acta. 18, 657 (1979)

129. Kiss, G. and Porter, R.S., J. Polym. Sci., Polym. Symp. 65, 193 (1978)

130. Kiss, G. and Porter, R.S., J. Polym. Sci., Polym. Phys. Ed. 18, 361 (1980)

131. Kiss, G. and Porter, R.S., Mol. Cryst. Liq. Cryst. 60, 267 (1980)

132. Kleman, M., Liebert, L. and Stzelecki, L., Polymer 24, 1299 (1983)

133. Kleinschuster, J.J., U.S. Patent No. 3,991,014 (1976)

134. Kleinschuster, J.J., U.S. Patent No. 4,066,620 (1978)

135. Kotaka, T., J. Chem. Phys. 30, 1566 (1959)

136. Krigbaum, W.R., in "Polymer Liquid Crystals", 275, ed. by Cifferi, A., Krigbaum, W.R. and Meyer, R.B., Academic Press, New York, NY (1982)

137. Krigbaum, W.R. and Watanabe, J., Polymer 24, 1299 (1983)

138. Kuhfuss, H.F. and Jackson, W.J., U.S. Patent No. 3,778,410 (1973)

139. Kuhfuss, H.F. and Jackson, W.J., U.S. Patent No. 3,804,805 (1974)

140. Kulichikhin, V.G., Platanov, V.A., Braverman, L.P., Belousova, T.A., Polyakov, V.F., Shablygin, M.V., Volokhina, A.V., Malkin, A.Ya. and Papkov, S.P., Vysokomol. Soedin (Polym. Sci. USSR) A18, 2656 (1976)

141. Kulichikhin, V.G., Vasileva, N.V., Servova, L.D., Platonova, V.A., Mil'kova, L.P., Andreyeva, L.N., Volokhina, A.V., Kudryavtsev, G.I. and Papkov, S.P., Vysokomol. Soedin (Polym. Sci. USSR) A18, 590 (1976)

142. Kwolek, S.L., U.S. Patent No. 3,671,542 (1972)

143. Kwolek, S.L., Morgan, P.W., Schaefgen, J.R. and Gulrich, L.W., Macromol. 10, 1390 (1977)

144. Laus, M., Angeloni, A.S., Ferruti, P., Galli, G. and Chiellini, E., J. Polym. Sci., Polym. Lett. Ed. 22, 587 (1984)

145. Lehman, O., Z. Physik. Chem. (Leipzig) 4, 462 (1889)

146. Lehman, O., Z. Physik. Chem. (Leipzig) 5, 435 (1890)

147. Lehman, O., Ann. Physik. (Leipzig) 4, 181 (1906)

148. Leslie, F.M., Quart. J. Mech. Appl. Math. 19, 357 (1966)

149. Lewis, D.N., Brann, J., Ko, W., Lin, C., Warner, D., and Westbrook, M., Polym. Eng. 5512 Lab Class Data (1983)

150. Lieser, G., J. Polym. Sci., Polym Phys. Ed. 21, 1611 (1983)

151. Lim, T., Uhl, J.T. and Prud'homme, R.K., J. Soc. Rheol. 28, 367 (1984)

152. Lobe, V.M. and White, J.L., Polym. Eng. Sci. 19, 617 (1979)

153. Mackley, M.R., Pinaud, F. and Siekmann, G., Polymer 24, 1299 (1983)

154. Marrucci, G., Mol. Cryst. Liq. Cryst. 72 (Lett.), 153 (1982)

155. Matsuo, M., Ozaki, F., Konno, Y., and Ogita, T., J. Polym. Sci., Polym. Phys. Ed. 19, 1531 (1981)

156. McFarlane, F.E. and Davis, T.G., U.S. Patent No. 3,890,256 (1975)

157. McFarlane, F.E., Nicely, V.A. and Davis, T.G., in "Contemporary Topics in Polymer Science", Vol. 2, 109 (1977)

158. McKinnon, A.J. and Tobolsky, A.V., J. Phys. Chem. 70, 1453 (1966)

159. McKinnon, A.J. and Tobolsky, A.V., J. Phys. Chem. 72, 1157 (1968)

160. McNeely, W.H. and Kang, K.S., in "Industrial Gums", 489, ed. by Whistler, R.L. and Bemiller, J.N., Academic Press, New York, NY (1973)

161. Menczel, J. and Wunderlich, B., J. Polym. Sci., Polym. Phys. Ed. 18, 1433 (1980)

162. Meyer, R.B., in "Polymer Liquid Crystals", 133, ed. by Ciferri, A., Krigbaum, W.R. and Meyer, R.B., Academic Press, New York, NY (1982)

163. Millaud, B., Thierry, A. and Skouious, A., J. Phys. (Paris) 39, 109 (1978)

164. Millaud, B., Thierry, A. and Skouious, A., J. Phys. Lett. (Paris) 40, L607 (1979)

165. Millich, F., Adv. Polym. Sci. 19, 117 (1975)

166. Minagawa, N. and White, J.L., J. Appl. Polym. Sci. 20, 501 (1976)

167. Miyoshi, A., Sasaka, A., Ikai, J., Gouhard, K. and Suzuki, Y., Japanese Patent Appl. No. 549-87683 (1974)

168. Morgan, P.W., Macromol. 10, 1381 (1977)

169. Morgan, P.W., J. Polym. Sci., Polym. Symp. 65, 1 (1978)

170. Morgan, R.J., Pruneda, C.O. and Steele, W.J., J. Polym. Sci., Polym. Phys. Ed. 21, 1757 (1983)

171. Navard, P. and Houdin, J. Br. Polym. J. 12, 174 (1980)

172. Nicely, V.A., "Structure Determination of Liquid Crystalline Polymers", Seminar at the Univ. of Tennessee, Knoxville, TN. (1985)

173. Nishio, Y., Yamane, T. and Takahashi, T., J. Polym. Sci., Polym. Phys. Ed. 23, 1043 (1985); 23, 1053 (1985)

174. Nishio, Y., Susuki, S., and Takahashi, T. Polym. J. (Japan) 17, 753 (1985)

175. Noel, C., Friedrich, C., Laupretre, F., Billard, J., Billard, J., Bosio, L. and Strazielle, C., Polymer 25, 263 (1984)

176. Northolt, M.G., Eur. Polym. J. 10, 799 (1974)

177. Northolt, M.G. and van Aartsen, J.J., J. Polym. Sci., Polym. Lett. Ed. 11, 333 (1973)

178. Omatete, O.O., Bodaghi, H., Fellers, J.F. and Browne, C.L., "Processing and Characterization of Cellulose Triacetate Films from Isotropic and Liquid Crystalline Solutions", PATRA Rept. No. 224, Univ. of Tennessee, Knoxville, TN (1985)

179. Onogi, S. and Asada, T., in "Rheology", Vol. 1, 127, ed. by Astarita, G., Marrucci, G. and Nicolais, L., Plenum Press, New York, NY (1980)

180. Onogi, Y., White, J.L. and Fellers, J.F., J. Non-Newt. Fluid Mech. 7, 121 (1980)

181. Ophir, Z. and Ide, Y., Polym. Eng. Sci. 23, 792 (1983)

182. Panar, M. and Wilcox, D.B., Offenlegungsschrift (German Patent Discloser) No. 2,705,382 (1977)

183. Panar, M., Avakian, P., Blume, R.C., Gardner, K.H., Gierke, T.D. and Yang, H.H., J. Polym. Sci., Polym. Phys. Ed. 21, 1955 (1983)

184. Papkov, S.P., Kulichikhin, V.G., Kalmykova, V.D. and Malkin, A.Ya., J. Polym. Sci., Polym. Phys. Ed. 12, 1753 (1974)

185. Parodi, O.J., J. Phys. (Paris) 31, 581 (1970)

186. Parry, D.A.D. and Elliott, A., J. Mol. Biol. 25, 1 (1967)

187. Patel, D.L and Gilbert, R.D., J. Polym. Sci., Polym. Phys. Ed. 19, 1231 (1981)

188. Patel, D. and DuPre', D.B., Mol. Cryst. Liq. Cryst. 53, 323 (1979)

189. Patel, D.L. and DuPre', D.B., J. Polym. Sci., Polym. Phys. Ed. 18, 1599 (1980)

190. Perec, V., Shaffer, T.D. and Nava, H., J. Polym. Sci., Polym. Lett. Ed. 22, 637 (1984)

191. Pletcher, T.C., U.S. Patent No. 3,991,013 (1976)

192. Pochan, J.M., in "Liquid Crystals, The Fourth State of Matter", 275, ed. by Saeva, F.D., Marcel Dekker, New York, NY (1979)

193. Prager, S., Trans. Soc. Rheol. 1, 53 (1957)

194. Prasadarao, M., Pearce, E.M. and Han, C.D., J. Appl. Polym. Sci. 27, 1343 (1982)

195. Prevorsek, D.C. in "Polymer Liquid Crystals", 346, ed. by Ciferri, A., Krigbaum, W.R. and Meyer, R.B., Academic Press, New York, NY (1982)

196. Prilutski, G.M., "The Rheology of Polymeric Liquid Crystals", PhD Dissertation, Univ. of Delware, Newark, DE (1984)

197. Prilutski, G.M. and Metzner, A.B., "The Rheology of Polymer Liquid Crystals", Soc. Rheol. Meeting, Blacksburg, VA (1984)

198. Rheometrics Mechanical Spectrometer, Model 7200 Electronics Manual, Rheometrics, Inc. (1974)

199. Rheometrics RMS 7200 Test Fixture Description Brochure, Rheometrics, Inc. (1976)

200. Reinitzer, F., Montasch. 9, 421 (1898)

201. Rigaku/Dmax Software Instruction Manual, Rigaku/USA (1973)

202. Robinson, C., Trans. Faraday Soc. 52, 571 (1956)

203. Robinson, C., Tetrahedron 13, 219 (1961)

204. Robinson, C. and Ward, J.C., Nature 180, 1183 (1957)

205. Robinson, C., Ward, J.C. and Beevers, R.B., Disc. Faraday Soc. 25, 29 (1958)

206. Roche, E.J., Takahashi, T., and Thomas, E.L., Amer. Chem. Soc. Symp., Fiber Diffraction Methods 141, 303 (1980)

207. Salamone, J.C., Clough, S.B., Salamone, A.B., Reid, K.I.G. and Jamison, D.E., Soc. Petrol. Eng. J. 22, 555 (1982)

208. Samuels, R.J., J. Polym. Sci., Pt. A-2 7, 1197 (1969)

209. Samulski, E.T. and Tobolsky, A.V., Nature 216, 977 (1967)

210. Samulski, E.T. and Tobolsky, A.V., Mol. Cryst. Liq. Cryst. 7, 433 (1969)

211. Samulski, E.T. and Wiercinski, R., Bull. Amer. Phys. Soc. 23, 296 (1978)

212. Sanderson, G.R., Br. Polym. J. 13, 71 (1981)

213. Sawyer, L.C., J. Polym. Sci., Polym. Phys. Ed. 22, 347 (1984)

214. Schneider, N.S., Furusaki, S. and Lenz, R.W., J. Polym. Sci., Pt. A 3, 933 (1965)

215. Shibaev, V.P., Tal'rose, R.V., Petrukhin, B.S., and Plate, N.V., Vysokomol. Soedin (Polym. Sci. USSR) A13, 493 (1971)

216. Shimamura, K., White, J.L. and Fellers, J.F., J. Appl. Polym. Sci. 26, 2165 (1981)

217. Simmens, S.C. and Hearle, J.W.S., J. Polym. Sci., Polym. Phys. Ed. 18, 871 (1980)

218. Simmoff, D.A. and Porter, R.S., Mol. Cryst. Liq. Cryst. 110, 1 (1984)

219. Sprague, B.S., Riley, J.L. and Noether, H.D., Text. Res. J. 28, 275 (1958)

220. Squire, I.M. and Elliott, A., Mol. Cryst. Liq. Cryst. 7, 457 (1969)

221. Stephen, M.J. and Straley, J.P., Rev. Modern Phys. 46, 617 (1974)

222. Subramanian, R. and DuPre', D.B., J. Polym. Sci., Polym. Phys. Ed. 22, 2207 (1984)

223. Suetsugu, Y. and White, J.L., J. Appl. Polym. Sci. 28, 1481 (1983)

224. Sugiyama, H., Lewis, D.N., White, J.L. and Fellers, J.F., J. Appl. Polym. Sci. 30, 2329 (1985)

225. Sugiyama, H., Lewis, D.N., White, J.L., and Fellers, J.F., unpublished data.

226. Suto, S., J. Polym. Sci., Polym. Phys. Ed. 22, 637 (1984)

227. Suto, S., White, J.L. and Fellers, J.F., Rheol. Acta. 21, 62 (1982)

228. Tadokoro, H., Soc. Cryst. Meeting Japan (1973)

229. Takeuchi, Y., Yamamoto, F., and Yamakawa, S. Polym. J. (Japan) 16, 579 (1984)

230. Tanaka, H. and White, J.L., Polym. Eng. Sci. 20, 950 (1980)

231. Tsvetkov, V.N., Shtennikova, I.N., Rjumtsev, E.I., and Getmanchuk, Y.P., Eur. Polym. J. 7, 767 (1971)

232. Tsvetkov, V.N., Rjumtsev, E.I., Shtennikova, I.N., Pogodina, N.V. and Peker, T.V., Eur. Polym. J. 11, 315 (1975)

233. Venkatraman, S., Berry, G.C. and Einaga, Y., J. Polym. Sci., Polym. Phys. Ed. 23, 1275 (1985)

234. Viney, C., Donald, A.M. and Windle, A.H., Polymer 26, 870 (1985)

235. Viola, G., Baird, D.G. and Gottis, A. " Studies of the Rheological Behavior of Liquid Crystalline Polymers", Soc. Rheol. Meeting, Blacksburg, Va. (1984)

236. Warner, S.B. and Jaffe, M., J. Cryst. Growth 48, 184 (1980)

237. Warren, R.C., Rheol. Acta. 23, 544 (1984)

238. Werbowyj, R.S. and Gray, D.G., Mol. Cryst. Liq. Cryst. 34 (Lett.), 97 (1976)

239. Whitcomb, P.J. and Macosko, C.W., J. Soc. Rheol. 22, 493 (1978)

240. White, J.L. and Fellers, J.F., J. Appl. Polym. Sci., Appl. Polym. Symp. 33, 137 (1978)

241. White, J.L. and Spruiell, J.E., J. Appl. Polym. Sci., Appl. Polym. Symp. 33, 91 (1978)

242. Wissbrun, K.F., Br. Polym. J. 12, 163 (1980)

243. Wissbrun, K.F., J. Soc. Rheol. 25, 619 (1981)

244. Zachariades, A.E., Economy, J. and Logan, J.A., J. Appl. Polym. Sci. 27, 2009 (1982)

245. Zachariades, A.E. and Logan, J.A., Polym. Eng. Sci. 23, 797 (1983)

246. Zachariades, A.E., Navard, P. and Logan, J.A., Mol. Cryst. Liq. Cryst. 110, 93 (1984)

VITA

David Neal Lewis was born in Macon, Georgia on August 9, 1955. He graduated from Southwest High School in June of 1973. The following September he entered Macon Junior College. After two years, he transferred to Georgia College in Milledgeville, Georgia and was awarded the Bachelor of Science degree in Chemistry in June of 1977. In the fall of 1977, he entered the Georgia Institute of Technology in Atlanta, Georgia and began study toward a Master of Science degree in Textiles. In December of 1979, he was awarded this degree.

In June of 1979, the author entered the University of Tennessee in Knoxville, Tennessee and began study toward a Doctorate degree in Polymer Engineering. He received the Doctor of Philosophy degree in June of 1986.

The author is a member of the Society of Plastics Engineers. He is currently a research associate in the Department of Material Science and Engineering.